Numerical and Experimental Evaluation of Microwave Treatment of Rocks for Application in Mining Excavation

by

Adel Ahmadihosseini

Department of Mining and Materials Engineering

McGill University, Montreal

August 2024

A thesis submitted to McGill University

in partial fulfilment of the requirements of the degree of

Doctor of Philosophy

Abstract

Efficiently breaking hard rocks remains a persistent challenge in mining and geotechnical engineering. Traditional explosive-based methods such as blasting, while effective in some cases, bring about a host of issues including but not limited to low productivity rate, noise pollution, dust, vibration, mine collapse, and safety hazards. Consequently, the mining sector seeks to transition from non-continuous explosive-based techniques to continuous mining approaches. However, continuous mining methods suffer from drawbacks such as the short life span of the cutting blades, especially when dealing with hard rocks. Rock pre-conditioning has emerged as a promising solution to address the challenges and facilitate the shift towards continuous mining. Among the various pre-conditioning methods, microwave treatment has achieved significant attention over the past decade. This research endeavours to assess the efficacy of microwave treatment as a rock pre-conditioning method through a combination of experimental and numerical analyses for field applications and introduce potential ways for its improvement. A comprehensive series of experiments, including microwave treatment, calorimetric measurements, thermal imaging, and rock mechanical testing, are conducted using a novel energy efficiency-based approach. Additionally, a fully coupled numerical model is developed to simulate heat transfer and energy absorption behaviours in rocks during microwave treatment and is validated against experiments conducted in this study. The developed numerical model is leveraged to enhance the energy efficiency of microwave treatment experiments. Through the integration of an energy efficiency-focused perspective, this research offers new insights into the potential application of microwave treatment for rock pre-conditioning in field settings. Moreover, the developed numerical model contributes to a deeper understanding of the mechanisms underlying microwave treatment and aids in achieving superior energy efficiency in experimental and potential field outcomes.

Résumé

Briser efficacement les roches dures reste un défi persistant en génie des mines et en géotechnique. Les méthodes traditionnelles basées sur les explosifs telles que le sautage, bien qu'efficaces dans certains cas, entraînent une multitude de problèmes, notamment le taux instable de productivité, le bruit, la poussière, les vibrations, l'effondrement des mines et les risques pour la sécurité. Par conséquent, le secteur minier cherche à passer de techniques discontinues basées sur des explosifs à des approches d'exploitation minière continue. Cependant, les méthodes continues d'exploitation minière souffrent d'inconvénients tels que la courte durée de vie des lames de coupe, en particulier lorsqu'il s'agit de roches dures. Le préconditionnement des roches est apparu comme une solution prometteuse pour relever les défis et faciliter la transition vers une exploitation minière continue. Parmi les différentes méthodes de préconditionnement, le traitement par micro-ondes a suscité une attention considérable au cours de la dernière décennie. Cette recherche vise à évaluer l'efficacité du traitement par micro-ondes en tant que méthode de préconditionnement des roches, appliquant une combinaison d'analyses expérimentales et numériques pour des applications sur le terrain et à introduire des moyens potentiels pour son amélioration. Une série complète d'expériences, notamment le traitement par micro-ondes, les mesures calorimétriques, l'imagerie thermique et les tests mécaniques des roches, sont menées à l'aide d'une nouvelle approche basée sur l'efficacité énergétique. De plus, un modèle numérique comprenant des phénomènes couplés est développé pour simuler les comportements de transfert de chaleur et d'absorption d'énergie dans les roches pendant le traitement par micro-ondes, validé par les expériences menées dans cette étude. Le modèle numérique développé est exploité pour améliorer l'efficacité énergétique des expériences de traitement par micro-ondes. Grâce à l'intégration d'une perspective axée sur l'efficacité énergétique, cette recherche offre de nouvelles perspectives sur l'application potentielle du traitement par micro-ondes pour le préconditionnement des

roches sur le terrain. De plus, le modèle numérique développé contribue à une compréhension plus approfondie des mécanismes sous-jacents au traitement par micro-ondes et aide à atteindre une efficacité énergétique supérieure dans les résultats expérimentaux et de meilleurs résultats potentiels sur le terrain.

“Madness is like gravity…all it takes is a little push.”

Joker- The Dark Knight

Acknowledgements

As I finalize the last steps of this thesis, I am compelled to express my profound gratitude for the unwavering support and guidance provided by my esteemed advisors. My supervisors, Prof. Ferri Hassani and Prof. Agus Sasmito, and my advisor, Prof. Ali Ghoreishi Madiseh, have been indispensable companions throughout this journey. Their steadfast mentorship, unwavering support, and boundless encouragement have been the cornerstone of my success. I am deeply grateful for their dedication and guidance, without which completing this endeavor would have been impossible.

I extend my heartfelt thanks to the support and technical staff at McGill University, whose assistance has been invaluable throughout my academic path: Ms. Marina Rosati, Ms. Barbara Hanley, Ms. Lucie Riffard, and Dr. William Cook. A special appreciation goes to Dr. Mehrdad Kermani for his indispensable aid in experimental setups and testing. I am also deeply grateful to all the members of the Geomechanics Lab and Mine Multiphysics Lab, who have been outstanding colleagues and cherished friends. I sincerely appreciate Prof. Alessandro Navarra for his insightful review of my work as a committee member over the years. Additionally, I extend my gratitude to Prof. Jamie Archibald, Prof. Luc Chouinard, Prof. Abdolhamid Akbarzadeh, Prof. Kristian Waters, Prof. Richard Chromic for their thorough review of this thesis.

I am deeply grateful to the individuals and organizations whose financial support has been instrumental in my journey. Special thanks to the McGill Engineering Doctoral Award, Fonds de Recherche du Quebec – Nature et Technologies (FRQNT), and Mitacs for their generous assistance throughout the years.

Last but not least, I would like to extend my appreciation to all friends and family who have been the brightest lights of the darkest nights. This thesis is dedicated to each and every one of you.

Contribution of Authors

The chapters of this research have been published or are under review in peer-reviewed journals. The contribution of the author of this thesis in each work is as follows:

- Chapter 2: **Ahmadihosseini, A.**, Shadi, A., Rabiei, M., Samea, P., Hassani, F., & Sasmito, A. P., 2022. Computational study of microwave heating for rock fragmentation; model development and validation. International Journal of Thermal Sciences, 181, 107746.

  Contributions: **Ahmadihosseini**: Methodology, Software, Validation, Formal analysis, Investigation, Writing-original draft, Writing-review & editing, Visualization, **Shadi**: Formal analysis, Writing-original draft, Writing-review & editing, **Rabiei**: Writing-review & editing, **Samea**: Writing-review & editing, **Hassani**: Conceptualization, Methodology, Investigation, Resources, Writing-review & editing, Supervision, Project administration, Funding acquisition, **Sasmito**: Conceptualization, Methodology, Investigation, Resources, Writing-review & editing, Supervision, Project administration, Funding acquisition

- Chapter 3: Ahmed, H. M., **Ahmadihosseini, A.**, Hassani, F., Hefni, M. A., Ahmed, H., Saleem, H. A., Moustafa, E. B. & Sasmito, A. P., 2023. Numerical and experimental analyses of rock failure mechanisms due to microwave treatment. Journal of Rock Mechanics and Geotechnical Engineering, 15(10), 2483-2495.

  Contributions: **Ahmed, H. M.:** Resources, **Ahmadihosseini**: Methodology, Software, Validation, Formal analysis, Investigation, Writing-original draft, Writing-review & editing, Visualization, **Hassani**: Conceptualization, Methodology, Investigation, Resources, Writing-review & editing, Supervision, Project administration, Funding acquisition, **Hefni**: Resources, **Ahmed, H.**: Resources, **Saleem**: Resources, **Moustafa**:

Resources, **Sasmito**: Conceptualization, Methodology, Investigation, Resources, Writing-review & editing, Supervision, Project administration, Funding acquisition

- Chapter 4: Deyab, S. M., **Ahmadihosseini, A.**, Rafezi, H., Hassani, F., & Sasmito, A. P., 2023. Investigating Microwave Treatment of Rocks Based on Fracture Mechanics Analysis in Mode I Fracture Toughness Test. Rock Mechanics and Rock Engineering, 56(7), 5275-5291.

  Contributions: **Deyab:** Methodology, Formal analysis, Investigation, Experimental design, Laboratory testing, Writing-original draft, Visualization, **Ahmadihosseini**: Methodology, Software, Validation, Formal analysis, Investigation, Writing-original draft, Writing-review & editing, Visualization, **Rafezi**: Methodology, Experimental design, Laboratory testing, Investigation, Writing-original draft, **Hassani**: Conceptualization, Methodology, Investigation, Resources, Writing-review & editing, Supervision, Project administration, Funding acquisition, **Sasmito**: Conceptualization, Methodology, Investigation, Resources, Writing-review & editing, Supervision, Project administration, Funding acquisition

- Chapter 5: **Ahmadihosseini, A.**, Hassani, F., Kermani, M., & Sasmito, A. P., 2024. Potential application of the microwave treatment in mining excavation evaluated using energy efficiency-based approach. International Journal of Rock Mechanics and Mining Sciences. (Under Review)

  Contributions: **Ahmadihosseini**: Methodology, Software, Validation, Formal analysis, Investigation, Writing-original draft, Writing-review & editing, Visualization, **Hassani**: Conceptualization, Methodology, Investigation, Resources, Writing-review & editing, Supervision, Project administration, Funding acquisition, **Kermani**: Investigation, Writing-review & editing, **Sasmito**: Conceptualization, Methodology, Investigation, Resources, Writing-review & editing, Supervision, Project administration, Funding acquisition

Additional journal and conference publications that the author of this thesis has contributed to are listed as follows:

- **Ahmadihosseini, A.**, Aslam, A., Rafiei, A., Hassani, F., Sasmito, A., 2024. Introducing a novel methodology for analysing the energy efficiency of microwave treatment in mine-to-mill operations. Applied energy. (Under Review)
- Shadi, A., **Ahmadihosseini, A.**, Ghoreishi Madiseh, A, Hassani, F, Sasmito, A, Rabiei, M, Samea, P., 2022. Numerical and experimental analysis of fully coupled electromagnetic and thermal phenomena in microwave heating of rocks. Minerals Engineering.
- **Ahmadihosseini, A.**, Aslam, A., Hassani, F., Sasmito, A., 2024. Evaluating the potential of microwave treatment as a rock pre-conditioning method in achieving a more sustainable mining. GeoMontreal, Montreal, Canada. (Accepted)
- **Ahmadihosseini, A.,** Aslam, A., Hassani, F., Sasmito, A., 2024. Experimental energy-based analysis of the efficiency of microwave treatment in mining operations. CIM Convention, Vancouver, Canada. (Accepted)
- **Ahmadihosseini, A.,** Aslam, A., Hassani, F., Sasmito, A., 2023. Investigating the efficiency of microwave treatment in mine-to-mill operations: an energy-based analysis. International Conference on Applied Energy, Doha, Qatar.
- Aslam, A., Rasyid, M., Rafiei, A., **Ahmadihosseini, A.,** Sasmito, A., Hassani, F., 2023. Potential benefits of microwave-assisted comminution in Kimberlite processing. Conference of Metallurgists, Toronto, Canada.

- **Ahmadihosseini, A.**, Hassani, F., Sasmito, A., 2023. Heat transfer analysis of microwave irradiation in rock grain minerals. International Heat Transfer Conference, Cape Town, South Africa.
- **Ahmadihosseini, A.,** Hassani, F., Sasmito, A., 2023. Numerical investigation of the energy efficiency of microwave-assisted comminution. CIM Convention, Montreal, Canada.
- Shadi, A., Rabiei, M., **Ahmadihosseini, A.**, Samea, P., Hassani, F., Sasmito, A., Ghoreishi Madiseh, A., 2022. Investigating the formation of damages in rocks due to microwave irradiation. CIM Convention, Vancouver, Canada.
- Madiseh, A., Shadi, A., Rabiei, M., **Ahmadihosseini, A.,** Hassani, A., Sasmito, A., 2021. Understanding the efficiency of microwave-assisted rock fragmentation. CIM Convention, Virtual.
- Rabiei, M., **Ahmadihosseini, A.**, Shadi, A., Samea, P., Ghoreishi Madiseh, A., 2022. The general rock failure modeling using discrete element method. CIM Convention, poster presentation, Vancouver, Canada.
- **Ahmadihosseini, A.**, Shadi, A., Hassani, A., 2021. Numerical and experimental analysis of rock energy absorption during microwave treatment. CIM Convention, poster presentation, Virtual.

Table of Contents

List of Tables

List of Figures

List of Abbreviations

ASTM: American society for testing and materials

BDF: Backward differentiation formula

BiCGStab: Biconjugate gradient stabilized method

BTS: Brazilian tensile strength

CCNBD: Cracked chevron notched Brazilian disc

CT: Computed tomography

DSC: Differential scanning calorimeter

EDX: Energy dispersive X-ray

FEM: Finite element method

FGMRES: Flexible generalized minimal residual method

GMRES: Generalized minimal residual method

HOME: Heat over microwave efficiency

IFBW: Intermediate frequency bandwidth

ISRM: International society of rock mechanics

LFA: Laser flash analyzer

LVDT: Linear variable differential transformer

NSCB: Notched semi-circle bend

PARDISO: Parallel direct solver

PLT: Point load test

SEM: Scanning electron microscopy

STD: Standard deviation

TE: Transverse electric

TFQMR: Transpose free quasi minimal residual method

TM: transverse magnetic

TMA: Thermo-mechanical analyzer

UCS: Uniaxial compressive strength

UTS: Uniaxial tensile strength

WOME: Weakening over microwave energy

XRD: X-ray diffraction

XRF: X-ray fluorescence

“You mustn’t be afraid to dream a little bigger darling.”

Eames- Inception

Chapter 1: Introduction

1.1. Background information and motivation

Mining emerges as one of the largest industries, confronting a myriad of challenges. Fundamentally, mining exerts immense energy demands, representing over 7% of global energy consumption—a statistic projected to soar more than eightfold over the next four decades. This energy consumption primarily relies on sources including electricity, diesel, oil, coal, natural gas, and gasoline (Aramendia et al., 2023; Holmberg et al., 2017; F. Lin et al., 2022). In addition to its substantial energy requirements, traditional non-continuous drill and blast mining methods pose issues such as mine collapse, pollution, low productivity, and safety hazards. These challenges necessitate engineers to reassess their approach in mine-to-mill practices by transitioning from non-continuous to continuous methods like mechanical excavation. This paradigm shift holds the potential for complete automation of mining excavation, removing personnel from mine surfaces, thereby enhancing safety, reducing costs, lowering energy consumption, and environmental pollution, while also mitigating risks like mine collapse and groundwater influx (Ma, Duan, Liu, et al., 2019; S. Wang et al., 2019). However, these methods encounter their own set of challenges, particularly when dealing with hard rocks due to the intricate nature of operations within this industry, such as rock breakage, crushing, grinding, and liberation, among others. Therefore, designing suitable continuous based equipment for mining through hard rocks carries issues such as costly designs and short lifespans of cutting equipment, heavy maintenance requirement and in summary, inefficient mining practices (Hassani, 2010).

This approach can be facilitated by employing rock pre-conditioning methods, wherein the rock mass is weakened prior to excavation through rock fragmentation techniques. These techniques enable the use of continuous methods even in hard rock formations (Wei et al., 2019). Engineered to induce micro/macro cracks within the rock mass before mining operations commence, these methods contribute to improvements in cost, energy efficiency, and overall sustainability. Among the most prominent pre-conditioning techniques are hydraulic fracturing, electrical methods, conventional heating, laser applications, and microwave treatment. Among these methods, microwave treatment has shown considerable promise in field applications over the years. This technique operates by exploiting the inherent variability of minerals within rocks to weaken their structure (Hassani, 2010).

Rocks typically comprise a diverse array of minerals, each exhibiting varying responses to microwave exposure. Mineral reactions range from absorption to reflection of microwave energy based on their dielectric properties, with the former resulting in material heating during microwave treatment. Given this variability, minerals that absorb microwaves undergo greater heating and expansion compared to those that reflect the energy. As a result, partial thermal expansion of the material exerts pressure on the surrounding rock matrix, inducing micro/macro cracks (Rasyid et al., 2023). Essentially, this method reduces the strength of the rock mass for subsequent mechanical excavation or breaking processes by pre-conditioning its properties in advance (Hassani et al., 2020).

The scope of this research is to assess the efficacy of microwave treatment as a rock pre-conditioning method to potentially enhance mechanical excavation. A comprehensive series of experiments is conducted within the Geomechanics Laboratory of McGill University, adopting an energy efficiency-based analysis approach that offers a novel perspective on evaluating the method's effectiveness. To facilitate this investigation, a fully coupled numerical model is developed to accurately simulate the energy absorption and heat transfer processes within the rocks during microwave treatment, with the model's outcomes validated against the experimental findings. The development of this numerical model not only helps in improving efficiency of microwave treatment but also yields fresh insights into the underlying physical mechanisms inherent in mining operations.

1.2. Literature review

Research on the application of microwave treatment to enhance rock fragmentation started to gain more attention in the early 2000s, experienced a notable increase over the past decade. Studies in this domain predominantly follow two main avenues: experimental testing and numerical modeling. This section aims to evaluate the existing literature in these areas to identify key knowledge gaps requiring attention. By pinpointing areas for improvement, this research seeks to steer the mining industry towards a more sustainable trajectory.

1.2.1. Experimental testing

During the early 2000s, substantial research studies started to evaluate microwave treatment as a rock pre-conditioning method. These studies initially focused on experimentally assessing the impact of microwaves on various rock characteristics, followed by investigations into the influence of different factors such as microwave mode, frequency, power, energy dosage, and rock type on the applicability of the method.

As one of the pioneering studies, Kingman et al. (2004) utilized microwave energy to weaken copper carbonatite ore. Employing an experimental setup comprising a 2.45 GHz magnetron for microwave energy generation, a single-mode transverse electric (TE mode 10n) applicator, and a short-circuit tuner to generate standing waves, they subjected samples to varying exposure times and power levels. Post-microwave treatment, the uniaxial compressive strength (UCS) of the samples was assessed using point load tests (PLT), revealing a significant reduction in ore strength alongside an increase in grindability (Kingman et al., 2004). Continuing their research, they investigated the response of lead-zinc ores to microwave treatment utilizing both single-mode and multi-mode cavities, employing powers ranging from 3 to 15 kW on relatively small sample sizes (<1 kg). Their findings highlighted that higher power density leads to more efficient microwave treatment, with single-mode cavities inducing higher strength reductions at the same input power.

Expanding the scope to different rock types, Satish et al. (2006) examined the impact of microwave energy with low powers (750 W) and a frequency of 2.45 GHz on basalt rocks, renowned for their hardness. They observed a linear increase in sample temperature up to 101°C after 360 seconds of exposure, followed by a reduction in PLT values. Their study suggested the potential application of microwave treatment in reducing the energy required for breaking basalt samples.

Peinsitt et al. (2010) compared the effects of microwave treatment on dry and water-saturated basalt, granite, and sandstone. Using a microwave system at a frequency of 2.45 GHz and power of 3 kW, they observed significant differences in heating rates among rock types, attributed to variations in dielectric properties. Water content exhibited varying effects on heating rates, with no change observed for basalt, a doubling for granite, and a fourfold increase for sandstone in water-saturated samples compared to dry ones.

To understand micro and macro crack development in rock samples during microwave treatment, Hartlieb et al. (2012) employed a 3.2 kW multi-mode cavity at a frequency of 2.45 GHz on cylindrical basalt samples. Their results indicated that after 60 seconds of exposure time, sample temperatures at the surface and centre reached 250°C and 400°C, respectively, accompanied by the formation of both axial and radial cracks.

In an effort to delve deeper into the fracture mechanics of basalt, Nejati et al. (2012) utilized microwave treatment on semi-circular samples designated for mode-I fracture toughness experiments, employing varying powers (1 to 5 kW) and exposure times (5 to 30 seconds). They observed a linear relationship between measured specimen temperatures and applied microwave energy, indicating the roles of both power and exposure time in achieving high temperatures within rocks, resulting in fracture toughness reduction.

In all the aforementioned studies, there was a significant emphasis on evaluating the influence of various factors such as rock type, microwave power and exposure time, frequency, etc., on the effectiveness of microwave treatment. These studies laid a solid foundation for research aimed at applying microwave treatment to improve rock fragmentation. Over the past decade, some researchers have continued along this trajectory, exploring the effects of a wider range of rock types under various microwave treatment conditions, taking into account advancements in microwave technology and the design of new systems.

For example, Zheng et al. (2017) investigated the effect of microwave treatment on the thermal properties of gabbro using a single-mode industrial microwave system with a maximum output power of 2 kW and a frequency of 2.45 GHz. Their study focused on measuring surface temperature, heating rates, and spatial temperature distribution to evaluate the effectiveness of microwave treatment in weakening the rock. They observed a linear increase in surface temperature and heating rates with power and exposure time, while spatial temperature distribution followed a reversed V-shape. Continuing their research, Zheng et al. (2020) performed experimental investigations into the thermal, mechanical, and cracking behaviours of three igneous rocks (gabbro, monzonite, and granite) under microwave treatment. They measured parameters such as heating rate, spatial temperature distribution, as well as mechanical parameters including elastic modulus, load-bearing capacity, crack pattern, and crack density of the rocks under different exposure times and powers. Their results indicated that microwave treatment weakened gabbro and monzonite rocks by generating cracks or causing melting and shattering of the specimens. In contrast, granite specimens experienced violent failures at high power levels. Additionally, applying 2 kW microwave power for 120 seconds reduced the elastic modulus by 13% and 27%, and load-bearing capacity by 34% and 43% for gabbro and monzonite, respectively.

Following a similar approach, Hassani et al., (2016) investigated the effect of microwave treatment on norite, granite, and basalt using UCS and Brazilian tensile strength (BTS) as strength criteria. They found that microwave treatment led to a linear decrease in heating rate on the rock surface with increasing distance from the microwave antenna, regardless of power level and exposure time. Furthermore, the tensile and compressive strengths of the rocks decrease with microwave power and exposure time. Continuing this research, Deyab et al. (2021) evaluated new rock types (kimberlite and granite) using an industrial microwave system with a maximum power of 15 kW at a frequency of 2.45 GHz. Comparing the rocks, they found that kimberlite exhibited better microwave energy absorption compared to granite, resulting in a more significant strength reduction. Their results also indicated that microwave treatment did not have a noticeable effect on the abrasivity of the rock samples.

Lu et al. (2020b) focused on the effect of microwave treatment on three rock types: basalt, gabbro, and granite. Their results indicated that the absorption capacity of rocks for microwaves was closely related to the imaginary part of the permittivity, with basalt exhibiting higher absorption capacity and heating rates compared to gabbro and granite.

In a comparative study, Meng et al. (2020) examined the breakage behaviour of oil shale with high grinding resistance using a 2.45 GHz multi-mode microwave cavity for treating oil shale samples. They found that microwave treatment significantly improved the grindability of oil shale compared to conventional heating, with a notable reduction in processing time. They observed a transformation from micro to macro cracks in oil shale samples treated with microwave heating, indicating enhanced reduction in structural integrity.

Several researchers have focused on exploring the influence of microwave treatment on the fracture mechanics characteristics of rocks, depicting its potential implications for various mining industry applications. For instance, Bai et al. (2021) investigated the fracture toughness of granite under the influence of microwave heating, employing different powers and exposure times. Their findings revealed a significant decrease of more than 35% in the fracture toughness of granite in certain cases, as well as a reduction in the failure time of the rock sample as the duration of microwave heating increased.

Ge et al. (2021) further analysed the effect of microwave treatment on fracture mechanics of granite samples with well-distributed lithofacies and minimal defects. Upon subjecting granite specimens to microwave treatment followed by mode-I fracture toughness tests, they observed a substantial reduction of approximately 40% in the fracture toughness parameters indicating a pronounced effect on the rock's mechanical properties.

Recognizing the significance of fracture mechanics, Li et al. (2021) delved deeper into the fracture behaviours of granite samples affected by microwave treatment. The samples were treated with microwave energy. The results showcased an exponential decrease in fracture toughness with heating time, suggesting increased ductility of the granite samples. Additionally, the analysis revealed a correlation between fracture toughness, fracture process zone size, and fractal surface dimension.

Li et al. (2021) investigated coal core fracturing using microwave energy. They compared crack propagation on the surface and interior of cores before and after microwave treatment. It was observed that microwave treatment induced new fractures and reduced pore sizes in coal cores, emphasizing the potential of microwave treatment for degassing coalbed methane and enhancing mining efficiency.

In a recent study by Shou et al. (2019), the deterioration of granite under microwave treatment and conventional heating was examined through experiments involving heating the rocks to temperatures ranging from 400°C to 1000°C. UCS results revealed a consistent pattern of initial strengthening, subsequent weakening, and final stabilization in the samples treated with both microwave and conventional heating within the 400°C -900°C range with the former exhibiting lower UCS values compared to conventional heating. Continuing the research on granite rocks, Lehmann et al., (2023) employed various geotechnical parameters, including UCS, BTS, PLT, and abrasivity, to assess the efficacy of microwave treatment. Utilizing an industrial microwave system with a power of 5 kW and a frequency of 915 MHz, they observed a more substantial weakening effect on BTS and PLT compared to UCS.

Some researchers have utilized new technologies to gain further understanding of the interactions between rocks and microwave irradiation. For instance, Lu et al. (2019a) employed a novel microwave system comprising a multi-mode microwave chamber with six magnetrons, each with a power input of 1 kW, for treating basalt specimens. This chamber was designed as a standing-wave field resonator heater, allowing for efficient utilization of microwave energy by facilitating repeated absorption of microwaves by the rock specimens. Surface temperature measurements were conducted using an infrared thermometer and a handheld infrared gun-type sensor. The study also utilized SEM and energy dispersive X-ray (EDX) for evaluating the grain minerals within the basalt samples. Their findings demonstrated that cracks resulting from microwave treatment primarily occurred around olivine grains, with intergranular cracks between olivine and plagioclase grains and within olivine grains.

Continuing the use of visual technologies, Lan et al. (2020) employed computed tomography (CT) scanning and SEM technology before and after microwave treatment of coal samples with different powers and exposure times. Through this approach, they identified three mechanisms of microcrack initiation in rocks: dewatering shrinkage of minerals, particle separation, and internal cracking of the body.

Xu et al. (2020) utilized thermal imaging, an ultrasonic testing system, and a digital microscope to observe the effect of microwave treatment on rocks. The results showed a direct correlation between microwave power, temperature distribution, P-wave velocity attenuation, and fracture pattern in specimens.

Li et al. (2020) investigated the influence of varying microwave exposure times up to 240 seconds on the dynamic fracture properties of granite. Damage properties were first quantified using CT scanning and P-wave velocity determinations, revealing a significant decrease in strength with increasing microwave irradiation duration. Dynamic fracture tests using a split Hopkinson pressure bar system with a laser gap gauge technique demonstrated that the initiation fracture toughness increased linearly with the loading rate. Additionally, microwave treatment had a pronounced weakening effect on fracture properties.

The damage properties of basaltic rocks under multilevel stress loading and microwave irradiation were the focus of the study by Liu et al. (2023). They conducted experiments to investigate the effects of microwave treatment on the mechanical strength and damage characteristics of basalt. Through X-ray image analysis, they showed a correlation between exposure time and the maximum temperature indicating a significant influence on the thermal behaviour of rocks.

Introducing novel and innovative approaches, Yao et al. (2021) employed a copper-foil-wrapping method to simulate real application scenarios and verified the feasibility of the experiments. The results showed that pore water not only increased the heating rate but also affected the temperature distribution inside the rock. During short heating periods, high-power microwave output led to rapid evaporation of pore water, resulting in a sharp rise in temperature and an exponential distribution in the rocks. Conversely, low-dielectric-loss minerals such as quartz and feldspar absorbed microwave energy after a longer heating period, leading to a reduction in heating rate and a more uniform temperature gradient.

Lu et al. (2020a) utilized the triaxial testing method to explore the potential significance of microwave-induced fracturing of hard rocks for stress release in deep rock masses. Their results indicated that the elastic modulus and Poisson's ratio of the basalts decreased quasi-linearly with increasing microwave exposure time under uniaxial compression, while showing minimal influence under triaxial compression. The cohesion of the basalt samples decreased linearly with prolonged microwave exposure time, indicating a weakening of the material over time.

Li et al. (2021) employed various experimental techniques to capture temperature variations, fracture toughness, acoustic emission events, strain fields, and fractal dimension of the fracture surfaces of granite during microwave treatment. Their results demonstrated an exponential decrease in the fracture toughness of the granite samples with increasing exposure time, indicating enhanced ductility. Furthermore, acoustic emission events recorded during fracture tests showed a prolonged active period and post-peak stage, further indicating increased ductility.

In a study by Yang et al. (2020) investigating the evolution of structure and mechanical properties of basalt induced by microwave irradiation, basalt samples were treated using a 2.45 GHz, 2 kW apparatus. This research focused on assessing the morphology, mineral characteristics, and mechanical performance of basalt samples heated to temperatures ranging from 100°C to 400°C. The results revealed that microwave irradiation induced rapid thermal stress within the basalt, resulting in significant structural damage characterized by transgranular and intergranular fractures. Notably, intergranular fractures predominated, especially at lower temperatures, while transgranular fractures became more prominent above 200°C. Additionally, the study highlighted a decrease in UCS and fracture toughness of basalt treated with microwave irradiation.

Zhang et al. (2022)evaluated the effect of microwave treatment on fracture mechanics by considering the effect of crack angle in fracture toughness experiments. A series of experiments were conducted to analyse the deformation and failure behaviours of hard rocks. The results indicated that the mode-I fracture toughness linearly decreased with exposure time for pure tensile failure at a crack angle of 0°, while it increased at other crack angles. Moreover, the crack angle was found to have a substantial influence on the deformation and failure behaviour of the granite, with mode-II fracture toughness showing varying trends based on the crack angle.

Over the past decade, significant research studies have focused on understanding the effect of rock mineralogy on the effectiveness of microwave treatment. For instance, Zeng et al. (2019) investigated the structural evolution of granite under high-temperature conditions induced by microwave treatment. They identified mineral compositions including alkali-feldspar, plagioclase, quartz, biotite, and trace minerals like titanite and zircon. Conducting microwave treatment experiments at temperatures ranging from 300°C to 800°C, they observed a spherical melt cavity with radial cracks near the biotite-rich components at 600°C, leading to complete rock disintegration at 800°C. The UCS of the granite showed a significant decrease with rising temperatures, highlighting the complex interplay between mineral characteristics, micro-crack propagation, and mechanical performance under high-temperature conditions.

Focusing on basalt, Yuan et al. (2020) conducted tests to evaluate its thermal responses using an industrial microwave system. The results showed that ilmenite rapidly heats up with microwave energy. Furthermore, observations using a SEM showed that rock failure was induced by the unstable extension of radial cracks around absorbing mineral grain boundaries.

Lu et al. (2017) conducted a comprehensive study on eleven rock-forming minerals in a multi-mode cavity at 2.45 GHz with a power of 2 kW to further understand the effect of mineralogy on the effectiveness of microwave treatment. The tests were conducted for a duration of 3 minutes for all samples. The study utilized SEM and EDX to determine the elemental distribution and mineralogical composition of the tested samples. They concluded that the presence of iron in rock-forming minerals influences their microwave absorption capacity and the interaction mechanisms between minerals and microwaves. Furthermore, different rock-forming minerals exhibit varying microwave absorption capacities, and a better microwave treatment can be achieved with the existence of mineral heterogeneity.

Batchelor et al. (2015) conducted a comprehensive characterization of the mineralogical and textural features of 13 commercially exploited nickel, copper, and lead-zinc ores. Utilizing a Mineral Liberation Analyser, they quantitatively and qualitatively related these features to the extent of reduction in ore competency for microwave treatment utilizing PLT. The results underscored the importance of mineralogical and textural characteristics in determining the effectiveness of microwave treatment on ore competency.

Temperature-dependent material characterization, especially dielectric properties, plays a crucial role in understanding the fundamental interaction of microwaves with rocks and ores, influencing both heating rate and microwave penetration depth. Bobicki et al. (2020) reported high-temperature measurements of dielectric properties, emphasizing their significance in various ores such as bauxite, chromite, limonitic laterite, silicate laterite, manganese carbonate, magnesium carbonate, silica, iron carbonate, and oolitic iron ores. These measurements provide essential information into the behaviour of ores under microwave irradiation, contributing to the optimization of ore processing methods.

In a broader scope, Hartlieb et al. (2016) presented the thermo-physical properties of granite, sandstone, and basalt in the temperature range of 25–1000°C. This information provides fundamental data on the behaviour of common rock types under varying temperature conditions, facilitating a better understanding of their response to microwave irradiation. Continuing their research, Hartlieb et al. (2018) evaluated the reaction of various rock types to low-power microwave irradiation in a multi-mode cavity to assess the potential for rock fragmentation. Utilizing controlled exposure times and a standard household microwave operating at 2.45 GHz with a power of 3.2 kW, they measured the relative p-wave velocity of small cylindrical samples to quantify the reduction of rock integrity in response to microwave irradiation. The results demonstrated that the reaction to microwave irradiation strongly depends on the mineralogy of the rock. Rocks with low contents of microwave absorbers, such as granite and sandstone, heat slowly and do not show significant physical changes. Conversely, rocks with better microwave absorption, like basalt and mafic volcanites, heat quickly leading to significant physical changes. These findings contribute to our understanding of the applicability of microwave treatment in rock fragmentation processes.

To further evaluate the effect of mineralogy on the effectiveness of microwave treatment, Zheng et al. (2020) conducted a study using a collection of 14 high-grade minerals, including 11 gangue minerals and 3 ore minerals commonly found in igneous and metamorphic hard rocks. These minerals were pulverized into the same grain size ranges to minimize the effect of grain size on the measurement results. The dielectric properties of the minerals were measured using a customized resonant cavity at 2.45 GHz and room temperature. The results revealed that the dielectric properties of the minerals increased as the bulk density increased, indicating a higher degree of mineral-microwave interaction with higher density.

Kahraman et al. (2020a) investigated the impact of microwave treatment on the strength of nine different igneous rocks. UCS and BTS tests were conducted on both untreated and treated rock samples. The study highlighted that even small amounts of metallic minerals could lead to substantial temperature increases in specimens, affecting their mechanical properties.

Zhao et al. (2020a) investigated the microwave sensitivities of minerals based on their heating rates. They classified the minerals into different sensitivity levels, revealing that hypersthene, hornblende, and biotite exhibited high sensitivity, while quartz, orthoclase, plagioclase, muscovite, forsterite, diopside, and hornblende were identified as insensitive minerals underscoring the significant impact of mineral group, crystal structure, and iron content on the microwave sensitivity of these minerals.

In a study evaluating the effect of microwave treatment on cracking in granitic rocks, Nicco et al. (2020) prepared core specimens from different types of granitic rocks, including biotite-bearing granite, the Mount Rosa granite, and the Mount Rosa amphibole-bearing granite. It was revealed that coarser-grained granites developed extensive networks of narrow cracks, while finer-grained granites exhibited fewer but wider cracks. The presence of adjacent grains with contrasting mineralogical, thermal, and microwave properties was crucial in generating stresses between grains, leading to cracking. However, strong microwave absorbers were not essential for the cracking process, indicating that even rocks containing weak microwave absorbers could be suitable targets for industrial applications of microwave-induced cracking.

To evaluate the impact of microwave treatment on copper ore breakage, Rizmanoski (2011) used modulated microwave power to induce stress between mineral phases. Mineralogical investigations using the mineral liberation analyser and X-ray diffraction (XRD) revealed the presence of microwave-absorbing minerals like chalcopyrite, grossularite, and galena within the ore matrix. The study revealed the potential of microwave treatment for ore strength reduction, especially when applying pulsed microwave power. The results also showed that higher energy inputs could lead to polymorphous transformations in absorbing minerals, impacting the ore's physical and chemical properties.

Hassani et al. (2020) introduced a novel calorimetric technique to quantify the achieved heating and damage within a microwave cavity on rocks and ores, addressing the overlooked aspect of energy efficiency in microwave treatment research. By proposing two new parameters to evaluate the effects of microwave-induced energy and thermally induced fracturing on mechanical strength degradation, their research offered a comprehensive understanding of the efficiency and effectiveness of microwave treatment. Experimental investigations conducted to determine optimum conditions for microwave treatment demonstrated that establishing optimal electromagnetic heating conditions significantly improves microwave-induced weakening. Meanwhile, Gao et al. (2020) investigated the effects of microwave heating on sandstone samples of varying sizes, showing how sample size influences the energy absorption and resulting changes in temperature. Through real-time monitoring of heating power, they calculated the absorbed microwave energy, revealing distinct relationships between temperature and energy across different sample sizes. These studies contribute significantly to understanding the energy efficiency and effectiveness of microwave treatment, offering valuable information for optimizing microwave-induced rock pre-conditioning methods for field applications.

In summary, research in this area has predominantly centered on exploring how the application of microwave energy affects the rock properties and its related behaviours. Although this approach has provided valuable insights, its practical applicability has been limited by a lack of attention to energy efficiency analysis. A notable advancement in the latest research is the incorporation of an energy efficiency-focused approach into the assessment of experimental findings. This shift in perspective enables us to not only understand the effects of microwave treatment on rocks but also evaluate its feasibility for real-world applications in the field. By considering energy efficiency alongside experimental data, we can better gauge the practicality and potential benefits of employing microwave technology in various geological contexts. This holistic approach not only enhances our understanding of microwave-rock interactions but also opens up avenues for sustainable and efficient utilization of this technology in geological processes.

1.2.2. Numerical modelling

The evolution of numerical modelling in understanding the effect of microwave treatment on rocks has been significant, transitioning from simpler 2-D models to more complicated coupled 3-D simulations. Researchers have used these models to investigate various aspects of microwave-assisted rock fragmentation, considering factors like power density, energy input, and mineral composition.

Whittles et al. (2003) initiated these studies with a quasi-static thermo-mechanical 2-D model, focusing on thermal stresses and fracturing induced by microwave energy. By considering electric field strength, microwave frequency, and dielectric properties, they predicted fracture locations and observed improved liberation of valuable minerals, particularly around grain boundaries. Jones et al. (2005) expanded on this approach with a 2-D model exploring the effects of power density on mineral breakage. Their finite difference simulations demonstrated that higher power densities could substantially reduce compressive strength, thus lowering grinding energy requirements. Continuing their research, Jones et al. (2007) delved into the impact of microwave energy delivery methods on ore sample strength reduction through a quasi-static thermo-mechanical 2-D model. The simulations unveiled a maximum reduction in UCS ranging between 45% and 50% at a power density of 1×10^{12} W/m^3, indicating complete development of thermally induced cracks.

Wang et al. (2008) introduced an innovative thermal-based particle modelling approach to examine the impacts of microwave-assisted breakage on ore materials, specifically a combination of calcite and pyrite. Their developed model aimed to explore microwave heating, thermal conduction, expansion, thermally induced fracturing, and stress-strain profiles associated with different input microwave energies. The study unveiled that microwave energy can trigger microcracking along the grain boundaries of ores, resulting in a decrease in the necessary mechanical breakage energy. Moreover, the research illustrated that microwave power density significantly influences the thermo-mechanical failure of the ores.

Ali and Bradshaw (2009) advanced the field by introducing a novel method to characterize damage in ore particles during microwave treatment. Their 2-D finite difference models, focusing on binary ore systems, highlighted the influence of power density and energy input on grain boundary damage, suggesting tailored approaches for different ore types. Continuing their work, Ali and Bradshaw (2010) explored fracture induction in mineral ores using discrete element modelling. They emphasized the role of power density in reducing energy input and localizing damage, particularly around grain boundaries.

Hartlieb et al. (2012) contributed further by developing a thermal and thermomechanical finite element model to analyse temperature distributions and induced stresses in basalt samples under microwave irradiation. Their findings showed significant temperature increases and crack formation due to tensile stresses exceeding the rock's strength.

Wang and Djordjevic (2014) employed a 2-D finite element method (FEM) to investigate thermal stress and crack development in rocks under short-pulse microwave energy exposure. They examined the thermal mismatch between microwave-absorbing parts and a low-absorbing matrix to understand its impact on stress distribution and crack development. The results indicated that the thermal mismatch between microwave-absorbing and low-absorbing minerals can generate significant localized thermal stresses in the rock when subjected to high-power microwave energy. The initial breakage primarily arises from tensile thermal stresses, leading to crack propagation in a radial direction from the calcite matrix.

Meisels et al. (2015) conducted a numerical analysis to explore how microwave propagation and absorption affect heterogeneous rocks. Their study introduces a 2-D numerical model of a two-component rock. The analysis incorporated absorbing parts within a non-absorbing matrix to mimic the heterogeneity of rocks. Employing the finite difference time domain method to solve Maxwell's equations, the study showed up to 20% changes in the intensity of the main radiation due to reflections at the interfaces and absorption in the discs. Subsequent thermo-mechanical FEM analysis revealed that the induced stresses reached significant levels, capable of initiating damage in the rocks.

Xu et al. (2020) employed a 2-D FEM electromagnetic-thermo-mechanical modelling approach, utilizing simplifying assumptions such as Lambert's Law to capture electromagnetic radiation. Combined with discontinuous deformation analysis, their simulation aimed to replicate the process of thermal failure and rock fracturing induced by microwave heating. They recognized thermal stress mismatch in local high-temperature areas as the primary factor for crack initiation while crack propagation was contingent on global temperature, sample geometry, and existing fractures.

As one of the early 3-D numerical models, Toifl et al. (2016) conducted a comprehensive study to investigate microwave-induced stresses in the microstructures of hard rocks. They employed a direct treatment of absorbed power density as a heat source in the heat conduction equation, which was numerically solved to simulate the transient inhomogeneous temperature field resulting from microwave treatment. The microstructure of the rocks was generated using a Voronoi tessellation algorithm with statistically distributed grain sizes and phase assignments, enabling the capture of sharp grain boundaries. Subsequent FEM stress simulation provided information regarding the stress formation, with statistical analysis used to predict stress and damage formation in the rock materials. The results revealed that considering microstructural details is crucial for determining reliable microwave-induced stresses in rocks with strongly absorbing phases. In a follow-up study, Toifl et al. (2017) assessed the effects of various microwave irradiation times under constant power and energy, leading to the evaluation of the transient temperature field and subsequent stress simulation.

The results indicated that microwave treatment has the potential to induce stresses high enough to facilitate fragmentation processes in hard rocks.

Li et al. (2019) investigated the effectiveness of microwave treatment by utilizing a fully coupled numerical model to examine the response of pegmatite specimens to microwave irradiation. The mineralogical composition of the pegmatite thin section, comprising quartz, orthoclase, plagioclase, and chlorite, was characterized using SEM to obtain a realistic microstructure for the model. The stress distribution within the pegmatite specimen exhibited a layered pattern with alternating high and low stresses. Stresses were highest in quartz and chlorite, indicating their good thermal conductivity and large thermal expansion coefficient. Different minerals within the pegmatite thin section showed varying levels of compressive stresses, with quartz experiencing the largest compressive stress and being more prone to plastic failure.

Using other numerical approaches, Li et al. (2022) developed a discrete element based model to capture the fracture behaviour of microwave-treated granite. The results demonstrated a strong correlation between temperature and confining stress on the fracture behaviour of microwave-heated samples. Specifically, the model revealed that higher temperatures resulted in smaller peak indentation force and penetration depth, attributed to an increase in thermal cracks and a decrease in rock brittleness. The model also identified three distinct stages of the fracture process: elastic deformation, fluctuating penetration, and post-peak, with the damage zone primarily comprising tensile cracks. Additionally, the model indicated that microwave treatment could mitigate the effect of high confining stresses on the damage zone, leading to improved hard-rock crushing efficiency.

Lin et al. (2017) presented a coupled electromagnetic and heat transfer model to investigate the thermal response of coal under microwave treatment. They explored the effects of microwave parameters (i.e., frequency and power), dielectric property, and size of the coal sample on heating behaviour. The results show that an increase in microwave power contributes to thermal heterogeneity.

Xu et al. (2021) investigated the utilization of microwave treatment for pre-conditioning hard rocks for the purpose of enhancing mineral resources recovery using a 3-D damage-based, electromagnetic-thermo-mechanical coupled numerical model. The research focused on low-porosity basalt samples subjected to microwave radiation in a box-type multi-mode cavity. The results showed a non-uniform temperature distribution in the rocks, leading to thermal mismatch-induced tensile cracks.

Zhao et al. (2022) used numerical simulations focused on analysing the effects of dielectric anisotropy on the temperature and stress distribution within coal samples under microwave irradiation. The results demonstrated significant differences in temperature and stress profiles based on the dielectric direction sensitivity and the dielectric constants of the material. Through a combination of numerical simulations and experimental observations, they observed significant thermal inhomogeneity within the coal samples due to the spatial variation of the electromagnetic field and material heterogeneity.

Pressacco et al. (2022) presented a numerical study on the effects of microwave irradiation on the mechanical properties of hard rock, specifically focusing on the weakening effect of microwave heating induced damage on the uniaxial compressive and tensile strength of granite-like rock. This study uses a damage-viscoplasticity model to simulate the thermo-mechanical behaviour of heterogeneous numerical rock specimens subjected to heating in a microwave oven and then to uniaxial compression and tension tests. The results show that the compressive and tensile strength of rock can be significantly reduced by microwave heating.

Liang et al. (2023) developed a fully coupled electromagnetic-thermal-mechanical model to investigate the fracture behaviour of basalt rock under microwave heating. Experimental validation involved heating basalt samples in a microwave cavity under varying power levels, showcasing a fluctuating increase in surface temperature compared to numerical results. Observations showed an inhomogeneous electric field distribution in the cavity and basalt rock during the energy conversion stage. Furthermore, it was identified that internal compression and external tension are the primary causes of basalt rock fracture under microwave irradiation.

Chun et al. (2022) utilized smoothed particle hydrodynamics and finite element method approaches to investigate how microwave pre-conditioning affects the strength of basalt rock. By conducting parametric sensitivity analysis, they calibrated the mechanical parameters for cohesion and internal friction angle for the basalt specimens treated with microwaves. The results suggest potential applications in optimizing processes such as rock cutting and drilling, with the aim of reducing equipment wear and extending machine service life.

1.3. Contributions to the original knowledge

This PhD thesis is focused on exploring the potential of microwave treatment as a viable field practice for engineers by addressing the existing knowledge gaps. By addressing the limitations of previous research studies, a methodology has been presented to provide insights and solutions that can improve the practical application of microwave treatment in various engineering contexts.

The experimental research in this field has primarily focused on understanding the impact of applying microwave energy on the characteristics and properties of rocks. While this approach has yielded valuable insights, it lacks practical applications due to neglecting the energy efficiency analysis. A significant contribution of the current research is the integration of an energy efficiency-based approach into the evaluation of experimental data. This perspective permits and assessment of the potential application of microwave treatment in the field. This approach follows two pathways: 1) quantifying the absorption of microwave energy by the sample, and 2) assessing the outcomes (e.g., damage) of the treatment per unit of input and absorbed microwave energy. A combination of calorimetric techniques and thermal imaging is used to analyse microwave energy absorption effectively.

This research also places emphasis on the numerical modelling of microwave treatment. The process of microwave heating of rocks is a complex coupled physical problem, involving electromagnetic irradiation, heat transfer resulting from the absorption of microwave energy by the material, and associated effects. Due to the intricate nature of this problem, previously developed numerical models in the literature often rely on simplifying assumptions to simulate this process such as: 1) employing Lambert's Law to simplify electromagnetic irradiation instead of utilizing Maxwell's equations or simplifying microwave heating within heat transfer equations, 2) utilizing inappropriate material properties as inputs for the numerical model, and 3) neglecting various mechanisms involved in microwave heating, such as convection and radiation. As a consequence of these limitations, these models often lack comprehensive validation against experimental data.

In the current research, a fully coupled numerical model has been developed to analyse the effects of microwave treatment on rocks. This model incorporates temperature-dependent material properties, including dielectric properties, thermal conductivity, heat capacity, and thermal expansion, which are measured and utilized as inputs. To ensure the accuracy of findings, the results of the numerical model undergo both quantitative and qualitative validation against experimental data. Moreover, employing an energy efficiency-based approach, the numerical model is successfully used to enhance the energy efficiency of the experimental investigations. By integrating the developed fully coupled numerical model with experimental research, quantitative insights are gathered into the potential applications of microwave treatment in the field.

“The greatest single human gift – the ability to chase down our dreams”.

Professor Hobby- A.I. Artificial Intelligence

Chapter 2: Computational study of microwave heating for rock fragmentation; model development and validation

2.1. Preface

Understanding the limitations of the existing literature on microwave treatment of rocks, this chapter aims to address them by developing a comprehensive numerical model that accurately represents the physical processes involved in microwave heating. Employing a finite element approach, the model is constructed based on the weak form of the partial differential equations governing the microwave heating process. The results of the numerical model are meticulously compared with experimental benchmarks conducted in this study, encompassing assessments of both energy absorption and temperature distribution. Following this comparison, a sensitivity analysis is conducted to provide further insights and understandings of the microwave treatment of rocks.

2.2. Abstract

Microwave heating can be useful in mining, tunneling and mineral processing by reducing the strength of rocks and ores. Understanding the multiphysics interaction between electric and magnetic waves on rocks due to microwave irradiation is of utmost importance in optimizing energy absorption (heating) and maximizing micro-crack generation. In this study, a coupled electromagnetic-thermal-flow-radiation model comprising conservation of mass, momentum, energy and Maxwell equations is derived, developed and solved using the finite element method. The model is validated against an experimental benchmark in terms of the overall heat absorption as well as the local temperature distributions over a range of operating parameters, i.e. distance from the antenna, microwave power and exposure time. Results show that the real and imaginary part of the dielectric permittivity of the rocks significantly affect the temperature distribution and intensity of the energy absorption, respectively. The energy absorption is also affected by the distance of the rocks from the antenna. Furthermore, at higher microwave energy dosages, the natural convective heat flow starts to develop and the effect of thermal radiation becomes more prominent, which adversely affects the energy absorption in the rock sample by more than 20% in some cases.

Keywords: Microwave treatment; Numerical modeling; Parametric study; Electromagnetic-thermal-flow-radiation analysis; Rock fragmentation

2.3. Introduction

One of the main challenges that engineers have struggled with since the inception of the mining industry is rock fragmentation. This process forms most of the costs in mining operations, tunneling and mineral processing (Gao-ming Lu et al., 2017; Walkiewicz et al., 1991). To date, several methods have been investigated with the intention of lowering the strength of rocks prior to drilling and thus reducing the costs associated with the excavation operations (R. Li et al., 2020). One of the most popular methods is by inducing thermal stresses into intact rocks and rock masses through microwave irradiation (Kingman et al., 2004). This method has not only been shown to be effective in reducing the required drilling forces applied during excavations (Hartlieb & Rostami, 2018) but also has revealed promising development in concrete treatment (Wei et al., 2019, 2021).

Researchers have investigated the microwave-assisted breakage of rocks by evaluating the influence of different factors, including microwave power, exposure time, shape and size of the sample, as well as the moisture content. For instance, Kingman et al. (2004) examined the effect of power density on rock strength reduction by applying the same energy dosage with different microwave powers. The study showed that the strength reduction could be achieved more efficiently at higher power densities. Satish (2005) and Satish et al. (2006) investigated the effect of microwave exposure time on the strength reduction of cylindrical basalt samples. The samples were irradiated with 750 W of microwave energy power for 60 s, 120 s, 180 s and 360 s, and major failures were observed at 180 s and higher exposure times.

Recent advances in this area include the incorporation of several modern techniques in expanding the understanding of the microwave-assisted breakage of rocks. Of related interest is a study by Lu et al. (2019a, 2017), who employed scanning electron microscopy (SEM) and energy dispersive X-ray (EDX) methods to evaluate the effect of microwave irradiation on different rocks and minerals. It was concluded that quartz and calcite are among weak microwave absorbent minerals. Therefore, marble and sandstone that are mainly composed of these minerals may not particularly take advantage of the use of microwave irradiation to enhance rock fragmentation. In another work, Hartlieb et al. (2012) extended the understanding of the effect of the mineralogy of the rocks on microwave-induced fragmentation. The results for different rock types with different mineralogy showed that even in relatively homogeneous rocks, such as basalt, microwave treatment can be effective for strength reduction.

Experimental investigation on microwave-assisted breakage of rocks provides useful information and leads to the improvement of this rock preconditioning method. However, the experimental microwave tests are relatively time-consuming and expensive as they require new technologies and equipment (H. Chen et al., 2020; J Zhu et al., 2007). These issues highlight the role of numerical models as they can provide information about the effectiveness of the microwave irradiation in different applications, such as rock fragmentation without utilizing expensive and delicate comminution testing (Kingman et al., 2004; Lee et al., 2021).

Numerical modelling of rock fragmentation due to microwave irradiation is complex and requires a fully coupled solution for electromagnetic wave propagation, heat transfer, and mechanical processes (Shadi et al., 2022). The complex nature of electromagnetic wave propagation and its numerical modelling has been the subject of several studies in this area. These include the electromagnetic wave distribution in rectangular waveguides (Cecot, 2005) coupled with other processes, such as phase change, thermal radiation, etc. (Abali & Reich, 2017), and different computational techniques in solving Maxwell's equations (Jin et al., 1999). The model becomes even more complicated and problematic when it takes into account the intrinsic heterogeneity of the rock. Such innate material complexity introduces high computational cost and possible convergence issues in the numerical study. To avoid these complications, some of the studies neglected the contribution of other phenomena, such as, electromagnetic wave distribution and convection in the cavity and employed unrealistic mathematical assumptions (Baiquan Lin et al., 2017; Jingyi Zhu et al., 2021). Hartlieb et al. (2012) used the finite element method (FEM) to examine the temperature and stress distributions during the microwave heating process on a homogeneous rock. It was shown that during microwave irradiation, the maximum stress occurs at the free boundaries of cylindrical samples. In the developed model, the heat generation and temperature distribution of the sample were introduced from the experimental data and the electromagnetic wave distribution was neglected. There are also several studies that have considered microwave absorbent particles, such as, pyrite, distributed in a transparent matrix like calcite to simplify the effect of rock heterogeneity during the microwave treatment. In these studies that either used continuum-based modelling (Ali & Bradshaw, 2009; D A Jones et al., 2007; Y. Wang & Djordjevic, 2014; Whittles et al., 2003) or discrete element modelling (Ali & Bradshaw, 2010; G. Wang et al., 2008), the microwave absorbent particles are considered as heat sources. The temperature of these particles increases at different rates based on the applied power density.

When the temperature increases, depending on the coefficient of thermal expansion, the volume of these particles increases. The volumetric strain of these absorbent particles applies stresses to their surrounding matrix leading to crack initiation.

In recent years, researchers have made major advances in simulating microwave heating of rocks by incorporating the electromagnetic wave distribution inside the microwave cavity. A number of issues have resulted in unrealistic and erroneous estimates in the energy absorption and temperature distribution captured by a numerical model. An example of such issues is given by Xu et al. (2020), in which Lambert's Law was employed instead of Maxwell's equations to capture the electromagnetic distribution inside the sample. Due to this simplification, the constructed model was only qualitatively validated. In a different study, Xue et al. (2019) employed a time-harmonic form of Maxwell's equations to capture the microwave heating of rocks in a field situation. However, the validity of the assumptions behind the time-harmonic form of Maxwell's equation in a field experiment was not justified, and thus further investigations are needed to thoroughly understand this process. This simplified method has been employed in other studies, including Lan et al. (2020) and Zhu et al. (2021) without a proper justification which makes the application of the time-harmonic form of Maxwell's equations one of the significant research subjects for future studies.

The use of simplified boundary conditions is another drawback in the existing numerical models in the literature. Examples of this are given by Toifl et al. (2017, 2016) where the sinusoidal excitation of the electromagnetic wave in the cavity was neglected during the simulation, and constant electric and magnetic fields were applied as boundary conditions. This simplification could result in the deviation of numerical results from the experiments. To fill these gaps, the main objectives of this paper are: (i) to develop a coupled electromagnetic-thermal-flow-radiation model of microwave heating for rocks and to validate the model against experimental results with regards to general heat absorption and local temperature distribution;

(ii) evaluate the effect of physical, design and operating parameters of microwave heating in rocks; and (iii) quantify the significance of natural convection on the energy absorbed by the rock due to microwave irradiation.

2.4. Methodology

2.4.1. Governing equations and assumptions

A coupled numerical model is developed by incorporating the equations for electromagnetic wave distribution along with the conservation equations of mass, momentum and energy. This section summarizes the governing equations and principal assumptions describing the electromagnetic heat transfer mechanism corresponding to the microwave irradiation process.

2.4.1.1. Propagation of the electromagnetic wave

Maxwell's equations describe the propagation of the electromagnetic wave through a medium. These equations include Faraday's Law of Induction (Eq. (2.1)), Maxwell-Ampere Law (Eq. (2.2)), and electric and magnetic forms of Gauss's Law (Eqs. (2.3) and (2.4)) (Hayt & Buck, 2012):

$$\nabla\times\mathbf{E}=-\frac{\partial\mathbf{B}}{\partial t} \tag{2.1}$$

$$\nabla\times\mathbf{B}=\varepsilon_0\mu_0\frac{\partial\mathbf{E}}{\partial t}+\mu_0\mathbf{J} \tag{2.2}$$

$$\nabla.\ \mathbf{E}=\frac{\rho^*}{\varepsilon_0} \tag{2.3}$$

$$\nabla.\ \mathbf{B}=0 \tag{2.4}$$

In these equations, **E**, is the electric field intensity, **B**, is the magnetic flux density, **J**, is the electric current density and ρ^*, is the electric charge density. The free space permittivity and permeability are $\varepsilon_0=8.854\times10^{-12}$ F/m and $\mu_0=4\pi\times10^{-12}$ H/m, respectively.

Eqs. (2.1)-(2.4) can be simplified further by employing a set of constitutive relations. First, it is assumed that rock is a dielectric material, and therefore, the applied electromagnetic field is not capable of breaking the bond between electrons and nuclei in the material. When a dielectric material faces electromagnetic radiation, the following relationships can be used to correlate the flux density to field intensity:

$$\mathbf{D}=\varepsilon\mathbf{E} \tag{2.5}$$

$$\mathbf{B}=\mu\mathbf{H} \tag{2.6}$$

Here, **D** is the electric flux density, and **H** is the magnetic field intensity. ε and μ, are respectively the complex permittivity and permeability of the material given by:

$$\varepsilon=\varepsilon'-i\varepsilon'' \tag{2.7}$$

$$\mu=\mu'-i\mu'' \tag{2.8}$$

Besides, applying an electric field to a dielectric material that contains free charges produces an electric flow. This flow forms an electric current, and its density can be calculated as:

$$\mathbf{J}=\sigma\mathbf{E} \tag{2.9}$$

where, σ, is the electric conductivity.

The constitutive relations in Eqs. (2.5), (2.6) and (2.9) are used in Eqs. (2.1)-(2.4), resulting in two time-dependent relations representing the electric and magnetic fields through the medium:

$$\frac{\partial\mathbf{H}}{\partial \mathrm{t}}=-\frac{1}{\mu}\nabla\times\mathbf{E}-\frac{\rho^*}{\mu}\mathbf{H} \tag{2.10}$$

$$\frac{\partial\mathbf{E}}{\partial \mathrm{t}}=-\frac{1}{\varepsilon}\nabla\times\mathbf{H}-\frac{\sigma}{\varepsilon}\mathbf{E} \tag{2.11}$$

The time-dependent form of Maxwell's equations is valid for dielectric materials. However, these equations can be further simplified by assuming the time-harmonic radiation of the electromagnetic wave. In these problems, a sinusoidal excitation is considered for the electric and magnetic fields:

$$\mathbf{E}(x,y,z,t)=\mathbf{E}(x,y,z)e^{i\omega t} \tag{2.12}$$

$$\mathbf{H}(x,y,z,t)=\mathbf{H}(x,y,z)e^{i\omega t} \tag{2.13}$$

where, ω, is the angular frequency. Using Eqs. (2.12) and (2.13) in (2.10) and (2.11) leads to a single time-harmonic equation that can be written as:

$$\nabla\times\left(\mu_r^{-1}\nabla\times\mathbf{E}\right)-k_0^2\left(\varepsilon_r-\frac{i\sigma}{\omega\varepsilon_0}\right)\mathbf{E}=0 \tag{2.14}$$

in which $k_0=\left(\omega^2\varepsilon_0\mu_0\right)^{1/2}$.

The aluminum surfaces of the cavity are considered perfect electric conductors satisfying the following constraint:

$$\hat{n}\times\mathbf{E}=0 \tag{2.15}$$

Rectangular ports are capable of radiating transverse electric (TE) and transverse magnetic (TM) waves. In this study, the experimental equipment radiates TE_{10} mode of the electromagnetic waves, which can be applied as a boundary condition by using the following constraint:

$$-\hat{n}\times(\hat{n}\times\mathbf{E})+ik_x\hat{n}\times(\hat{n}\times\mathbf{E})=-2ik_xE_0\sin\left(\frac{\pi y}{a}\right)e^{-ik_xz} \tag{2.16}$$

In this equation, a, is the longer dimension of the cross-section of the port, E_0, is the maximum electric field generated by the source, and k_x, is given by the following relation:

$$k_x=\sqrt{k_0^2-\left(\frac{\pi}{a}\right)^2} \tag{2.17}$$

If the square root expression is less than zero, k_x will be a complex number meaning that the frequency of the electromagnetic wave in the waveguide is below the cut-off frequency; therefore, the wave stops propagating. Except for TE_{10}, other radiation modes have not been considered in the current study as the geometry of the experimental equipment dictates the TE_{10} propagation mode only. The equations for other modes are presented in Appendix B following Jin et al. (2008).

2.4.1.2. Heat transfer

The heat transfer equation in solids and fluids is implemented based on the energy conservation law given by:

$$\rho C_P \frac{\partial T}{\partial t} + \rho C_P \mathbf{u}.\nabla T + \nabla.(-k\nabla T) = Q \qquad (2.18)$$

in which, ρ, is the density, C_P, is the heat capacity, T, is the temperature, **u**, is the velocity vector, k, is the thermal conductivity, and Q, is the heat source. During the microwave heating process, the heat is sourced from the electromagnetic heating and can be obtained using the following relation:

$$Q = \omega\varepsilon_0\varepsilon_r'' \bar{\mathbf{E}}^2 + \omega\mu_0\mu_r'' \bar{\mathbf{H}}^2 \qquad (2.19)$$

The aluminum surfaces of the cavity are adiabatic and satisfy the following equation:

$$-n.(-k\nabla T) = 0 \qquad (2.20)$$

2.4.1.3.Flow

During the heating process, the air in the cavity works as a fluid that is heated during microwave irradiation. This phenomenon results in natural convection in the cavity that could potentially cause energy loss. The effect of natural convection can be evaluated by considering the continuity and momentum equations for a single-phase fluid given as Eqs. (2.21) and (2.22), respectively:

$$\frac{\partial\rho}{\partial t} + \nabla.(\rho\mathbf{u}) = 0 \qquad (2.21)$$

$$\frac{\partial(\rho\mathbf{u})}{\partial t} + \nabla.(\rho\mathbf{u}\times\mathbf{u}) = -\nabla p + \nabla.\ \mathbf{S} + \mathbf{F} \qquad (2.22)$$

In these equations, p, is the pressure, **S**, is the viscous stress tensor, and **F**, is the volume force vector which is applied based on gravity. When the flow equations are coupled with heat transfer, Eqs. (2.21) and (2.22) and the second term of Eq. (2.18) are simultaneously solved for the velocity vector. In other words, the pressure and the stress field affect the fluid velocity and consequently change the second term in Eq. (2.18) and the energy absorptions of the sample. The aluminum boundaries of the cavity satisfy the no-slip boundary condition given by:

$$\mathbf{u}=0 \tag{2.23}$$

2.4.1.4. Thermal radiation

The heat loss due to thermal radiation has been taken into account by applying Eq. (2.24) to entire surfaces including the sample and aluminum surfaces of the cavity (Vajdi et al., 2020):

$$q=\epsilon\sigma_{SB}\left(T_S^4-T_a^4\right) \tag{2.24}$$

In Eq. (2.24), q, is the radiative heat transfer, ϵ, is the surface emissivity, σ_{SB}, is the Steffen-Boltzmann constant, T_s, is the surface temperature, and T_a, is the temperature of the area surrounding the targeted surface which in this context is the same as T for the air in the cavity calculated by the heat transfer equations explained in Section 2.2.3.

2.4.1.5. Solution procedure

In this study, first, the Maxwell's equations are solved in a stationary study. An iterative solver is used in this step, with a damped version of Newton's Method. For this study step, different iterative solvers, including Generalized Minimal Residual Method (GMRES), Flexible Generalized Minimal Residual Method (FGMRES), Transpose Free Quasi Minimal Residual Method (TFQMR) and Biconjugate Gradient Stabilized Method (BiCGStab) are implemented and compared to find the optimized solver concerning the computation time. A similar model with the exact discretization is carried out in order to compare the effect of different solvers on the generated electric field. It should be noted that the computation time changes based on the number of CPU cores that are employed for the simulation. Therefore, the same computational system configuration is used for all solvers. Table 2.1 tabulates the computational time, minimum, maximum and the average value of the electric field created in the sample. Figure 2.1 depicts the convergence graphs for the simulations carried out using different solvers. The magnitude of the electric fields and the numerical errors obtained for different solvers provide inconsiderable differences. The computation time corresponding to the FGMRES is significantly lower than for the other solvers and hence it is selected to carry out the simulations in this study.

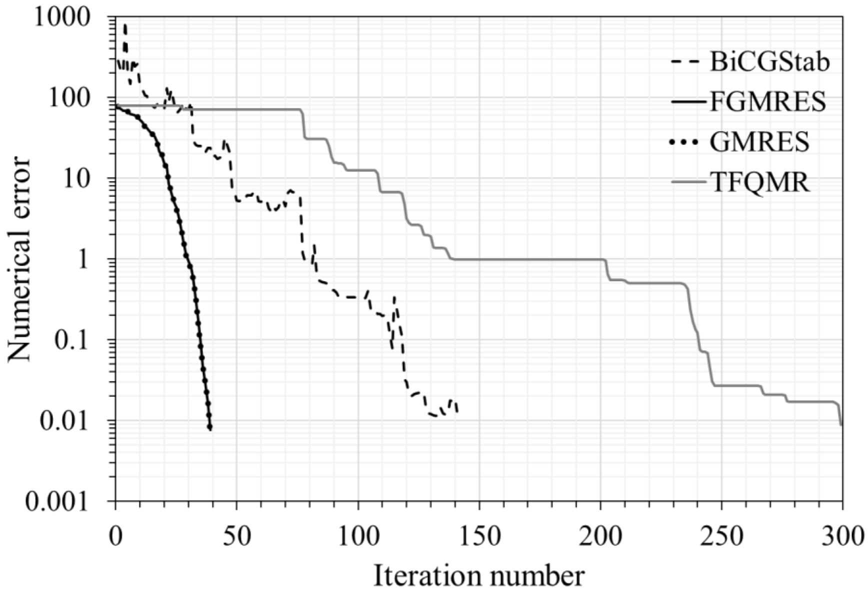

Figure 2.1 The convergence plots for solving Maxwell's equations using BiCGStab, FGMRES, GMRES and TFQMR iterative solvers.

Table 2.1 The computational time and the minimum, maximum and average electric field generated in the sample by different solvers.

Solver	Computational time (s)	Max electric field (V/m)	Min electric field (V/m)	Avg electric field (V/m)
GMRES	202	21738	1113.3	10844
FGMRES	195	21738	1113.4	10844
TFQMR	957	21738	1113.7	10845
BiCGStab	610	21738	1113.4	10844

The calculated electric and magnetic fields in the stationary study step are used as inputs to calculate the heat generation in the next study step. A time-dependent study is performed for the simultaneous solution of the heat transfer, flow, and thermal radiation equations. A Parallel Direct Solver (PARDISO) is used in this study step with air in the cavity working as a weakly compressible fluid with temperature-dependent properties (Multiphysics, 1998). The backward differentiation formula (BDF) is used for the time stepping algorithm. The study steps of the simulation are summarized in a flowchart shown in Figure 2.2.

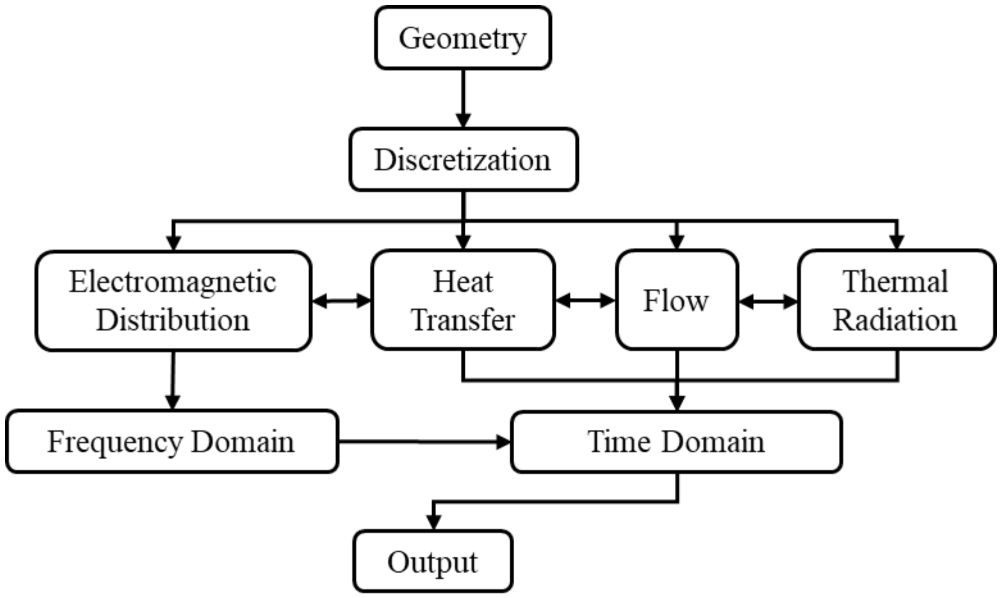

Figure 2.2 The flowchart presenting the summary of the study steps.

2.4.2. Experimental procedure

2.4.2.1. Sample preparation

The sample used in this study is prepared by cutting a basalt block into a rectangular geometry with the dimensions of 15 cm×10 cm×2 cm in order to fit the size of the antenna. The results for the mineralogy analysis based on the X-Ray Fluorescence (XRF) method and their resulting normative mineralogy are detailed in (Motlagh, 2015). The following paragraphs elaborate on the measurements of the rock properties for the data analysis and simulations.

The dielectric properties of the rock are measured using a high-temperature coaxial probe. This method has been shown to be very accurate when dealing with solid and high absorptive rocks, such as, basalt (X. Wang et al., 1999). Prior to the measurements, the surfaces are treated using sandpapers with different grit sizes to ensure a smooth and proper contact between the rock and the probe. The rock surface is polished for 10 mins with each sandpaper (grit designations of 80, 120, 240, 320, and 400), starting from the lowest numbers to highest. The surface of the rock before and after polishing can be seen in Figure 2.3. The sample is then dried in a conventional oven at 60 °C for 24 hours. The coaxial probe is used on the smoothened surface at different locations for the measurements of the dielectric properties. These measurements are performed at an intermediate frequency bandwidth (IFBW) of 300.00 Hz and a power of 5.0 dBm. At each location, five measurements are taken and the average value is chosen as the representative of the location. The measurements are made at different points on the sample to ensure consistency of the estimates and to confirm the homogeneity of the rock. The material properties used in this study are given in Table 2.2.

Thermal properties of the rock include the heat capacity and the thermal conductivity. Heat capacity is measured by calorimetry and the thermal conductivity is measured by the transient heated needle method using a KD2Pro thermal conductivity meter. For both heat capacity and thermal conductivity, the sample property is chosen based on the average value of three repeated tests.

The values for other parameters including relative permeability, surface emissivity and electrical conductivity have been used based on the information provided in (Mineo & Pappalardo, 2021; Motlagh, 2015), and (Hassani et al., 2016), respectively.

It should be noted that basalt is constituted of different minerals including plagioclase, diopside, olivine, etc. (Motlagh, 2015); however, based on the measurements performed in this study, it is observed that these minerals are distributed uniformly throughout the sample ensuring the validity of the homogeneous assumption for the rock. This idea has been emphasized for two main reasons in this study: i) the repeatability of the physical property measurements; and ii) the repeatability of the microwave heating tests with regard to both temperature distribution and energy absorptions.

Table 2.2 Properties of basalt used in the microwave heating tests.

Parameter	Value	Unit
Thermal conductivity	1.59	W/(m.K)
Density	2870	kg/m^3
Heat capacity	840	J/(kg.K)
Relative permittivity	10-1.1j	1
Surface emissivity	0.94	1
Relative permeability	1	1
Electrical conductivity	5×10^{-5}	S/m

2.4.2.2. Microwave heating tests

Microwave heating experiments are performed using industrial microwave equipment (Figure 2.3a) to provide data for the validation of the numerical results. With the help of a control system, the power output of the equipment can change from 0 to 15 kW. The waves can propagate only at the frequency of 2.45 GHz.

For the heating experiments, the sample is exposed to a microwave power of 3 kW for 4.35 s at different distances from the antenna. The microwave energy is irradiated from the magnetron into the waveguide (TE_{10} single-mode propagation). After each heating experiment, the energy absorption of the sample is measured by performing a calorimetric study. The calorimetric study includes putting the heated sample inside a thermally isolated chamber (calorimeter) filled with water. The sample needs to stay inside the calorimeter until thermal equilibrium between the rock and water is ensured. Then, based on the initial temperatures of water and the sample and the temperature after equilibrium, the amount of energy absorbed by the rock during the microwave heating experiment can be determined. Using the measured absorbed energy in the sample and the input energy irradiated from the microwave, the energy efficiency of the experiment can be calculated using a parameter referred to as the Heat Over Microwave Efficiency (HOME) following Hassani et al. (Hassani et al., 2020):

$$\text{HOME }(\%) = \frac{\text{Absorbed Energy}}{\text{Input Energy}} \times 100 \tag{2.26}$$

At the end of each heating experiment, the sample is placed inside a conventional oven at 60°C for 24 hours to remove the water that is absorbed during the calorimetric study. The dried sample is then cooled down to room temperature until a thermal equilibrium is achieved with the surrounding air. The sample is then reused for the next microwave heating experiment. At each test distance from the antenna, the heating experiment is performed 3 times to make sure of the repeatability of the experiments and that the average value of the absorbed energy is reported. A fourth test is performed at each distance to capture the temperature distribution on the surface of the sample using an infrared thermal imaging camera immediately after the microwave irradiation exercise.

2.4.3. Description of the model

The partial differential equations presented in Section 2.2.1 are numerically solved by implementing the weak form of the equations in the FEM code. A detailed discussion on obtaining the weak form of the partial differential equations is provided in Appendix A.

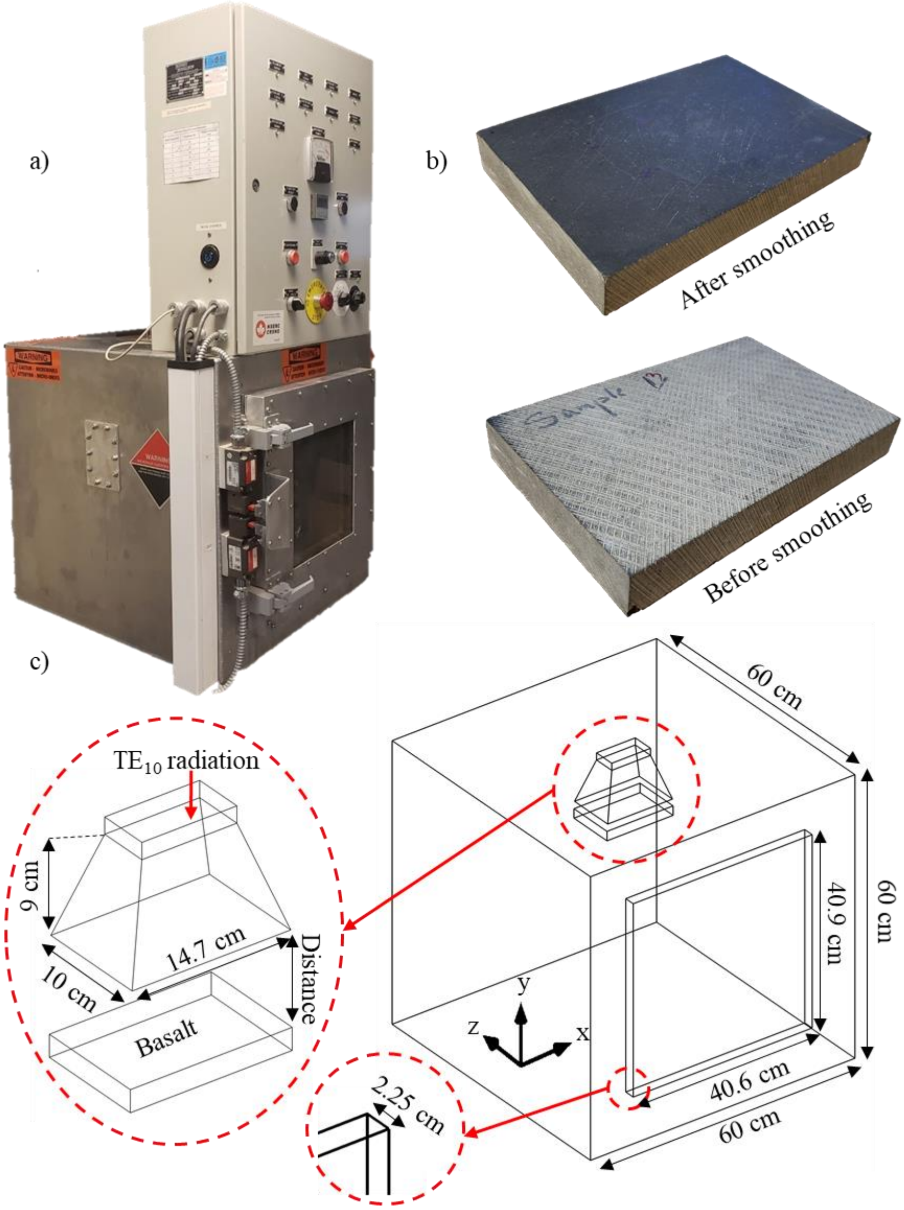

Figure 2.3 a) The industrial microwave system in the Geomechanics Laboratory of McGill; b) Sample's surface before and after polishing; c) The geometry of the developed numerical model for the simulation of microwave heating experiments including the details of the sample and antenna.

The geometry of the cavity (designed based on the experiment set-up) is a cuboid with the dimensions of 60 cm×60 cm×60 cm. At the center of the upper boundary, a cube with the dimensions of 8.8 cm×4.6 cm×1.5 cm is specified, representing the port of the cavity. The antenna is a Horne-shaped aluminum sheet at the top that connects the cavity to the waveguide. The microwave door adds an extra interior boundary to the cavity, which is included in the model (Figure 2.3c). Also, the geometry of the model is designed to include a rectangular block with the dimensions of 15 cm×10 cm×2 cm representing the basalt slab placed inside the cavity, as shown in Figure 2.3c. The coordinates of the sample are changed within the geometry of the cavity to study the heating behavior of the samples when exposed to microwave irradiation at different distances.

The initial temperature for the sample and the entrapped air are set at room temperature at 20 °C, and the air pressure is set to 1 atm. There is no initial electric and magnetic field in the cavity. For the heat transfer equation, the six aluminum boundaries representing the sides of the cavity are adiabatic. The surface emissivity for all the aluminum boundaries including the six sides and the antenna is considered to be 0.1 based on the values presented in the literature (Infrarde & Termografije, 2018). These boundaries follow the no-slip condition according to Eq. (2.23). The port boundary condition radiates the TE_{10} mode of the electromagnetic wave into the cavity and is considered an open boundary for the flow of fluid.

Mesh discretization and the element quality are important factors in numerical modeling of complicated coupled equations as in electromagnetic heating. In this study, tetrahedral elements are used for discretizing the geometry. A mesh independency analysis is performed to find the optimized element size with sufficient quality. In this study, attention is mostly focused on the effect of different parameters on HOME. Figure 2.4 presents the change in the value of HOME against the maximum element size for 4.35 s of microwave irradiation with 3 kW power at 65 mm distance from the antenna. It should be mentioned that HOME is chosen as a representative parameter to quantify microwave heating phenomena in order to compare the numerical simulations with the laboratory results. Also, the average electric field magnitude calculated inside the sample during the microwave irradiation is considered a second parameter to ensure mesh independency. In Figure 2.4, the element quality on the top surface of the sample is shown based on the skewness mesh quality measure. According to the results, the mesh with the maximum element size of 1.8 cm, minimum element size of 0.0923 cm, and maximum element growth rate of 1.35 is selected for all the simulations. A total of 635591 tetrahedral elements are used to discretize the entire geometry. This discretization scheme provides acceptable element quality and yields mesh-independent results.

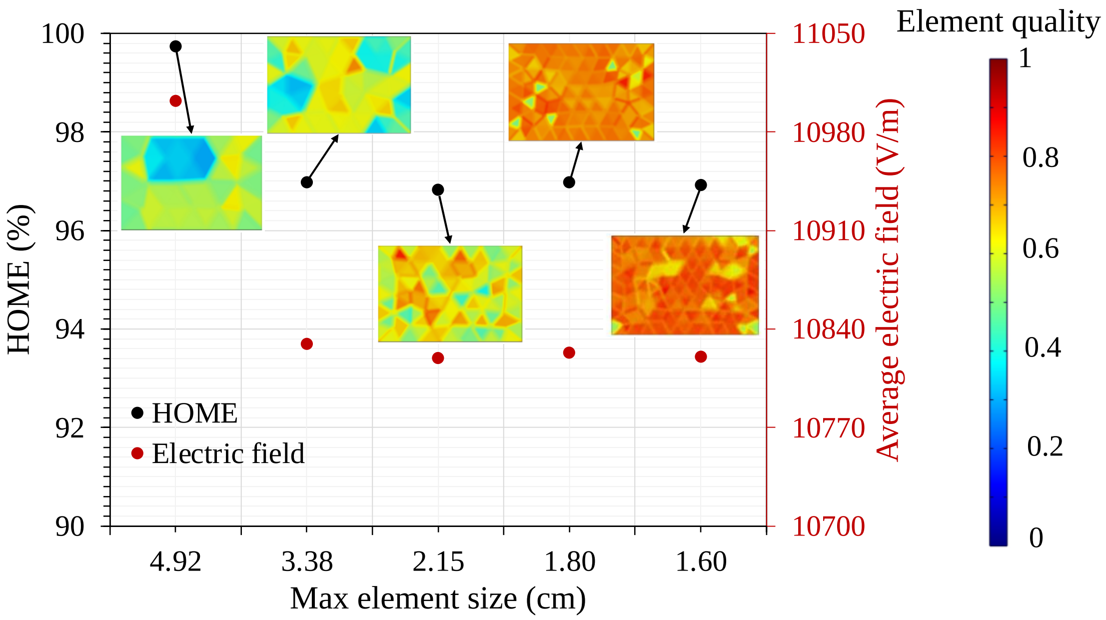

Figure 2.4 The results for HOME, electric field magnitude and element quality at different mesh sizes.

The developed model is validated against the laboratory results carried out in this research. According to Section 2.2.2, the experiments have been performed at low energy dosages with the power and exposure time of 3 kW and 4.35 s, respectively. Because of the low energy dosage, there is no major increase in the temperature of the sample due to microwave irradiation. Therefore, it is assumed that the material properties are temperature-independent and are constant during the test. For the series of high energy dosage simulations performed in this study, the intention is restricted to evaluate the significance of natural convection and thermal radiation. Indeed, in order to validate the numerical model for field investigations, it is deemed necessary to consider the temperature-dependent material properties. Consideration of this matter however falls out of the scope of the current research.

2.5. Results

2.5.1. Validation and verifications of the proposed model

A numerical model is developed based on the procedures explained in the previous sections. The overall heat absorption and the local temperature distribution of the basalt slab at different distances from the antenna are used to compare the numerical model and the laboratory results. Furthermore, the flow and radiation equations are coupled to the model to evaluate the effect of natural convection and thermal radiation during microwave treatment, respectively.

Figure 2.5 compares the experimental and the numerical results for the energy absorption for different sample-to-antenna distances due to microwave irradiation with the power of 3 kW and the exposure time of 4.35 s. The numerical estimate for the HOME value against the distance of the sample follows the same trend as in the experiments, thus, ensuring the accuracy of the model. For instance, in both the experiments and the numerical model, the maximum and minimum energy absorption occur at 15 mm and 65 mm distance from the microwave antenna, respectively. The numerical results show a reliable representation of the experimental data for a 15 mm to 95 mm distance, with less than 7% difference in the HOME value.

The effect of natural convection and thermal radiation has been evaluated in Table 2.3. In this table, the difference between the HOME value when the effect of natural convection and thermal radiation is included to the model is also given. The results demonstrate that the effect of both natural convection and thermal radiation is negligible at low energy dosages used for the experimental benchmark by causing less than 1% difference in the HOME value.

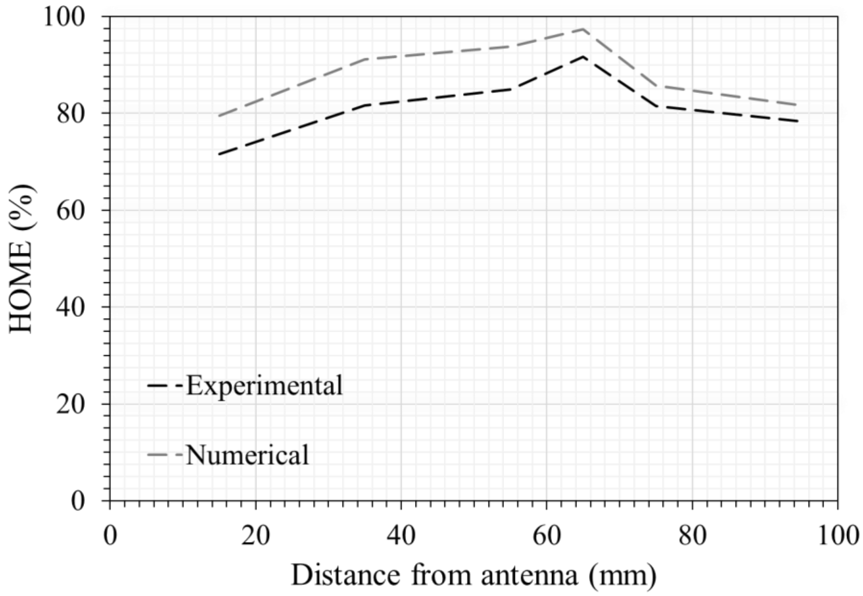

Figure 2.5 Validation of the numerical model using the overall energy absorption when the sample is exposed to the power of 3 kW and exposure time of 4.35 s.

To improve the validation of the numerical model, the local temperature distribution on the top surface of the sample in the experiments and the simulations has been compared. This comparison is given in Figure 2.6 at 55 mm distance from the antenna. The major hot zones on the surface of the sample are highlighted with a black circle to emphasize the comparability of the numerical simulations and the experiments. In order to quantify the comparison between the data for the local temperature distribution of the numerical simulations and the experiments, two horizontal lines are selected on the sample through which the surface temperature distribution is evaluated. The comparison between the temperatures obtained from the numerical simulations and the experiments are given in Figures 2.7a and b. It should be noted that comparing the temperature at certain points of the sample is highly susceptible to change due to experimental errors in measuring the rock thermal properties and the heterogeneous nature of the rock sample. Moreover, capturing thermal images requires additional handling time to take the sample out of the cavity. This handling time adds extra heat loss that is not included in the numerical models. Figures 2.7a and b confirm this concept as the experimental values lie below the numerical values signifying the importance of heat loss during the handling time. The validation of the numerical model with regard to the overall energy absorption and the local temperature distribution confirms the applicability of the time-harmonic form of Maxwell's equations during the microwave irradiation in the cavity.

Table 2.3 Evaluation of adding the effect of thermal radiation and natural convection and the decrease that they cause in the HOME value during the simulation.

	HOME (%) calculated based on		
Distance (mm)	The basic numerical model	Adding the effect of natural convection	Adding the effect of thermal radiation
15	79.52	79.40	79.39
35	91.10	90.80	90.93
55	93.73	93.51	93.55
65	97.35	97.13	97.16
75	85.71	85.58	85.55
95	81.65	81.45	81.52

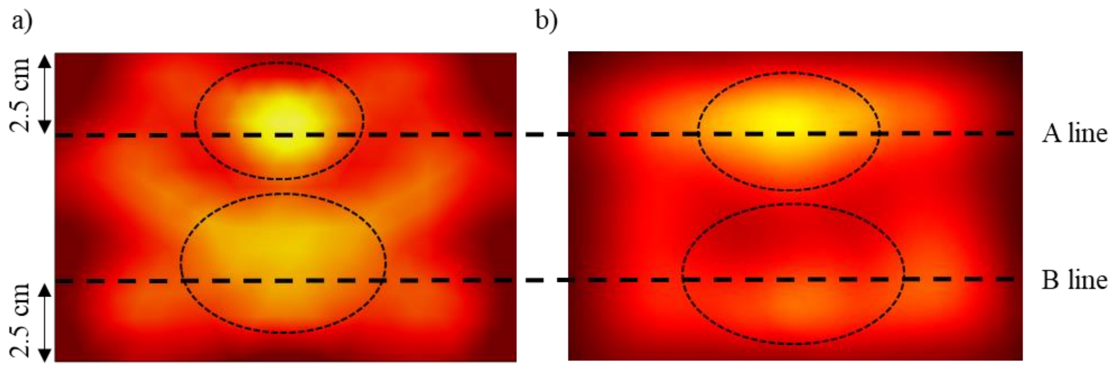

Figure 2.6 The temperature distribution at the top surface of the sample at 55 mm distance from the antenna after microwave treatment; a) numerical results, and b) experimental results.

The numerical model is employed to scrutinize the procedure through which the sample gets heated during microwave irradiation. According to Eq. (2.19), during microwave irradiation, electric and magnetic fields are generated inside the rock sample that are responsible for the heating. This process can be further investigated by comparing the electric and magnetic fields in the sample (Figure 2.8) and the temperature distribution on the exterior faces (Figure 2.6a). The overall shape of the temperature and electric field contours are highly compatible. Also, the points with the highest and lowest electric fields correspond to the points with the highest and lowest temperatures, respectively. However, the generated magnetic field in the sample is not comparable with the temperature distribution in any meaningful way.

In Figure 2.9, the streamlines for the fluid (air) flow, created due to the natural convection, are depicted around the sample at the end of the 4.35 s of exposure time. The velocity magnitudes are low (less than 0.1 m/s), emphasizing the negligible effect of natural convection at low energy dosages. Nevertheless, this effect needs to be further investigated at higher energy dosages as well.

In order to verify the algorithm that has been utilized to develop the numerical model, the results of the current study are compared to previously published literature. Shadi et al. (2022) used the commercial software COMSOL Multiphysics to capture the energy absorption of basalt samples during microwave irradiation. The comparison between the results of the current study and Shadi et al. (2022) is shown in Figure 2.10. This figure shows that the overall trend for the energy absorption due to microwave irradiation at different distances from the antenna is the same in both studies. The difference in HOME at each distance is less than 5% between the two numerical models. This discrepancy is mainly due to the difference in assigned properties and the geometry of the model. Shadi et al. (2022) used temperature-dependant dielectric properties in their model, whereas constant dielectric properties measured at room temperature are introduced to the models developed for this study (see Section 2.2.7). A discussion is also made on using the complete geometry of the cavity including the entire waveguide (Shadi et al., 2022). This study considers a part of the waveguide for reducing the computation time while this can impose a negligible difference (less than 2%) on the final results. Considering the mentioned possible potential differences between the two numerical models, the proximity of the results confirms the verification of the developed code.

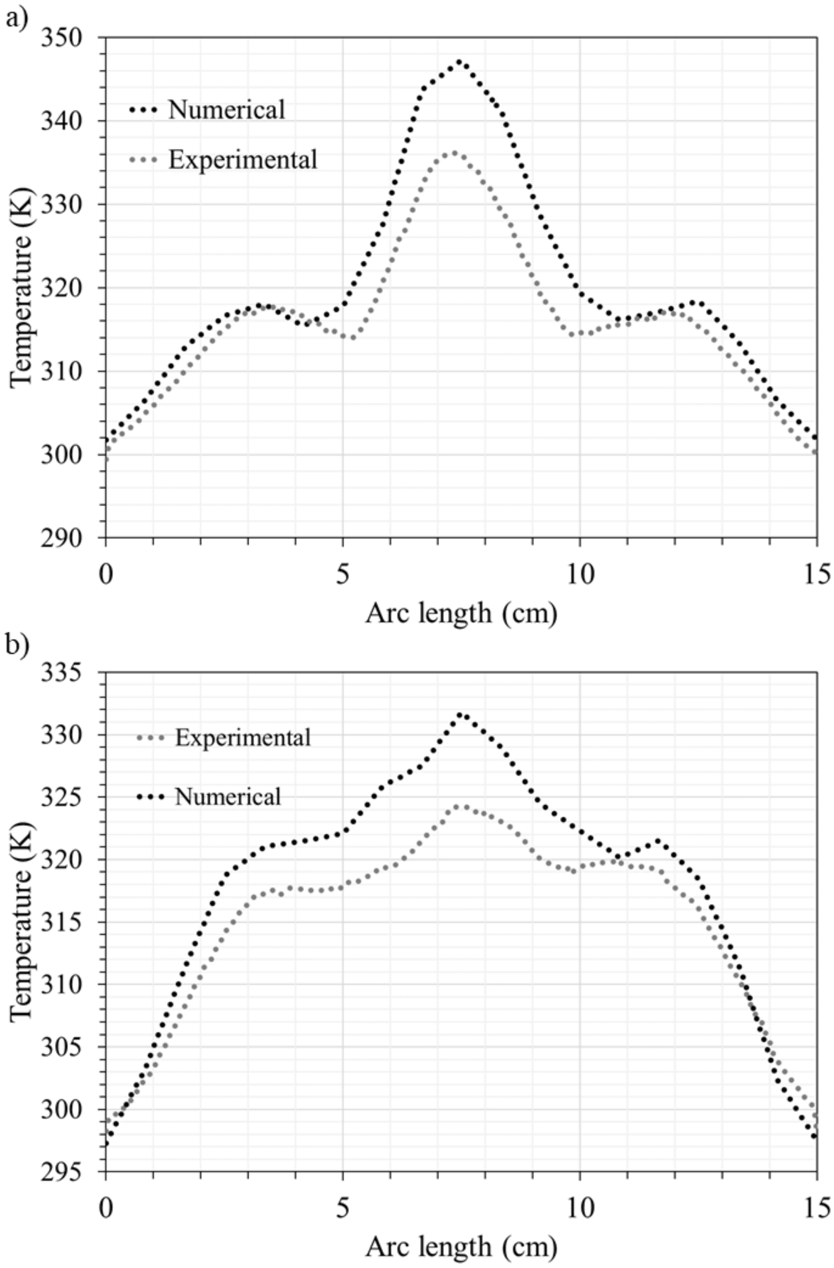

Figure 2.7 Comparison between the temperature at the surface of the sample along a) the A line and b) the B line when the sample is placed at 55 mm distance from the antenna and after 4.35 s of exposure time.

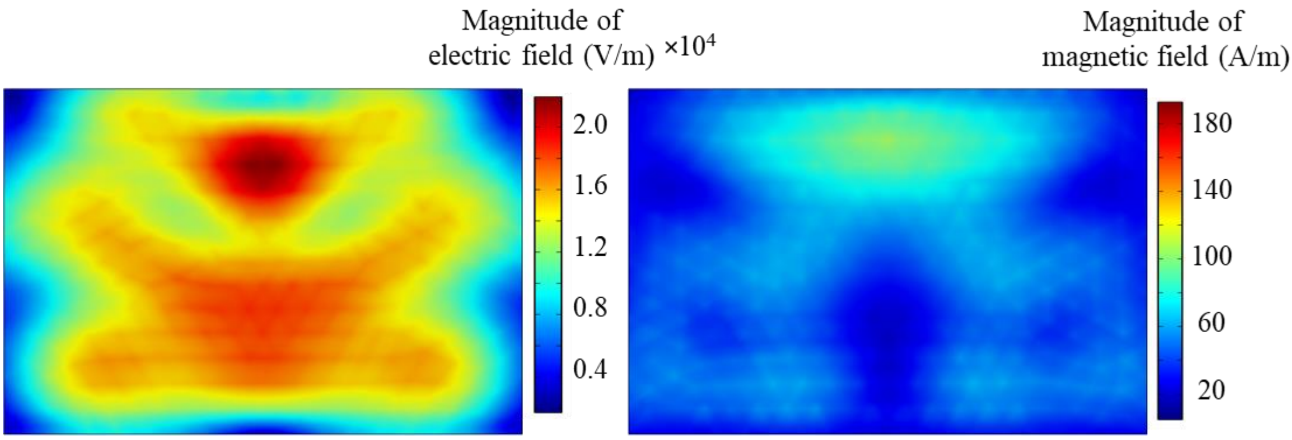

Figure 2.8 The magnitude of the electric field (left) and the magnetic field (right) generated on the surface of the sample during microwave treatment at 55 mm distance from the antenna.

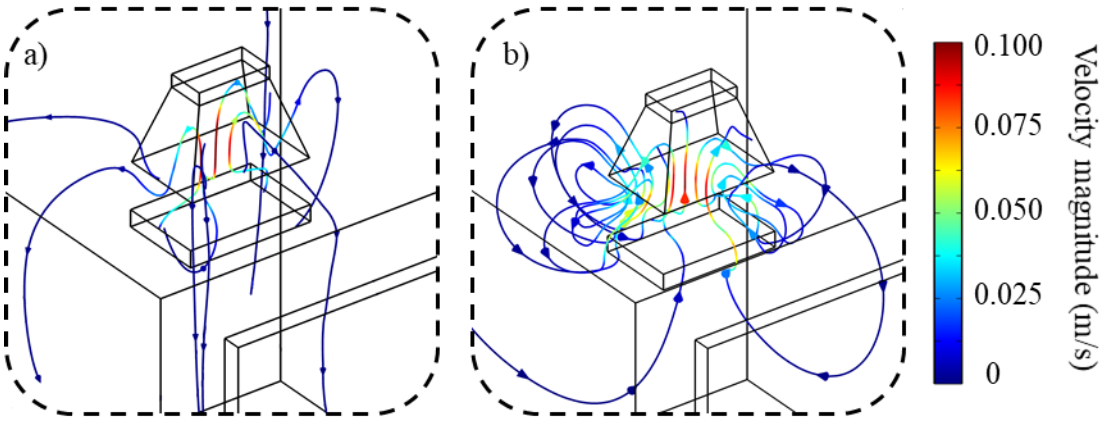

Figure 2.9 The streamlines of fluid flow during microwave treatment for a) 55 mm and b) 75 mm distance from the antenna.

2.5.2. *Sensitivity analysis on the dielectric properties*

A parametric study is carried out to investigate the effect of material properties that define the electromagnetic distribution inside the cavity and the rock sample. The values for the permittivity parameters are chosen based on the measured and reported results from the literature, including the studies carried out by Hassani et al. (2016), Hartlieb and Rostami (2018) and Hartlieb et al. (2012).

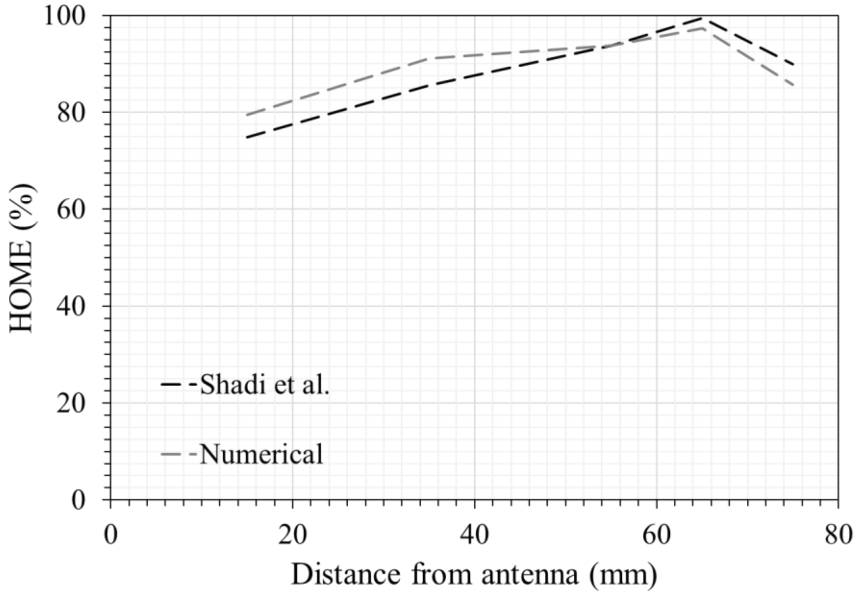

Figure 2.10 The comparison between the current study and Shadi et al. (2022) with regard to the calculated HOME after microwave heating for basalt samples placed at different distances from the antenna.

The effect of the real part of the relative permittivity on the energy absorption and temperature distribution is shown in Figures 2.11a and 2.12. Figure 2.11a shows that a change in ε_r' while keeping ε_r'' at a constant value of 1.1 can significantly affect the trend of the HOME-distance curves. For instance, for the case of ε_r'=10, the maximum and minimum HOMEs are achieved at 65 mm and 15 mm distances, while these values are achieved at 55 mm and 95 mm distances for ε_r'=8. This observation can be further investigated by comparing the temperature distribution for different values of permittivity. While the hot temperature zone is concentrated in the middle of the sample for ε_r'=8 and ε_r'=9, it is distributed more uniformly over the surface for ε_r'=10 (Figure 2.12). Figure 2.11b shows the value of HOME at different distances and ε_r'' values while keeping ε_r' at a constant value of 10. Comparing the charts in Figure 2.11 shows that although ε_r' changes the overall pattern of the energy absorption and the temperature distribution, ε_r'' only affects the intensity of the energy absorption as given in Eq. (2.19). Therefore, this change is more focused on the amount of energy absorbed rather than changing the trend and the temperature distribution (Figure 2.11b and 12). For instance, Figure 2.12 shows that similar temperature distributions are achieved at different ε_r'' values, and this parameter only affects the intensity of the heating.

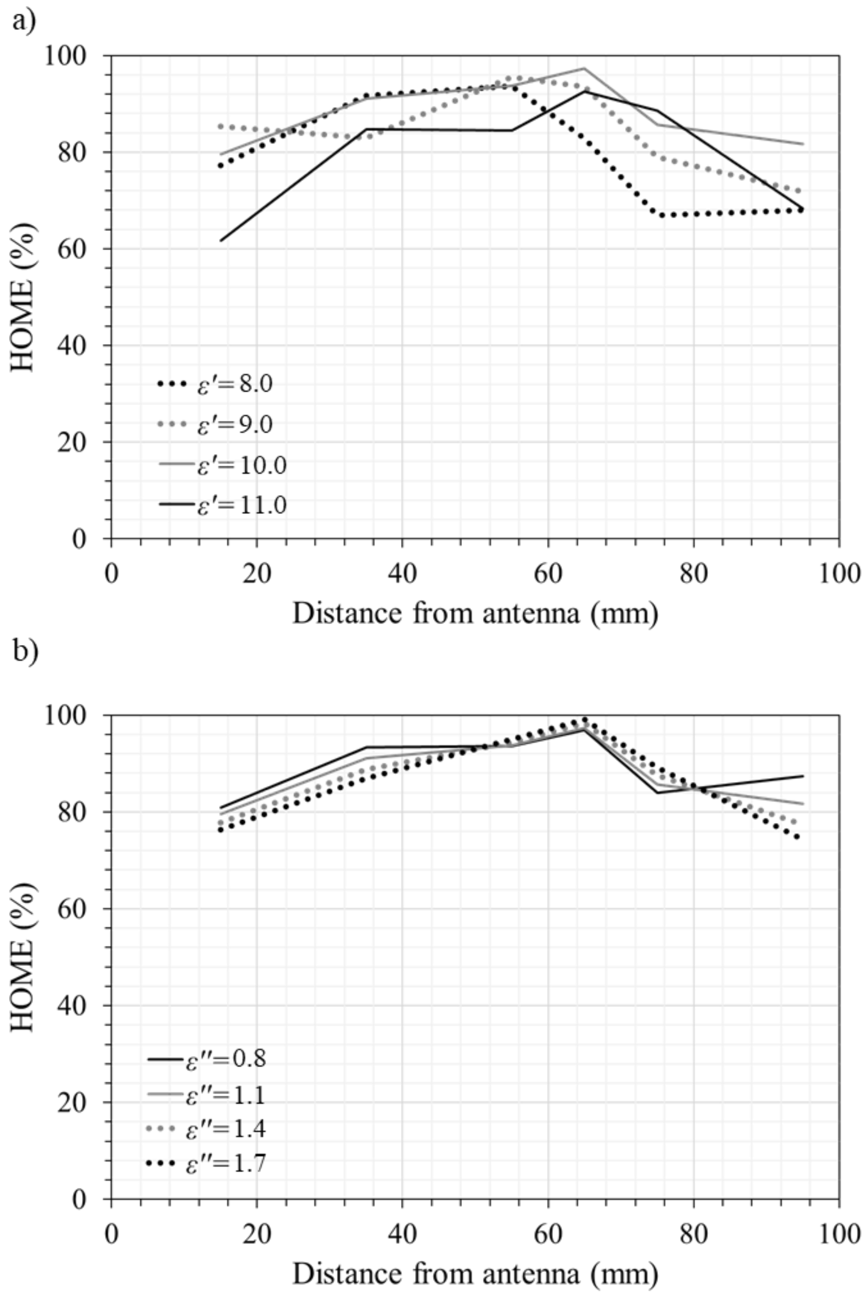

Figure 2.11 The effect of a) real and b) imaginary parts of the relative permittivity on the overall energy absorption of the sample due to microwave treatment after 4.35 s of exposure time.

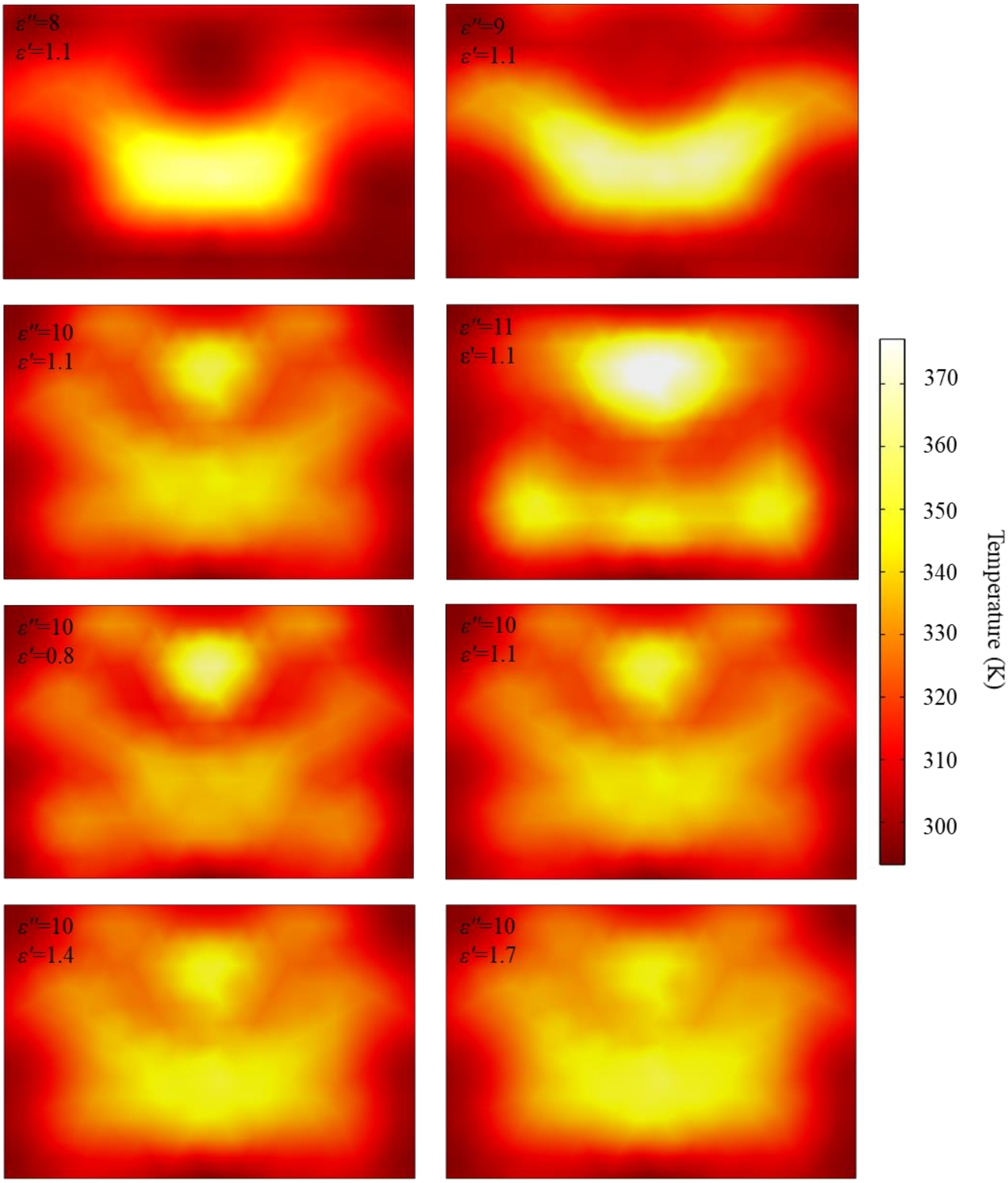

Figure 2.12 The effect of the real and imaginary parts of the relative permittivity on the local temperature distribution on the top surface of the sample after 4.35 s of microwave irradiation at 65 mm distance from the antenna with the power and frequency of 3 kW and 2.45 GHz, respectively.

2.5.3. *Effect of natural convection*

In this section, the effect of natural convection in the cavity is investigated at different exposure times and for a constant sample-to-antenna distance (65 mm). A sensitivity analysis is performed to evaluate the effect of power and exposure time on the energy loss values due to natural convection. Microwave powers of 1, 5, 10, and 15 kW with exposure times of up to 100 s are used for this sensitivity study. In order to observe the effect of natural convection, the differences in the values of HOME and the maximum temperature of the sample with and without considering the natural convection are measured.

The 3D graph shows the change in HOME values when the natural convection is included in the model (Figure 2.13a). The results show that the energy loss caused by natural convection increases for higher exposure times. The energy loss could be as large as 4% at 100 s of exposure time even at low powers, making it a significant factor in design considerations. The effect of power is more complicated, and while the energy loss increases with an increase in the power from 1 kW to 5 kW, it starts to decrease when the power goes up to 15 kW. The reason for this phenomenon is that at high power and exposure times, there is a high temperature layer of air created around the sample which reduces the amount of heat loss from the sample. As shown in Figure 2.13a, this effect is negligible for low power and exposure times.

The 3D graph depicted in Figure 2.13b shows the change in the maximum temperature of the sample at the end of the microwave heating with the natural convection included in the model. The maximum change in the highest value of the temperature within the sample is 35 K—which is negligible—considering that in some cases, the temperature of the sample is increased up to more than 1500 K. Nevertheless, the effects of power and exposure time on the change in the maximum temperature need to be further investigated. Figure 2.13b shows that when the applied power is high enough for low exposure times, the generated natural convection creates an isolated layer around the sample, which causes an increase in the maximum temperature. This effect fades away when the power is decreased or when the exposure time is longer than 50 s.

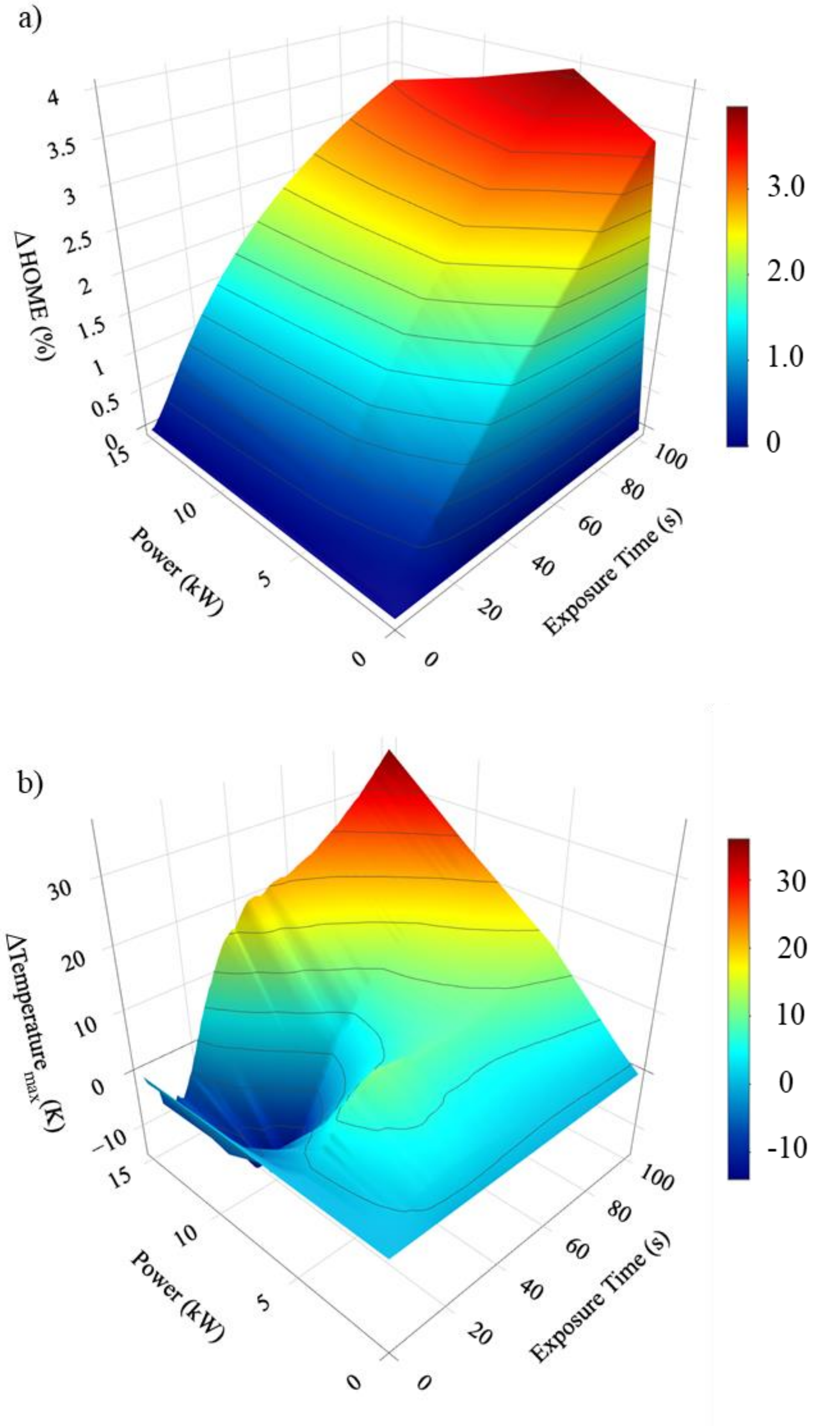

Figure 2.13 The difference between a) energy absorption and b) maximum temperature of the sample with and without the effect of natural convection.

Figure 2.14 shows the streamlines for the fluid flow at different powers after 100 s of exposure time. The general direction of the flow inside the cavity, which is toward the open boundary, remains unchanged. However, the velocity values are different and increase with increasing power. It should be noted that the increase in the velocity of the fluid with increasing power is not significant. For instance, doubling the power from 5 kW to 10 kW would increase the maximum velocity from 0.75 m/s to 0.9 m/s. This observation supports the conclusions of Figure 2.13.

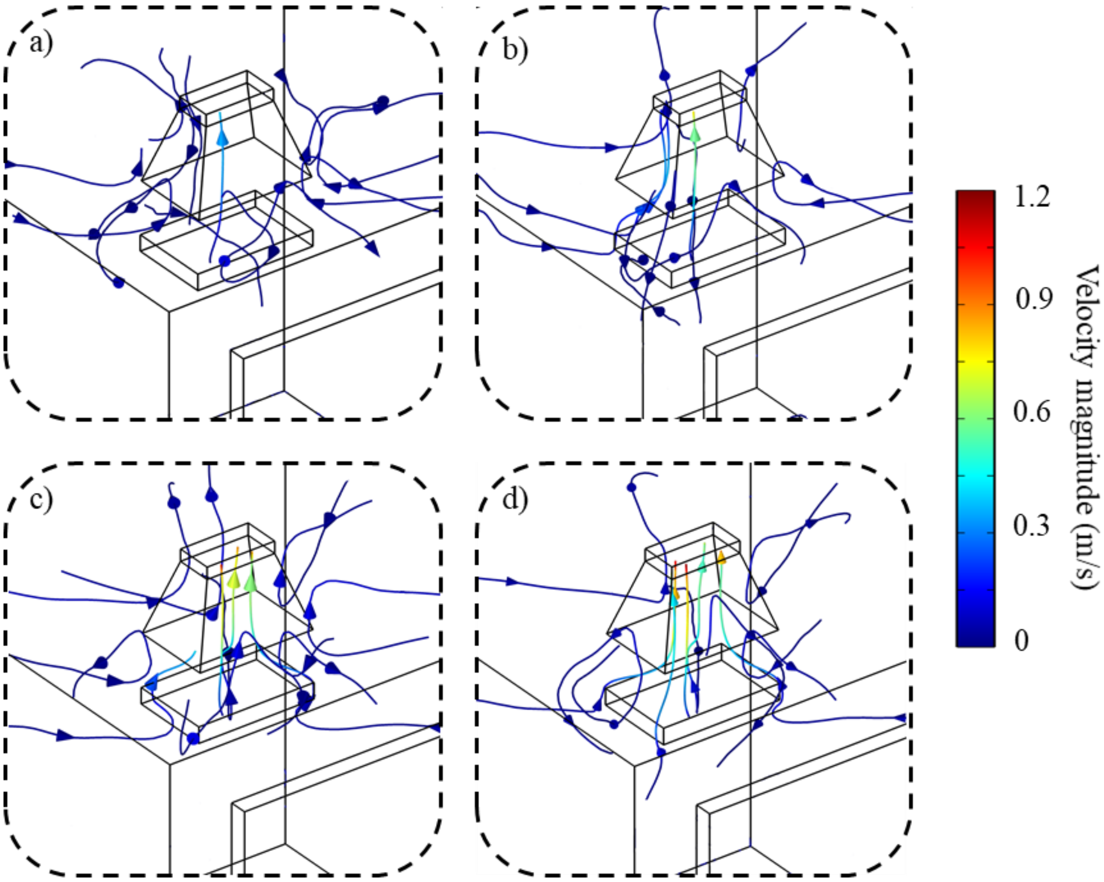

Figure 2.14. The streamlines of the fluid flow at 100 s of exposure time for applied powers of a) 1 kW, b) 5 kW, c) 10 kW, and d) 15 kW.

Further investigation has been performed to study the effect of natural convection during microwave irradiation. In this case, it is assumed that the sample is exposed to total microwave energy of 90 kJ. To apply this amount of energy, the powers of 1, 5, 10 and 15 kW are employed with the exposure times of 90, 18, 9, and 6 s, respectively. The results for HOME and the maximum temperature in the sample at the end of exposure times are shown in Figure 2.15. In this figure, a comparison is made between the models with natural convection and the models that only consider the heat transfer due to the conduction.

Figure 2.15a evaluates the effect of power on HOME with and without the consideration of natural convection. It can be observed that if the effect of natural convection is neglected, HOME does not change when power is decreased. However, when the flow equations are considered in the model, reducing the power and increasing the exposure time increases the effect of natural convection, which can cause a more than 4% decrease in HOME. For instance, the power of 1 kW and exposure time of 90 s resulted in HOME values of 83% and 77% percent with and without including the effect of natural convection, respectively.

One of the main reasons for the rock failure during microwave irradiation is the uneven and non-uniform heating of different parts of the sample. When the temperature of a part increases while the adjacent parts have lower temperatures, tensile stresses are generated due to thermal expansions; this could cause chipping and even more extensive failures at higher exposure times can be observed throughout the sample. The tensile stress is increased when the temperature difference increases. Therefore, the maximum temperature of the sample becomes more prominent as a representative of the tensile stress generation. Figure 2.15b depicts the maximum temperature of the sample with respect to the change in applied microwave power. Even when the effect of natural convection is not taken into account, the maximum temperature of the sample drastically decreases by reducing the power. For instance, the maximum temperature of the sample after the exposure time of 6 s with the power of 15 kW reaches 674 K. However, when the power is reduced to 1 kW, it decreases to 502 K, which shows a maximum temperature differential of 172 K. This emphasizes the generation of larger tensile stresses in high powers.

a)

b)

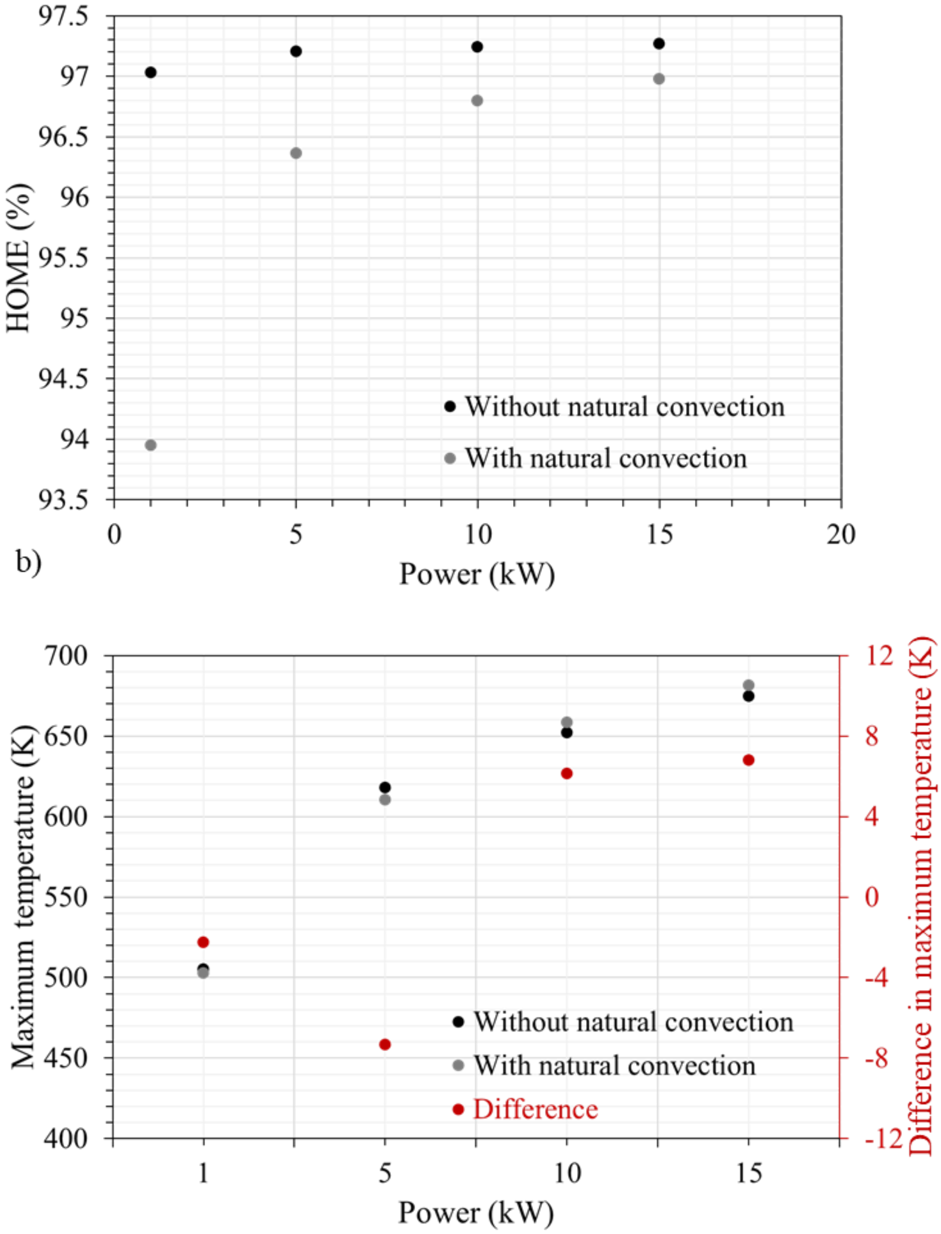

Figure 2.15 The effect of natural convection on a) the HOME value and b) the maximum temperature during the microwave treatment at different powers.

2.5.4. *Effect of thermal radiation*

This section evaluates the effect of thermal radiation at different powers and exposure times when the distance between the sample and the antenna is 65 mm. A sensitivity analysis is carried out at different microwave powers and exposure times to analyze the effect of thermal radiation during microwave treatment of rocks.

Figure 2.16 shows the reduction in the numerically achieved HOME when the thermal radiation equation is included. The sensitivity analysis follows the same parameter selection as Section 2.3.4 with powers of 1, 5, 10, and 15 kW and up to 100 s of exposure time. The results show that the energy loss caused by thermal radiation increases with both power and exposure times. The energy loss due to thermal radiation can be significant causing more than 25% decrease in the HOME value. These results would make thermal radiation a significant factor for design considerations, especially for field applications where high power and exposure times might be used.

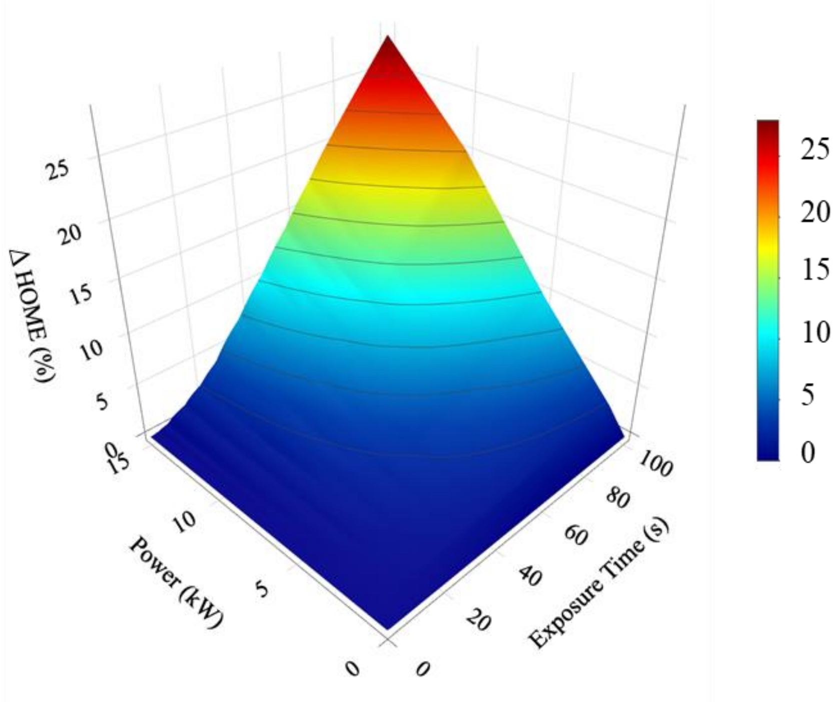

Figure 2.16. The difference between the energy absorption of the sample with and without the effect of thermal radiation.

2.6. Conclusion

This study provided a fundamental study of FEM-based numerical modeling for the microwave irradiation of rocks. The mathematical heat transfer, flow, thermal radiation and Maxwell's equations are implemented in the weak form of the partial differential equations and solved using the finite element method. The model considers a homogeneous rock slab in a microwave cavity with a waveguide that radiates the microwave energy. Among the well-known solvers for Maxwell's equations, FGMRES is shown to be the most efficient one in terms of the computation time while providing almost the same accuracy. The comparison of the numerical model against the experimental benchmark tests shows the reliability of the numerical model in representing the actual electromagnetic heating phenomenon by capturing the energy absorption with less than 7% difference.

The heat generation in basalt slabs has a direct relationship with the electric field created within the sample during microwave irradiation as the generated heat increases with an increase in the electric field intensity. The electric permittivity is the main parameter affecting the electric field in the cavity and the sample. The real part of the electric permittivity changes the temperature distribution and therefore the trend of the energy absorption of the sample when it is placed at different distances from the antenna. On the other hand, the imaginary part of the electric permittivity only affects the intensity of the energy absorption without causing any significant effect on the trend of energy absorption at different distances from the antenna.

Exposure time is an important factor in design considerations. Exposure time has a significant effect on the natural convection created during the microwave heating, causing less than 0.5% and more than 4% energy loss for 5 s and 100 s of exposure time, respectively. The same exposure time with different irradiation powers will generate a similar energy loss percentage by considering the natural convection in the cavity. With the same amount of energy, higher powers with lower exposure times create higher temperatures in the sample that leads to faster fragmentation and strength reduction.

Thermal radiation is found to be negligible in low energy dosages but at high powers and exposures times, it can significantly affect the value of HOME during the microwave irradiation in some cases by more that 25% which makes it an influential factor in design considerations.

Appendix 2.A: Weak form of the partial differential equations

In this appendix, the weak forms of the partial differential equations explained in Section 2.2.1 are introduced. First, for Maxwell's equations, the time-harmonic form of the partial differential equations is defined in Section 2.2.1 as follows:

$$\nabla\times\left(\mu_r^{-1}\nabla\times\mathbf{E}\right)-k_0^2\left(\varepsilon_r-\frac{i\sigma}{\omega\varepsilon_0}\right)\mathbf{E}=0 \tag{2.A.1}$$

Eq. (2.A.1) is applicable over the volume enclosed by the boundaries (V) of the computational domain. In order to solve the problem defined in Eq. (2.A.1), the equation is multiplied by a testing function (**W**) and then integrated over the volume V leading to:

$$\int_V \mathbf{W}.\left[\nabla\times\left(\mu_r^{-1}\nabla\times\mathbf{E}\right)-k_0^2\left(\varepsilon_r-\frac{i\sigma}{\omega\varepsilon_0}\right)\mathbf{E}\right]dV=0 \tag{2.A.2}$$

By incorporating vector identity and Gauss's Theorem, the weak form of the time-harmonic form of Maxwell's equations can be given as follows:

$$\int_V \left[(\nabla\times\mathbf{W}).\mu_r^{-1}.(\nabla\times\mathbf{E})-k_0^2\left(\varepsilon_r-\frac{i\sigma}{\omega\varepsilon_0}\right)\mathbf{W}.\ \mathbf{E}\right]dV \tag{2.A.3}$$

As for the mass and momentum conservation equations, the weak forms are specified in Eqs. (2.A.4) and (2.A.5) that can be written as:

$$\int_0^t\int_V \left[\rho\frac{\partial\mathbf{W}}{\partial t}+\rho\mathbf{u}.\nabla.\mathbf{W}\right]dVdt=0 \tag{2.A.4}$$

$$\int_0^t\int_V \left[\rho\mathbf{u}.\frac{\partial\mathbf{W}}{\partial t}+\rho(\mathbf{u}\times\mathbf{u}):\nabla\mathbf{W}+p\nabla.\mathbf{u}\right]dVdt=\int_0^t\int_V [\mathbf{S}:\nabla\mathbf{u}-\mathbf{F}.\mathbf{W}]\,dVdt \tag{2.A.5}$$

Appendix 2.B: Radiation modes

Rectangular waveguides, depending on their dimensions, are capable of transmitting different modes of electromagnetic radiation. The equations for TE and TM field components of a rectangular waveguide can be calculated based on the expressions in Table (2.1.A) in which *a* is the shorter and *b* is the longer dimension of the waveguide and other parameters can be calculated based on the following equations:

$$k_{c,nm}=\sqrt{\left(\frac{n\pi}{a}\right)^2+\left(\frac{m\pi}{b}\right)^2} \tag{2.A.6}$$

$$\beta_{nm}=\sqrt{k_0^2-k_{c,nm}^2} \tag{2.A.7}$$

$$\lambda_{c,nm}=\frac{2ab}{\sqrt{n^2b^2+m^2a^2}} \tag{2.A.8}$$

Table 2.A.1 The electromagnetic field components of radiation for different TE and TM modes.

	TE_{nm}	TM_{nm}
H_z	$\cos\left(\frac{n\pi x}{a}\right)\cos\left(\frac{m\pi y}{b}\right)\exp(-j\beta_{nm}z)$	0
E_z	0	$\sin\left(\frac{n\pi x}{a}\right)\sin\left(\frac{m\pi y}{b}\right)\exp(-j\beta_{nm}z)$
E_x	$Z_{H,nm}H_y$	$-j\frac{\beta_{nm}n\pi}{ak_{c,nm}^2}\cos\left(\frac{n\pi x}{a}\right)\sin\left(\frac{m\pi y}{b}\right)\exp(-j\beta_{nm}z)$
E_y	$-Z_{H,nm}H_x$	$-j\frac{\beta_{nm}m\pi}{bk_{c,nm}^2}\sin\left(\frac{n\pi x}{a}\right)\cos\left(\frac{m\pi y}{b}\right)\exp(-j\beta_{nm}z)$
H_x	$j\frac{\beta_{nm}n\pi}{ak_{c,nm}^2}\sin\left(\frac{n\pi x}{a}\right)\cos\left(\frac{m\pi y}{b}\right)\exp(-j\beta_{nm}z)$	$-\frac{E_y}{Z_{E,nm}}$
H_y	$-j\frac{\beta_{nm}m\pi}{bk_{c,nm}^2}\cos\left(\frac{n\pi x}{a}\right)\sin\left(\frac{m\pi y}{b}\right)\exp(-j\beta_{nm}z)$	$\frac{E_x}{Z_{E,nm}}$
$Z_{H,nm}$	$\frac{k_0}{\beta_{nm}}Z_0$	0
$Z_{E,nm}$	0	$\frac{\beta_{nm}}{k_0}Z_0$

References

Abali, B. E., & Reich, F. A. (2017). Thermodynamically consistent derivation and computation of electro-thermo-mechanical systems for solid bodies. Computer Methods in Applied Mechanics and Engineering, 319, 567–595.

Ali, A. Y., & Bradshaw, S. M. (2009). Quantifying damage around grain boundaries in microwave treated ores. Chemical Engineering and Processing: Process Intensification, 48(11–12), 1566–1573.

Ali, A. Y., & Bradshaw, S. M. (2010). Bonded-particle modelling of microwave-induced damage in ore particles. Minerals Engineering, 23(10), 780–790.

Cecot, W. (2005). Modeling of electromagnetic fields in rectangular waveguides by coupled finite–infinite elements. Computer Methods in Applied Mechanics and Engineering, 194(2–5), 549–558.

Chen, H., Li, T., Wang, Z., Ye, R., & Li, Q. (2020). Effect of dielectric properties on heat transfer characteristics of rubber materials via microwave heating. International Journal of Thermal Sciences, 148, 106162.

Hartlieb, P., Leindl, M., Kuchar, F., Antretter, T., & Moser, P. (2012). Damage of basalt induced by microwave irradiation. Minerals Engineering, 31, 82–89.

Hartlieb, P., & Rostami, J. (2018). Rock mechanics implications of microwave treatment of rock as part of a hybrid system for mechanical excavation of rock for civil and mining applications. ISRM EUROCK, ISRM-EUROCK.

Hassani, F., Nekoovaght, P. M., & Gharib, N. (2016). The influence of microwave irradiation on rocks for microwave-assisted underground excavation. Journal of Rock Mechanics and Geotechnical Engineering, 8(1), 1–15.

Hassani, F., Shadi, A., Rafezi, H., Sasmito, A. P., & Ghoreishi-Madiseh, S. A. (2020). Energy analysis of the effectiveness of microwave-assisted fragmentation. Minerals Engineering, 159, 106642.

Hayt, W., & Buck, J. (2012). Engineering electromagnetics.

Infrarde, E., & Termografije, E. (2018). Emissivity of aluminium alloy using infrared thermography technique. Mater. Tehnol, 52, 323–327.

Jin, J.-M., & Riley, D. J. (2008). Finite element analysis of antennas and arrays. John Wiley & Sons.

Jin, J.-M., Zunoubi, M., Donepudi, K. C., & Chew, W. C. (1999). Frequency-domain and time-domain finite-element solution of Maxwell's equations using spectral Lanczos decomposition method. Computer Methods in Applied Mechanics and Engineering, 169(3–4), 279–296.

Jones, D. A., Kingman, S. W., Whittles, D. N., & Lowndes, I. S. (2007). The influence of microwave energy delivery method on strength reduction in ore samples. Chemical Engineering and Processing: Process Intensification, 46(4), 291–299.

Kingman, S W, Jackson, K., Cumbane, A., Bradshaw, S. M., Rowson, N. A., & Greenwood, R. (2004). Recent developments in microwave-assisted comminution. International Journal of Mineral Processing, 74(1–4), 71–83.

Kingman, S W, Jackson, K., Bradshaw, S. M., Rowson, N. A., & Greenwood, R. (2004). An investigation into the influence of microwave treatment on mineral ore comminution. Powder Technology, 146(3), 176–184.

Lan, W., Wang, H., Zhang, X., Fan, H., Feng, K., Liu, Y., & Sun, B. (2020). Investigation on the mechanism of micro-cracks generated by microwave heating in coal and rock. Energy, 206, 118211.

Lee, G. L., Law, M. C., & Lee, V.-C. (2021). Numerical modelling and investigation of microwave heating and boiling phenomena in binary liquid mixtures using OpenFOAM. International Journal of Thermal Sciences, 159, 106538.

Li, R., Zhang, C., & Huang, Z. (2020). Quenching and rewetting of rock in liquid nitrogen: Characterizing heat transfer and surface effects. International Journal of Thermal Sciences, 148, 106161.

Lin, B., Li, H., Chen, Z., Zheng, C., Hong, Y., & Wang, Z. (2017). Sensitivity analysis on the microwave heating of coal: A coupled electromagnetic and heat transfer model. Applied Thermal Engineering, 126, 949–962.

Lu, G.-M., Feng, X.-T., Li, Y.-H., Hassani, F., & Zhang, X. (2019). Experimental investigation on the effects of microwave treatment on basalt heating, mechanical strength, and fragmentation. Rock Mechanics and Rock Engineering, 52(8), 2535–2549.

Lu, G., Li, Y., Hassani, F., & Zhang, X. (2017). The influence of microwave irradiation on thermal properties of main rock-forming minerals. Applied Thermal Engineering, 112, 1523–1532.

Mineo, S., & Pappalardo, G. (2021). Rock emissivity measurement for infrared thermography engineering geological applications. Applied Sciences, 11(9), 3773.

Motlagh, P. N. (2015). Physical and mechanical properties of rocks exposed to microwave irradiation: potential application to tunnel boring. McGill University (Canada).

Multiphysics, C. (1998). Introduction to comsol multiphysics®. COMSOL Multiphysics, Burlington, MA, Accessed Feb, 9(2018), 32.

Satish, H, Ouellet, J., Raghavan, V., & Radziszewski, P. (2006). Investigating microwave assisted rock breakage for possible space mining applications. Mining Technology, 115(1), 34–40.

Satish, Hemanth. (2005). Exploring microwave assisted rock breakage for possible space mining applications.

Shadi, A., Ahmadihosseini, A., Rabiei, M., Samea, P., Hassani, F., Sasmito, A. P., & Ghoreishi-Madiseh, S. A. (2022). Numerical and experimental analysis of fully coupled electromagnetic and thermal phenomena in microwave heating of rocks. Minerals Engineering, 178, 107406.

Toifl, M., Hartlieb, P., Meisels, R., Antretter, T., & Kuchar, F. (2017). Numerical study of the influence of irradiation parameters on the microwave-induced stresses in granite. Minerals Engineering, 103, 78–92.

Toifl, M., Meisels, R., Hartlieb, P., Kuchar, F., & Antretter, T. (2016). 3D numerical study on microwave induced stresses in inhomogeneous hard rocks. Minerals Engineering, 90, 29–42.

Vajdi, M., Moghanlou, F. S., Sharifianjazi, F., Asl, M. S., & Shokouhimehr, M. (2020). A review on the Comsol Multiphysics studies of heat transfer in advanced ceramics. Journal of Composites and Compounds, 2(2), 35–43.

Walkiewicz, J. W., Clark, A. E., & McGill, S. L. (1991). Microwave-assisted grinding. IEEE Transactions on Industry Applications, 27(2), 239–243.

Wang, G., Radziszewski, P., & Ouellet, J. (2008). Particle modeling simulation of thermal effects on ore breakage. Computational Materials Science, 43(4), 892–901.

Wang, X., Guo, H., Wang, C., Chen, P., & Shi, Y. (1999). Relative dielectric constant from dry rocks. Chinese Science Bulletin, 44, 2286–2293.

Wang, Y., & Djordjevic, N. (2014). Thermal stress FEM analysis of rock with microwave energy. International Journal of Mineral Processing, 130, 74–81.

Wei, W., Shao, Z., Qiao, R., Chen, W., Zhou, H., & Yuan, Y. (2021). Recent development of microwave applications for concrete treatment. Construction and Building Materials, 269, 121224.

Wei, W., Shao, Z., Zhang, Y., Qiao, R., & Gao, J. (2019). Fundamentals and applications of microwave energy in rock and concrete processing–A review. Applied Thermal Engineering, 157, 113751.

Whittles, D. N., Kingman, S. W., & Reddish, D. J. (2003). Application of numerical modelling for prediction of the influence of power density on microwave-assisted breakage. International Journal of Mineral Processing, 68(1–4), 71–91.

Xu, T., He, L., Zheng, Y., Zou, X., Badrkhani, V., & Schillinger, D. (2020). Experimental and numerical investigations of microwave-induced damage and fracture formation in rock. Journal of Thermal Stresses, 44(4), 513–528.

Xue, Y., Cao, Z., Dang, F., Ma, Z., & Gao, J. (2019). Numerical simulation of damage and permeability evolution mechanism of coal seam under microwave radiation. Thermal Science, 23(3 Part A), 1355–1361.

Zhu, J, Kuznetsov, A. V, & Sandeep, K. P. (2007). Mathematical modeling of continuous flow microwave heating of liquids (effects of dielectric properties and design parameters). International Journal of Thermal Sciences, 46(4), 328–341.

Zhu, Jingyi, Yi, L., Yang, Z., & Duan, M. (2021). Three-dimensional numerical simulation on the thermal response of oil shale subjected to microwave heating. Chemical Engineering Journal, 407, 127197.

"*We need to fail down here, so we don't fail up there".*

Neil Armstrong- First Man

Chapter 3: Numerical and experimental analyses of rock failure mechanisms due to microwave treatment

3.1. Preface

In the preceding chapter, a numerical model was developed to capture the heat transfer and energy absorption behaviour during microwave treatment of rocks. In this chapter, the developed model is utilized to delve deeper into comprehending the impact of microwave treatment on various rock types, particularly those containing microwave-absorbing minerals. Building upon experimental observations indicating that samples incorporating microwave-absorbing minerals exhibit faster failure at lower energy dosages compared to homogeneous samples, the utilization of the developed numerical model offers a fresh perspective on identifying suitable candidates for the potential application of microwave treatment to enhance rock failure properties. Through this investigation, we aim to refine our understanding and optimize the efficacy of microwave treatment for rocks.

3.2. Abstract

Despite the extensive studies conducted on the effectiveness of microwave treatment as a novel rock pre-conditioning method, there is yet to be found reliable data on the rock failure mechanisms created by microwave heating. In addition, there is no significant discussion on the energy efficiency of the method as one of the important fracture pre-conditioning factors among the mining and geotechnical engineers in the industry. This study presents a novel

experimental method to evaluate two main rock failure mechanisms due to microwave treatment without applying any mechanical forces, i.e. distributed and concentrated heating. This research shows that the existence of a small and concentrated fraction of a strong microwave absorbing mineral will change the failure mechanism from the distributed heating to the concentrated heating, which can increase the weakening over microwave efficiency (WOME) by more than 10 fold. This observation is further investigated using the developed coupled numerical model. It is shown that at the same input energy, the existence of microwave absorbing minerals can cause major heat concentration inside the rock and increase the maximum temperature by up to three times.

Keywords: Microwave treatment; Numerical modeling; Failure mechanism; Energy efficiency; Rock pre-conditioning

3.3. Introduction

Rock excavation and associated problems are significant in the mining industry and geotechnical engineering (Rostami & Ozdemir, 1993). Engineers employ either non-continuous or batch (e.g. drilling and blasting) or continuous (e.g. mechanical excavation) methods to address this problem. The uncertainties of the non-continuous methods such as mine collapse and groundwater inrush along with low mine productivity due to longer cycle time needed to clear-out blasting fumes and its environmental effect have made the mining industry lean toward continuous methods (Ma, Duan, Li, et al., 2019; Ma, Duan, Liu, et al., 2019; S. Wang et al., 2019). Nevertheless, continuous methods have their own limitations. For example, mechanical excavation suffers from slow excavation rate, short life span of the cutting discs and periodic equipment maintenance (Kahraman, Canpolat, Fener, et al., 2020). In order to address the issues of continuous methods, rock pre-conditioning has been introduced in which one of the most promising methods is the microwave treatment (Hassani, 2010).

In a general view, microwave irradiation can heat up some minerals like pyrite, while it does not have any effect on others like allanite (T. T. Chen et al., 1984). Therefore, during microwave treatment, there are some minerals that are heated and expanded due to thermal expansion which induce stress to their contact surfaces with other surrounding minerals. The generated internal stress creates micro/macro cracks inside the rock that results in a strength reduction of the microwaved sample before excavation starts and consequently, addresses the issues of the continuous excavation methods to some extent (Hassani, 2010; Jones et al., 2005; Y. Zheng et al., 2020; Y L Zheng et al., 2020).

Increasing either power or exposure time increases the microwave output energy dosage that gives rise to a higher temperature and potentially, a higher strength reduction in the rock (Nekoovaght Motlagh, 2009). In this regard, many studies have investigated the effect of different dosages of microwave energy on rock strength parameters. These studies are jointed together by stating that increasing the energy dosage would cause more strength reduction. For instance, Peinsitt et al. (2010) treated sandstone, granite, and basalt rocks with a microwave power of 3 kW and exposure times of 60 s, 120 s, 180 s, 240 s, and 300 s. They emphasized the strength reduction of the samples caused by microwave energy by comparing uniaxial compressive strength (UCS) values of the rocks before and after treatment. Moreover, Nejati et al. (2012) evaluated the effect of microwave treatment on the fracture toughness of basalt. Different powers of 1-5 kW with an exposure time of up to 30 s was used to treat small cylindrical samples with a diameter of 50 mm and a height of 15 mm, which resulted in large microwave energy dosages and a reduction of stress intensity factor. These studies have been continuing over the past decade. For example, Bisai et al. (2020) investigated the effect of microwave energy on uniaxial tensile strength (UTS) and UCS reduction in granite and sandstone rocks. Yuan et al. (2020) investigated crack propagation in olivine basalt at different powers and exposure times and it was shown that there is an increase in the crack density after microwave treatment. In previous studies, it is mentioned that the strength reduction and crack density are increased when the microwave power and exposure time are increased. However, to the best of the authors' knowledge, there has not been a thorough evaluation of the energy efficiency of the microwave treatment of rocks, especially for the heterogeneous samples (Bai et al., 2021; Hartlieb et al., 2018; Hassani et al., 2011; D A Jones et al., 2007; X. Li et al., 2020; G.-M. Lu, Feng, Li, & Zhang, 2019; Gaoming Lu, Feng, et al., 2020). One should consider that neglecting the amount of energy spent on reducing rock strength with microwave energy can cause major conceptual issues in the studies. To address this issue, Hassani et al. (2020) proposed an innovative approach by adding calorimetric measurements to microwave heating studies of rock materials. After each microwave heating experiment, the sample is put inside a calorimeter to measure the energy absorption of rock samples. Measuring the energy absorptions led to the introduction of two new parameters named heat over microwave efficiency (HOME) and weakening over microwave energy (WOME), which can quantify the evaluation of the energy efficiency of the microwave treatment method.

Experimentally investigating the effect of microwave treatment on improving mining excavation can be time-consuming and expensive. Developing numerical models can address a lot of these issues (Salsman et al., 1996; Whittles et al., 2003). A variety of research works have been conducted to numerically evaluate the effect of microwave energy on rock strength reduction. Numerical investigation of complex coupled phenomena such as microwave heating of rocks can face several challenges including but not limited to high computational cost and convergence issues. To overcome these challenges, researchers have implemented different numerical approaches (e.g. discrete element method (Ali & Bradshaw, 2010; G. Wang et al., 2008) and continuum methods (Ali & Bradshaw, 2009; G. Wang et al., 2008; Y. Wang & Djordjevic, 2014; Whittles et al., 2003), simplified assumptions (e.g. using Lambert's Law instead of Maxwell's equations to find the electromagnetic distribution in the space (Xu et al., 2020)) and simplified boundary conditions (e.g. disregarding the accurate design of the cavity (Toifl et al., 2016, 2017)). The limitations in the conducted methods and especially the simplified assumptions create major differences between numerical modeling, field, and experimental data, leading to improper validation and verification of the developed models (J. Li et al., 2019; Pressacco et al., 2022).

Recent advancements in the development of numerical models as well as increased accessibility to high-power computer systems have resulted in major improvements in the developed numerical models. For instance, Toifl et al. (2017, 2016) developed a three-dimensional (3D) numerical model to investigate the damage caused by microwave treatment on heterogeneous rock. However, not using proper boundary conditions created a deviation between the reality and the model. In one of the most recent examples in Shadi et al. (2022), they have been able to capture the energy absorption of the homogeneous samples during microwave treatment with less than 3% error. Continuing the development of these numerical models can significantly improve the understanding of the effect of microwave treatment on the rock's strength reduction.

To address the knowledge gap and build upon the previous research works, it is intended to introduce a new experimental procedure by concentrating on energy as the major parameter as well as the study of heterogeneous rocks that constitute high microwave absorbing minerals. The effect of the existence of the major microwave absorbing minerals in the rock mass has been evaluated both numerically and experimentally.

3.4. Methodology

3.4.1. Experimental procedure

This section describes the experimental procedure followed in this study to evaluate the effect of microwave treatment on reducing the strength of rocks. The experimental investigation is conducted in two parts. First, the characteristics of the rocks are evaluated using different experiments and techniques. The gathered results provide some insight into the nature of the rocks used for microwave treatment experiments. Some of these results are also used as input parameters for the developed numerical model. Second, the procedure for the microwave treatment experiments is provided in detail by describing the industrial microwave system used in the study and the specifications of the heating experiments, such as power, exposure time, and microwave frequency. The detail of each subsection is provided as follows.

3.4.1.1. Material characterization

The samples used in this study are categorized as rhyolite rocks and are gathered from the Najran Area in Saudi Arabia (Ahmed et al., 2022). The samples are taken out in intact form using core drilling with a diameter of 50 mm. The surfaces of the cores are polished to reach a tolerance of 0.04 according to the ASTM standard (D4543, 2019) (see Figure 3.1). There are two visually distinctive patterns for the rocks which can be categorized in light and dark, as shown in Figure 3.1a and b, respectively. Furthermore, different techniques, such as scanning electron microscopy (SEM), X-ray fluorescence (XRF), and X-ray Diffraction (XRD), are employed to characterize the samples in a more quantified manner (Tables 3.1-3.3). The significant variation in the weight percentage of different minerals and elements between the samples discussed in Tables 3.1-3.3 and the distinct visual patterns shown in Figure 3.1 emphasize the heterogeneous nature of the rocks used in this study. It should be noted that some of the minerals, such as pyrite, are microwave absorbent, and their percentage in the sample can significantly change the response of the rock to the microwave energy.

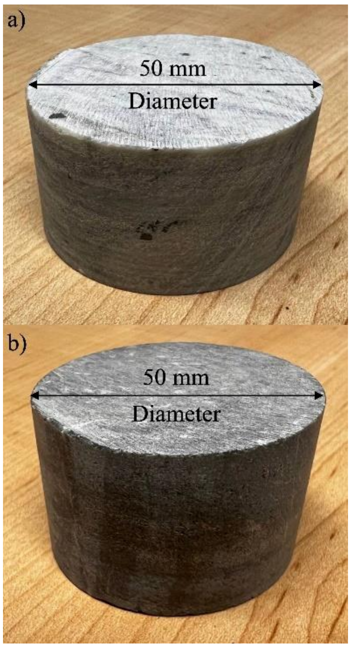

Figure 3.1 Two visually distinctive patterns among the samples used for the microwave treatment experiment: (a) Light pattern, and (b) Dark pattern.

Table 3.1. Elemental compositions (%) of samples.

Sample	C	O	Na	Mg	Al	Si	S	K	Ca	Fe	Cu
I	4.33	51.84	3.09	1.49	12.13	15.65	0	0.55	0.53	10.38	0
II	7.6	46.86	2.93	0	4.98	32.47	0	0.87	1.62	2.66	0
III	1.8	55.69	1.56	0.65	11.82	22.75	0.14	3.37	0	1.65	0.57

Table 3.2 Chemical composition (%) of samples determined by XRF.

Sample	CaO	Al_2O_3	Fe_2O_3	SiO_2	P_2O_5	TiO_2	MnO	MgO	Na_2O	K_2O	SO_3	CL	LOI*
I	6.21	13.79	9.72	50.11	0.2	0.28	0.21	2.92	2.93	0.65	1.35	<0.01	11.54
II	2.8	13.15	2.61	70.9	0.06	0.16	0.34	0.34	5.10	1.03	1.32	<0.01	2.39
III	3.47	12.47	4.45	68.95	0.05	0.11	0.14	1.69	2.43	0.96	0.66	<0.01	4.58

*LOI: Loss on ignition.

Table 3.3 Mineral phase identification of the samples and their weight percentage (%).

Sample	Albite	Aragonite	Quartz	Pyrite	Chlorite	Dolomite	Sphalerite	Chalcopyrite	Galena
I	36.1	0	28.3	1.7	15.4	18.5	0	0	0
II	54.5	22.4	11.6	2.5	9	0	0	0	0
III	0	1	48.4	5.7	40.4	0	2.1	2	0.4

The core diameters are 50 mm, and they are cut into 100 mm sections to provide UCS-sized samples with a height to diameter ratio of 2:1. Afterward, the top and the bottom surfaces of each sample are ground using a mechanical grinding machine to ensure that the flat surfaces are horizontal and parallel and also, the dimensions are consistent.

The heat capacity is calculated by measuring the heat transfer between rock and water when they have different temperatures until reaching thermal equilibrium. The thermal conductivity is measured by employing a KD2Pro probe. It should be noted that the tests for measuring both heat capacity and thermal conductivity are repeated three times and the average value is reported to ensure the reliability of the results in representing the rock characterization parameters (Table 3.4).

The thermal expansion of the sample is measured using a thermomechanical analyzer (TMA) apparatus. The main concept of the TMA is to measure the change in the dimension of the sample when the temperature changes. The procedure for each test includes multiple steps as follows:

(1) The temperature is set at 298.15 K;

(2) The sample and equipment stay isothermal for 1 min at 298.15 K;

(3) The temperature is increased at the rate of 3 K/min up to 673.15 K;

(4) The temperature is decreased at the rate of 3 K/min down to 298.15 K; and

(5) Steps 3 and 4 are repeated.

For the sample to be used in the thermal expansion coefficient measurement, the inclusion of two parallel surfaces is required. The initial distance between the two parallel surfaces is 24.57 mm. During the entire test, the deformation of the sample between the two parallel surfaces is recorded. Figure 3.2 depicts the dimension change versus the temperature, which also shows a cyclic behavior for the thermal expansion of the rock. However, considering the fact that there is no cyclic phenomenon during the microwave heating tests, the values of the first heating cycle should be considered as the main parameter in microwave treatment.

Table 3.4 Rock material properties.

Parameter	Unit	Value
Thermal conductivity	W/(m K)	2.51
Density	kg/m^3	2800
Heat capacity	J/(kg K)	716
Relative permeability	-	1
Electrical conductivity	S/m	0

The electromagnetic properties of the rocks include three main parameters: relative permittivity, relative permeability, and electrical conductivity. When the rock is not constituted of any major magnetic or electrically conductive minerals, the relative permeability and electrical conductivity parameters are approximately 1 and 0, respectively. The relative permittivity of the samples in this study is measured using two different methods.

The first method to measure the dielectric properties is by use of the coaxial probe. In this method, a high-temperature coaxial probe is employed. Applying this method to solid materials requires that they have flat and smooth surfaces to ensure proper contact between the probe and the rock. Therefore, two samples are chosen randomly, and their surfaces are smoothened using sandpapers to ensure proper contact between the rock and the probe. The probe is used at three different surface locations and in each location the measurement is repeated three times to ensure that the results are reliable. The experiments are performed at the intermediate frequency bandwidth (IFBW) of 300 Hz and the power of 10 dBm. The samples used for the measurements have a diameter of 50 mm and a length of 30 mm. The recommended test specifications are detailed in Table 3.5 (Keysight, 2017a, 2017b). It should be noted that Rhyolite rocks are not good microwave absorbents and therefore, the recommendations for the loss tangent values might not be satisfied.

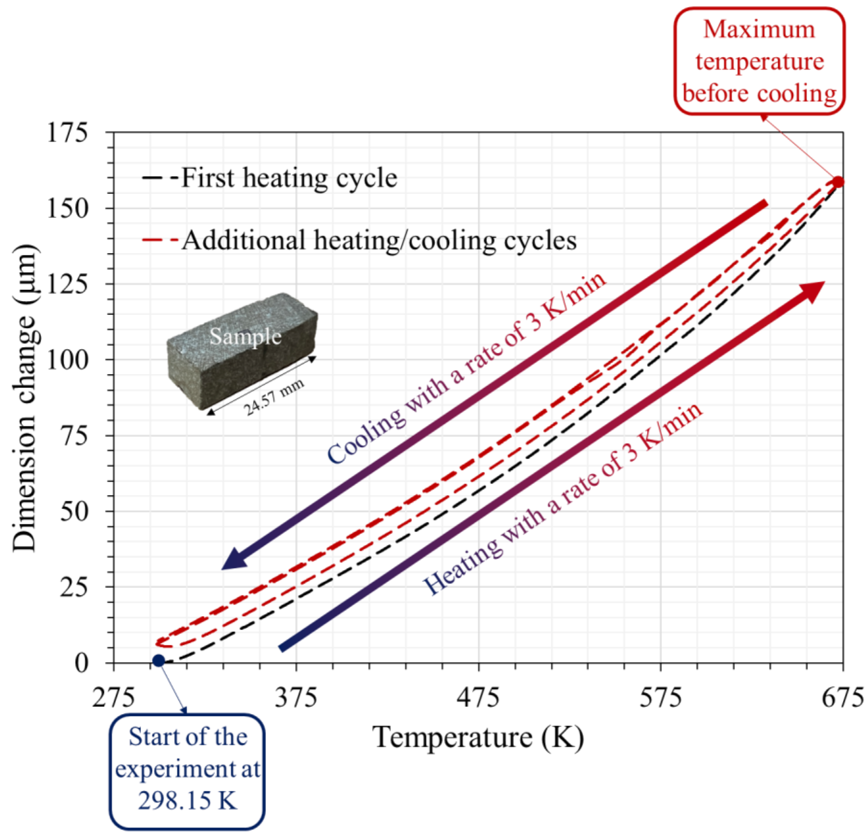

Figure 3.2 The TMA experiment results of the sample's thermal expansion behavior in different continuous heating cycles. Since there is no cooling during the microwave treatment, the first heating line (depicted in black) is more important.

Table 3.5 Recommendations for the test specifications for the measurement of the dielectric properties using the coaxial probe.

Parameter	Recommendation/Specification
Sample size	Diameter: > 20 mm Thickness: > 20 mm/$\sqrt{\lvert \boldsymbol{\varepsilon}_{\mathbf{r}} \rvert}$ Granule size: < 0.3 mm
Expected value	$\varepsilon_r^{'}$<100 Loss tangent: > 0.05

Note: ε_r is the relative permittivity,

Using a coaxial probe for the measurement of the dielectric properties for the samples with low microwave energy absorption might not provide accurate results. Therefore, in this study, the cavity perturbation method is utilized as an alternative method for the measurement of the dielectric properties. This method is performed based on the system developed by (Hutcheon, Jong, & Adams, 1992; Hutcheon, Jong, Adams, et al., 1992), which includes using small-sized samples (diameter of 3.71 mm and a length of 12.32 mm). In this method, the sample is encountered with an electric field and afterward, the change in the frequency and the introduced electromagnetic energy is related to the complex dielectric properties of the material. One of the advantages of using this method is its capability in measuring the dielectric properties at high temperatures up to 1400°C. This method has been previously used in literature to measure the temperature-dependent permittivity of rock materials (Bobicki et al., 2020; Hartlieb et al., 2016; Samouhos et al., 2012; Shadi et al., 2022). However, because of the small-size samples, it is difficult to provide useful information for heterogeneous rocks. Furthermore, compared to other methods like the coaxial probe, the measurements are more time-consuming.

In this study, both of the introduced methods of dielectric properties measurements are employed and compared.

3.4.1.2. Microwave heating experiments

The purpose of the microwave heating experiments in this study is to evaluate the required microwave energy to break rock samples. The heating experiments are performed using an industrial microwave cavity working at the frequency of 2.45 GHz. The detailed dimensions of the cavity are shown in Figure 3.3. The electromagnetic wave is radiated through a rectangular waveguide with length and width of 88 mm and 46 mm, respectively. For each experiment, the UCS-sized sample is placed inside the cavity where the distance between the waveguide port and the top surface of the sample is 15 mm. Then, the sample is exposed to a microwave power of 3 kW. The microwave radiation continues until a major failure is observed in the sample. Immediately after the major failure is observed, the radiation is stopped and the sample is put inside a calorimeter to measure the absorbed energy during the microwave heating. Then, based on the absorbed and input energies, the HOME is calculated as follows:

$$\text{HOME } (\%) = \frac{\text{Absorbed Energy}}{\text{Input Energy}} \times 100 \tag{3.1}$$

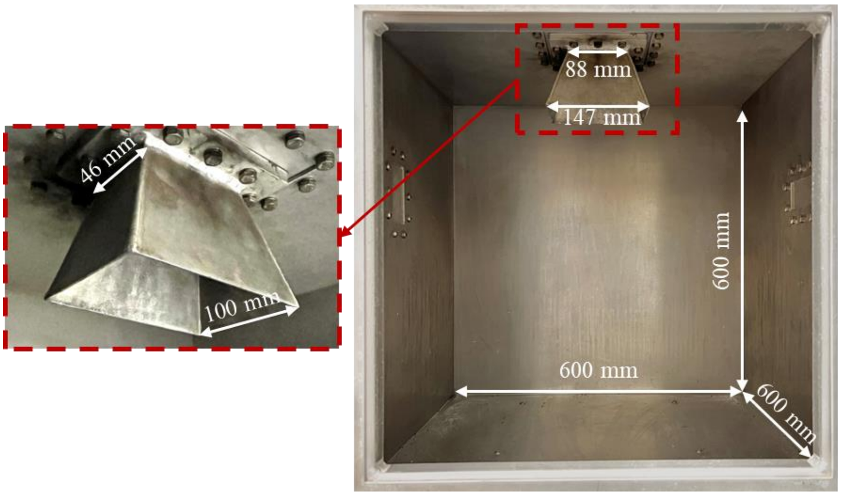

Figure 3.3 The industrial microwave cavity and its dimensions used for the microwave heating experiments.

Furthermore, considering the major destruction of the sample during the heating experiments, it is assumed that the applied energy has caused a 100% strength reduction of the material. Therefore, the WOME can be calculated:

$$\text{WOME (\%/kW h/ton)} = \frac{1}{\text{Input Energy/Mass}} \times 100 \tag{3.2}$$

3.4.2. Numerical model

A 3D coupled numerical model is developed to investigate the energy absorption and the temperature change at different locations of the rock during the microwave treatment. This model has been previously verified, validated, and explained in detail in (Ahmadihosseini et al., 2022). This section is only focused on the main points of the developed numerical model and the readers are referred to Ahmadihosseini et al. (2022) for a detailed description.

3.4.2.1. Governing equations

To describe the electromagnetic wave distribution throughout the cavity, the time harmonic form of the Maxwell's equations is used as follows:

$$\nabla\times\left(\mu_r^{-1}\nabla\times\mathbf{E}\right)-k_0^2\left(\varepsilon_r-\frac{i\sigma}{\omega\varepsilon_0}\right)\mathbf{E}=0 \tag{3.3}$$

where **E** is the electric field intensity; σ is the electrical conductivity; ω is the angular frequency; μ_r is the relative permeability; i is the unit imaginary number; ε_0 is free space permittivity; and k_0 is the wavenumber in free space, which can be calculated as follows:

$$k_0=\left(\omega^2\varepsilon_0\mu_0\right)^{1/2} \tag{3.4}$$

where μ_0 is the free space permeability. It should be noted that for rocks, the relative permittivity and permeability are complex numbers constituting real and imaginary parts as follows:

$$\varepsilon_r=\varepsilon_r'-i\varepsilon_r'' \tag{3.5}$$

$$\mu_r=\mu_r'-i\mu_r'' \tag{3.6}$$

Since in most rocks, there is no magnetic loss ($\mu_r \approx 1$), the relative permittivity becomes the main parameter governing the electromagnetic distribution in the cavity and therefore, in order to capture correctly the electromagnetic distribution in the material, it is necessary to have accurate measurements of both the real and imaginary parts of the relative permittivity.

The energy absorption of the sample is calculated by solving the energy conservation equation as follows:

$$\rho C\frac{\partial T}{\partial t}+\nabla(-k\nabla T)=Q \tag{3.7}$$

where ρ is the density of rock, C is the heat capacity, T is the temperature, k is the thermal conductivity, and Q is the heat source that is generated inside the material during the microwave treatment and can be obtained using Eq. (3.8) as follows:

$$Q=\omega\varepsilon_0\varepsilon_r''\,\bar{\mathbf{E}}^2+\omega\mu_0\mu_r''\,\bar{\mathbf{H}}^2 \tag{3.8}$$

where H is the magnetic field intensity.

The solution procedure of the aforementioned equations in the numerical model is depicted in Figure 3.4.

3.4.2.2. Boundary conditions

The following boundary conditions are considered for the development of the numerical model:

1) All the internal and external aluminum boundaries of the microwave cavity are perfect electric conductors;
2) The electromagnetic wave is radiated through the port boundary condition into the cavity with mode 10 of transverse electric field (TE_{10}) into the cavity; and
3) The external aluminum surfaces are adiabatic boundary conditions.

In order to elaborate the boundary surfaces, they are depicted in different colors in Figure 3.5b.

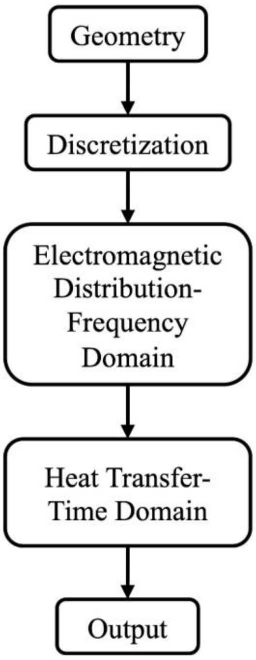

Figure 3.4 The flowchart specifying the solution procedure for the developed numerical model.

3.4.2.3. Model description

The geometry of the cavity in the numerical model is designed based on the experimental equipment in the geomechanics laboratory of McGill University (Figure 3.5a). The geometry includes two cubes with the dimensions of 600 mm × 600 mm × 600 mm (length × width × height), and 88 mm×46 mm×15 mm (length × width × height) to represent the cavity and the port of the microwave, respectively. (Shadi et al., 2022) investigated the effect of a full-length waveguide geometry compared to a simple cube and showed that a simplified cubic geometry is a good representative of the port for rectangular waveguides. Therefore, in this study, the port geometry is chosen with the length and width representing the waveguide and a height of 15 mm. The waveguide port is depicted as a shape of a horn with the detailed dimensions shown in Figure 3.5a and c. It should be mentioned that an internal boundary is added to the model to represent the door of the microwave with a length of 22.5 mm in the z-direction, as shown in Figure 3.5a. The sample is included in the design as a cylinder with a diameter of 50 mm and a length of 100 mm to represent the UCS-sized samples in the cavity. Three extra geometries are designed to consider a core with different material properties in the middle of the sample representing the microwave absorbent minerals. To evaluate the temperature distribution and electric field inside the sample after microwave treatment, a cross-section is considered that cuts the sample in half and is parallel to the xy plane. As for the initial conditions, the temperature is set at 293.15 K, and both the electric and magnetic fields are set at 0.

The geometry is discretized using tetrahedral elements. The details of the mesh independency analysis are provided in (Ahmadihosseini et al., 2022), which includes the final size criteria with the maximum element size of 18 mm, minimum element size of 0.923 mm, and maximum element growth of 1.35. This creates a total of approximately 660,000 tetrahedral elements for the whole geometry.

3.5. Results and discussion

3.5.1. Permittivity properties analysis

To measure the relative permittivity of the rock using the methods described in Section 3.2.1.1, two samples (Sample I and Sample II) are chosen randomly. First, the coaxial probe is employed to measure the dielectric properties of each sample. The measurement is performed at three different locations for each sample and the average value is used as the representative value of the sample. Afterward, a smaller cylindrical sample proper for the cavity perturbation method is drilled from each of the two samples and the measurement of the dielectric properties is performed using the second method. The results of the measurements are shown in Figure 3.6.

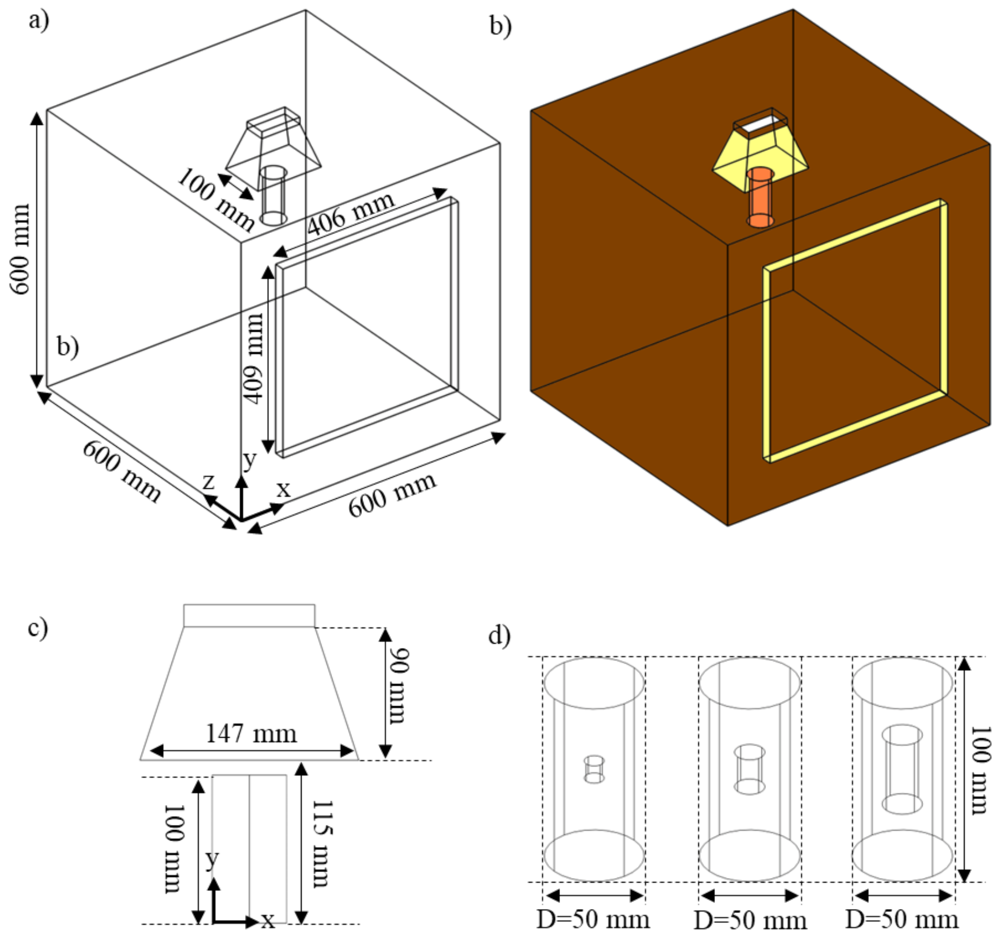

Figure 3.5 (a) The geometry of the numerical model; (b) The sample, external, and internal boundary conditions specified in the geometry in different colors of orange, brown, and yellow, respectively; (c) The dimensions of the waveguide port and the sample; and (d) The different core sizes considered inside the sample with diameters of 10 mm, 15 mm and 20 mm and lengths of 10 mm, 20 mm, and 40 mm for the smallest size to the biggest size, respectively.

Figure 3.6a depicts the real part of the permittivity of the two rocks captured using two measurement methods. The values obtained by the cavity perturbation method are larger than those by the coaxial probe method in all the frequencies. This could be due to the imperfect contact between the surfaces of the probe and the rock. Furthermore, the results show that there is no significant change in the real part of the permittivity when the frequency changes. In summary, at the frequency of 2.45 GHz, the average value of all four measurements of the real part of the permittivity is 6.11.

Figure 3.6b compares the imaginary part of the relative permittivity measured using the two probes for the selected two samples. Even though the same samples are used for the measurement of dielectric properties, there is a noticeable difference between the captured values between the two methods. The difference is more significant in Figure 3.6b, which compares the imaginary part of the permittivity at different frequencies. The trends of the charts in Figure 3.6b are more irregular compared to the real part of the permittivity shown in Figure 3.6a. The results of the coaxial probe show that the values of the imaginary part of the permittivity increase when the frequency increases. However, for the cavity perturbation method, while the same trend can be observed for Sample II, there is no significant change in the imaginary part of the relative permittivity for Sample I when the frequency changes. Another explanation for the difference between the two measurement methods is the fact that the rhyolite rocks used in this study are weak microwave absorbers. This fact adds further error in the results presented by the coaxial probe. The results of Figure 3.6b show that the average value of the imaginary part of the permittivity at the frequency of 2.45 GHz is 0.112 with an approximate range of 0.06-0.18.

The effect of temperature on the real and imaginary parts of the permittivity is shown in Figure 3.6c and d. The results of the permittivity at high temperatures are captured only using the cavity perturbation method. The charts for samples I and II have a noticeable difference due to the heterogeneous nature of the rocks used in this study. Figure 3.6c shows that there is an overall increasing trend in the real part of the permittivity for both samples when the temperature increases. However, this trend is different for the imaginary part as there is a peak in the values at 380 K approximately for both samples. In other words, the values for the imaginary part of the permittivity increase until 380 K to a maximum of approximately 0.23 and beyond the peak temperature, the values start to decrease. The following points can be deduced by comparing the two methods of measuring the relative permittivity of the rocks:

1) Even though the coaxial probe is an appropriate method to capture the permittivity of the solid materials, establishing the perfect contact between the surfaces of the rocks and the probe is rather difficult;
2) The coaxial probe is easier and quicker to employ for permittivity measurements;
3) The coaxial probe provides the average value of the permittivity surrounding the contact surface of the rock and the probe, while cavity perturbation can provide more detailed information since it requires smaller samples;
4) Using the cavity perturbation method for the heterogeneous samples is time-consuming and expensive as it requires the measurement of several samples, and directions, etc.;
5) The cavity perturbation method can provide information at higher temperatures while the coaxial probe can only be used at room temperature; and
6) For the samples that are weak microwave absorbers, the cavity perturbation method has superiority over the coaxial probe measurements.

Considering the advantages and disadvantages of each method, it is up to engineers to make the decision on which method to use for different microwave applications.

3.5.2. Failure mechanisms due to microwave treatment

The samples are exposed to microwave power of 3 kW for all the experiments. For each test, the exposure time is continued until a major failure occurs. The thermal images taken from the samples after the microwave treatment show two general forms of distributed and concentrated heating as shown in Figure 3.7a, and Figure 3.7b-d, respectively. In the distributed heating, the whole sample is heated uniformly, while in concentrated heating there is a major heating zone where the failure initiates. The visual observation also confirms extreme microwave absorption and accordingly burning of some minerals in the rocks failing with concentrated heating. Figure 3.8 shows the specific burning spots of the samples after microwave irradiation. According to Tables 3.1-3.3, this burning can be related to some of the minerals in the rocks with high microwave absorption, such as pyrite. In general, the samples with concentrated heating fail at a shorter exposure time compared to the distributed heating.

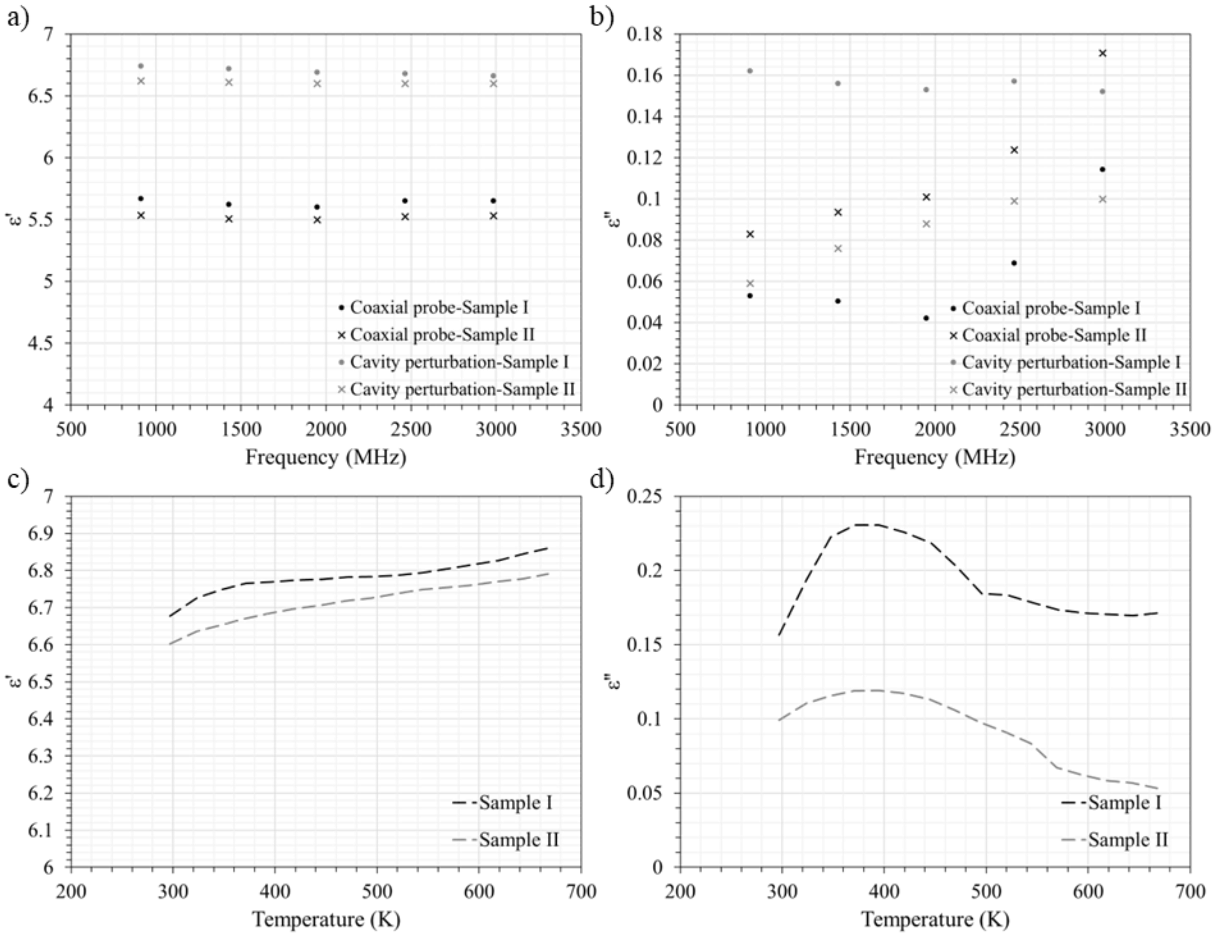

Figure 3.6 Comparison between the results of the coaxial probe and cavity perturbation methods at different frequencies for (a) Real part, and (b) Imaginary part of the permittivity. The temperature dependency of (c) Real part, and (d) Imaginary part of the permittivity measured using the cavity perturbation method.

To further evaluate the distributed and concentrated heating, the cumulative percentage of the samples that fail at different exposure times is shown in Figure 3.9a. For instance, approximately 78% of the samples failed before 240 s of microwave exposure time with a power of 3 kW. In Figure 3.9a, two major steps can be observed. The first and second steps start at approximately 20 s and 80 s, respectively. The experimental observations with the help of thermal images showed that the first step is the transition between concentrated and distributed heating. In other words, the general trend of the failure modes due to microwave heating shows the samples that fail before the first step follow the concentrated heating, while the samples that fail after the first step follow the distributed heating. Therefore, this step is used to differentiate between the two failure modes during microwave heating.

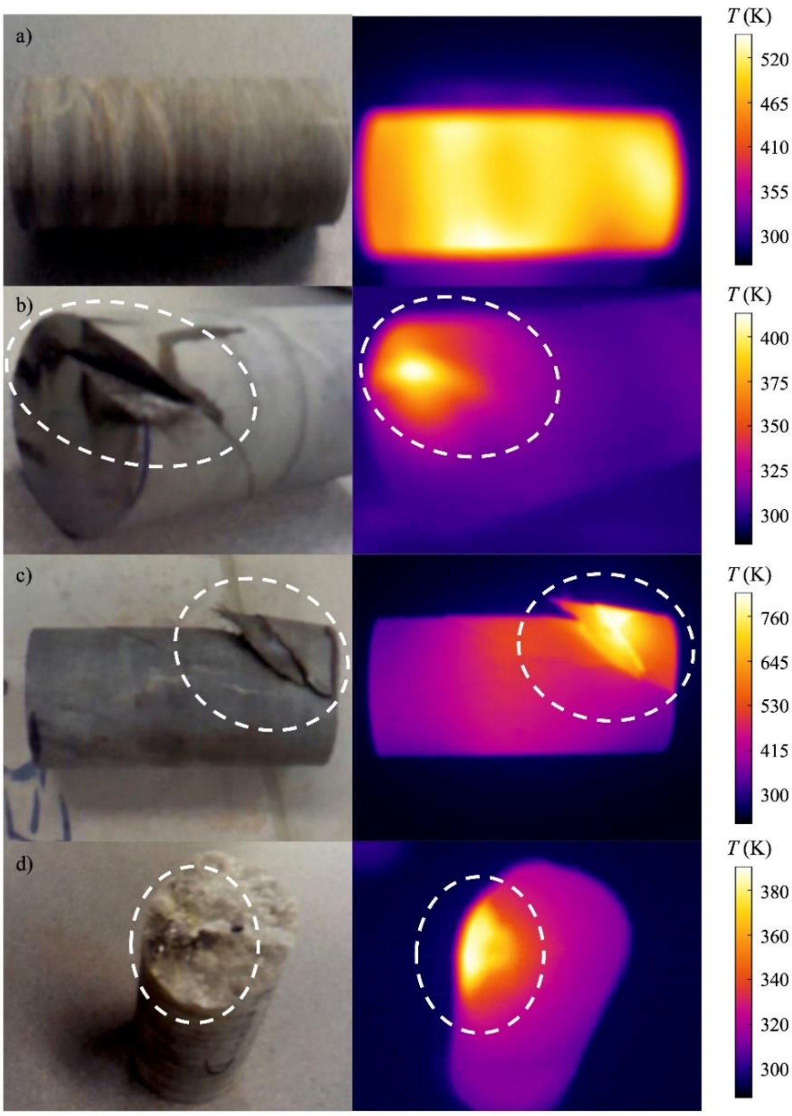

Figure 3.7 Different types of heat distribution after microwave treatment with 3 kW: (a) Distributed heating; and (b-d) Concentrated heating.

It has been shown that there is a correlation between HOME and WOME parameters during microwave treatment (Hassani et al., 2020). They used basalt as the main rock to investigate this theory. However, basalt is considered a relatively homogeneous rock that is treated in the same manner as distributed heating. This theory has been further investigated in this study for both sets of concentrated and distributed heating. Therefore, Figure 3.9a can be divided into two zones, Zone 1 and Zone 2, which are the representatives of concentrated and distributed heating. The correlation between HOME and WOME has been evaluated for both zones and it is observed that the results for Zone 2 show a good correlation with R2 of more than 0.8 (Figure 3.9b), while the results for the concentrated heating in Zone 1 are not correlated in any meaningful way. Moreover, the comparison between the two zones shows that the average WOME in Zone 1 is 6.28 %/kW h/ton while this value is 0.46 %/kW h/ton which shows over 10 times better efficiency.

Figure 3.8 Different observations from the samples after the failure. The samples that fail due to concentrated heating show burning in some locations while there is no sign of burning in the samples with distributed heating.

Concerning the experimental results in Figure 3.9b, two data points are with HOME values of more than 40% and deviated from the general trendline. It is believed that the results are related to potential sources of errors during the experiments, especially the calorimetric study for the samples with high HOME values and the distinction between distributed and concentrated heating for some of the samples. In other words, when the energy absorption of the samples is high, the potential heat loss increases during the treatment and calorimetric study, which is not included in the calculation and can add to the error. Furthermore, in some cases, the distinction between concentrated and distributed heating is difficult to observe because there is a heat concentration in a part of the sample, but the general rock body is also heated considerably. In this case, it is hard to judge whether the sample has failed based on distributed or concentrated heating which can increase the error in the calculations.

3.5.3. Heat absorbing minerals in the rock

In this section, the comparison between concentrated and distributed heating is further investigated using the developed numerical model. A series of parametric studies has been conducted to evaluate the effect of heat absorbing minerals on the efficiency of the microwave treatment of rocks. To represent different sizes of heat absorbing minerals in the sample, three different geometries are considered in the modeling process as mentioned in Section 3.2.2.3. Then, different permittivity values have been assigned to the main rock and the mineral core. Subsequently, the energy absorption of the sample is computed using the numerical model after an exposure time of 10 s with a power of 3 kW. The temperature distribution of the sample on the defined cross section is used to compare the different cases. This parametric study has been performed in two parts. In the first part, it is assumed that the composition of the mineral core is of the same type as the main rock. Therefore, for the main rock, the average values of the real and imaginary parts of the permittivity (ε_r'=6.11 and ε_r''=0.112) are assigned. However, for the mineral core, while the average value is used for the real part of the permittivity

(ε_r'=6.11), three different values are chosen for the parametric study on the imaginary part of the permittivity (ε_r''=0.06, 0.12, and 0.18). The results of the parametric study are depicted in Figure 3.10. It can be observed that in all the nine cases shown in Figure 3.10, there is no significant change in the average temperature of the sample. As for the maximum temperature, no significant change can be observed in Figure 3.10a and b. There is a major change in the maximum temperature of the sample (more than 85 K) when the largest mineral core size is considered in the model and ε_r'' is increased from 0.06 to 0.18 (Figure 3.10c).

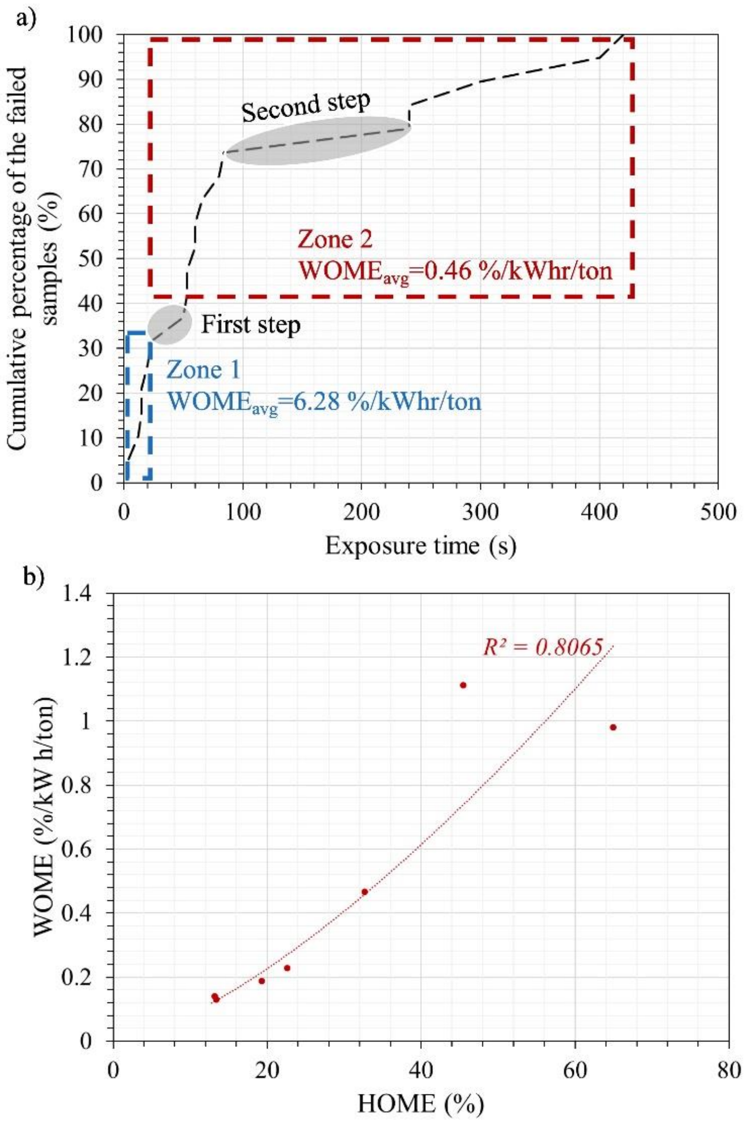

Figure 3.9 (a) Exposure time when the samples fail due to microwave power of 3 kW and the division of the samples' failure into Zone 1 and 2; and (b) The relation between HOME and WOME for samples that fail in Zone 2.

In the second part, the parametric study is expanded to assign the mineral cores and the permittivity values of specific microwave absorbing minerals. In this study, magnetite and pyrite are considered as examples of strong microwave absorbing minerals. According to the study of (Y. Zheng et al., 2020; Y L Zheng et al., 2020), magnetite and pyrite have relative permittivities of 14.5-2.5×i and 8.25-1×i, respectively. For all the cases, the average permittivity values (ε_r'= 6.11 and ε_r''= 0.112) are assigned to the main rock while the permittivity values of the core change based on the assumed mineral. The comparison is also performed at different core sizes. As displayed in Figure 3.11a, in terms of the smallest core size, when the strong microwave absorbing minerals are added to the model, there is no significant change in the average temperature of the whole sample, but the maximum temperature can increase by more than 30 K and 180 K when pyrite and magnetite are the mineral cores, respectively. Figures 3.11a and b show that increasing the core size can increase the maximum temperature up to 850 K and 1550 K when pyrite and magnetite are the core minerals, respectively. It should be mentioned that there is no significant change in the average temperature of the sample with the pyrite core; however, for the magnetite core, approximately a 10 K increase can be observed. Moving to a larger core size as shown in Figure 3.11a to b increases the maximum temperature. Figures 3.11b and c shows that increasing the core size does not always result in an increase in the temperature. For instance, the maximum and the average temperatures are decreased by 550 K and 9 K, respectively when the magnetite core size diameter increases from 15 mm to 20 mm. Figure 3.11 depicts a significant change in the temperature distribution in the sample after microwave treatment when the pyrite and magnetite cores are added. Overall, the temperature increase is more uniformly distributed throughout the sample when there is no mineral core, and it is more concentrated in the core when pyrite or magnetite are assumed in the model.

To further evaluate the effect of including microwave absorbing minerals in the rock, the electromagnetic field distribution in the cavity during microwave heating is investigated. As mentioned in Eq. (3.8), one of the main parameters affecting the heating rate during microwave irradiation in non-magnetic materials is the electric field intensity. Table 3.6 summarizes the minimum, maximum, and average electric fields in the cavity when the mineral core is added to the model in different sizes. It is evident that adding a mineral core to the material can drastically change the electric field intensity as there are major changes in the average and maximum electric field intensities in the cavity, which can be up to 17% in some cases. To further evaluate the effect of adding mineral cores on the electromagnetic distribution, the electric field intensities in the cross section of the numerical model for the whole cavity and the sample are shown in Figures 3.12 and 3.13, respectively. There is a significant effect for adding the mineral cores which drastically changes the electric field distribution in the cavity and the sample. The change in the electric field results in a change in the heating rate and temperature distribution. These data further support the results as depicted in Figure 3.11.

It should be noted that only the heat transfer and electromagnetic distribution equations are solved in the current model and the damage caused by microwave treatment in the model is not calculated. However, as shown in Figures 3.10 and 3.11, it is shown that when a mineral with high microwave energy absorption exists in the model, with the same energy input, a more significant and concentrated increase in temperature can be achieved. Thus, there will be a higher expansion rate and more cracks, resulting in a high strength reduction. This understanding is very important for mining engineers as the efficiency of the microwave-assisted rock fragmentation method can be much higher for heterogeneous rocks (especially when the rock constitutes microwave absorbing minerals) compared to homogeneous samples.

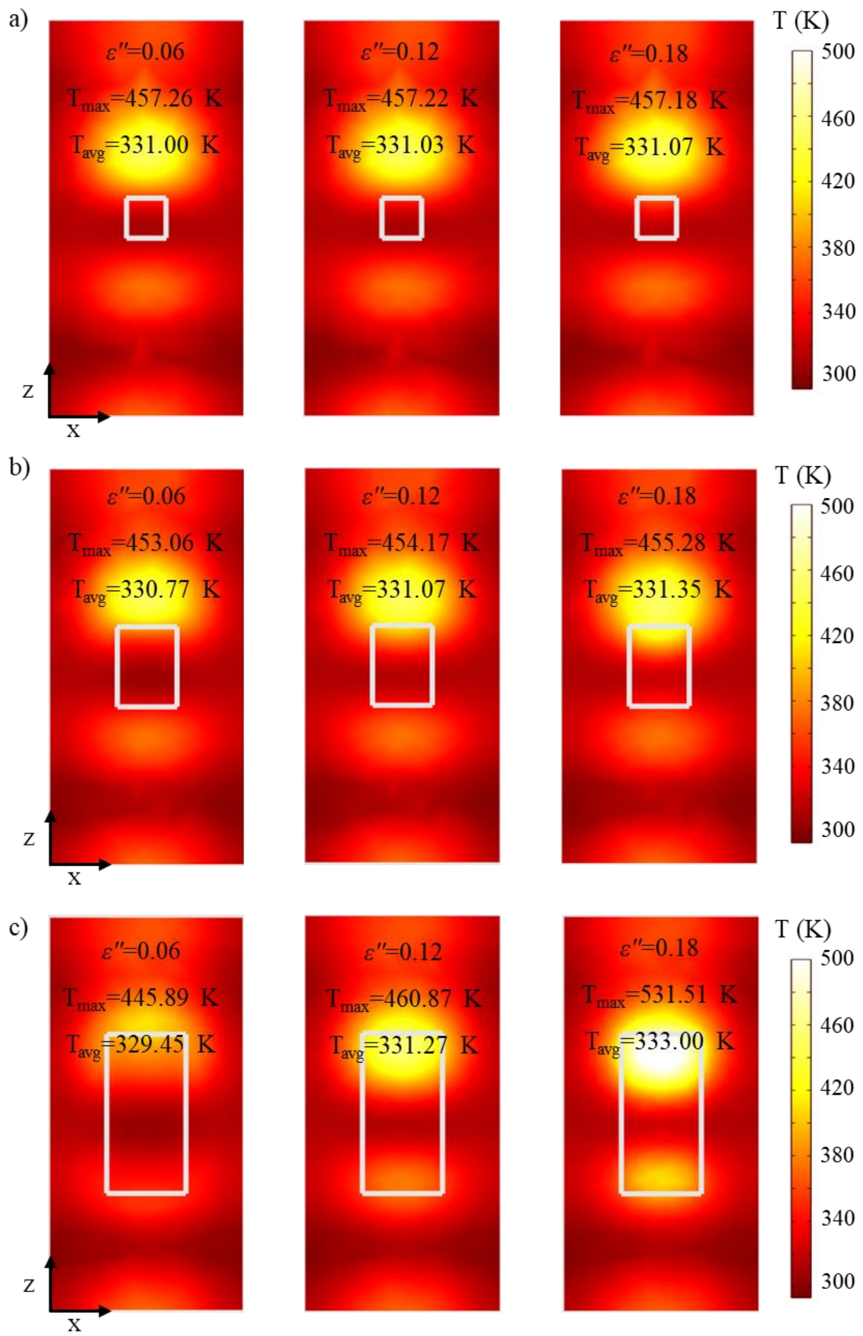

Figure 3.10. The effect of changing the imaginary part of the permittivity of the core while the average value is used for all the other parts of the sample considering three different core sizes with the diameters of (a) 10 mm, (b) 15 mm and (c) 20 mm.

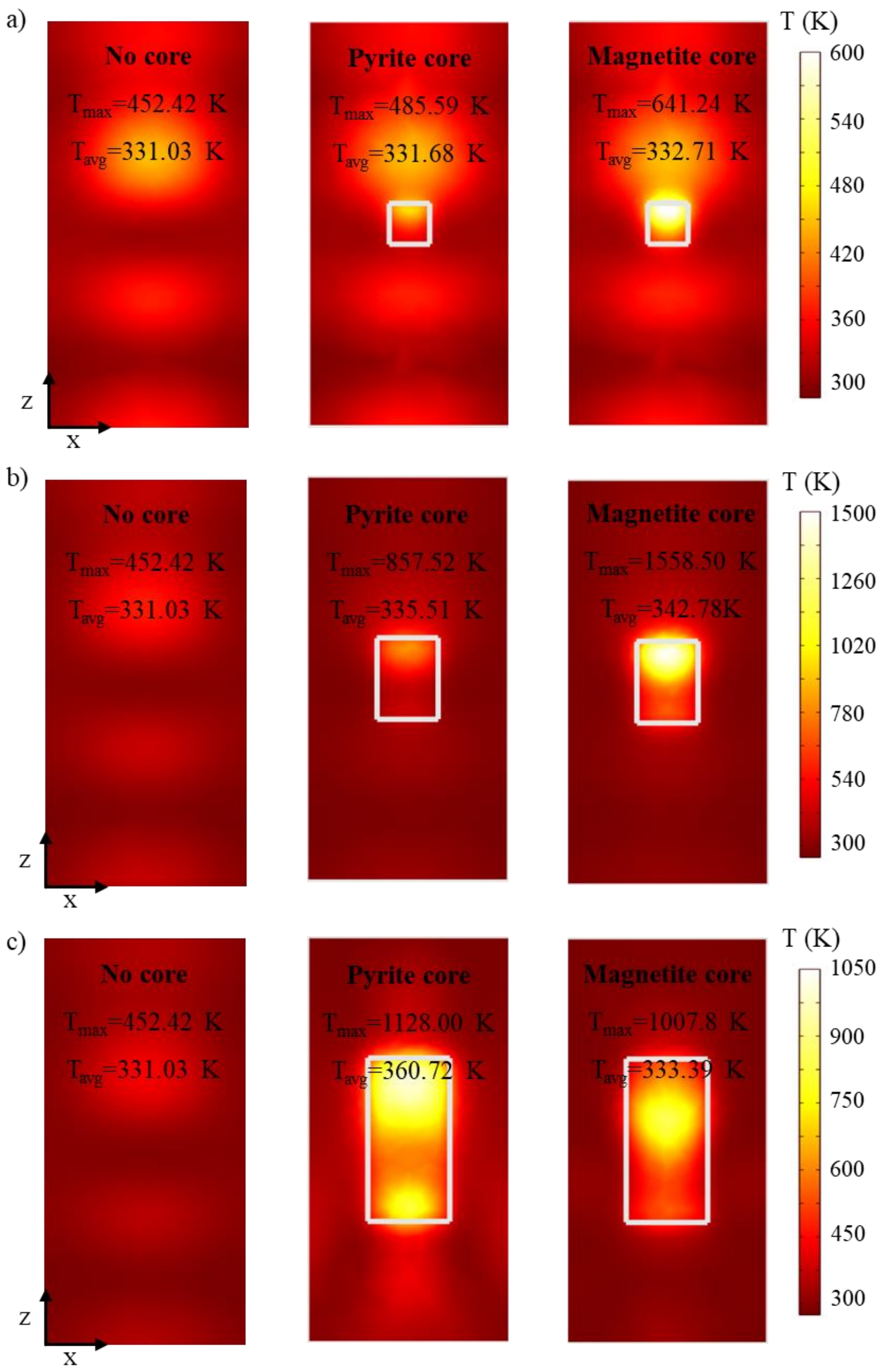

Figure 3.11 The effect of considering different core minerals inside the sample on the energy absorption and temperature distribution after microwave treatment for different core size with the diameters of (a) 10 mm, (b) 15 mm and (c) 20 mm.

Table 3.6 The average and maximum electric field intensities in the cavity.

Case	Electric field (10^5 V/m)	
	Average	Maximum
No core	1.3924	2.2483
Small pyrite core	1.3951	2.263
Small magnetite core	1.4051	2.307
Medium pyrite core	1.3889	2.3293
Medium magnetite core	1.4007	2.5559
Large pyrite core	1.6411	2.6909
Large magnetite core	1.3549	2.5394

3.6.Conclusions

This study evaluated different failure mechanisms of rocks due to microwave treatment. To understand the behaviors of the rhyolite rocks during microwave treatment, their relative permittivity is investigated using both coaxial probe and cavity perturbation methods. It is concluded that the coaxial probe method is simpler and faster to implement, while the cavity perturbation method can provide results with higher accuracy at different temperatures.

A novel experimental procedure is introduced to evaluate the failure of the samples affected only by microwave energy and without any external mechanical forces. It is concluded that the UCS-sized samples follow two patterns of distributed and concentrated heating due to microwave treatment. The heating patterns result in their related failure mechanisms. The concentrated heating failure mechanism is caused by a microwave absorbent mineral inside the sample. Concentrated heating failure has over 10 times higher efficiency compared to distributed heating having an average WOME value of 6.28 %/kW h/ton, which is the highest reported value in the literature for the UCS-sized samples.

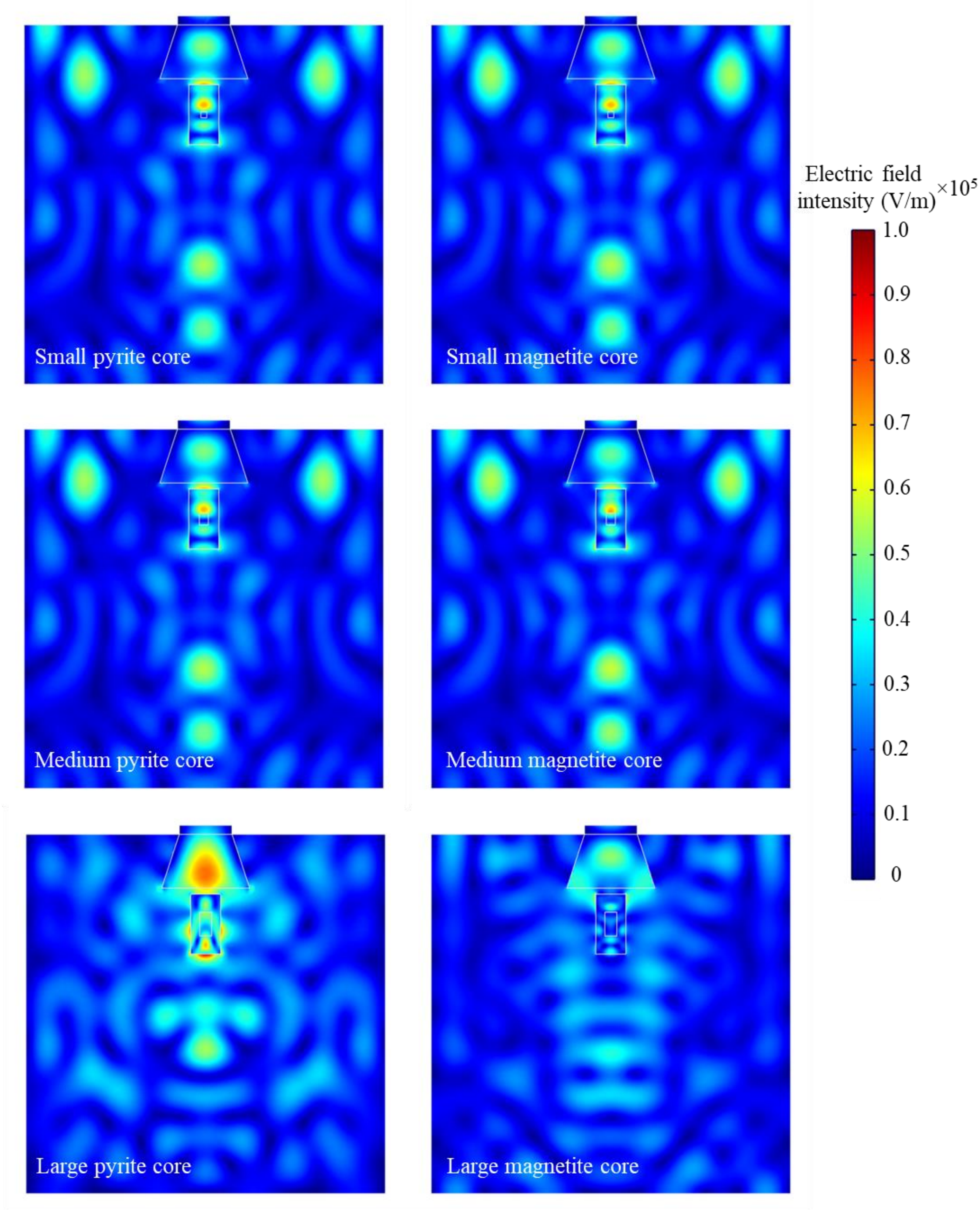

Figure 3.12 The electric field distribution in the cross section of the cavity after microwave radiation with a power of 3 kW.

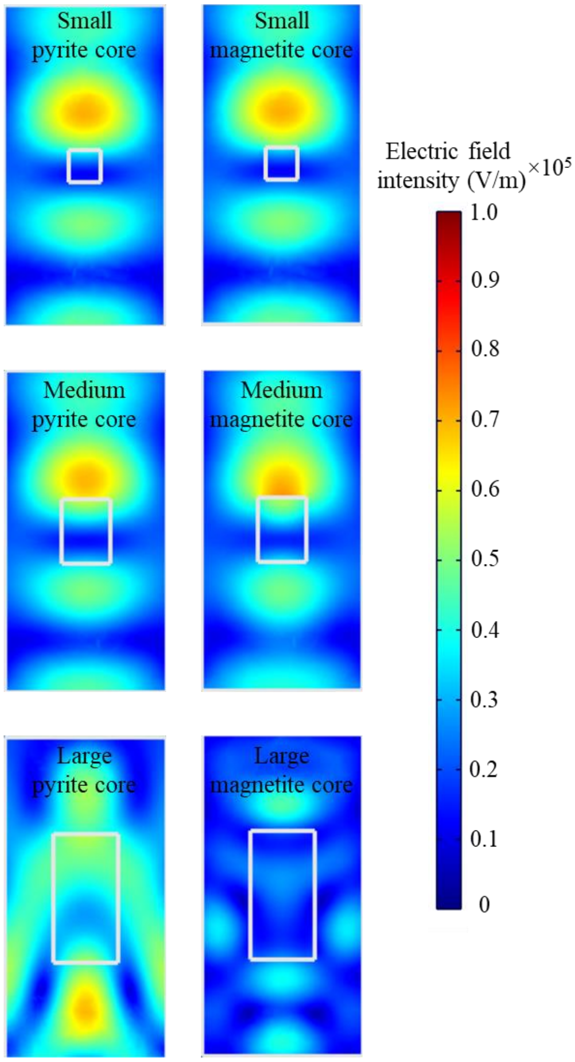

Figure 3.13 The electric field distribution in the cross section of the sample after microwave radiation with a power of 3 kW.

The developed numerical model is employed to further evaluate failure mechanisms caused by distributed and concentrated heating. It is shown that even a small heterogeneity in a rock such as a 0.12 difference in the ε_r'' of the mineral core can change the maximum temperature by over 85 K. Moreover, having a small microwave absorbing mineral core like magnetite or pyrite in the rock specimen can change the heat distribution drastically and create concentrated heating. In some cases, the maximum temperature of the sample is increased by more than 1000 K with the same input energy.

References

Ahmadihosseini, A., Shadi, A., Rabiei, M., Samea, P., Hassani, F., & Sasmito, A. P. (2022). Computational study of microwave heating for rock fragmentation; model development and validation. International Journal of Thermal Sciences, 181, 107746.

Ahmed, H. M., Hefni, M. A., Ahmed, H. A. M., Adewuyi, S. O., Hassani, F., Sasmitob, A. P., Saleem, H. A., Moustafa, E. B., & Hassan, G. S. A. (2022). Effect of Elevated Temperature on Rhyolitic Rocks' Properties. Materials, 15(9), 3204.

Ali, A. Y., & Bradshaw, S. M. (2009). Quantifying damage around grain boundaries in microwave treated ores. Chemical Engineering and Processing: Process Intensification, 48(11–12), 1566–1573.

Ali, A. Y., & Bradshaw, S. M. (2010). Bonded-particle modelling of microwave-induced damage in ore particles. Minerals Engineering, 23(10), 780–790.

Bai, G., Sun, Q., Jia, H., Ge, Z., & Li, P. (2021). Variations in fracture toughness of SCB granite influenced by microwave heating. Engineering Fracture Mechanics, 258, 108048.

Bisai, R., Palaniappan, S. K., & Pal, S. K. (2020). Influence of individual and combined pre-treatment on the strength properties of granite and sandstone. Arabian Journal of Geosciences, 13(1), 1–10.

Bobicki, E. R., Pickles, C. A., Forster, J., Marzoughi, O., & Hutcheon, R. (2020). High temperature permittivity measurements of selected industrially relevant ores: Review and analysis. Minerals Engineering, 145, 106055.

Chen, T. T., Dutrizac, J. E., Haque, K. E., Wyslouzil, W., & Kashyap, S. (1984). The relative transparency of minerals to microwave radiation. Canadian Metallurgical Quarterly, 23(3), 349–351.

D4543. (2019). Standard practices for preparing rock core as cylindrical test specimens and verifying conformance to dimensional and shape tolerances. ASTM International.

Hartlieb, P., Kuchar, F., Moser, P., Kargl, H., & Restner, U. (2018). Reaction of different rock types to low-power (3.2 kW) microwave irradiation in a multimode cavity. Minerals Engineering, 118, 37–51.

Hartlieb, P., Toifl, M., Kuchar, F., Meisels, R., & Antretter, T. (2016). Thermo-physical properties of selected hard rocks and their relation to microwave-assisted comminution. Minerals Engineering, 91, 34–41.

Hassani, F. (2010). Review of explosive-free rock breakage (EFRB) technologies. McGill University. Montreal, Canada, 450.

Hassani, F, Nekoovaght, P. M., Radziszewski, P., & Waters, K. E. (2011). Microwave assisted mechanical rock breaking. 12th ISRM Congress.

Hassani, Ferri, Shadi, A., Rafezi, H., Sasmito, A. P., & Ghoreishi-Madiseh, S. A. (2020). Energy analysis of the effectiveness of microwave-assisted fragmentation. Minerals Engineering, 159, 106642.

Hutcheon, R., Jong, M. de, & Adams, F. (1992). A system for rapid measurements of RF and microwave properties Up to 1400° C. Part1: theoritical development of the cavity frequency-shift data analysis equations. Journal of Microwave Power and Electromagnetic Energy, 27(2), 87–92.

Hutcheon, R., Jong, M. de, Adams, F., Wood, G., McGregor, J., & Smith, B. (1992). A System for Rapid Measurements of RF and Microwave Properties Up to 1400° C. Part 2: Description of Apparatus, Data Collection Techniques and Measurements on Selected Materials. Journal of Microwave Power and Electromagnetic Energy, 27(2), 93–102.

Jones, D A, Kingman, S. W., Whittles, D. N., & Lowndes, I. S. (2007). The influence of microwave energy delivery method on strength reduction in ore samples. Chemical Engineering and Processing: Process Intensification, 46(4), 291–299.

Jones, Dafydd Aled, Kingman, S. W., Whittles, D. N., & Lowndes, I. S. (2005). Understanding microwave assisted breakage. Minerals Engineering, 18(7), 659–669.

Kahraman, S., Canpolat, A. N., Fener, M., & Kilic, C. O. (2020). The assessment of the factors affecting the microwave heating of magmatic rocks. Geomechanics and Geophysics for Geo-Energy and Geo-Resources, 6(4), 1–16.

Keysight. (2017a). Basics of measuring the dielectric properties of materials— application note. http://literature.cdn.keysight.com/litweb/%0Apdf/5989-2589EN.pdf

Keysight. (2017b). Keysight 85070E dielectric probe kit 200 MHz to 50 GHz—technical overview. https://literature.cdn.keysight.com/%0Alitweb/pdf/5989-0222EN.pdf?id=364444

Li, J., Kaunda, R. B., Arora, S., Hartlieb, P., & Nelson, P. P. (2019). Fully-coupled simulations of thermally-induced cracking in pegmatite due to microwave irradiation. Journal of Rock Mechanics and Geotechnical Engineering, 11(2), 242–250.

Li, X., Wang, S., Xu, Y., Yao, W., Xia, K., & Lu, G. (2020). Effect of microwave irradiation on dynamic mode-I fracture parameters of Barre granite. Engineering Fracture Mechanics, 224, 106748.

Lu, G.-M., Feng, X.-T., Li, Y.-H., & Zhang, X. (2019). The microwave-induced fracturing of hard rock. Rock Mechanics and Rock Engineering, 52(9), 3017–3032.

Lu, G., Feng, X., Li, Y., & Zhang, X. (2020). Influence of microwave treatment on mechanical behaviour of compact basalts under different confining pressures. Journal of Rock Mechanics and Geotechnical Engineering, 12(2), 213–222.

Ma, D., Duan, H., Li, X., Li, Z., Zhou, Z., & Li, T. (2019). Effects of seepage-induced erosion on nonlinear hydraulic properties of broken red sandstones. Tunnelling and Underground Space Technology, 91, 102993.

Ma, D., Duan, H., Liu, J., Li, X., & Zhou, Z. (2019). The role of gangue on the mitigation of mining-induced hazards and environmental pollution: an experimental investigation. Science of the Total Environment, 664, 436–448.

Nejati, H., Hassani, F., & Radziszewski, P. (2012). Experimental investigation of fracture toughness reduction and fracture development in basalt specimens under microwave illumination. In Earth and Space 2012: Engineering, Science, Construction, and Operations in Challenging Environments (pp. 325–334).

Nekoovaght Motlagh, P. (2009). An investigation on the influence of microwave energy on basic mechanical properties of hard rocks. Concordia University.

Peinsitt, T., Kuchar, F., Hartlieb, P., Moser, P., Kargl, H., Restner, U., & Sifferlinger, N. (2010). Microwave heating of dry and water saturated basalt, granite and sandstone. International Journal of Mining and Mineral Engineering, 2(1), 18–29.

Pressacco, M., Kangas, J. J. J., & Saksala, T. (2022). Numerical Modelling of Microwave Heating Assisted Rock Fracture. Rock Mechanics and Rock Engineering, 55(2), 481–503.

Rostami, J., & Ozdemir, L. (1993). A new model for performance prediction of hard rock TBMs. Proceedings of the Rapid Excavation and Tunneling Conference, 793.

Salsman, J. B., Williamson, R. L., Tolley, W. K., & Rice, D. A. (1996). Short-pulse microwave treatment of disseminated sulfide ores. Minerals Engineering, 9(1), 43–54.

Samouhos, M., Taxiarchou, M., Hutcheon, R., & Devlin, E. (2012). Microwave reduction of a nickeliferous laterite ore. Minerals Engineering, 34, 19–29.

Shadi, A., Ahmadihosseini, A., Rabiei, M., Samea, P., Hassani, F., Sasmito, A. P., & Ghoreishi-Madiseh, S. A. (2022). Numerical and experimental analysis of fully coupled electromagnetic and thermal phenomena in microwave heating of rocks. Minerals Engineering, 178, 107406.

Toifl, M., Hartlieb, P., Meisels, R., Antretter, T., & Kuchar, F. (2017). Numerical study of the influence of irradiation parameters on the microwave-induced stresses in granite. Minerals Engineering, 103, 78–92.

Toifl, M., Meisels, R., Hartlieb, P., Kuchar, F., & Antretter, T. (2016). 3D numerical study on microwave induced stresses in inhomogeneous hard rocks. Minerals Engineering, 90, 29–42.

Wang, G., Radziszewski, P., & Ouellet, J. (2008). Particle modeling simulation of thermal effects on ore breakage. Computational Materials Science, 43(4), 892–901.

Wang, S., Li, X., Yao, J., Gong, F., Li, X., Du, K., Tao, M., Huang, L., & Du, S. (2019). Experimental investigation of rock breakage by a conical pick and its application to non-explosive mechanized mining in deep hard rock. International Journal of Rock Mechanics and Mining Sciences, 122, 104063.

Wang, Y., & Djordjevic, N. (2014). Thermal stress FEM analysis of rock with microwave energy. International Journal of Mineral Processing, 130, 74–81.

Whittles, D. N., Kingman, S. W., & Reddish, D. J. (2003). Application of numerical modelling for prediction of the influence of power density on microwave-assisted breakage. International Journal of Mineral Processing, 68(1–4), 71–91.

Xu, T., He, L., Zheng, Y., Zou, X., Badrkhani, V., & Schillinger, D. (2020). Experimental and numerical investigations of microwave-induced damage and fracture formation in rock. Journal of Thermal Stresses, 44(4), 513–528.

Yuan, Y., Shao, Z., Qiao, R., Fei, X., & Cheng, J. (2020). Thermal response and crack propagation of mineral components in olivine basalt under microwave irradiation. Arabian Journal of Geosciences, 13(14), 1–11.

Zheng, Y. L., Zhao, X. B., Zhao, Q. H., Li, J. C., & Zhang, Q. B. (2020). Dielectric properties of hard rock minerals and implications for microwave-assisted rock fracturing. Geomechanics and Geophysics for Geo-Energy and Geo-Resources, 6(1), 1–17.

Zheng, Y., Ma, Z., Zhao, X., & He, L. (2020). Experimental investigation on the thermal, mechanical and cracking behaviours of three igneous rocks under microwave treatment. Rock Mechanics and Rock Engineering, 53(8), 3657–3671.

"Which would be worse - to live as a monster, or to die as a good man?"

Teddy Daniels- Shutter Island

Chapter 4: Investigating microwave treatment of rocks based on fracture mechanics analysis in mode I fracture toughness test

4.1. Preface

The previous chapter demonstrated how a numerical model can improve understanding of the physics underlying microwave treatment of the rock samples. As fracture mechanics characteristics are integral to every rock, this chapter extends the previous work by utilizing the developed numerical model to optimize microwave treatment efficiency, with fracture toughness alteration being the evaluation criterion. Building upon the insights gained in the previous chapter, the numerical model is used to further investigate the impact of microwave treatment on rocks' fracture toughness. By employing an energy efficiency-based approach in conducting experiments, this section aims to achieve two objectives: firstly, to gain a deeper understanding of the current efficacy of microwave treatment in field applications, and secondly, to utilize the numerical model as a tool for enhancing experimental outcomes.

4.2. Abstract

During the past decade, numerous research has been conducted to evaluate the effectiveness of microwave treatment in improving rock fragmentation. While these studies focused on investigating the effect of microwave treatment on rock parameters, the current research approaches the problem from another perspective by studying the applicability of mode I fracture toughness parameters to evaluate the effectiveness of the microwave treatment as a

rock pre-conditioning method based on energy analysis. Different rock sizes are investigated, and it is shown that for the basalt rock used in this study, the minimum required diameter for the fracture toughness experiments is 70 mm. In a novel approach, a finite element based numerical model is employed to maximize the energy absorption of the sample in the cavity. It is shown that optimizing the location of the rock sample in the cavity can increase the heat over microwave efficiency (HOME) and weakening over microwave energy (WOME) by more than 40% and 30%, respectively. Furthermore, it is concluded that although increasing the exposure time results in more K_{IC} value reduction, it decreases the WOME value by more than 50% in some cases. Finally, the applicability of fracture toughness experiments in evaluating the effectiveness of microwave treatment is discussed in detail.

Keywords: Numerical simulations; Mode I fracture toughness; Microwave treatment; Failure mechanism; Energy efficiency

4.3. Introduction

There are varieties of applications for the microwave treatment in the mining industry including but not limited to heating the ore body to differentiate waste from ore for sorting purposes (Deyab et al., 2021; Hassani et al., 2016; G. M. Lu et al., 2016), strength reduction of the rocks to improve the rock excavation efficiency, and creating micro-cracks to enhance the energy efficiency of the comminution part of the mining processes (Deyab et al., 2020; Hassani et al., 2020; Kingman et al., 2004). The advantages of microwave treatment of rocks in the mining industry originate from the mineral-based composition of rock materials. Different minerals in the rock have different thermal expansion and heating rates when irradiated by microwave energy which causes differential volume change of the minerals within the rock. This phenomenon creates thermal stresses between the rock mineral particles and leads to the generation of micro-cracks and therefore, the weakening of the rocks. The microwave-treated rocks are easier to excavate through due to their reduced strength which results in potentially more efficient excavation, comminution, and equipment maintenance (Hassani, 2010; G. M. Lu et al., 2016; Scott, 2006).

Multiple studies have been conducted to evaluate the effect of microwave irradiation on the mechanical properties of rocks. These studies focused on different factors affecting the effectiveness of the microwave treatment method such as microwave power (e.g. Deyab et al., 2021), exposure time (e.g. Hassani et al., 2011), rock types (e.g. granite and kimberlite in Deyab et al., 2021; basalt in Lu et al., 2019; red sandstone in Yao et al., 2021; gabbro Zheng et al., 2017), cooling rate (e.g. Rafezi et al., 2020), and rock water content (e.g. Peinsitt et al., 2008). The central focus of the literature was to evaluate the change in the mechanical properties of the rocks gathered from well-known and easy to implement experiments, such as uniaxial compressive strength (UCS), and Brazilian tensile strength (BTS) tests, after the treatment to investigate the effectiveness of the method. For instance, Hassani et al. (2016) and Lu et al. (2019) evaluated the effect of microwave treatment on the reduction of UCS in basalt samples. They emphasized how microwave treatment could be a potential method to improve rock excavation. Although in many studies, researchers have reported a significant strength reduction after the treatment, in some cases the effect of microwave treatment has been less promising. Researchers addressed this issue by increasing the microwave power density (Dafydd Aled Jones et al., 2005). One significant aspect missing in these studies is understanding the crack propagation effects and the change in the failure mechanism of the rocks before and after the treatment which can justify observing a less efficient pre-conditioning response. According to Chang et al. (2002), crack propagation is the main reason for the failure of quasi-brittle materials such as rocks, and fracture toughness is an essential parameter in this regard, providing useful information for rock failures. Performing complex experiments such as determination of fracture toughness requires following certain failure mechanisms to be accepted by the standards (Kuruppu et al., 2014). Regardless of its complexity, however, determination of fracture toughness is an essential experiment since it provides data for the rock parameters that researchers cannot gather from other simpler and more widely used experiments such as UCS determination (Whittaker et al., 1992). Furthermore, the results gathered from fracture toughness experiments can be widely used for the interpretation of geological features, stability analysis, and also modeling of the fracture process in rocks (Ouchterlony, 1988).

In the field of rock mechanics, fracture toughness refers to the ability of a rock to resist fracturing and crack diffusion (Feng et al., 2017). The parameter that describes the intensity of stress at the tip of the crack is called the stress intensity factor. Different modes of fracture toughness are defined based on the orientation of the applied stress in relation to the fracture which is categorized under three different modes: mode I, II, and III (Kuruppu et al., 2014). Currently, mode I is the most advanced and popular mode in use (Callister Jr & Rethwisch, 2020). The International Society of Rock Mechanics (ISRM) has suggested several testing methods for determining the mode I fracture toughness of rocks. These methods include Chevron Bending (Iqbal & Mohanty, 2007; Ouchterlony, 1988), Short Rod (Ouchterlony, 1989), Cracked Chevron Notched Brazilian Disc (CCNBD), and Notched Semi-Circle Bend (NSCB) (Fowell et al., 1995). The latter method is recommended for measuring mode I fracture toughness of rocks due to its simpler geometry structure, and the preparation process (Kuruppu et al., 2014).

Researchers have studied the effect of heating on the fracture toughness of rocks. For example, Yin et al. (2020) used the Cracked Straight Through Brazilian Disc method to study the effect of high-temperature treatment on the mixed-modes I+II of biotite granite samples. Their study indicated that increasing the temperature affects both the mixed-mode fracture toughness values and the fracture initiation angle. In an earlier study, Nasseri et al. (2007) used the CCNBD method to study the effect of thermal damage on mode I fracture toughness of granite rocks. The results demonstrated that the mechanical strength and dynamic elastic properties of the rock decreased after the heat treatment. In another related work, Peng et al. (2020) used the NSCB method to examine the effect of various temperatures on mode I fracture toughness and fracture energy for granite rocks at different burial depths. The results of these tests revealed that fracture toughness and fracture energy decrease as the temperature increases. In recent years, there have been more studies investigating the effect of microwave treatment on fracture toughness and fracture energy of rocks. For instance, Li et al. (2021, 2020) used the NSCB method and found that fracture toughness of granite decreased with the increase in the microwave exposure time. All these studies are focused on the effect of microwave treatment on the fracture energy and fracture toughness values without considering the failure mechanism and fracture propagation in different modes of the fracture toughness tests.

All the aforementioned studies employed an experimental approach to address the research questions regarding the effectiveness of temperature and microwave treatment on rock fragmentation. While the experimental approach provides close to reality and field observations, they are time-consuming and expensive to conduct. Additionally, the lack of appropriate numerical models with proper verification and validation discouraged the researchers and engineers from employing numerical simulations to improve the experimental results. Recent advancements in numerical methods have created a major improvement in the applicability of the numerical models in evaluating the effectiveness of the microwave treatment (Lan et al., 2020; Toifl et al., 2017). These advancements resulted in validated and verified numerical models that are capable of predicting the behaviour of rocks during microwave irradiation (Ahmadihosseini et al., 2022; Shadi et al., 2022). Using these models provides researchers with the opportunity to improve the efficiency of the microwave treatment as a rock pre-conditioning method and reduce the potential cost of conducting numerous experiments.

The novelty of the current research to address the knowledge gap in this field is taking into account the complications that are added to the rock failure mechanisms in mode I fracture toughness due to microwave treatment. Moreover, for the first time, the previously developed and validated numerical models are successfully utilized to improve the efficiency of the microwave treatment as a rock pre-conditioning method. Using the numerical model has reduced the number of experiments required to achieve conclusive remarks. Furthermore, all the data analysis has been conducted with an energy based approach to improve the understanding of researchers on the energy efficiency of the microwave treatment of rocks.

4.4. Methodology

4.4.1. Experimental procedure

4.4.1.1. Sample preparation

The test samples for this study are basalt rocks received in the form of intact blocks from quarries located in Chifeng, China. The intact blocks of basalt are drilled at the McGill Geomechanics laboratory using a radial drilling machine to obtain cylindrical core samples with diameters of 50, 70, and 100 mm. The cylindrical samples are cut into disks with thickness of 20, 30, and 40 mm for the cores with the smallest to the largest diameters, respectively, using a wet diamond saw. Both ends of the samples were then ground and flattened using a diamond wheel grinder machine. Afterward, the disk samples are cut into two halves with semi-circular shapes and then a notch was created using the wet diamond saw (Figure 4.1a). All the dimensions follow the ISRM suggested method and are detailed in Table 4.1.

4.4.1.2.Test procedures

- Microwave treatment

An industrial microwave system with a frequency of 2450 MHz and a controllable power ranging from 0 to 15 kW with a TE_{10} radiation mode is utilized for the microwave treatment experiments (Figure 4.1b). After each experiment, the samples are put inside a calorimeter to measure the energy absorption of the sample during the microwave treatment. By calculating the absorbed energy, the heat over microwave efficiency (HOME) can be measured as follows (Hassani et al., 2020):

$$\text{HOME } (\%) = \frac{\text{Absorbed energy during microwave treatment}}{\text{Total energy used for treatment}} \times 100 \tag{4.1}$$

a) b)

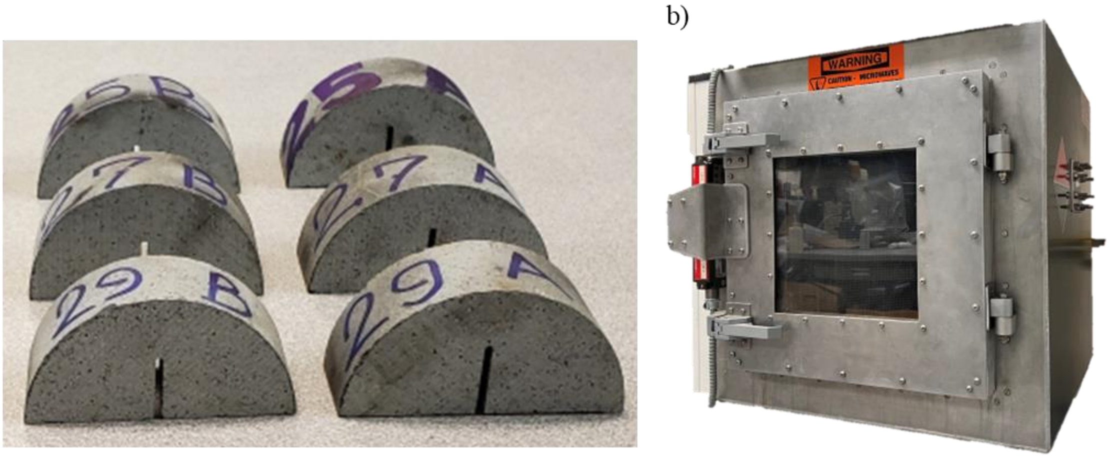

Figure 4.1 a) The samples prepared for the fracture toughness experiment, and b) the cavity used for the microwave treatment experiments.

Table 4.1 The specifications of the dimensions of the samples used for the fracture toughness tests in the study.

Parameter	Symbol	Value (mm)		
Diameter	D	50	70	100
Thickness	B	21	30	40
Crack length	a	11	20	29
Span length	s	39	45	65

- Fracture toughness

The main focus of the current study is to evaluate the effectiveness of microwave treatment as a rock pre-conditioning method based on mode I fracture toughness characterization. To achieve this goal, the fracture toughness of the samples is measured before and after the treatment. A specific apparatus consisting of three cylindrical rods are designed and placed on a Humboldt compression machine for the fracture toughness measurements (Figure 4.2). For each test, the sample is placed between the rods which apply force in three different locations of the sample to represent mode I fracture toughness. The experiments follow a displacement-controlled testing procedure in which the bottom plate (bottom rods) moves upwards at a constant rate of 0.5 mm/min. The displacement data is captured using an external Linear Variable Differential Transformer (LVDT) in every 1 s time step. Furthermore, the applied forces are recorded using a load cell that is connected to the top rod. The force values are then used in Eq. (4.2) to calculate the K_{IC} value (critical K value in mode I) as follows:

$$K_{IC} = Y' \frac{P_{max}\sqrt{\pi a}}{2RB} \tag{4.2}$$

where P_{max} is the maximum load at the failure, R is the radius of the sample, and Y' is the dimensionless stress intensity factor which is calculated as follows:

$$Y' = -1.297+9.516\left(\frac{s}{2R}\right)-\left(0.47+16.457\left(\frac{s}{2R}\right)\right)\beta+(1.071+34.401\left(\frac{s}{2R}\right))\beta^2 \tag{4.3}$$

where β=a/R. Also, to evaluate the efficiency of the microwave treatment as a rock pre-conditioning method, a parameter introduced by Hassani et al. (2020) named Weakening Over Microwave Energy (WOME) is utilized. In this study this parameter is defined based on the input and absorbed energy as follows:

$$WOME_{Absorbed} = \frac{\text{Percentage of } K_{IC} \text{ reduction}}{\text{Absorbed energy/mass}} \tag{4.4}$$

$$WOME_{Input} = \frac{\text{Percentage of } K_{IC} \text{ reduction}}{\text{Input energy/mass}} \tag{4.5}$$

The results of this paper make a comparison between WOME and K_{IC} reduction due to microwave treatment. One of the main applications of microwave treatment of rocks, which is also the main focus of the present study, is to achieve a more efficient excavation process. The main superiority of WOME over the K_{IC} value is the inclusion of the energy input in the parameter calculations, which makes it possible to observe how much reduction in the K_{IC} is achieved considering the amount of energy used in the form of microwave irradiation. In other words, WOME analysis makes it possible to analyse whether the microwave energy applied can efficiently enhance a reduction in the K_{IC} value.

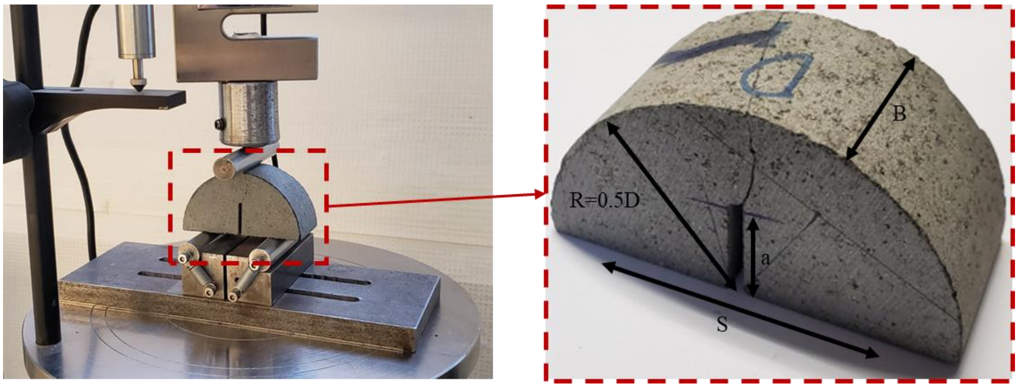

Figure 4.2 The specifications of the sample and the apparatus for the fracture toughness test.

This study conducted more than 150 mode I fracture toughness experiments on both treated and untreated samples over the range of sample diameters and thicknesses manufactured to provide at least three repeats that are acceptable based on the ISRM suggested method for fracture toughness in each test specification. Unacceptable results were caused by several reasons the most important of which were fractures not propagating in the correct direction and the early failure of the samples before the fracture toughness experiment could be conducted due to microwave treatment and heating fracture damage.

4.4.2. Numerical procedure

This study utilizes the previously developed numerical model introduced by Ahmadihosseini et al. (2022) to optimize the efficiency of the microwave treatment as a rock pre-conditioning method. This section provides a brief explanation of the governing equations, boundary conditions, and the general description of the model. The readers are referred to Ahmadihosseini et al. (2022) for detailed information.

4.4.2.1. Equations and assumptions

In this study, the numerical model is developed based on the following assumptions:

- The basalt rock samples are homogeneous.
- The microwave energy is radiated through the port with TE_{10} radiation mode.
- The aluminium surfaces of the cavity are perfect electric conductors.
- The time harmonic form of Maxwell's equations is valid to capture the electromagnetic field distribution in the cavity.
- Basalt surfaces have heat loss due to convection with a heat loss factor of 300 W/(m^2.K) due to exposure to air during the microwave treatment (Shadi et al., 2022).

Based on the aforementioned assumptions, Eqs. (4.6) and (4.7) are implemented to capture electromagnetic field distribution and heat transfer, respectively, as follows:

$$\nabla\times\left(\mu_r^{-1}\nabla\times\mathbf{E}\right)-\mathrm{k}_0^2\left(\varepsilon_r-\frac{i\sigma}{\omega\varepsilon_0}\right)\mathbf{E}=0 \tag{4.6}$$

$$\rho\mathrm{C}\frac{\partial\mathrm{T}}{\partial\mathrm{t}}+\nabla.(-\mathrm{k}\nabla\mathrm{T})=\mathrm{Q} \tag{4.7}$$

where, $\mathbf{E}$ is the electric field intensity, σ is the electrical conductivity, ω is the angular frequency, ε_r is the relative permittivity, μ_r is the relative permeability, k_0 is the wavenumber in the free space, ρ is the density, C is the heat capacity, T is the temperature, k is the thermal conductivity, and Q is the heat source. Eqs. (4.6) and (4.7) are related by implementing Eq. (4.8) to calculate the heat source created based on the microwave heating as follows:

$$\mathrm{Q}=\omega\varepsilon_0\varepsilon_r''\,\bar{\mathbf{E}}^2+\omega\mu_0\mu_r''\,\bar{\mathbf{H}}^2 \tag{4.8}$$

where ε_r'' and μ_r'' are the imaginary parts of the relative permittivity and permeability, respectively, and $\mathbf{H}$ is the magnetic field intensity.

4.4.2.2. Model description

The geometry of the numerical model needs to be designed based on the experimental setup to represent the microwave treatment experiments. Therefore, the exact dimensions of the experimental cavity are measured and implemented for designing the geometry. The details are depicted in Figure 4.3a which shows the internal and external aluminium boundaries in silver and white, respectively, and the sample in brown. This study evaluates two different approaches for preparing mode I fracture toughness testing specimens from intact cylinders. In the first approach, the cylindrical samples are cut after the microwave treatment while in the second approach the samples are treated after the cutting process. Three different geometry designs are considered to evaluate the energy absorption of the sample during the treatment and provide a comparison between the two approaches (Figure 4.3c). For the samples that are cut before the microwave treatment (geometry designs 2 and 3) the considered space between the two half cylinder parts is 1 mm and the thickness of the notch is 1.7 mm. The model has an initial temperature of 293.15 K with zero electric and magnetic fields. Furthermore, the basalt rock parameters have been measured in the previous studies and are used here as the inputs for the numerical model (Table 4.2) (Ahmadihosseini et al., 2022).

To discretize the geometry of the model, 3D tetrahedral elements are used. In order to choose the right size for the elements, a mesh independency study is performed. For all the cases shown in Figure 4.4, the sample is treated with a microwave power of 3 kW and an exposure time of 4.35 s. Figure 4.4 depicts the absorbed energy of the samples with different sizes versus the number of meshes used to discretize the model. It is observed that the samples with smaller sizes are more sensitive to the mesh size. The details of the final meshing system used in this study that ensures the independence of the numerical model from mesh sizes for all the different sample sizes are provided in Table 4.3. Furthermore, in Figure 4.5, the final mesh is depicted for the different parts of the geometry.

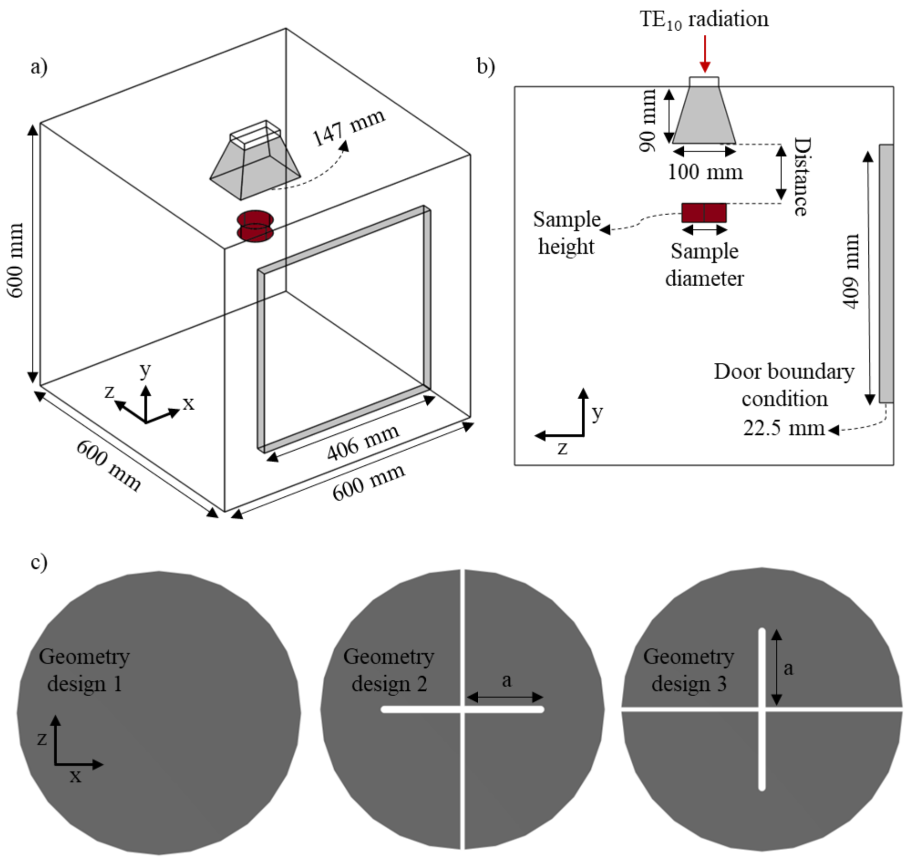

Figure 4.3 The geometry of the numerical model used to evaluate the energy absorption of the sample during microwave treatment in a) isometric view, b) yz plane view and c) different sample geometry designs to represent two approaches of cutting the sample before and after the microwave treatment.

Table 4.2 The rock parameters used as the input for the numerical model (Ahmadihosseini et al., 2022).

Parameter	Symbol	Value	Unit
Thermal conductivity	k	1.59	W/(m.K)
Density	ρ	2870	Kg/m^3
Heat capacity	C	840	J/(kg.K)
Relative permittivity	ε_r	10-1.1j	1
Relative permeability	μ_r	1	1
Electrical conductivity	σ	5×10^{-5}	S/m

Table 4.3 The final parameters of the meshing system used for the simulations of the study.

Parameter	Sample	Cavity	Unit
Maximum element size	5	13.00	mm
Minimum element size	0.12	0.12	mm
Maximum element growth rate	1.3	1.3	1
Curvature factor	0.2	0.2	1

4.5. Results and discussion

4.5.1. Effect of sample size

According to the ISRM suggested method, there is no definitive requirement for the size of the samples for mode I fracture toughness measurement using the NSCB method (Kuruppu et al., 2014). The suggested procedure to find the appropriate size includes measuring the K_{IC} for different sample diameters. K_{IC} converges to a certain value as the diameter of the sample increases. The minimum required diameter should be chosen as the smallest diameter that leads to a K_{IC} consistent with the converged value. In this study, the same procedure is followed by comparing the measured K_{IC} value of the untreated basalt for three different sample diameters: 50, 70, and 100 mm. Table 4.1 provides detailed information on the size specifications of the samples. The results of the K_{IC} values at different sample diameters are shown in Figure 4.6. It can be observed that the samples with diameters of 50 mm have the highest standard deviation (STD) with a value of 0.11 MPa.m$^{0.5}$. The average K_{IC} for this size is 1.30 MPa.m$^{0.5}$ while this value for samples with diameters of 70 mm and 100 mm is 1.26 MPa.m$^{0.5}$ with an STD of less than 0.03 MPa.m$^{0.5}$. In other words, the sample with a diameter of 70 mm is the smallest size in this study that has a K_{IC} value consistent with the final converged value. Therefore, the samples with diameters of 70 mm are chosen as the acceptable diameter for the rest of the NSCB mode I fracture toughness experiments in this study.

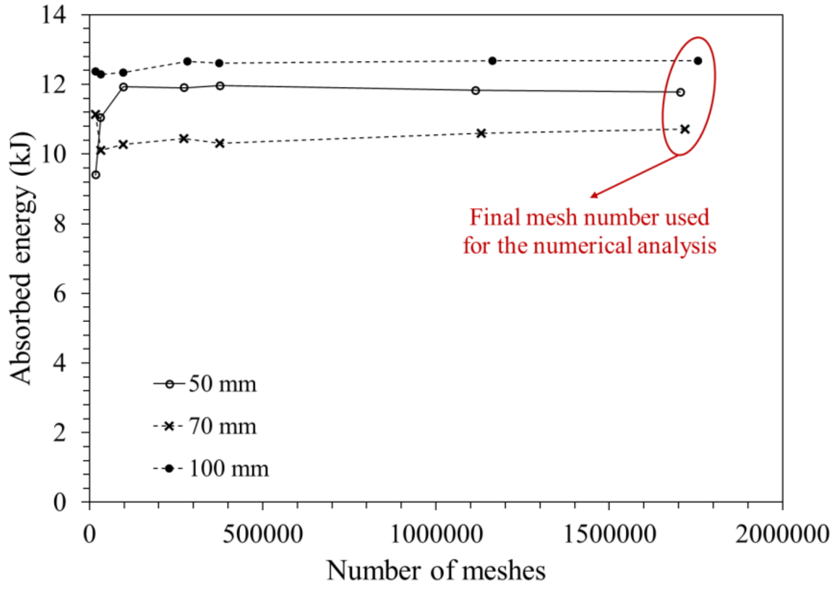

Figure 4.4 The result of the mesh independency analysis for the samples with different sizes.

4.5.2. Validation and verification

The developed numerical model used in this study has been previously validated and verified in previously published work. For the complete detail regarding the model's validity, the readers are referred to Ahmadihosseini et al. (2022). The focus of the current study in the following sections is to utilize the developed numerical model to increase the energy efficiency of the microwave treatment of rocks as a rock pre-conditioning method. However, in this section, to showcase the reliability of the numerical model in representing the experimental data, a comparison is made between the numerically and experimentally captured temperature distribution data after the microwave treatment. A full cylindrical sample with a diameter of 70 mm that is used for the fracture toughness experiment is radiated with a microwave power of 3 kW and an exposure time of 4.35 s located at a 15 mm distance from the antenna. Figure 4.7 depicts the temperature distribution on the sample after microwave irradiation for both the numerical model and the experiment. The results emphasize the accuracy of the numerical model in representing the physical phenomena involved in the experiment by correctly capturing the temperature distribution in the sample after the microwave treatment.

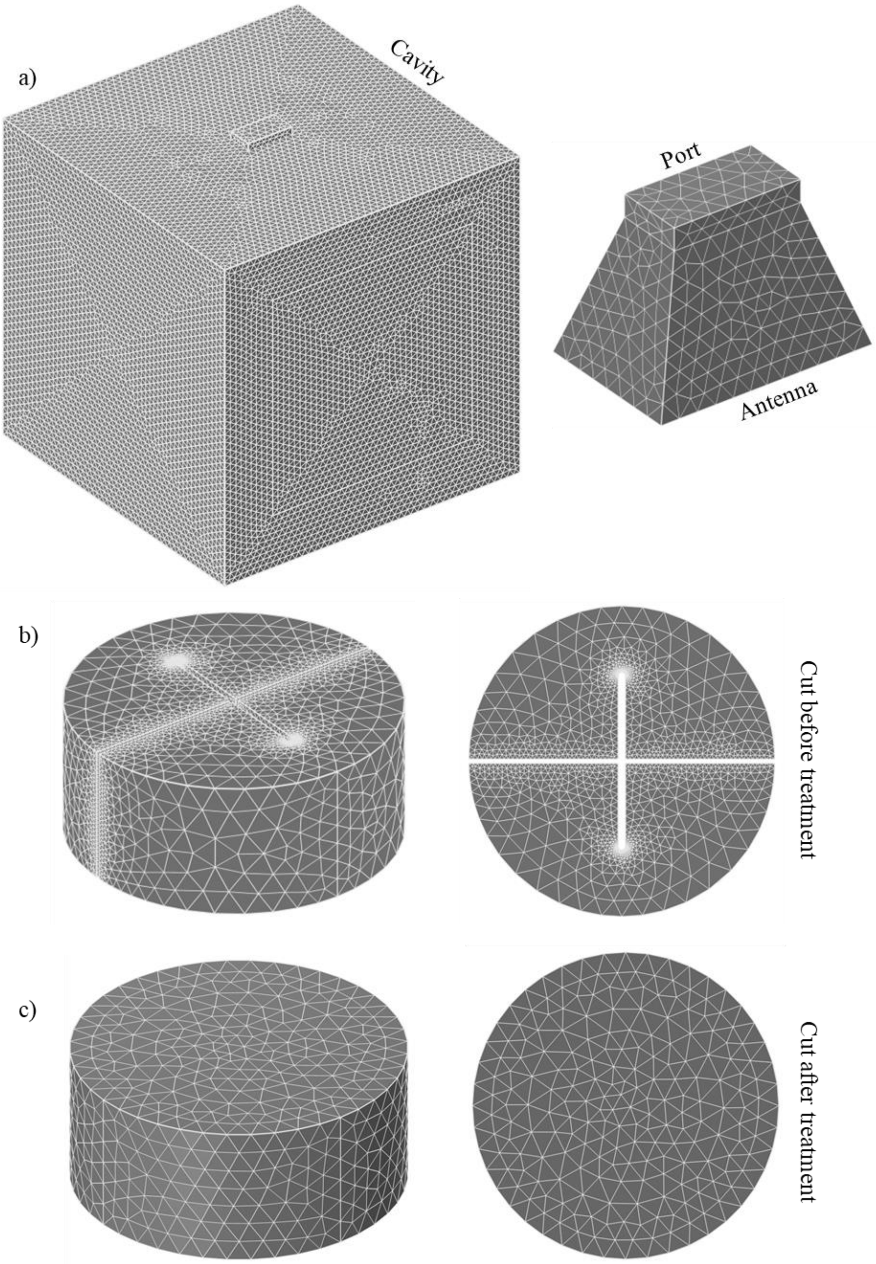

Figure 4.5 The final mesh used for the numerical simulations for a) cavity, port and the waveguide, b) samples that are cut before the treatment, and c) samples that are cut after the treatment.

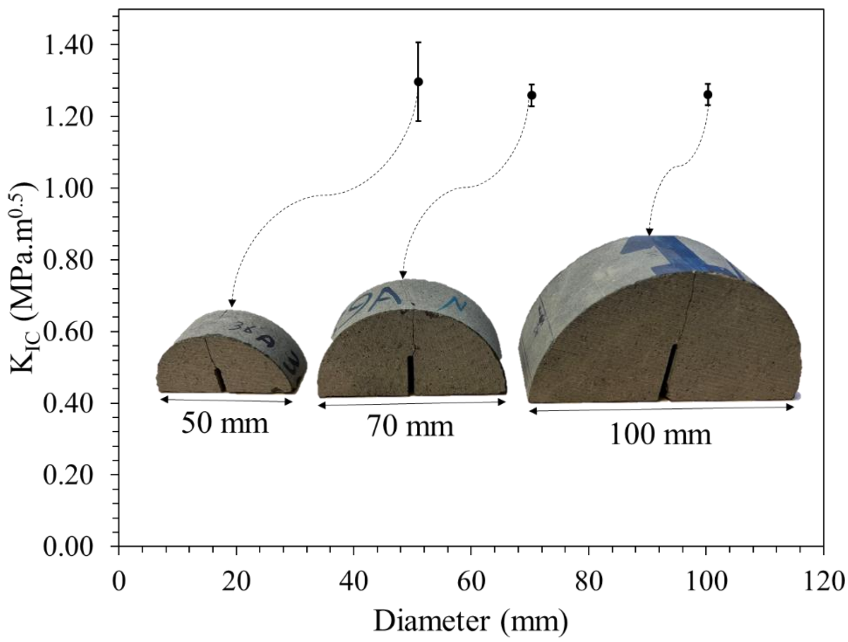

Figure 4.6 The experimentally measured K_{IC} and its STD in different sample diameters for the basalt used in this study.

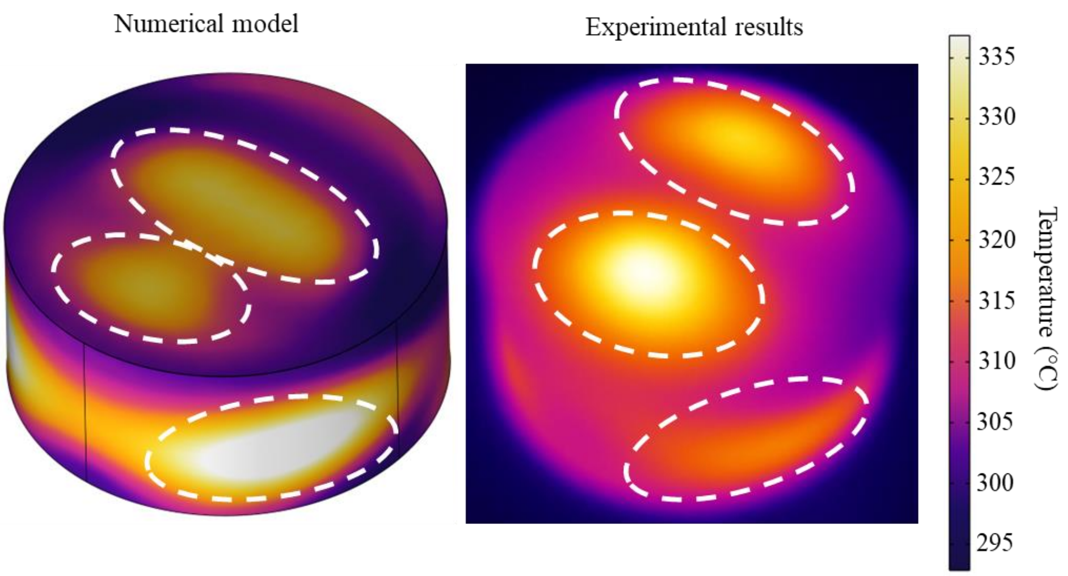

Figure 4.7 The comparison between the temperature distribution captured in the experiment and the numerical model after microwave treatment with a power of 3 kW and an exposure time of 4.35 s.

4.5.3. *Optimising the energy absorption*

The importance of microwave energy absorption in achieving better microwave assisted fragmentation of rock has been previously emphasized by Hassani et al. (2020). It was shown that in the same test specifications, achieving a higher HOME led to a higher WOME resulting in a better microwave treatment efficiency. In this section, with a novel approach, the previously developed and validated numerical model explained in Section 4.2.2 is utilized to analyse the energy absorption of the samples at different locations of the cavity to potentially improve HOME during microwave treatment experiments. For the numerical simulation, the samples are treated with a microwave power of 3 kW and for an exposure time of 4.35 s. The geometry of the numerical model is changed to represent the placement of the sample at different distances from the antenna, different sample sizes, and cutting before and after the microwave treatment.

The energy absorption of the samples during microwave treatment is evaluated at different distances from the antenna (Figure 4.8a). The comparison between the charts representing different sample sizes illustrates that the largest sample sizes have the highest HOME value among the three sizes. Furthermore, the dependence of the HOME value on distance is more significant when the sample sizes are smaller. For instance, 50 mm diameter samples absorb approximately 90% of the input energy when placed at a distance of 15 mm from the antenna but this value significantly reduces to less than 45% when they are placed at a 75 mm distance. This trend is different for the 100 mm diameter samples as the difference between the minimum and maximum HOME when the samples are located at different distances is less than 10%. Changing the sample size not only changes the maximum and minimum values of the energy absorption but also highly affects the locations at which these optimum values are achieved. For example, the minimum energy absorption for the samples with diameters of 50 mm, 70 mm, and 100 mm is achieved at 75 mm, 95 mm, and 35 mm distances from the antenna, respectively. Disregarding the effect of sample size can highly affect the microwave treatment efficiency as a distance that results in a high energy absorption for one size could lead to a low energy absorption for another size. An example of this is shown by the comparison between 70 mm and 100 mm diameter samples at a 75 mm distance from the antenna which leads to low and high energy absorption for the former and the latter, respectively. In this study, based on Section 4.3.1, the selected diameter of the samples for the experiments is 70 mm. According to Figure 4.8, for this sample size, the maximum HOME is achieved at 15 mm and 55 mm distances with an approximate HOME value of 80%. In this study, to minimize the effect of spacers used to place the sample at different locations in the cavity, the samples are hung from the antenna using a thin plastic non-microwave absorbent band. The sample is more stable on the plastic band when it is closer to the antenna. The further the sample is placed from the antenna, the harder it is to stabilize its location. Therefore, between 15 mm and 55 mm distance from the antenna, the shorter distance position was chosen for the microwave treatment experiments in order to minimize sample instability during testing.

To further evaluate the development of electromagnetic field and temperature conditions in the sample due to microwave treatment, the electric field intensity magnitude and temperature are integrated within the sample volume using Eqs (4.9) and (4.10) as follows:

$$E_{Integral}=\iiint \bar{\mathbf{E}}dV \tag{4.9}$$

$$T_{Integral}=\iiint TdV \tag{4.10}$$

Furthermore, the STD of each parameter is calculated and drawn alongside their respective integration within the volume at different distances in Figures 4.8b and c. The comparison between the two figures shows that the variation of $E_{Integral}$ at different distances is smaller as compared to $T_{Integral}$. This fact can be further scrutinized by evaluating the relative calculated STD of each parameter at different distances which shows that overall, at all the distances, the temperature chart shows a larger STD. This fact can be justified by delving into Eqs. (4.7) and (4.8) in more detail. According to Eq. (4.8), there is a power of 2 correlation between the electric field intensity magnitude and the heat source. On the other hand, Eq. (4.7) depicts a power of 1 correlation between the heat source and the temperature which emphasizes that changes in the electric field intensity would change the temperature of the sample exponentially with a power of 2.

One significant discussion that can be made on the topic of microwave treatment considering the data shown in Figure 4.8, is the difference between conventional and microwave heating. In conventional heating, when a material is closer to the heat source, it absorbs more energy in the form of heating. A clear example of conventional heating is heating with fire. The closer the material is to the fire, the more energy it absorbs and the warmer it gets. However, heating during microwave radiation works differently. In microwave heating, the heat is generated from within the sample because of the response of the material particles to the electric and magnetic fields generated inside the material. The amount of energy that is generated in the sample in the form of heating is calculated using Eq. (4.8) which shows the direct impact of the electric and magnetic fields on the generated heat source. Comparison between Figure 4.8b and Figures 4.8a and c further emphasizes this point by showing that the trend in the $E_{Integral}$ versus distance is the same as $T_{Integral}$ and HOME. In other words, a higher HOME and $T_{Integral}$ is achieved at a distance from the antenna where a higher electric field has been generated in the sample. Because of the wavelike nature of electromagnetic waves, the electric and magnetic fields generated in the material during microwave radiation vary significantly with the distance from the antenna. Maxwell's equations (Eq. (4.6)) can be used to find the generated electric and magnetic fields in the material. This is another point of superiority for using numerical models. While it is hard to find analytical solutions for Maxwell's equations and experimental investigations, which are expensive and time-consuming to implement, to predict the generated electric and magnetic fields inside the material for complicated geometries and real applications, numerical models can extensively be used.

The STD values for temperature and the electric field intensity magnitude shown in Figures 4.8b and 4.8c emphasize one of the important characteristics of microwave treatment which is the non-uniform distribution of temperature within the rocks during the heating experiments. Increasing the temperature of one part of the rock without heating the other parts causes the generation of stress within the sample due to thermal expansion which leads to fragmentation and strength reduction. The heating pattern in the sample significantly depends on the geometry of the sample and its location in the cavity. Figure 4.9 supports this claim by showing how significantly the temperature distributions within the samples change based on their size and distance from the antenna.

Sample preparation for the mode I fracture toughness experiments is very delicate and complex which includes cutting cylindrical shaped samples into half longitudinally and also creating the notch. This study investigates the effect of cutting the sample before and after the microwave treatment. The three sample geometry designs detailed in Section 4.2.2.2 are evaluated and compared.

Figure 4.10 shows the temperature distribution after the microwave treatment with a power of 3 kW and an exposure time of 4.35 s for all three geometry designs including the calculated HOME and the maximum temperature in the samples. The results show that sample cutting time (before and after treatment), as well as the cutting direction, affects the energy absorption of the sample to some extent which can accordingly affect K_{IC} values. Comparison between the geometry designs shows that geometry design 3 leads to the highest HOME while resulting in almost the same maximum temperature as in geometry design 1. Alternately, geometry design 2 has a maximum temperature of 446.1 K which is the highest among the three geometry designs. Two main reasons can justify the difference in the HOME value and the maximum temperature realized between geometry designs 2 and 3, shown in Figure 4.10. First, it is assumed that the principal cut, which splits the rock into two halves, does not remove any material from the rock. However, the notch design in the geometry removes some mass from the rock, which creates a difference in the effect of the principal cut and the notch on the HOME value and the maximum temperature, especially when their length and thickness are different (Figure 4.3). Second, because of the door boundary condition, the model's geometry is only symmetrical on the yz plane, splitting the cavity in half. Therefore, the temperature distribution in different cut planes (yz in geometry design 2 and xy in geometry design 3) is different, which means the notch removes parts with varying amounts of absorbed energy. In this study, geometry design 2 is chosen over 3 to represent cutting the sample before the microwave treatment due to its easier placement in the experimental cavity, higher maximum temperature, and the cutting plane being in the symmetrical plane direction which leads to two similarly heated fracture toughness samples. Furthermore, the samples that are cut after the treatment (geometry design 1) are all cut in the same orientation as geometry design 2. In other words, they are cut in half on the diametric plane parallel to the yz plane. In the following sections, the experimental results and the K_{IC} values for cutting the sample before and after the microwave treatment are provided and compared.

4.5.4. *Effect of microwave treatment on K_{IC} value*

In this section, the effect of microwave treatment on mode I fracture toughness of basalt is evaluated. For each microwave treatment experiment, the disk consisting of two NSCB fracture toughness samples is treated with microwave energy. Two different approaches for preparing the NSCB samples out of the disk-shaped basalt for the fracture toughness experiments are implemented and compared. In the first approach, the sample is cut, and the notch is created before the microwave treatment. Then, the two NSCB samples are put together to represent the disk-shaped basalt for the microwave treatment experiments. In the second approach, the intact disk-shaped sample is used for the treatment, therefore, the disk is cut into two NSCB samples after the microwave radiation. Each full disk sample is treated with a power of 3 kW and exposure times of 10, 20, and 30 s. The resulted K_{IC} values against the exposure time are shown in Figure 4.11. Table 4.A.1 in the Appendix which details all the data points has been provided for the reference. Two main observations should be emphasized based on the results shown in Figure 4.11. First, there is a decrease in the K_{IC} with an increase in the exposure time. Second, a higher reduction in the K_{IC} value is achieved when the sample is cut before the treatment. Some hypotheses justify the difference between cutting the samples before and after the treatment. When the intact cylindrical rock sample is treated, the created microcracks are distributed throughout the sample. However, when the sample is cut before the microwave treatment, the created microcracks are focused on the weak spots of the sample with a potential stress concentration which in this case is the notch. Analysing the temperature distribution results shown in Figure 4.10 can further evaluate this hypothesis. In Figure 4.10, a comparison between the temperature distribution after the microwave treatment for geometry designs 1 and 2 (geometry designs used for the experiments) shows that when the sample is cut before the treatment, the temperature increase is focused more on the notch. The maximum temperature is also increased on the notch surroundings when the sample is cut before the treatment. Higher heat concentration around the notch can increase the thermal stress, which, consequently, could cause the failure of the rock sample in the fracture toughness experiment at lower forces resulting in lower K_{IC} values. Further analysis of the distribution of cracks throughout the rocks during the microwave treatment is outside the scope of the current study and is considered for future research on this topic. In general, the results of this study have shown that changing the approach from cutting the sample after to before the microwave treatment can decrease the K_{IC} value by more than 35% in some cases.

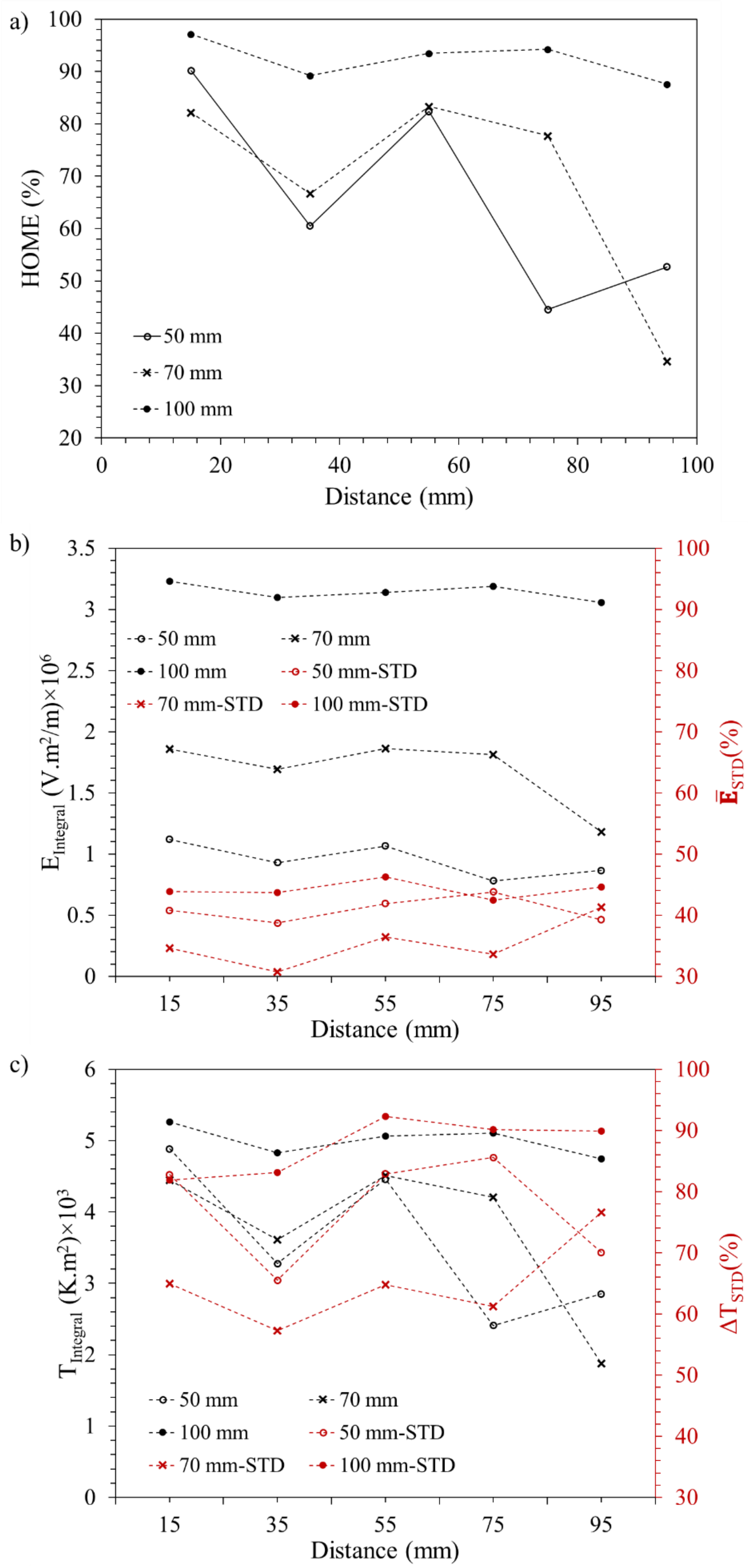

Figure 4.8 The distance test analysis of the disk-shaped samples using the developed numerical model for a) HOME, b) electric field intensity magnitude, and c) temperature considering a power of 3 kW and an exposure time of 4.35 s.

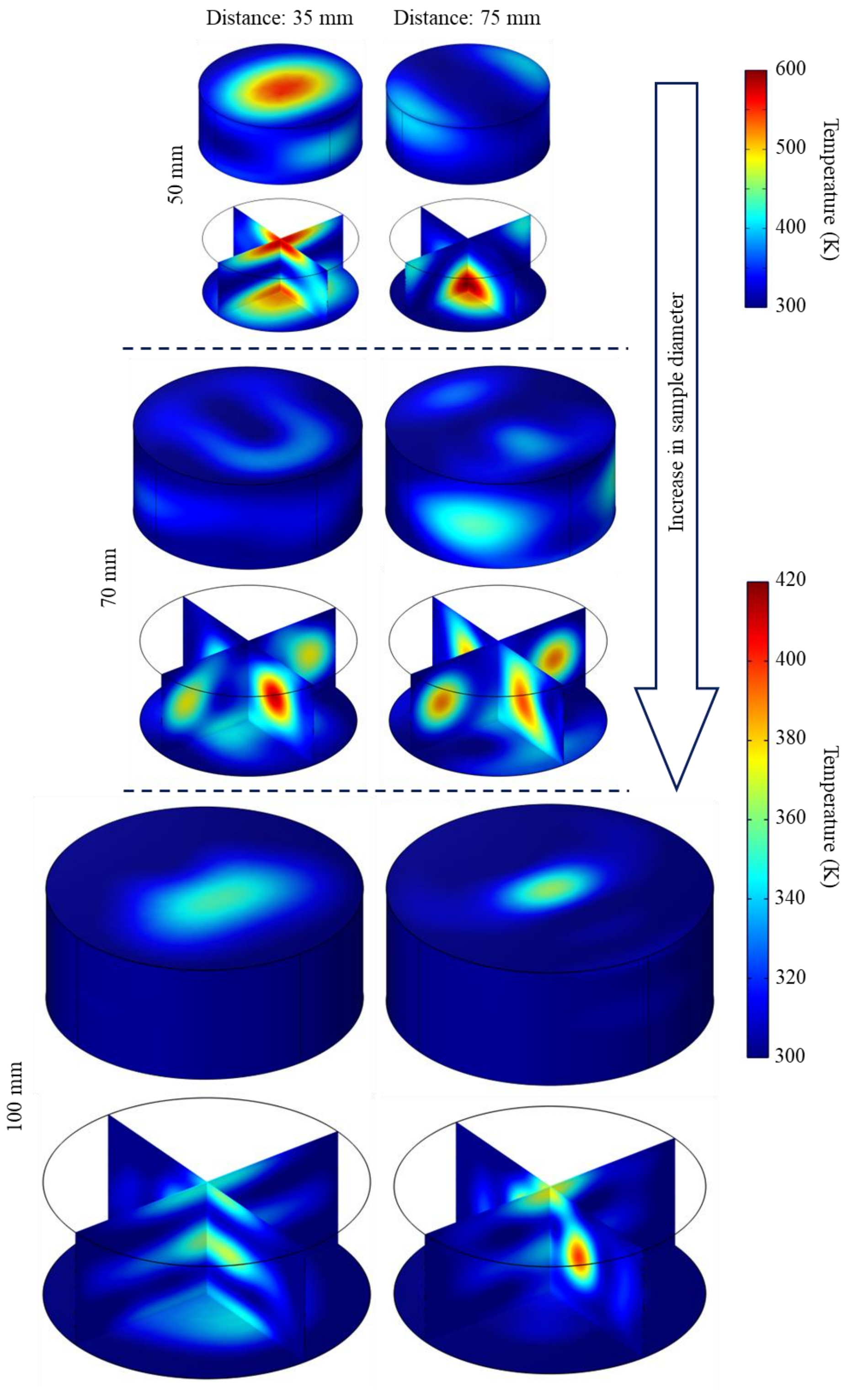

Figure 4.9 The temperature distribution of the surface of the samples with different sizes and at different distances from the antenna after microwave treatment with a power of 3 kW and an exposure time of 4.35 s using the numerical model. The left and right sides of the figure represent 35 mm and 75 mm distances from the antenna, respectively.

Summarizing the results gathered from Figures 4.10 and 4.11, it seems intuitive that a more effective microwave treatment can be observed when the sample is cut before the treatment since a high heat concentration is generated at the tip of the notch where the K_{IC} is measured. Considering the real application of microwave treatment, even though cutting the sample before the treatment might not be a true representative of intact rocks, it can showcase the weakening of rocks at the tip of existing cracks, making them easier to cut.

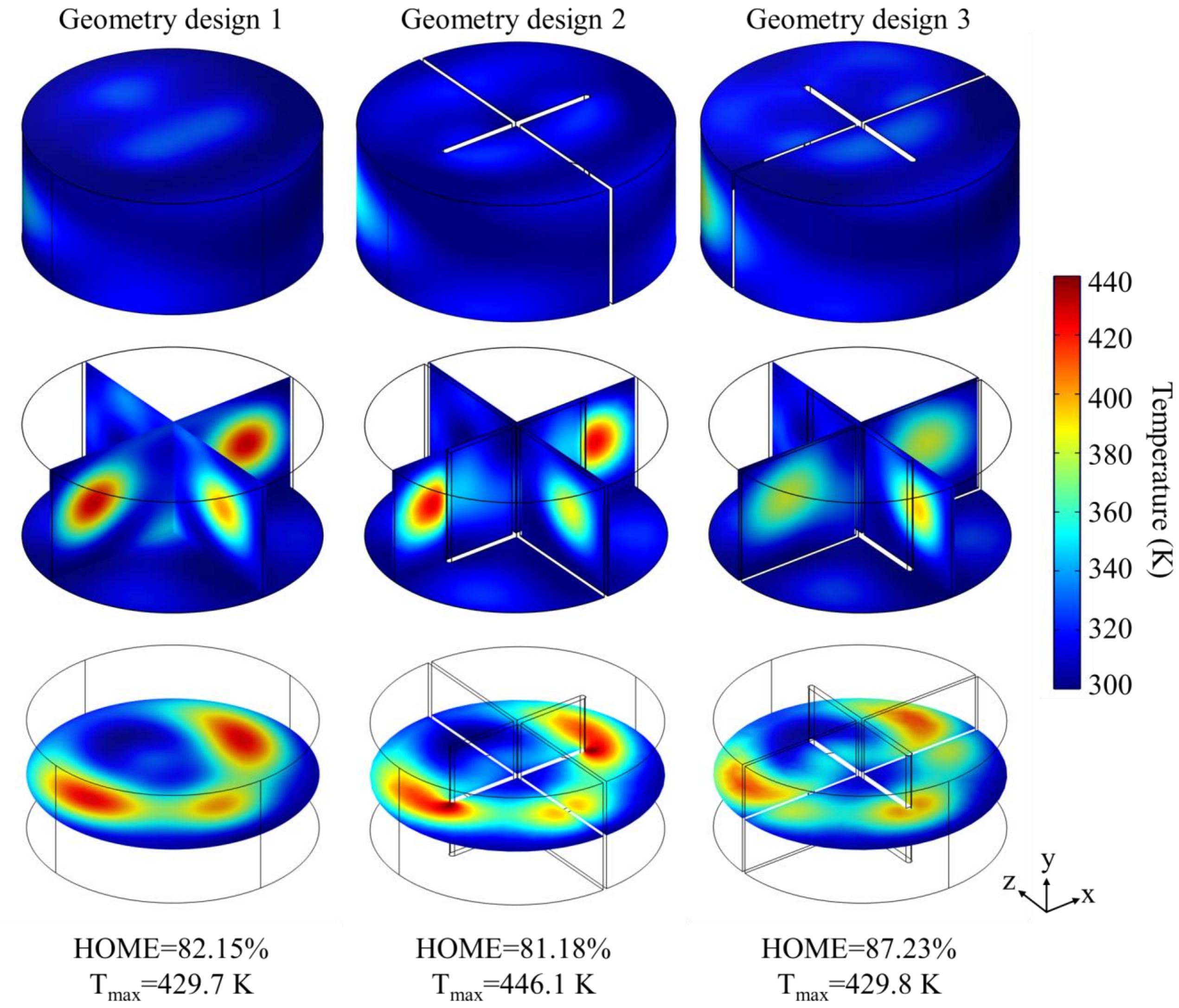

Figure 4.10 The numerical comparison between the three geometry designs after the microwave treatment with a power of 3 kW and an exposure time of 4.35 s.

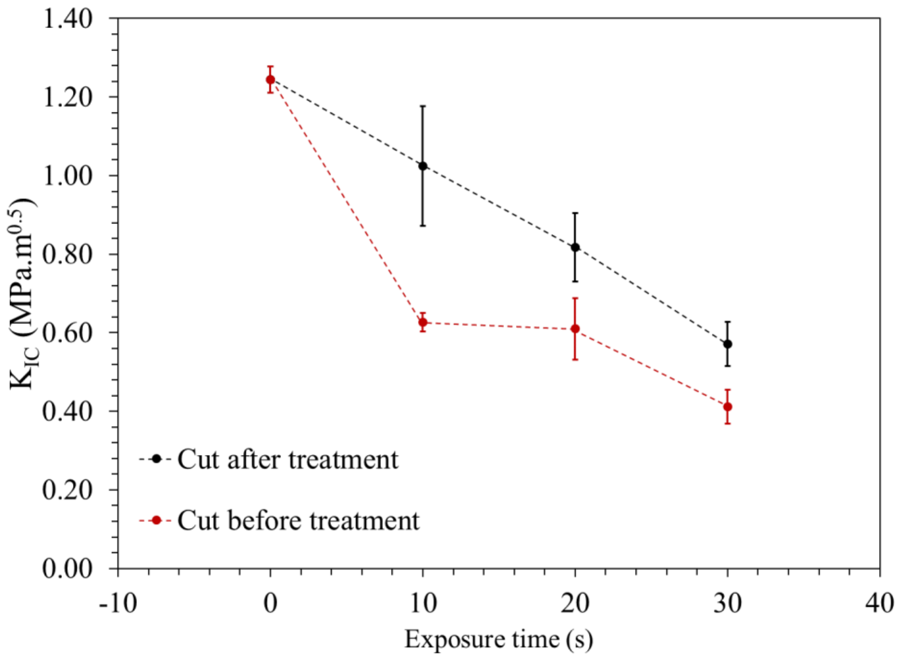

Figure 4.11 Experimental results on the effect of 3 kW power of microwave treatment at different exposure times on the K_{IC} value and comparison between the two approaches of cutting the sample before and after the microwave treatment.

To further evaluate the efficiency of the microwave treatment as a rock pre-conditioning method, the achieved K_{IC} and $WOME_{Input}$ values at different exposure times are compared for the samples that were cut before the treatment (Figure 4.12). The results show that while increasing the exposure time causes more reduction in the K_{IC} value, it decreases $WOME_{Input}$, meaning that the extra energy that is put into the sample does not assist to reduce the K_{IC} value with the same efficiency as with shorter exposure times. For instance, comparing 10 s and 30 s of exposure times, while increasing the exposure time creates more than an additional 18% reduction in the K_{IC} value, it decreases $WOME_{Input}$ from 2.32 %/kWhr/ton to 0.96 %/kWhr/ton. This observation emphasizes the importance of optimizing the energy input in order to maximize $WOME_{Input}$ for future studies on evaluating the effect of microwave treatment on rock parameters.

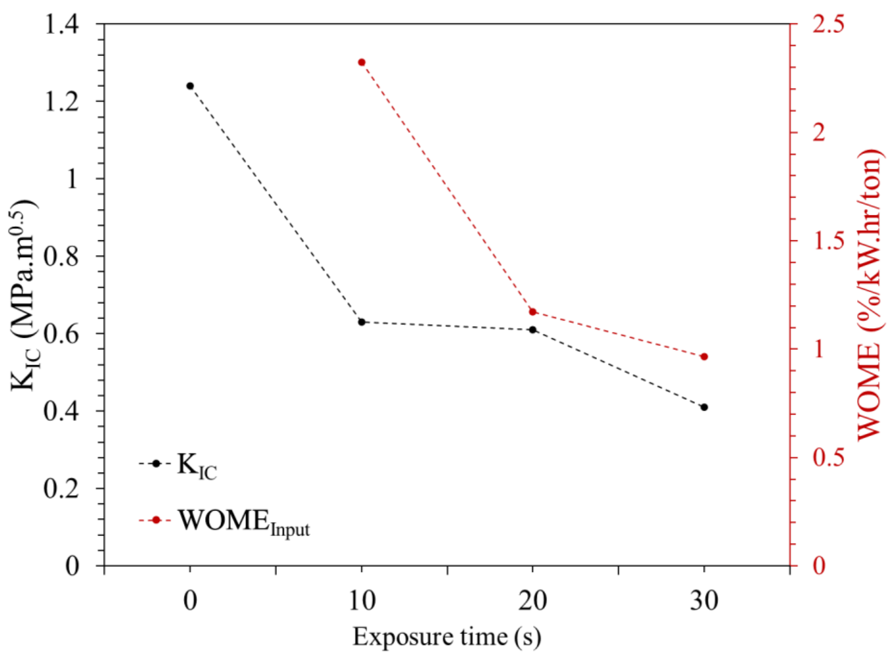

Figure 4.12 Experimental data showing a comparison between the calculated WOME and K_{IC} at different exposure times when samples are treated with microwave power of 3 kW.

Figure 4.13 compares $WOME_{Input}$ and $WOME_{Absorbed}$ at different exposure times. $WOME_{Absorbed}$ represents the efficiency of the microwave treatment when there is an assumed ideal HOME of 100% during the microwave treatment. This figure shows that achieving 100% HOME can in some cases increase WOME by a significant value of more than 35%. This understanding signifies the importance of optimizing the energy absorption of the sample (HOME) during microwave treatment experiments. The development of the numerical models can provide extraordinary information with regard to the energy absorption of the samples to improve the efficiency of the microwave treatment as a rock pre-conditioning method such as optimizing the location of the sample in the cavity.

4.5.5. Discussion on the failure modes

Fracture toughness is known as one of the complex experiments for rock parameter measurement. According to the ISRM suggested method for measuring fracture toughness (Kuruppu et al., 2014), this test requires a specific failure pattern dictating that the deviation of fracture propagation from the notch plane should be less than 0.05D. If this condition is exceeded, the gathered test results are considered invalid and further test repeats need to be conducted to compensate for the unacceptable results. This section investigates this issue and discuss the failure pattern in the NSCB mode I fracture toughness experiment as an obstacle in evaluating the effectiveness of microwave treatment on rock fragmentation.

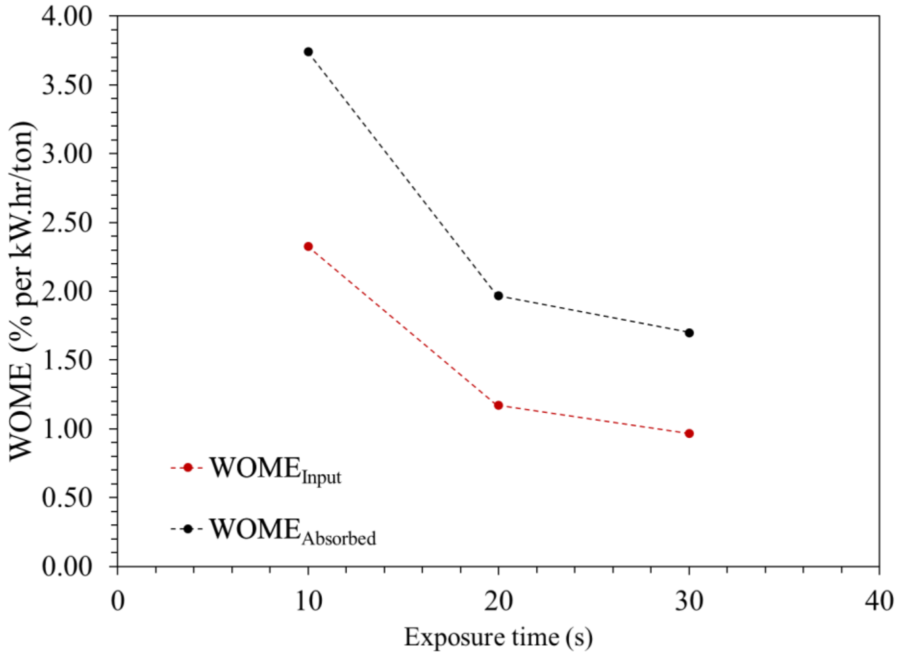

Figure 4.13 Comparison between WOME$_{Input}$ and WOME$_{Absorbed}$ at different exposure times using the experimental data gathered in this study.

Microwave treatment affects the rocks by creating micro-fractures within the sample which leads to local damaged zones. After the treatment, there are two types of fractures in the sample. Some are micro-scale and difficult to observe unaided and the other ones are the prominent fractures that are visible throughout the sample. For some mechanical tests such as UCS, all the micro-fractures contribute to the failure of the sample which leads to a potential strength reduction. In the mode I fracture toughness test, however, the failure of the samples requires the propagation of a crack on the notch plane without any major deviation. In this study, after each microwave treatment experiment, the visible fractures were marked in black as shown in Figure 4.14. Afterward, the samples were used in the fracture toughness apparatus for the K_{IC}

measurement. In a significant number of the test cases, the fractures started to propagate from the damaged zones (black marked areas) instead of following the created notch. This phenomenon depicts two major disadvantages in evaluating the effectiveness of microwave treatment with respect to the fracture toughness data. First, there are a large number of data points that are invalid because of the improper failure modes such as shown by the failed samples in Figure 4.14. Therefore, to provide at least three acceptable repeats for each test specification, there need to be several additional tests since many of the test results would be invalid (in some cases of this study, more than eight NSCB fracture toughness experiments needed to be conducted to provide three acceptable repeats). The number of unacceptable failure modes increases by increasing the power and exposure time as shown in Figure 4.15. Second, there are damage zones that do not take part in the failure of the samples during the mode I fracture toughness experiment. In other words, in some rock mechanical strength experiments such as UCS, most of the damage zones caused by microwave treatment take part in the strength reduction, however, only a small portion of the created damage takes part in the NSCB mode I fracture toughness test. This means that the effectiveness of the microwave treatment as a rock pre-conditioning method is higher than what the available data for fracture toughness shows which can be a promising point for engineers who are looking into improving the efficiency of rock excavation using microwave treatment.

Figure 4.14 The marked visible fractures of the NSCB samples after the microwave treatment and the failure pattern after the fracture toughness experiment.

4.6. Conclusions

This study aimed to evaluate the effectiveness of microwave treatment as a rock pre-conditioning method by conducting mode I fracture toughness experiments on NSCB samples before and after the treatment. The heating experiments were performed at different powers and exposure times on cylindrical basalt samples with diameters of 70 mm. In a novel approach, the previously developed numerical model was utilized to optimize the energy absorption of the sample during the microwave treatment. The key conclusions of the study are summarized as follows:

- Different sample sizes for mode I fracture toughness were evaluated and it was shown that the minimum sample diameter for the basalt used in this study should be 70 mm.
- The optimised distance to achieve the maximum HOME depends highly on the sample size and geometry. For 70 mm diameter samples, the maximum energy absorption of the cylindrical samples during the microwave treatment was achieved at 15 and 55 mm distances from the antenna. Changing the distance of the sample from the antenna could result in a significant decrease in the energy absorption of the sample which in some cases can be as large as 40%. Combining numerical modelling and experimental work can highly benefit researchers and engineers to improve the efficiency of microwave treatment as a rock pre-conditioning method. Neglecting either experimental or numerical efforts can lead to inapplicable results and a waste of time and materials.
- A comparison between cutting the samples before and after the microwave treatment showed that the effect of microwave treatment is more significant for the samples with weak spots (the samples that are cut before the treatment). In some cases, the existence of the weak spots created over 35% more reduction in the K_{IC} value after microwave treatment.
- Increasing the exposure time leads to more K_{IC} value reduction but decreases WOME. Depending on the application, researchers and engineers need to link different parameters such as WOME, K_{IC} reduction, and excavation energy to establish a rationale for optimizing the microwave treatment method in the field.

- Achieving a better energy absorption during microwave heating with the same energy input can lead to a higher WOME. Numerical models can be utilized in order to maximize the energy absorption of the samples.
- The K_{IC} value only provides a partial representation of the effect of microwave treatment on rock properties and not all the damaged zones take part in the evaluation. Therefore, the actual effect of microwave treatment on the rock is much more severe.

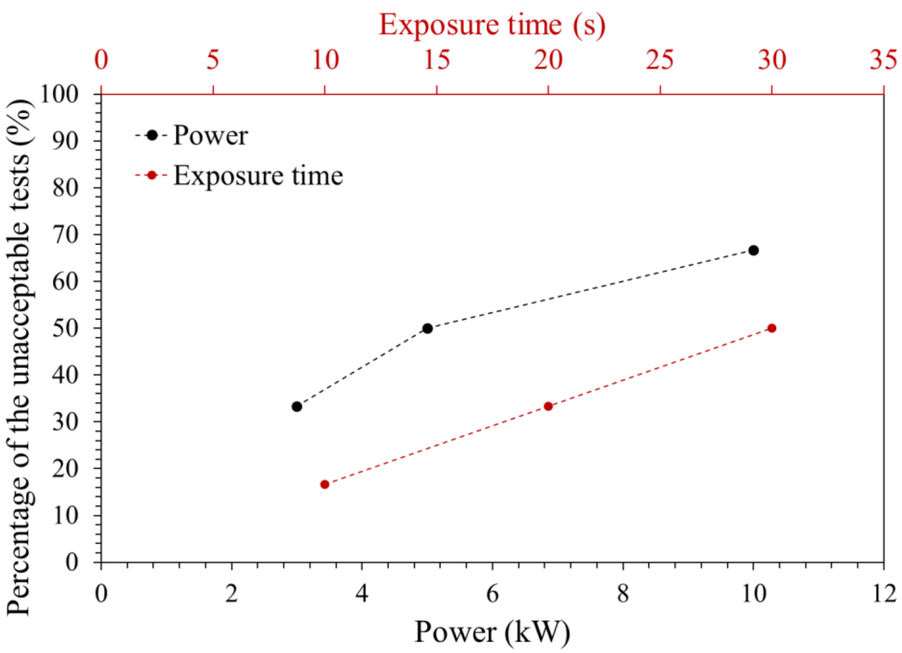

Figure 4.15 The percentage of invalid fracture toughness experiments and its relationship with microwave power and exposure time.

4.7. Future work

There are some limitations in the current state numerical model used in this study that can be the subject of future works. First, the present research paper uses constant rock properties as the inputs of the numerical model. While this approach is appropriate for low energy dosages, it is important to extend the model to include a two-way, fully coupled modeling approach for high energy dosages, especially in field applications. Furthermore, applying the model in the field requires defining new boundary conditions to represent an open field for both heat transfer and Maxwell's equations. Additionally, the current model can capture the electromagnetic and thermal behavior of rocks, and the damage is measured experimentally. The model can be coupled with the equations for the mechanical analysis so that the damage caused by the microwave treatment of rocks can be numerically captured.

Appendix

In this appendix, the data points representative of the fracture toughness experiments included in Figure 4.11 are provided in Table 4.A.1.

Table 4.A.1 The data points for the K_{IC} values of the fracture toughness samples representative of the chart in Figure 11.

<table>
<tr><th>Description</th><th>Power (kW)</th><th>Exposure time (s)</th><th>Repeat number</th><th>K_{IC} (MPa.m$^{0.5}$)</th></tr>
<tr><td rowspan="5">Untreated sample</td><td rowspan="5">N.A</td><td rowspan="5">N.A</td><td>1</td><td>1.24</td></tr>
<tr><td>2</td><td>1.19</td></tr>
<tr><td>3</td><td>1.26</td></tr>
<tr><td>4</td><td>1.27</td></tr>
<tr><td>5</td><td>1.26</td></tr>
<tr><td rowspan="11">The notch is created after the microwave treatment</td><td rowspan="4">3</td><td rowspan="4">10</td><td>1</td><td>1.20</td></tr>
<tr><td>2</td><td>0.83</td></tr>
<tr><td>3</td><td>1.03</td></tr>
<tr><td>4</td><td>1.04</td></tr>
<tr><td rowspan="4">3</td><td rowspan="4">20</td><td>1</td><td>0.82</td></tr>
<tr><td>2</td><td>0.89</td></tr>
<tr><td>3</td><td>0.87</td></tr>
<tr><td>4</td><td>0.70</td></tr>
<tr><td rowspan="3">3</td><td rowspan="3">30</td><td>1</td><td>0.63</td></tr>
<tr><td>2</td><td>0.57</td></tr>
<tr><td>3</td><td>0.52</td></tr>
<tr><td rowspan="9">The notch is created before the microwave treatment</td><td rowspan="3">3</td><td rowspan="3">10</td><td>1</td><td>0.63</td></tr>
<tr><td>2</td><td>0.65</td></tr>
<tr><td>3</td><td>0.60</td></tr>
<tr><td rowspan="3">3</td><td rowspan="3">20</td><td>1</td><td>0.66</td></tr>
<tr><td>2</td><td>0.65</td></tr>
<tr><td>3</td><td>0.52</td></tr>
<tr><td rowspan="3">3</td><td rowspan="3">30</td><td>1</td><td>0.46</td></tr>
<tr><td>2</td><td>0.41</td></tr>
<tr><td>3</td><td>0.37</td></tr>
</table>

References

Ahmadihosseini, A., Shadi, A., Rabiei, M., Samea, P., Hassani, F., & Sasmito, A. P. (2022). Computational study of microwave heating for rock fragmentation; model development and validation. International Journal of Thermal Sciences, 181, 107746.

Callister Jr, W. D., & Rethwisch, D. G. (2020). Fundamentals of materials science and engineering: an integrated approach. John Wiley & Sons.

Chang, S.-H., Lee, C.-I., & Jeon, S. (2002). Measurement of rock fracture toughness under modes I and II and mixed-mode conditions by using disc-type specimens. Engineering Geology, 66(1–2), 79–97.

Deyab, S. M., Rafezi, H., Hassani, F., Kermani, M., & Sasmito, A. P. (2021). Experimental investigation on the effects of microwave irradiation on kimberlite and granite rocks. Journal of Rock Mechanics and Geotechnical Engineering, 13(2), 267–274.

Deyab, S. M., Rafezi, H., Hassani, F., Sasmito, A. P., & Kermani, M. (2020). The effect of microwave irradiation on the mechanical properties of kimberlite and limestone. Selçuk-Teknik Dergisi, 19(4), 97–109.

Feng, G., Kang, Y., Meng, T., Hu, Y., & Li, X. (2017). The influence of temperature on mode I fracture toughness and fracture characteristics of sandstone. Rock Mechanics and Rock Engineering, 50(8), 2007–2019.

Fowell, R. J., Hudson, J. A., Xu, C., & Zhao, X. (1995). Suggested method for determining mode I fracture toughness using cracked chevron notched Brazilian disc (CCNBD) specimens. International Journal of Rock Mechanics and Mining Sciences and Geomechanics Abstracts, 7(32), 322A.

Hassani, F. (2010). Review of explosive-free rock breakage (EFRB) technologies. McGill University. Montreal, Canada, 450.

Hassani, F, Nekoovaght, P. M., Radziszewski, P., & Waters, K. E. (2011). Microwave assisted mechanical rock breaking. 12th ISRM Congress.

Hassani, F, Nekoovaght, P. M., & Gharib, N. (2016). The influence of microwave irradiation on rocks for microwave-assisted underground excavation. Journal of Rock Mechanics and Geotechnical Engineering, 8(1), 1–15.

Hassani, F, Shadi, A., Rafezi, H., Sasmito, A. P., & Ghoreishi-Madiseh, S. A. (2020). Energy analysis of the effectiveness of microwave-assisted fragmentation. Minerals Engineering, 159, 106642.

Iqbal, M. J., & Mohanty, B. (2007). Experimental calibration of ISRM suggested fracture toughness measurement techniques in selected brittle rocks. Rock Mechanics and Rock Engineering, 40(5), 453–475.

Jones, D. A., Kingman, S. W., Whittles, D. N., & Lowndes, I. S. (2005). Understanding microwave assisted breakage. Minerals Engineering, 18(7), 659–669.

Kingman, S. W., Jackson, K., Cumbane, A., Bradshaw, S. M., Rowson, N. A., & Greenwood, R. (2004). Recent developments in microwave-assisted comminution. International Journal of Mineral Processing, 74(1–4), 71–83.

Kuruppu, M. D., Obara, Y., Ayatollahi, M. R., Chong, K. P., & Funatsu, T. (2014). ISRM-suggested method for determining the mode I static fracture toughness using semi-circular bend specimen. Rock Mechanics and Rock Engineering, 47(1), 267–274.

Lan, W., Wang, H., Zhang, X., Fan, H., Feng, K., Liu, Y., & Sun, B. (2020). Investigation on the mechanism of micro-cracks generated by microwave heating in coal and rock. Energy, 206, 118211.

Li, Q., Li, X., & Yin, T. (2021). Effect of microwave heating on fracture behavior of granite: An experimental investigation. Engineering Fracture Mechanics, 250, 107758.

Li, X., Wang, S., Xu, Y., Yao, W., Xia, K., & Lu, G. (2020). Effect of microwave irradiation on dynamic mode-I fracture parameters of Barre granite. Engineering Fracture Mechanics, 224, 106748.

Lu, G.-M., Feng, X.-T., Li, Y.-H., Hassani, F., & Zhang, X. (2019). Experimental investigation on the effects of microwave treatment on basalt heating, mechanical strength, and fragmentation. Rock Mechanics and Rock Engineering, 52(8), 2535–2549.

Lu, G. M., Li, Y. H., Hassani, F., & Zhang, X. W. (2016). Review of theoretical and experimental studies on mechanical rock fragmentation using microwave-assisted approach. Chin J Geotech Eng, 38(8), 1497–1506.

Nasseri, M. H. B., Schubnel, A., & Young, R. P. (2007). Coupled evolutions of fracture toughness and elastic wave velocities at high crack density in thermally treated Westerly granite. International Journal of Rock Mechanics and Mining Sciences, 44(4), 601–616.

Ouchterlony, F. (1988). Suggested methods for determining the fracture toughness of rock. International Journal of Rock Mechanics and Mining Sciences, 25(2), 71–96.

Ouchterlony, F. (1989). On the background to the formulae and accuracy of rock fracture toughness measurements using ISRM standard core specimens. International Journal of Rock Mechanics and Mining Sciences & Geomechanics Abstracts, 26(1), 13–23.

Peinsitt, T., Kuchar, F., Kargl, H., Restner, U., Sifferlinger, N., & Moser, P. (2008). Microwave heating of rocks with different water content. In Proceedings of Microwave Technology'08 (pp. 1–9).

Peng, K., Lv, H., Zou, Q., Wen, Z., & Zhang, Y. (2020). Evolutionary characteristics of mode-I fracture toughness and fracture energy in granite from different burial depths under high-temperature effect. Engineering Fracture Mechanics, 239, 107306.

Rafezi, H., Deyab, S. M., Hassani, F., Ghoreishi-Madiseh, S. A., & Micallef, D. (2020). A comparative study of the cooling-rate effect on rock strength reduction after microwave irradiation. Experimental Results, 1.

Scott, G. (2006). Microwave pretreatment of a low grade copper ore to enhance milling performance and liberation. Stellenbosch: University of Stellenbosch.

Shadi, A., Ahmadihosseini, A., Rabiei, M., Samea, P., Hassani, F., Sasmito, A. P., & Ghoreishi-Madiseh, S. A. (2022). Numerical and experimental analysis of fully coupled electromagnetic and thermal phenomena in microwave heating of rocks. Minerals Engineering, 178, 107406.

Toifl, M., Hartlieb, P., Meisels, R., Antretter, T., & Kuchar, F. (2017). Numerical study of the influence of irradiation parameters on the microwave-induced stresses in granite. Minerals Engineering, 103, 78–92.

Whittaker, B. N., Singh, R. N., & Sun, G. (1992). Rock fracture mechanics. Principles, design and applications.

Yao, J., Tao, M., Zhao, R., Hashemi, S. S., & Wang, Y. (2021). Effect of microwave treatment on thermal properties and structural degradation of red sandstone in rock excavation. Minerals Engineering, 162, 106730.

Yin, T., Wu, Y., Wang, C., Zhuang, D., & Wu, B. (2020). Mixed-mode I+ II tensile fracture analysis of thermally treated granite using straight-through notch Brazilian disc specimens. Engineering Fracture Mechanics, 234, 107111.

Zheng, Y. L., Zhang, Q. B., & Zhao, J. (2017). Effect of microwave treatment on thermal and ultrasonic properties of gabbro. Applied Thermal Engineering, 127, 359–369.

"I figured, since I'd gone this far, I might as well just turn back, keep right on going."

Forrest Gump- Forrest Gump

Chapter 5: Potential application of the microwave treatment in mining excavation evaluated using energy efficiency-based approach

5.1. Preface

In the previous chapter, the focus was on analyzing fracture toughness values to assess the efficacy of microwave treatment as a rock preconditioning method. While fracture toughness offers valuable insights into the fracture mechanics of rocks, it provides a limited perspective on their overall characteristics. This chapter extends the energy efficiency-based analysis approach to a more widely used experiment, namely the UCS test. By incorporating UCS into the evaluation, the results of this chapter aim to provide a more comprehensive understanding of the potential of microwave treatment as a rock preconditioning method in mining applications.

5.2. Abstract

Over the past two decades, microwave treatment has emerged as a promising method for enhancing efficiency and resource utilization in mining excavation and comminution processes. While previous studies have explored the effects of microwave energy on rock characteristics, there remains a notable gap in energy efficiency analysis crucial for practical application. As part of an overall research study on microwave treatment of rocks and ores at the Geomechanics Laboratory of McGill University, over 200 experiments were conducted, covering material characterization, microwave treatment, thermal imaging, calorimetric measurements, and mechanical testing. Detailed temperature-dependent material properties of basalt are measured and analyzed to predict the outcome of microwave treatment. Integrating thermal imaging and calorimetric measurements provided comprehensive insights into temperature dynamics within samples during treatment. Optimizing the treatment scenarios significantly enhanced heat over microwave efficiency by over 15% and weakening over microwave energy by more than 4 times in select cases. The energy efficiency-based analysis offers quantitative data on the influence of microwave treatment on uniaxial compressive strength, elastic modulus, Poisson's ratio, and strain energy of basalt. Additionally, insights into the impact of power levels on treatment efficacy are uncovered, revealing exponential increases in rock weakening over microwave energy from 0.15 to 66.92%/kWhr/t with an increase in power from 3 to 100 kW. Optimizing the microwave energy absorption resulted in higher weakening over microwave energy compared to previous literature. These findings present a novel approach for engineers and researchers to leverage microwave treatment in mining operations, ultimately enhancing efficiency and resource utilization in the mining industry.

Keywords: Microwave treatment; Energy efficiency; Basalt; Mining excavation; Material characterization

5.3. Introduction

One of the primary challenges faced by mining engineers revolves around the considerable energy demands of mining operations. Currently, the mining industry accounts for over 7% of global energy consumption, with energy supplied from sources such as electricity, diesel, oil, coal, natural gas, and gasoline (Aramendia et al., 2023). Projections suggest that this demand could increase by a factor of eight over the next four decades. Among the most energy-intensive processes within mining operations are rock breaking, crushing, and grinding (Holmberg et al., 2017; F. Lin et al., 2022). Over the past three decades, researchers have explored alternative approaches to enhance rock breakage, aiming to mitigate energy consumption in excavation and comminution processes. These alternatives include hydraulic fracturing, electrical methods, conventional heating, laser applications, and microwave treatment, with the latter demonstrating promising potential for practical field applications (Bai-quan Lin et al., 2020; Wei et al., 2019).

The microwave treatment technique takes advantage of the inherent mineral heterogeneity within rocks to weaken their structure. Rocks typically comprise a diverse array of minerals, with each exhibiting unique responses to microwave irradiation. These responses can range from absorbing to reflecting microwave energy, with absorption manifesting as heating during irradiation (Ahmadihosseini et al., 2022; Q. H. Zhao, Zhao, Zheng, Li, He, & Zou, 2020). The presence of various minerals within a rock sample means that the parts constituting good microwave absorbers will heat up and experience a temperature rise relative to the parts that are non-absorbent or energy reflective. The thermal heating causes the microwave-absorbing regions to expand, exerting pressure on the surrounding material. As temperature increases, this pressure intensifies, eventually leading to the formation of micro/macro cracks and the eventual failure of the sample. This process results in a reduction in the strength of the rock, facilitating its easier breakage (Lan et al., 2020).

Research into the effectiveness of microwave treatment as a rock pre-conditioning method majorly started in the early 2000s. Whittles et al. (2003) conducted pioneering studies investigating the impact of microwave treatment on the uniaxial compressive strength (UCS) of rocks. Their findings revealed that high power densities can significantly diminish the strength of ore materials, offering potential economic benefits compared to conventional rock-breaking tools. Building upon this work, Jones et al. (2005) furthered the research by exploring microwave-assisted breakage through a 2D, two phase numerical model. Their study underscored the critical role of power density in influencing weakening during microwave treatment. Moreover, they observed that cracks tended to form around the grain boundaries between absorbent and transparent parts of the rock, suggesting potential improvements in mineral liberation for mining operations. Subsequently, researchers continued to investigate microwave treatment as a rock pre-conditioning method, examining various specifications such as power, exposure time, and frequency, across different rock types including basalt (Nejati et al., 2012; Satish et al., 2006), granite (Peinsitt et al., 2010), sandstone (Peinsitt et al., 2010), etc. These studies consistently emphasized the significance of high power densities and the presence of microwave-absorbing minerals in a reflective matrix to achieve efficient microwave treatment (Ali & Bradshaw, 2009, 2010; D A Jones et al., 2007; G. Wang et al., 2008). Collectively, these investigations established a comprehensive understanding of microwave-assisted breakage systems, serving as a foundation for future studies in this field.

Over the past decade, research studies have predominantly pursued two avenues of investigation. Firstly, there has been a continued emphasis on evaluating various factors such as microwave power (Batchelor et al., 2015), exposure time (Y L Zheng et al., 2017), rock types (Hartlieb et al., 2018; Kahraman, Canpolat, & Fener, 2020; Lehmann et al., 2023; Y. Zheng et al., 2020), radiation mode (Deyab et al., 2021), moisture content (Yao et al., 2021), and mechanical testing methods (Hassani et al., 2016; Gaoming Lu, Feng, et al., 2020; Y L Zheng et al., 2021) to evaluate the effectiveness of microwave treatment as a rock pre-conditioning method. Concurrently, researchers have employed a range of technologies to delve deeper into the mechanisms of rock failure during microwave treatment. Among the most commonly utilized technologies are scanning electron microscopy (SEM) and energy dispersive X-ray (EDX), which facilitate the determination of elemental distribution and mineral composition of rock samples (Gao-ming Lu et al., 2017). Lu et al. (2019a) employed these methods and demonstrated that enstatite minerals are primarily responsible for fracture generation during microwave treatment of basalt. Utilizing SEM, Lan et al. (2020) identified three mechanisms of microcrack initiation in rocks: dewatering shrinkage of minerals, particle separation, and internal cracking of the body. Additionally, Xu et al. (2020) integrated three tools—wave velocity measurement, thermal camera imaging, and microscopic imaging—to conduct a comprehensive analysis of rock damage caused by microwave treatment, highlighting the importance of employing higher power densities for effective treatment. Analyzing the mineralogical composition of a pegmatite thin section using SEM, Li et al. (2019) revealed key constituents of the rock as the input for computational modeling, which aids in understanding rock behavior under microwave treatment. Computational models are another technological approach to understanding the behavior of the material under microwave irradiation. These models have evolved from initial implementations with simplified assumptions for electromagnetic irradiation, heat transfer, and mechanical degradation (Baiquan Lin et al., 2017; Pressacco et al., 2022; Toifl et al., 2016, 2017; Y. Wang & Djordjevic, 2014) to more sophisticated models incorporating diverse heat transfer phenomena, Maxwell's equations, and mechanical constitutive models, resulting in fully validated models against experimental data (Ahmed et al., 2023; Deyab et al., 2023; Shadi et al., 2022; Cui et al., 2020). Throughout these studies, there has been a strong focus on comprehending the mechanisms and phenomena involved in microwave treatment of rocks. However, there remains a significant gap in data regarding the energy efficiency of the method which is a crucial factor for assessing its potential implementation in the mining industry.

Energy efficiency in microwave treatment can be examined from two angles: the energy absorbed by the rock relative to the total input microwave energy and the enhancements in mining operations achieved per unit of input microwave energy. Current research endeavors to suggest a new pathway by addressing the existing knowledge gaps prioritizing energy efficiency analysis in the microwave treatment of rocks. To calculate the absorbed microwave energy, a calorimetric technique is employed. Moreover, changes in parameters representative of improvements in various mining operations are evaluated through the lens of energy analysis, offering a comprehensive understanding of the method's efficiency. This novel approach not only opens avenues for the adoption of microwave treatment technology in the mining industry but also aids in charting future research directions.

5.4. Methodology

5.4.1. Sample preparation

The rock samples utilized in this study are basalt sourced from the Chifeng area in China (Rabiei et al., 2023), received in the form of intact blocks measuring 600×600×600 mm^3. To prepare the cylindrical samples required for UCS experiments, cores with diameters of 50 mm are first extracted from the basalt blocks using a radial drilling machine. These cores are then cut to a length of 100 mm to achieve a 2:1 length-to-diameter ratio for the cylinders, following ASTM recommendations (Standard, 2010). Subsequently, both ends of the samples are ground using a diamond wheel grinder machine to ensure parallelism and suitability for the UCS experiment. Additionally, the side surfaces of the samples are smoothed using sandpaper #400 to facilitate the attachment of strain gauges for deformation and strain measurements during mechanical testing. The initial water content of the samples is determined to be 1%. To mitigate any potential effects on the microwave treatment characteristics, the samples are subjected to heating at a 60°C standard temperature in a conventional oven for 24 hours to ensure their complete dryness.

5.4.2. Property measurements

Accurate data analysis and interpretation in rock studies necessitate comprehensive rock characterization, which includes the measurement of various temperature-dependent rock properties such as density, thermal expansion, heat capacity, thermal conductivity, and electromagnetic parameters. This section offers detailed insights into the measurement procedures employed for determination of these properties and their corresponding values. It is important to note that different samples were utilized for each property measurement. This approach serves two primary purposes: firstly, to mitigate errors arising from repeated heating of samples, and secondly, to accommodate the diverse sample preparation requirements of different apparati. Given these considerations, employing different samples for various experiments ensures the integrity and reliability of the data collected.

The density of the sample is initially determined at room temperature using Archimedes' principle (Spierings et al., 2011), yielding a value of 2870 kg/m³. To assess density at higher temperatures, with the assumption that the mass of the sample remains constant, the density can be calculated using the thermal expansion coefficient as follows:

$$\rho_{(T)}=\frac{M}{V_{(T)}} \tag{5.1}$$

$$V_{(T)}=V_0+\Delta V \tag{5.2}$$

$$\Delta V=3\alpha V_0\Delta T \tag{5.3}$$

In Eqs. (5.1-5.3), T represents temperature, with the subscript (T) denoting the value of the related parameter at temperature T, ρ is the density, M is the mass, V is the volume and α is the linear thermal expansion coefficient. The linear thermal expansion coefficient is determined using a Thermo-Mechanical Analyzer (TMA). Following the standard ASTM procedure, a sample with two parallel surfaces is prepared. Initially, the sample is equilibrated at 25°C and maintained at this temperature for 1 minute. Then, the temperature is increased at a rate of 3°C/min up to 400°C, while the change in the sample's length is continuously measured during the heating process using a linear variable differential transformer (LVDT) (ASTM, 2006). The linear thermal expansion coefficient can then be calculated using Eq. (5.4) as follows:

$$\alpha=\frac{\Delta L}{L_0\Delta T} \tag{5.4}$$

Here, L represents the length of the sample. The calculated linear thermal expansion coefficient is illustrated in Figure 5.1a. Utilizing the obtained values of the thermal expansion coefficient, the density at higher temperatures is computed using Eqs. (5.1-5.3), as depicted in Figure 5.1b.

Heat capacity measurements are conducted using a Differential Scanning Calorimeter (DSC) system following ASTM standard (E1269-11, 2011). A small chunk of basalt rock is crushed into powder form and utilized in the DSC equipment (less than 100 mg). Initially, the sample temperature is reduced in the isothermal chamber to 0°C. Subsequently, the sample is heated at a temperature rate of 20°C/min up to 400°C, while the input energy and, consequently, the heat capacity are continuously recorded. The results of the heat capacity measurement are illustrated in Figure 5.1c.

The thermal diffusivity of the material is determined using the standard ASTM procedure with a Laser Flash Analyzer (LFA) (Measurements, 2007). For this equipment, a disc-shaped sample with a diameter of 12.7 mm and a thickness of 1-3 mm needs to be prepared. The sample is then placed in the chamber, where it undergoes isothermal conditions at every 20°C temperature interval to receive laser energy pulses for the measurement of thermal diffusivity. At each temperature step, the pulses are sent three times to ensure the reliability of the readings. The thermal diffusivity is subsequently correlated to the thermal conductivity as follows:

$$k=\rho C_p D \tag{5.5}$$

Here, k is the thermal conductivity, C_p is the heat capacity, and D is the thermal diffusivity. The results for the thermal diffusivity measurement are illustrated in Figure 5.1d.

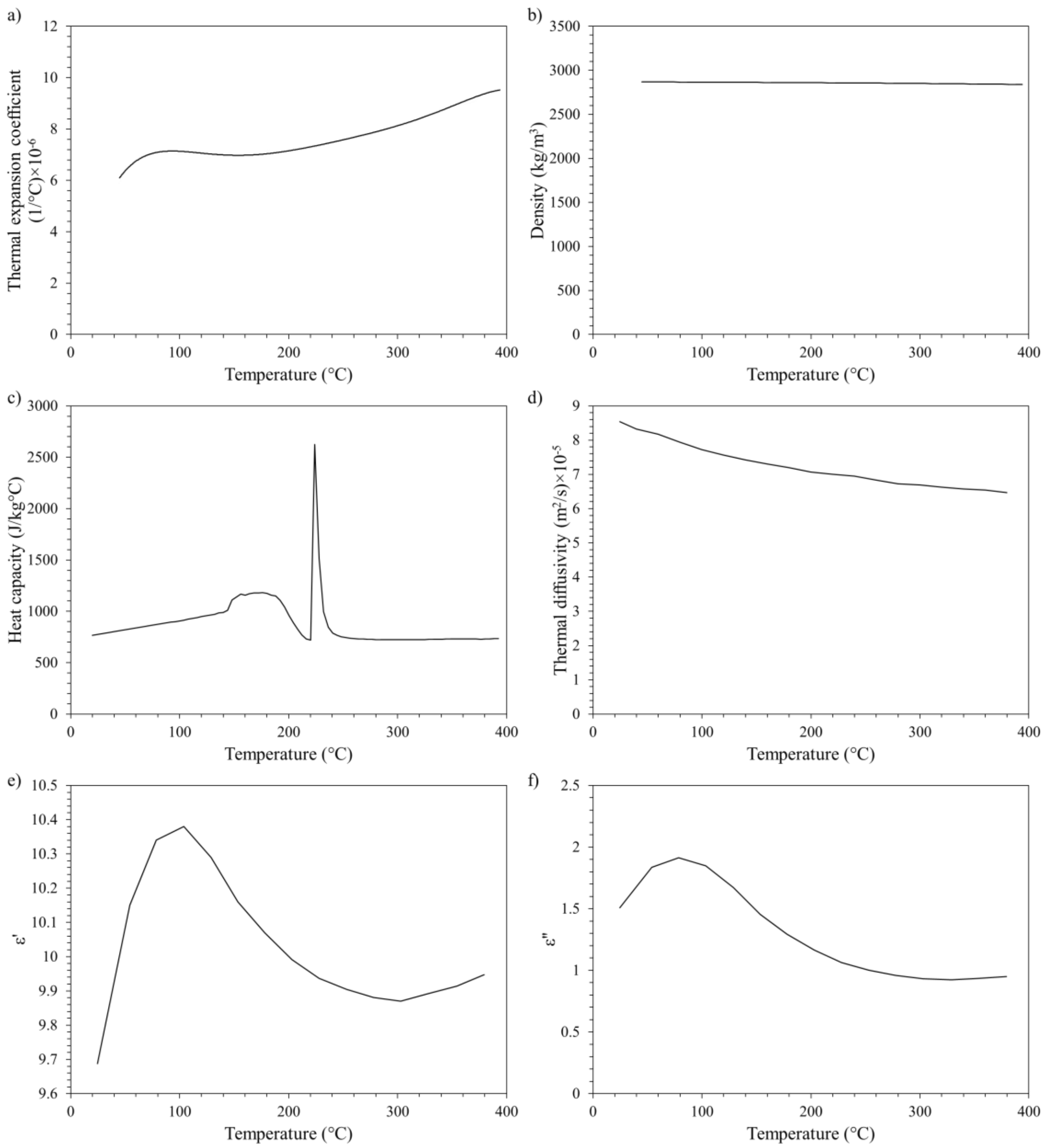

Figure 5.1 The temperature-dependent material properties measured for the basalt rock used in this study: a) thermal expansion coefficient, b) density, c) heat capacity, d) thermal diffusivity, e) real part of the dielectric properties, and f) imaginary part of the dielectric properties.

Arguably, the most critical parameter in the microwave treatment of rocks is the dielectric properties, which comprise both real and imaginary parts and is reported as a complex number, as follows:

$$\varepsilon=\varepsilon'-i\varepsilon'' \tag{5.6}$$

where ε' is the real part and ε'' is the imaginary part of the dielectric properties, with the latter directly influencing heat generation within the rock, as follows:

$$P=2\pi f\varepsilon''\bar{\mathbf{E}}^2+2\pi f\mu''\bar{\mathbf{H}}^2 \tag{5.7}$$

In Eq. (5.7), P is the power by which heat is generated within the sample, f is the frequency, **E** is the electric field intensity, **H** is the magnetic field intensity, and μ'' is the imaginary part of the magnetic permeability of the material. Since the rock used in this study is non-magnetic basalt, its magnetic permeability is expressed as 1, simplifying Eq. (5.7) as follows:

$$P=2\pi f\varepsilon''\bar{\mathbf{E}}^2 \tag{5.8}$$

Following the suggestions by Hutcheon et al. (1992b, 1992a), the dielectric properties of the rock are measured using the cavity perturbation method. With this approach, both the real and imaginary parts of the dielectric properties of the sample are measured at every 25°C temperature step up to 400°C, as depicted in Figures 5.1e and f, respectively.

The summary of material properties at room temperature is presented in Table 5.1. These results, along with their potential influence on the microwave treatment of rocks, will be further discussed in the Results and Discussion section.

Table 5.1. The summary of the measured material properties at room temperature.

Parameter	Symbol	Value	Unit
Thermal diffusivity	D	8.54×10^{-5}	m^2/s
Density	ρ	2870	kg/m^3
Heat capacity	C_p	766	J/(kg°C)
Relative dielectric properties	ε_r	9.69-1.51i	1
Thermal expansion coefficient	α	5.9×10^{-6}	1/°C

5.4.3. Microwave treatment

5.4.3.1. Microwave equipment

An industrial microwave system operating at a frequency of 2.45 GHz is employed for the microwave treatment experiments. The forwarded power of the microwave can be controlled using a gauge ranging from 0 to 15 kW. The cavity is designed for single-mode microwave irradiation with Transverse Electric radiation in mode 10. Additionally, a horn-shaped antenna is positioned at the entrance of the electromagnetic waves to direct energy toward the targeted sample, thereby enhancing absorption per input energy. Figure 5.2a illustrates the design of the microwave cavity used in this study.

5.4.3.2.Post-treatment measurements

To calculate the energy absorbed by the sample during microwave treatment, a calorimetric technique is employed. In this method, following the microwave treatment of each sample, the rock is placed in a calorimeter—a heat-isolated container filled with water (Figure 5.2a). Sufficient time is allowed for the sample to reach an energy equilibrium state with the water, during which both the water and the rock sample attain the same temperature. Subsequently, the total energy absorbed by the sample during microwave treatment can be calculated as follows:

$$Q=M_{w}C_{p_{w}}(T_{e}-T_{0w})+M_{r}C_{p_{r}}(T_{e}-T_{0r}) \tag{5.9}$$

In Eq. (5.9), the subscripts *w* and *r* represent water and rock, respectively. Additionally, the subscript *e* signifies the thermal equilibrium status between rock and water. With the absorbed energy by the rock known, the heat over microwave efficiency (HOME) parameter is defined as follows:

$$\text{HOME}\ (\%)=\frac{Q}{P\times t}\times 100 \tag{5.10}$$

where P is the forwarded microwave power and t is the microwave exposure time.

Calorimetric measurements offer valuable insights into the overall energy absorption of the sample during microwave treatment. However, for a more detailed understanding of temperature distribution and its development within the sample, thermal imaging techniques are employed using a thermal camera (Figure 5.2a). Following each microwave treatment experiment, a thermal image is captured of the sample, providing detailed temperature distribution on its surface.

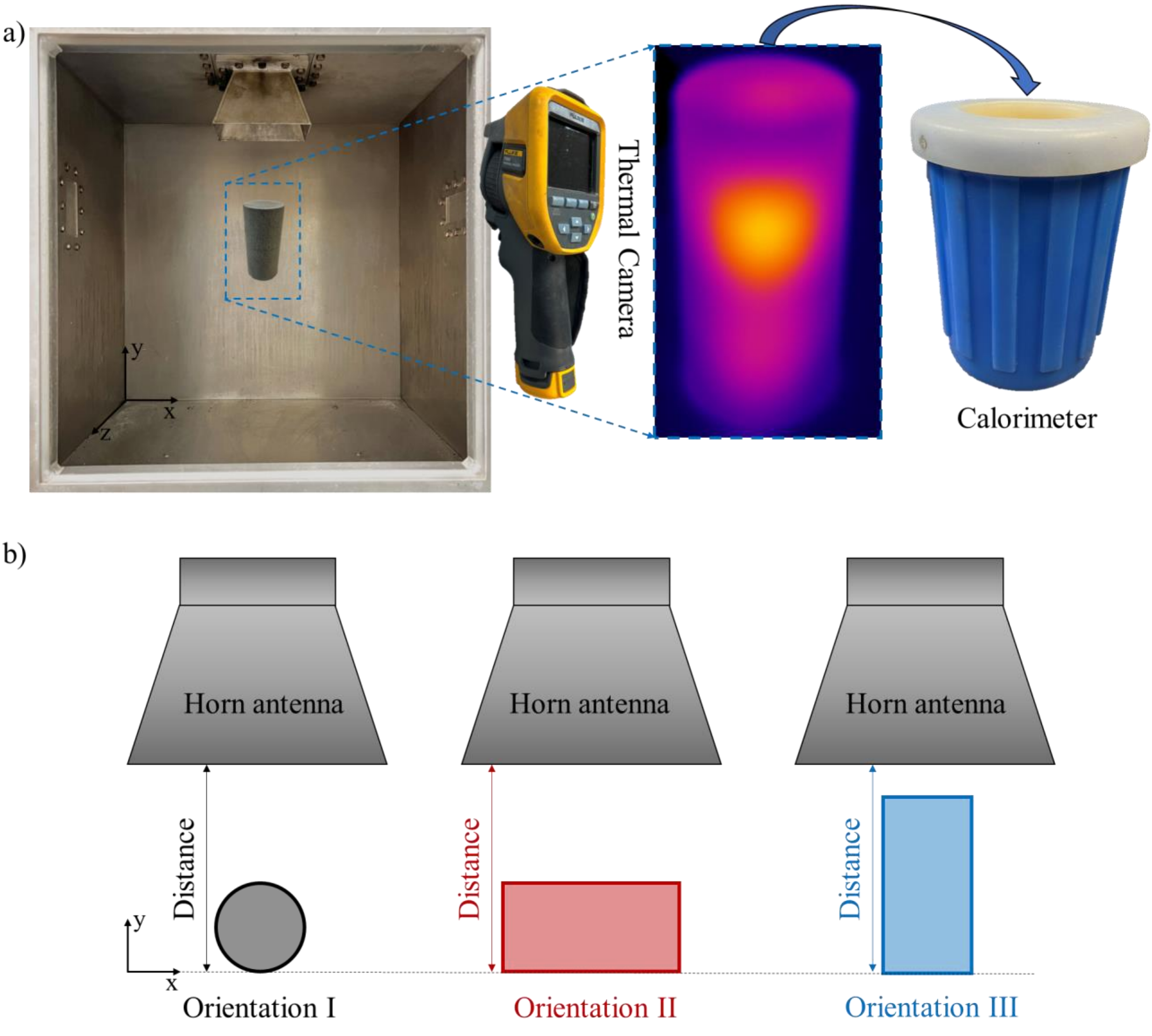

Figure 5.2 a) The experimental equipment used for the microwave treatment experiments, b) the orientation and distance of the sample relative to the antenna.

5.4.3.3.Heating experiment specifications

This study explores two different scenarios for microwave treatment of UCS-sized samples. Initially, samples are irradiated with a low energy dosage (power of 3 kW and exposure time of 4.32 s) while positioned at various locations and orientations within the cavity to optimize HOME (Figure 5.2b). It is noteworthy that for this set of experiments, the same sample is used repeatedly to mitigate the effect of rock heterogeneity. Moreover, the low energy dosage is selected to minimize potential changes in the rock's characteristics due to heating, ensuring that the maximum temperature reached in the sample remains below 80°C. Based on the results obtained from the first scenario, the optimized sample location within the cavity is determined. This optimized location is then utilized in the second scenario for the treatment of UCS-sized basalt samples at different powers and exposure times. Three power levels—3, 7, and 12 kW—are considered, and for each power level, two energy dosages are administered, representing low energy dosage (approximately 20 kWhr/t input microwave energy) and high energy dosage (approximately 50 kWhr/t input microwave energy). Detailed experimental specifications are provided in Table 5.2. In both scenarios, thermal camera imaging and calorimetric results are utilized to facilitate data analysis post-treatment. To ensure the reliability of the results, at each sample location, microwave power, and exposure time, a minimum of three test repetitions are conducted.

5.4.4. Mechanical analysis

UCS tests are conducted on the samples treated with microwave energy following the ASTM standard (Standard, 2010). Additionally, three untreated samples undergo UCS testing using an MTS Rock Testing System to provide insight into the intrinsic mechanical properties of the base material. Strain gauges, consisting of two axial and two radial sensors, are installed on each sample to capture displacement characteristics during the strength test. Throughout each test, data for force, as well as axial, and radial strains are continuously recorded over time, offering insights into UCS, elastic modulus, Poisson's ratio, and strain energy characteristics of this rock material. UCS represents the highest achievable sample stress during the experiment. The change in UCS value after microwave treatment is examined through an energy efficiency-based perspective by analysing the achieved reduction in UCS value per microwave energy. This analysis is conducted using a parameter defined as weakening over microwave energy (WOME), as follows:

$$\text{WOME (\%/kWhr/t)}=\frac{\Delta UCS/UCS_{untreated}\times 100}{\text{Microwave Energy/M}} \tag{5.11}$$

In Eq. (5.10), either the input or absorbed microwave energy can be used to calculate WOME which results in the following definitions:

$$\text{WOME}_{gross}\text{ (\%/kWhr/t)}=\frac{\Delta UCS/UCS_{untreated}\times 100}{\text{Input Microwave Energy/M}} \tag{5.12}$$

$$\text{WOME}_{net}\text{ (\%/kWhr/t)}=\frac{\Delta UCS/UCS_{untreated}\times 100}{\text{Absorbed Microwave Energy/M}} \tag{5.13}$$

Table 5.2 Specifications of the microwave treatment experiments conducted in this research.

Scenario	Power (kW)	Exposure time (s)	Average input microwave energy (kWhr/t)	Number of tests
Scenario I: Location optimization	3	4.32	5.99	3 (for each location)
Scenario II: Microwave treatment	3	14.32	19.04	5
	3	38.32	51.79	6
	7	6.53	20.66	6
	7	16.51	51.06	5
	12	3.68	19.65	6
	12	9.68	51.28	5

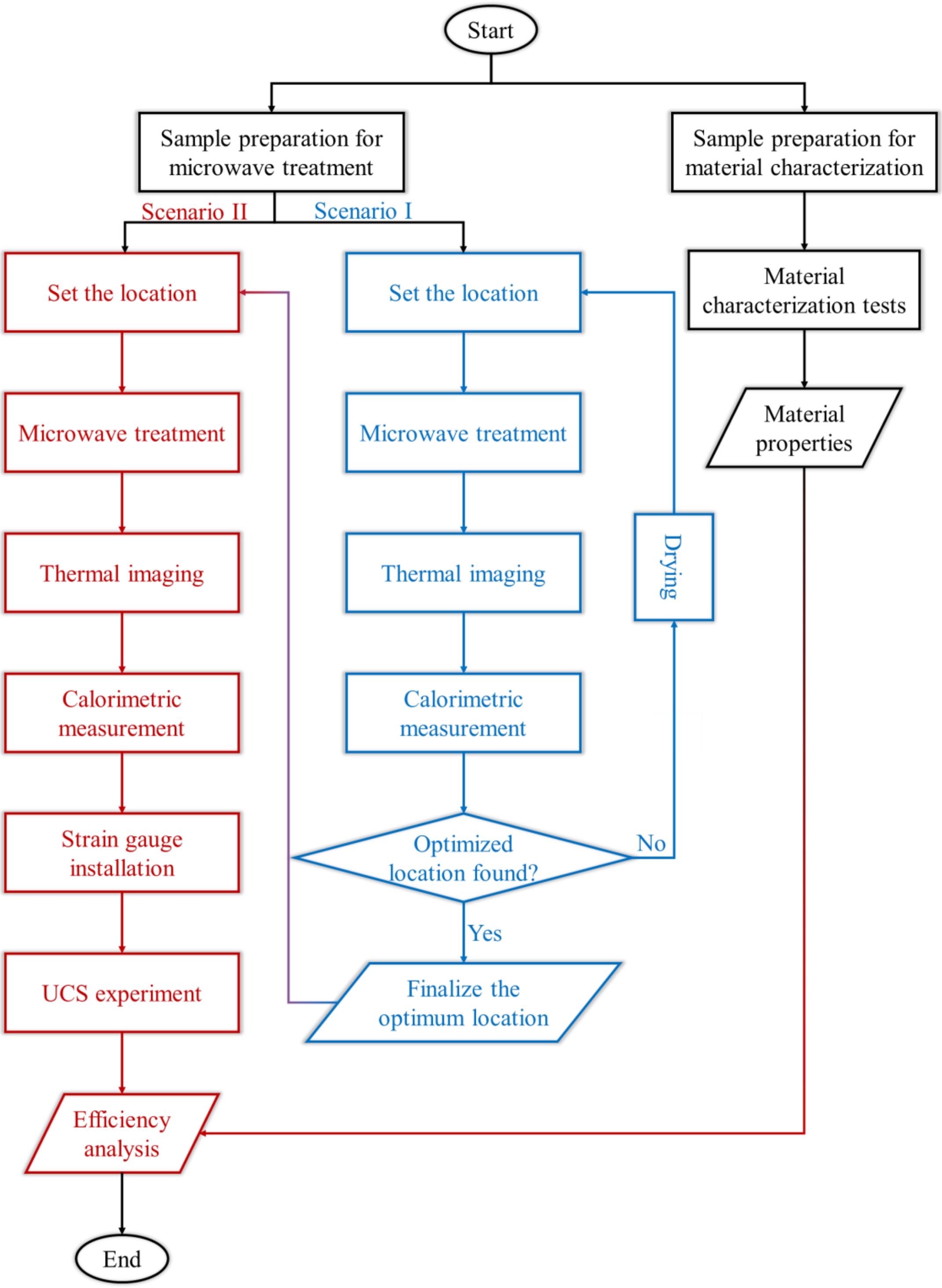

Figure 5.3 The flowchart summarizing the employed methodology in this research.

The slope of the linear elastic section of the stress-strain curve and the ratio of the slopes of the radial and axial strain curves over this same section represent the elastic modulus and Poisson's ratio, respectively. The area under the force-displacement curve is calculated to determine strain energy, which represents the work required to deform the material until the sample breaks.

In summary, this study entails conducting over 70 microwave treatment experiments, followed by corresponding strength tests under UCS specifications and displacement analysis captured using a strain gauging system. The data are analyzed from a novel energy efficiency-based perspective aimed at guiding researchers toward new pathways in understanding the effectiveness of microwave treatment as a rock pre-conditioning method. Figure 5.3 illustrates a flowchart summarizing the methodology employed in this study.

5.5.Results and discussion

5.5.1. Material properties

Understanding material properties is essential for effective microwave treatment, as it enables prediction of the material's behavior when subjected to microwave energy. Key basalt rock parameters—density, thermal expansion coefficient, heat capacity, thermal diffusivity, and dielectric properties—were measured using a temperature-dependent approach up to 400°C (Figure 5.1). The thermal expansion coefficient and real and imaginary parts of the dielectric properties exhibit a peak around 100°C. While the thermal expansion coefficient shows a continuous increase at higher temperatures, dielectric values peak at this temperature. Additionally, density remains relatively constant within the temperature range studied. However, heat capacity exhibits a prominent peak around 230°C, possibly indicating a phase change. Conversely, thermal diffusivity demonstrates a consistent decrease from room temperature to 400°C, decreasing from 8.54×10^{-5} m²/s to less than 7×10^{-5} m²/s. These material properties play a crucial role in the analysis of microwave treatment data.

Among the rock parameters, the dielectric properties of the rock are the most crucial in characterizing energy absorption during microwave treatment. The real and imaginary parts of the complex dielectric properties influence the response of the rock material to microwave irradiation in distinct ways. Firstly, the imaginary part (ε'') directly influences energy absorption according to Eq. (5.8). Assuming the electric field remains constant, an increase in ε'' leads to higher energy absorption. Moreover, both the real and imaginary parts of dielectric properties affect the electric field distribution and its intensity within the sample, similarly influencing energy absorption as per Eq. (5.8). Thus, due to the intricate relationship between the real and imaginary parts of permittivity and sample energy absorption, finding an optimized microwave treatment plan is essential to enhance HOME and WOME.

5.5.2. Optimizing energy absorption

Prior to microwave treatment experiments, it is crucial to distinguish between the information provided by calorimetric studies and thermal imaging for a better understanding of rock behavior. Firstly, calorimetric measurements do not yield temperature distribution of the sample post-microwave treatment, making it impossible to capture the maximum temperature—a vital parameter for evaluating potential damage to rock samples. Conversely, thermal camera images cannot offer a comprehensive understanding of overall energy absorption during microwave treatment, as their results are limited to the surface of the sample.

This study investigates the approach of using the average surface temperature from thermal camera images to calculate overall energy absorption. The sample in orientation I (shown in Figure 5.2) is positioned at various distances from the antenna, and immediately after microwave treatment, a thermal image is captured (Figure 5.2b). Subsequently, the sample is placed inside the calorimeter for overall energy absorption measurement. Energy absorption is calculated for sample placed at different distances using the average surface temperature from the thermal images. The results from thermal images are then compared with calorimetric measurements as shown in Figure 5.4. Across all distances, it is observed that the calculation from thermal images underestimates the energy absorption of the sample, indicating the presence of higher temperature points inside the sample. The discrepancy between the two methods can be as large as 20% at certain distances. These findings underscore the importance of utilizing both thermal imagery and calorimetric measurements to understand the effect of microwave treatment on rocks.

To maximize energy absorption and thus, HOME of the samples during microwave treatment for potentially achieving the most efficient treatment, the sample location in the cavity must be optimized. The sample is placed at various distances from the antenna with three different orientations for this purpose, as shown in Figure 5.2b. The results of the distance test analysis for both calorimetric measurement and thermal imagery are presented in Figure 5.5. It's observed that the trend of energy absorption versus distance differs significantly depending on the orientation used. For orientations I, II, and III, the maximum energy absorption occurs at points 5, 3, and 2 of their respective colours, respectively. Regarding temperature distribution, two thermal images are taken for each sample (one from each side) to provide a comprehensive understanding of surface temperature distribution. This enables capturing an average surface temperature of the sample. Based on the results in Figure 5.5, the distance of point 5 (155 mm from the antenna) for orientation I is selected for two reasons. Firstly, this point exhibits the highest energy absorption compared to other distances and orientations with approximate HOME value of 72%. Secondly, the surface temperature is relatively low, indicating a higher temperature concentration inside the sample, which could potentially cause more damage to the sample (Hassani et al., 2020).

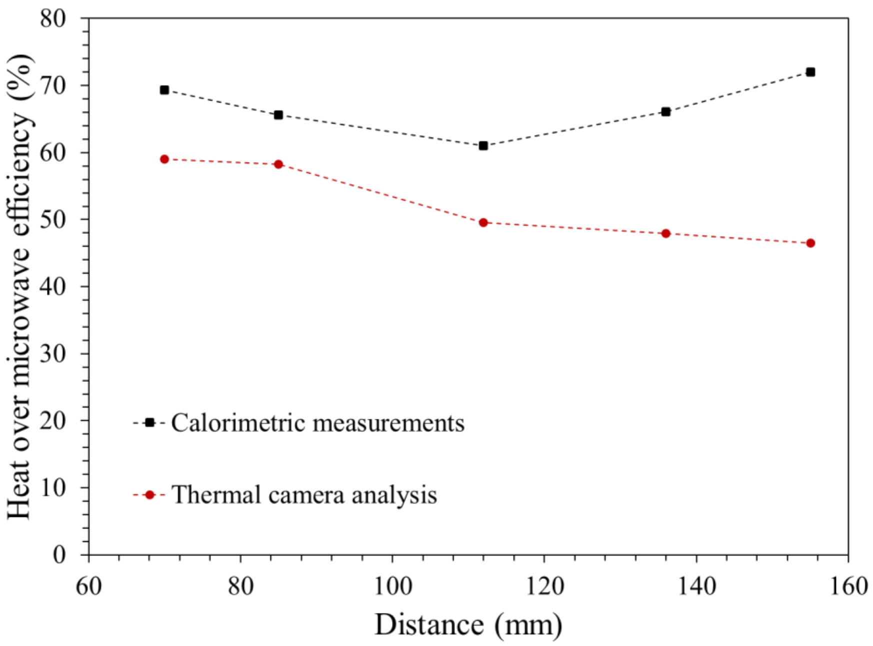

Figure 5.4 Comparison between the HOME calculated from thermal camera images and calorimetric measurements.

5.5.3. *Microwave treatment efficiency*

After optimizing the distance and location of the sample within the cavity, microwave treatment experiments are conducted. The samples are treated with microwave energy at three different powers (3, 7, and 12 kW) and two energy dosages (approximately 20 and 50 kWhr/t of input microwave energy). Following the treatment experiments, both thermal imagery and calorimetric measurements are conducted.

Comparison between thermal images and calorimetric measurements for low and high powers, as well as low and high energy dosages, is depicted in Figure 5.6. Several points can be interpreted from the results. Firstly, the larger energy dosage is almost 2.5 times greater than the lower energy dosage, yet the temperature distributions observed in the thermal images show a maximum temperature less than twice as large. This phenomenon primarily occurs due to two reasons. Firstly, the effect of the rock's thermal conductivity causes heat generated in the sample during microwave exposure to transfer from areas of higher temperature to those of lower temperature, thereby reducing the maximum temperature of the sample. Secondly, the higher energy dosage requires a longer exposure time, allowing the sample more time to be in contact with the surrounding air, leading to natural or turbulent convection which reduces the overall surface temperature.

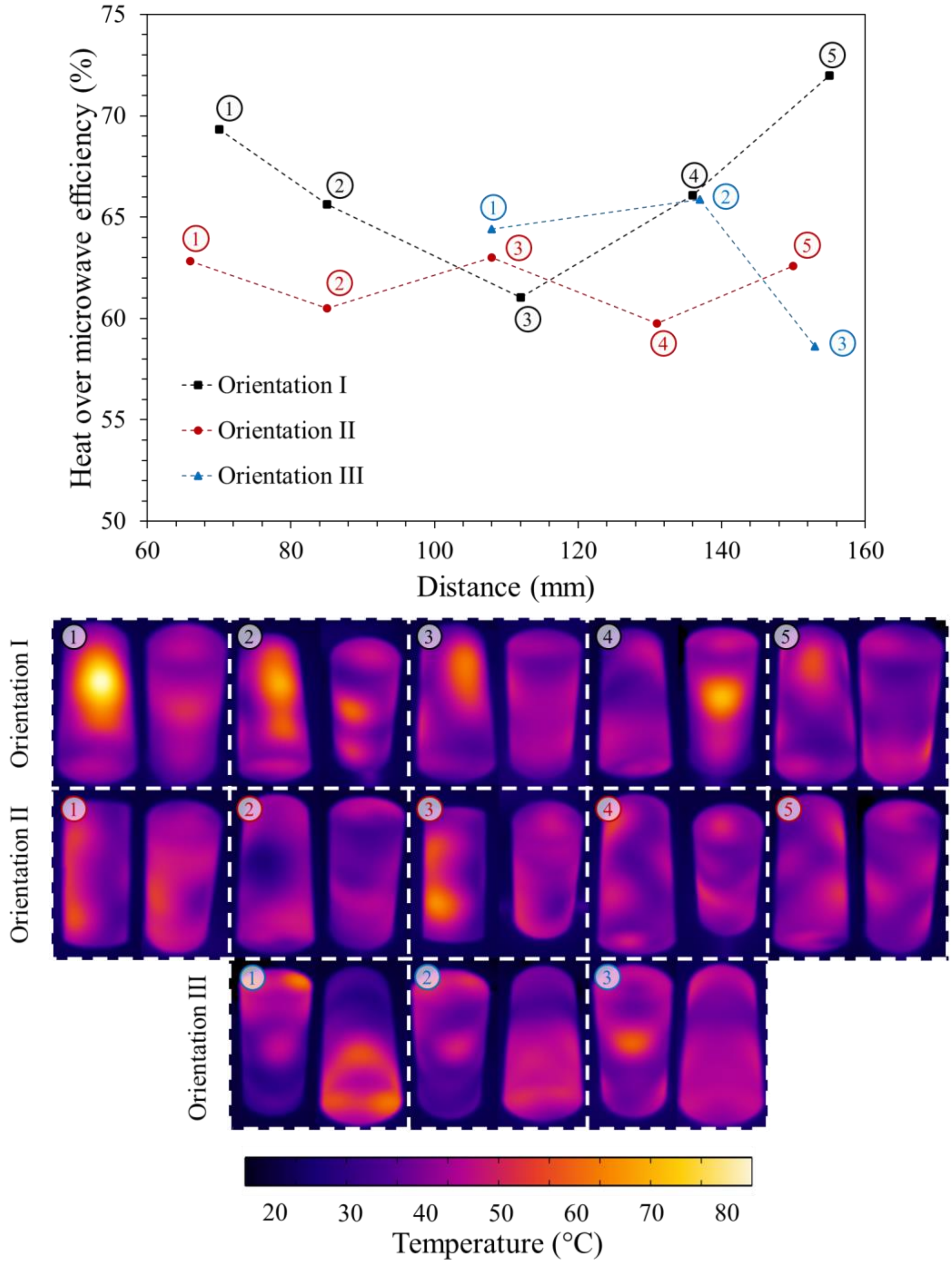

Figure 5.5 The results of the distance test analysis depicting the temperature distribution and calorimetric measurements.

Regarding calorimetric measurements, it is observed that the overall percentage of energy absorbed by the sample is lower for larger energy dosages. This can be attributed to the longer exposure time required for achieving a larger energy dosage. During this extended exposure time, the sample loses some of the absorbed energy due to natural or turbulent convection upon contact with surrounding air, factors not accounted for in calorimetric measurements. Therefore, heat loss due to convection increases as exposure time increases, resulting in a lower overall energy absorption percentage. Furthermore, the dielectric properties of the material are temperature-dependent. Specifically, at 100°C, there is a peak for the real and imaginary parts of the dielectric properties, which aligns closely with the maximum temperature observed for low energy dosage in the thermal images. As temperatures increase with higher energy dosages, the samples surpass the peak point for dielectric properties, changing the overall energy absorption behaviour.

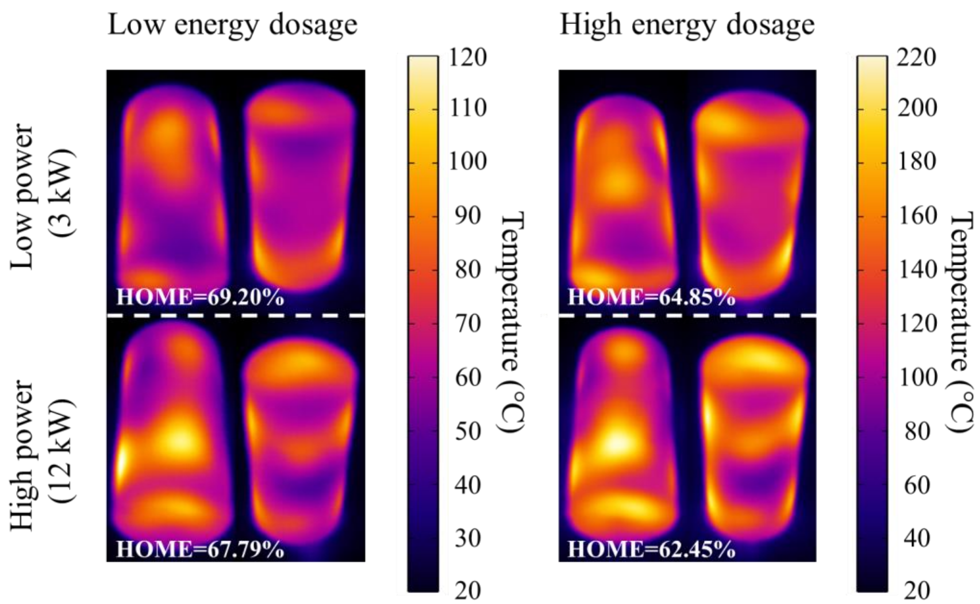

Figure 5.6 The temperature distribution and HOME of the samples after microwave treatment for high and low powers and energy dosages.

After the microwave treatment experiments, four strain gauges—two axial and two radial—were attached to each sample to measure the elastic modulus and Poisson's ratio. Subsequently, the samples were subjected to UCS testing. Figure 5.7 presents the UCS values obtained at varying powers and exposure times. Notably, an increase in exposure time resulted in a decrease in UCS values, with this reduction being more intense at higher powers. While Figure 5.7 demonstrates the achieved strength reduction resulting from microwave treatment, it does not fully elucidate the efficiency of the method. The evaluation parameters are changed to achieve a better understanding of the energy efficiency of the microwave treatment. First, the input and absorbed microwave energy is utilized instead of exposure time on the horizontal axis. This adjustment equalizes the scale of the horizontal axis for different powers used, facilitating more meaningful comparisons. Additionally, rather than solely focusing on UCS values, the change in strength is evaluated based on microwave energy ($WOME_{gross}$ and $WOME_{net}$). This approach offers a more nuanced understanding of the microwave treatment's efficiency in enhancing mining excavation (Figure 5.8).

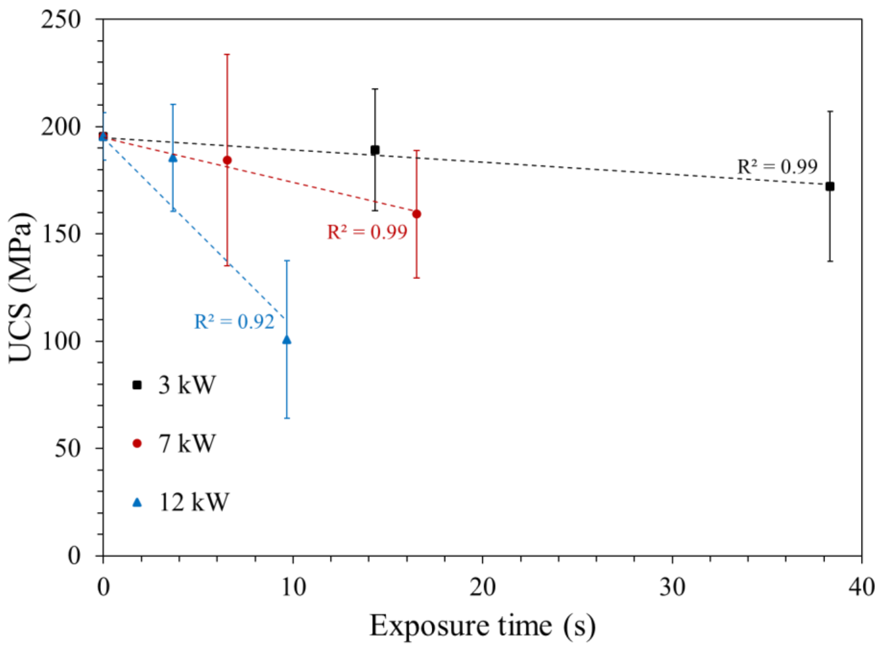

Figure 5.7 The UCS values after microwave treatment at different powers and exposure times.

The results of the UCS data are analyzed with an energy efficiency-based approach in Figure 5.8. The evaluated parameters are UCS, $WOME_{gross}$, and $WOME_{net}$, which are drawn versus input and absorbed microwave energy. A linear relationship exists between the three parameters and the microwave energy depicted through the linear trendline with R-squared values of more than 0.90. For instance, Figure 5.8c shows $WOME_{gross}$ versus input microwave energy for different powers. The trendline demonstrates a linear correlation between the microwave energy and $WOME_{gross}$, with R-squared values of 0.95, 0.93, and 0.99 for 3, 7, and 12 kW, respectively. Additionally, WOME increases with microwave energy across all cases. This phenomenon is because, at the low microwave energy used in this study, the sample's temperature does not increase sufficiently to create significant fractures, resulting in lower WOME. However, as the energy dosage increases, fractures become more pronounced, leading to more significant UCS reduction and higher WOME. Furthermore, consistent with previous observations, higher powers exhibit greater efficiency than lower powers. Quantitative analysis reveals that increasing power from 3 to 12 kW for the same microwave energy can enhance WOME by over four times in certain cases.

Comparing the charts for absorbed and input microwave energy in Figure 5.8 shows a steeper trendline slope when the horizontal axis is the absorbed microwave energy. This is because the sample only partially absorbs the input microwave energy (around 65%), and the rest does not take part in heating and damaging the samples. Therefore, the range at which the microwave treatment experiments are conducted is smaller for the absorbed microwave energy than the input microwave energy (approximately 0-35 kWhr/t to 0-50 kWhr/t). Using absorbed microwave energy instead of input is physically more meaningful. This way, the question for assessing the efficiency of the microwave treatment is divided into two sub-questions: I) how much of the input microwave energy is transferred to the rock and II) how much damage is caused to the sample due to the absorbed microwave energy. In order to achieve a more energy-efficient microwave treatment, not only the overall microwave energy absorption but also, the damage caused by the absorbed microwave energy needs to increase.

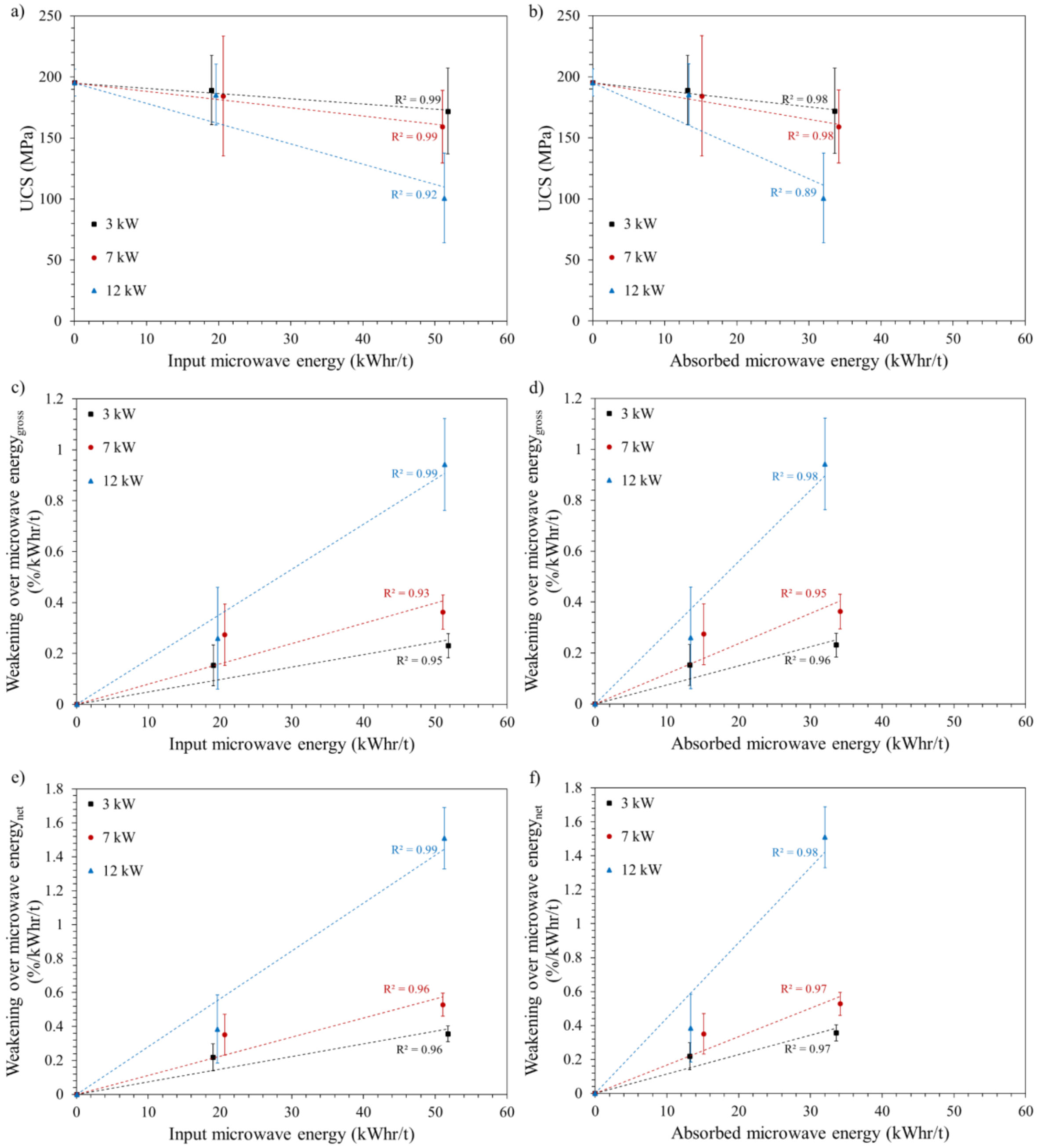

Figure 5.8 Evaluating the influence of microwave treatment on the rocks' strength reduction by analyzing a) changes in the UCS versus input microwave energy, b) changes in UCS versus the absorbed microwave energy, c) changes in $WOME_{gross}$ versus input microwave energy, d) changes in $WOME_{gross}$ versus absorbed microwave energy, e) changes in $WOME_{net}$ versus input microwave energy, c) changes in $WOME_{net}$ versus absorbed microwave energy.

Using strain gauge measurements, the elastic modulus and Poisson's ratio at different energy dosages are determined. Figures 5.9a and 5.9b illustrate the elastic modulus and Poisson's ratio versus the input microwave energy, respectively. Unlike the UCS values shown in Figure 5.9a, no clear linear relationship is observed between these parameters and the input microwave energy. This discrepancy can be attributed to several factors. Firstly, the nature of the material remains relatively unchanged during microwave treatment, as the energy levels employed are not sufficient to induce significant alterations. Additionally, micro/macro fractures occur throughout the sample during microwave treatment. While strain gauges effectively capture deformation characteristics at the localized points of attachment upon the surface of samples, they may not fully account for fractures occurring deep within and throughout such samples. For accurate consideration of fractures in Poisson's ratio and elastic modulus calculations, extensometers are preferable as they measure deformation from top to bottom of the sample during the UCS experiment.

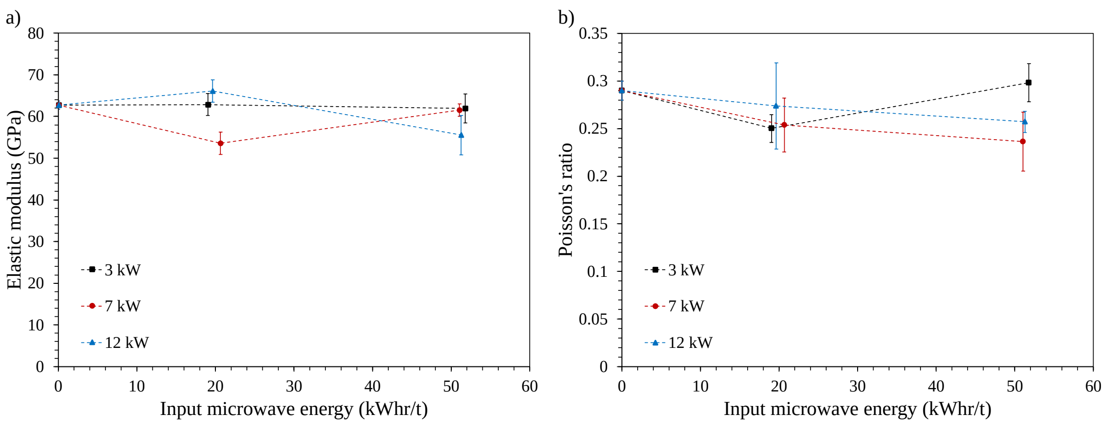

Figure 5.9 The effect of microwave treatment on the elastic modulus and the Poisson's ratio of the basalt rock.

The analysis of Poisson's ratio and elastic modulus parameters alongside the general reduction in UCS with increasing power and exposure time has provided new insights into the impact of microwave treatment on rocks. By calculating the strain energy using force-deformation curves, a more comprehensive understanding of microwave treatment effectiveness is achieved, as it captures both strength reduction and deformation characteristics simultaneously. The results reveal a significant reduction in the area under the stress-strain curve (strain energy) compared to untreated samples (Figure 5.10). Notably, a linear relationship is observed between input microwave energy and the area under the curve, with R-squared values of 0.95, 0.94, and 0.99 for 3, 7, and 12 kW, respectively. Moreover, the disparity between different powers is pronounced, with lines representing 3 and 7 kW being closely clustered, while the 12 kW line exhibits a more drastic reduction in the area under the curve.

5.5.4. Potential application

Following the understanding of the effect of microwave treatment on the characteristics of rocks from an energy efficiency perspective, there are several discussions to be had regarding its potential applications in the mining industry.

The analysis of the results presented in Figure 5.8 reveals the presence of relatively large error bars for certain data points, despite conducting more than 5 repeats in some cases. This variability can be attributed to the heterogeneous nature of rocks, coupled with the unpredictable effects of microwave treatment. Addressing this issue is imperative for the practical application of microwave treatment in the field. Potential solutions include increasing the number of tests and repetitions, as well as implementing several experimental methodologies alongside each other. By adopting these approaches, we can not only enhance the reliability of the data but also gain a more comprehensive understanding of the effectiveness of microwave treatment on rocks, paving the way for its practical implementation in field settings.

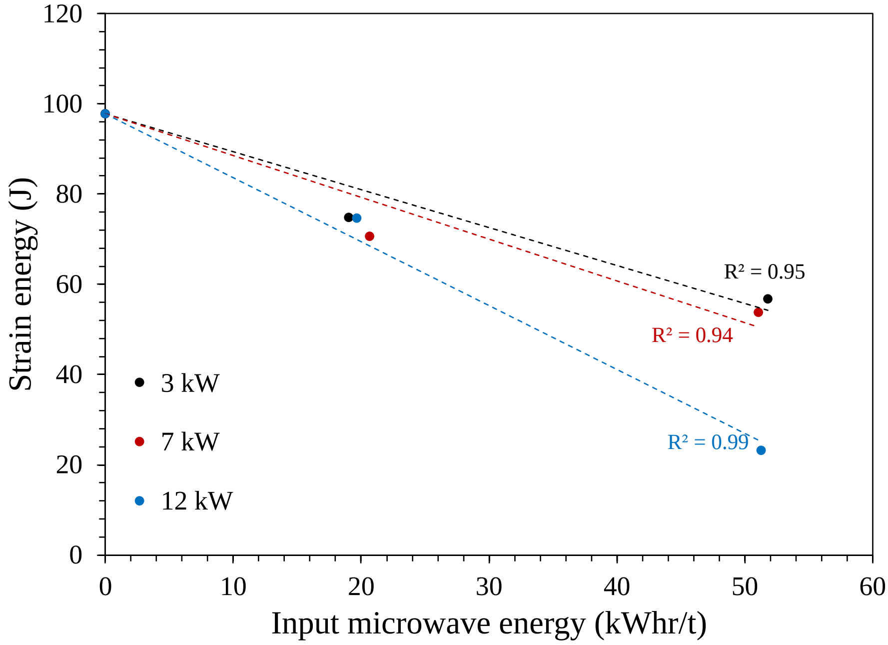

Figure 5.10 Strain energy calculated for samples at different powers and microwave energies.

The results depicted in Figures 5.8 and 5.10 underscore the importance of employing higher powers to enhance the efficiency of microwave treatment. Higher power trendlines exhibit steeper slopes, indicative of increased WOME (representing microwave treatment efficiency) with higher powers. Notably, the trendlines for 3 and 7 kW powers closely resemble each other, while the trendline for 12 kW (Figure 5.8) demonstrates a more pronounced increase in slope, suggesting an exponential rise in WOME with increasing power. This hypothesis is further explored in Figure 5.11, where $WOME_{gross}$ and $WOME_{net}$ are plotted against power for scenarios involving the high energy dosage. Figure 5.11a reveals that a second-degree polynomial trendline yields a strong correlation (R-squared > 0.95) between WOME and power. Extrapolating from this trendline predicts a substantial increase in WOME with higher power usage. For instance, $WOME_{gross}$ could increase from approximately 0.15%/kWhr/t for 3 kW to 66.92%/kWhr/t for 100 kW. Notably, while the power increases by 33.33, $WOME_{gross}$ increases by 446.13 times. Furthermore, Figure 5.11b emphasizes the importance of high microwave absorption as a comparison between the charts related to $WOME_{net}$ and $WOME_{gross}$ shows that at 100 kW power, while WOMEgross value is at 66.92%/kWhr/t, the value for

$WOME_{net}$ is predicted to be much lower at 35.90%/kWhr/t. That being said, achieving such high power densities presents challenges due to current technological limitations. Although engineers have achieved 100 kW power microwave energy, it operates at lower frequencies (around 0.91 GHz), impacting samples' energy absorption. Furthermore, applying 50 kWhr/t of microwave energy with a 100 kW power requires only 1.15 seconds of exposure time for UCS sized samples used in this study. Given the ramp-up time needed for microwave generators to achieve high power, reaching promising power density levels remains challenging. Nonetheless, with ongoing advancements in microwave technology, this goal may soon be attainable, marking a significant advancement in method implementation within the mining industry.

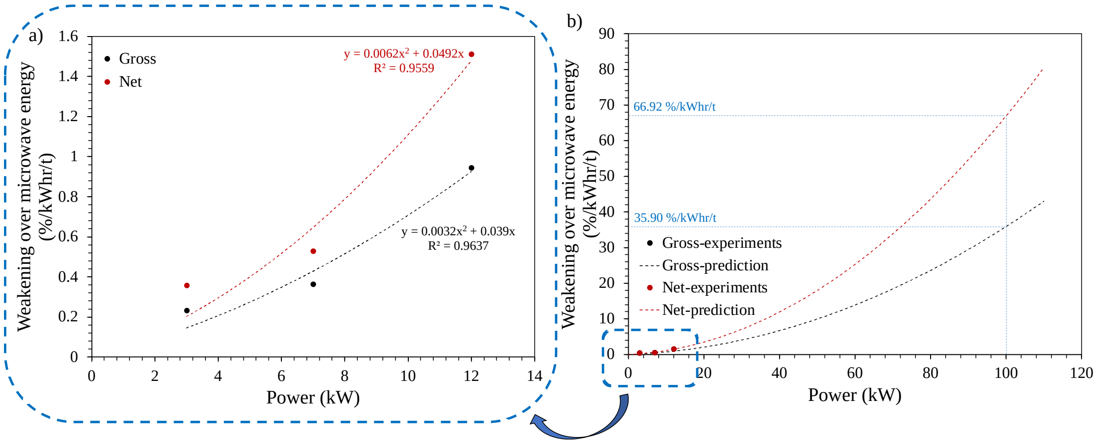

Figure 5.11 The effect of power on WOME at the high energy dosage for a) the powers used in the experiments and b) theoretical increased powers.

While this study primarily examines the efficacy of microwave treatment in mining excavation, recent research indicates that its application in one mining operation can significantly influence the product input and output of subsequent processes (Ahmadihosseini et al., n.d.). Utilizing microwave treatment during excavation stages may not only enhance efficiency in extraction but also yield benefits in operations such as crushing, liberation, and comminution. This ripple effect could result in exponential improvements in treatment efficiency across the mining industry as a whole. Future investigations could delve deeper into understanding the effects of microwave treatment in one operation on the subsequent stages of the mining process.

5.6. Conclusions

The current study utilizes a novel energy efficiency-based methodology to assess the efficacy of microwave treatment for enhancing mining excavation. Conducting over 200 experiments including material characterization, microwave treatment of UCS samples at varying powers and energy dosages, thermal imaging, calorimetric measurements, and mechanical testing, this approach yielded quantitative insights into the potential of microwave treatment in practical field applications. The data analysis is looked at with a fresh perspective using parameters, namely HOME and WOME, which provide valuable insight for the engineers using microwave treatment in mining applications. The key findings can be summarized as follows:

- Comprehensive temperature-dependent material characteristic data up to 400°C for basalt is provided emphasizing the importance of accurate material characterization for proper data analysis in experimental research.
- Energy efficiency-based analysis underscores the significance of employing both thermal imaging and calorimetric measurements. While thermal imaging offers detailed surface temperature distribution data, calorimetry provides insights into overall energy absorption. Integrating these datasets enhances the understanding of temperature dynamics within the sample.
- Optimization of sample placement significantly enhances energy absorption, yielding improvements of over 15% in some cases.
- Employing an energy efficiency-based perspective provides quantitative evidence supporting the potential of microwave treatment for enhancing mining excavation.

- Optimizing the microwave treatment scenarios selected for this research has increased the efficiency by more than 4 times in some cases.
- Quantitative analysis highlights the importance of utilizing higher microwave powers to improve treatment efficiency. Increasing power from 3 to 100 kW results in exponential increases in WOME, from 0.15 to 66.92%/kWhr/t, the high range of which is within the scope of field application by engineers.

References

Ahmadihosseini, A., Aslam, A., & Ferri Hassani, A. S. (n.d.). Investigating the Efficiency of Microwave Treatment in Mine-to-Mill Operations: An Energy-Based Analysis.

Ahmadihosseini, A., Shadi, A., Rabiei, M., Samea, P., Hassani, F., & Sasmito, A. P. (2022). Computational study of microwave heating for rock fragmentation; model development and validation. International Journal of Thermal Sciences, 181, 107746.

Ahmed, H. M., Ahmadihosseini, A., Hassani, F., Hefni, M. A., Ahmed, H. M., Saleem, H. A., Moustafa, E. B., & Sasmito, A. P. (2023). Numerical and experimental analyses of rock failure mechanisms due to microwave treatment. Journal of Rock Mechanics and Geotechnical Engineering, 15(10), 2483–2495.

Ali, A. Y., & Bradshaw, S. M. (2009). Quantifying damage around grain boundaries in microwave treated ores. Chemical Engineering and Processing: Process Intensification, 48(11–12), 1566–1573.

Ali, A. Y., & Bradshaw, S. M. (2010). Bonded-particle modelling of microwave-induced damage in ore particles. Minerals Engineering, 23(10), 780–790.

Aramendia, E., Brockway, P. E., Taylor, P. G., & Norman, J. (2023). Global energy consumption of the mineral mining industry: Exploring the historical perspective and future pathways to 2060. Global Environmental Change, 83, 102745.

ASTM, E. (2006). Standard test method for linear thermal expansion of solid materials by thermomechanical analysis. ASTM E228-17, West Conshohocken, PA.

Batchelor, A. R., Jones, D. A., Plint, S., & Kingman, S. W. (2015). Deriving the ideal ore texture for microwave treatment of metalliferous ores. Minerals Engineering, 84, 116–129.

Cui, G., Chen, T., Feng, X., Chen, Z., Elsworth, D., Yu, H., Zheng, X., & Pan, Z. (2020). Coupled multiscale-modeling of microwave-heating-induced fracturing in shales. International Journal of Rock Mechanics and Mining Sciences, 136, 104520.

Deyab, S. M., Ahmadihosseini, A., Rafezi, H., Hassani, F., & Sasmito, A. P. (2023). Investigating Microwave Treatment of Rocks Based on Fracture Mechanics Analysis in Mode I Fracture Toughness Test. Rock Mechanics and Rock Engineering, 56, 5275–5291.

Deyab, S. M., Rafezi, H., Hassani, F., Kermani, M., & Sasmito, A. P. (2021). Experimental investigation on the effects of microwave irradiation on kimberlite and granite rocks. Journal of Rock Mechanics and Geotechnical Engineering, 13(2), 267–274.

E1269-11, A. (2011). Standard test method for determining specific heat capacity by differential scanning calorimetry. Am. Soc. Test. Mater, 1, 1–6.

Hartlieb, P., Kuchar, F., Moser, P., Kargl, H., & Restner, U. (2018). Reaction of different rock types to low-power (3.2 kW) microwave irradiation in a multimode cavity. Minerals Engineering, 118, 37–51.

Hassani, F., Nekoovaght, P. M., & Gharib, N. (2016). The influence of microwave irradiation on rocks for microwave-assisted underground excavation. Journal of Rock Mechanics and Geotechnical Engineering, 8(1), 1–15.

Hassani, F., Shadi, A., Rafezi, H., Sasmito, A. P., & Ghoreishi-Madiseh, S. A. (2020). Energy analysis of the effectiveness of microwave-assisted fragmentation. Minerals Engineering, 159, 106642.

Holmberg, K., Kivikytö-Reponen, P., Härkisaari, P., Valtonen, K., & Erdemir, A. (2017). Global energy consumption due to friction and wear in the mining industry. Tribology International, 115, 116–139.

Hutcheon, R., Jong, M. de, & Adams, F. (1992). A system for rapid measurements of RF and microwave properties Up to 1400° C. Part1: theoritical development of the cavity frequency-shift data analysis equations. Journal of Microwave Power and Electromagnetic Energy, 27(2), 87–92.

Hutcheon, R., Jong, M. de, Adams, F., Wood, G., McGregor, J., & Smith, B. (1992). A System for Rapid Measurements of RF and Microwave Properties Up to 1400° C. Part 2: Description of Apparatus, Data Collection Techniques and Measurements on Selected Materials. Journal of Microwave Power and Electromagnetic Energy, 27(2), 93–102.

Jones, D A, Kingman, S. W., Whittles, D. N., & Lowndes, I. S. (2007). The influence of microwave energy delivery method on strength reduction in ore samples. Chemical Engineering and Processing: Process Intensification, 46(4), 291–299.

Jones, Dafydd Aled, Kingman, S. W., Whittles, D. N., & Lowndes, I. S. (2005). Understanding microwave assisted breakage. Minerals Engineering, 18(7), 659–669.

Kahraman, S., Canpolat, A. N., & Fener, M. (2020). The influence of microwave treatment on the compressive and tensile strength of igneous rocks. International Journal of Rock Mechanics and Mining Sciences, 129, 104303.

Lan, W., Wang, H., Zhang, X., Fan, H., Feng, K., Liu, Y., & Sun, B. (2020). Investigation on the mechanism of micro-cracks generated by microwave heating in coal and rock. Energy, 206, 118211.

Lehmann, G., Mayr, M., Käsling, H., & Thuro, K. (2023). Microwave pre-conditioning of granite and concrete and the implications on their geotechnical parameters. International Journal of Rock Mechanics and Mining Sciences, 164, 105294.

Li, J., Kaunda, R. B., Arora, S., Hartlieb, P., & Nelson, P. P. (2019). Fully-coupled simulations of thermally-induced cracking in pegmatite due to microwave irradiation. Journal of Rock Mechanics and Geotechnical Engineering, 11(2), 242–250.

Lin, Bai-quan, Zhu, C., Wang, Z., Liu, J., Saffari, P., & Nie, W. (2020). Image and ultrasonic analysis-based investigation of coal core fracturing by microwave energy. International Journal of Rock Mechanics and Mining Sciences, 127, 104232.

Lin, Baiquan, Li, H., Chen, Z., Zheng, C., Hong, Y., & Wang, Z. (2017). Sensitivity analysis on the microwave heating of coal: A coupled electromagnetic and heat transfer model. Applied Thermal Engineering, 126, 949–962.

Lin, F., Feng, X.-T., Yang, C.-X., Li, S.-P., Zhang, J.-Y., Su, X.-X., & Tong, T.-Y. (2022). Experimental study on improving mechanical mining efficiency of deep banded iron ore by microwave presplitting. International Journal of Rock Mechanics and Mining Sciences, 159, 105233.

Lu, G.-M., Feng, X.-T., Li, Y.-H., Hassani, F., & Zhang, X. (2019). Experimental investigation on the effects of microwave treatment on basalt heating, mechanical strength, and fragmentation. Rock Mechanics and Rock Engineering, 52(8), 2535–2549.

Lu, Gao-ming, Li, Y., Hassani, F., & Zhang, X. (2017). The influence of microwave irradiation on thermal properties of main rock-forming minerals. Applied Thermal Engineering, 112, 1523–1532.

Lu, Gaoming, Feng, X., Li, Y., & Zhang, X. (2020). Influence of microwave treatment on mechanical behaviour of compact basalts under different confining pressures. Journal of Rock Mechanics and Geotechnical Engineering, 12(2), 213–222.

Measurements, A. C. E. on T. (2007). Standard Test Method for Determining Thermal Diffusivity by the Flash Method. ASTM International.

Nejati, H., Hassani, F., & Radziszewski, P. (2012). Experimental investigation of fracture toughness reduction and fracture development in basalt specimens under microwave illumination. In Earth and Space 2012: Engineering, Science, Construction, and Operations in Challenging Environments (pp. 325–334).

Peinsitt, T., Kuchar, F., Hartlieb, P., Moser, P., Kargl, H., Restner, U., & Sifferlinger, N. (2010). Microwave heating of dry and water saturated basalt, granite and sandstone. International Journal of Mining and Mineral Engineering, 2(1), 18–29.

Pressacco, M., Kangas, J. J. J., & Saksala, T. (2022). Numerical Modelling of Microwave Heating Assisted Rock Fracture. Rock Mechanics and Rock Engineering, 55(2), 481–503.

Rabiei, M., Samea, P., Shadi, A., & Ghoreishi-Madiseh, S. A. (2023). A discrete element analysis for general failure behavior of basalt. International Journal of Rock Mechanics and Mining Sciences, 167, 105394.

Satish, H., Ouellet, J., Raghavan, V., & Radziszewski, P. (2006). Investigating microwave assisted rock breakage for possible space mining applications. Mining Technology, 115(1), 34–40.

Shadi, A., Ahmadihosseini, A., Rabiei, M., Samea, P., Hassani, F., Sasmito, A. P., & Ghoreishi-Madiseh, S. A. (2022). Numerical and experimental analysis of fully coupled electromagnetic and thermal phenomena in microwave heating of rocks. Minerals Engineering, 178, 107406.

Spierings, A. B., Schneider, M. u, & Eggenberger, R. (2011). Comparison of density measurement techniques for additive manufactured metallic parts. Rapid Prototyping Journal, 17(5), 380–386.

Standard, A. (2010). D7012–10 (2010) Standard test method for compressive strength and elastic moduli of intact rock core specimens under varying states of stress and temperatures.

Annual Book of ASTM Standards, American Society for Testing and Materials, West Conshohocken, PA, 495–498.

Toifl, M., Hartlieb, P., Meisels, R., Antretter, T., & Kuchar, F. (2017). Numerical study of the influence of irradiation parameters on the microwave-induced stresses in granite. Minerals Engineering, 103, 78–92.

Toifl, M., Meisels, R., Hartlieb, P., Kuchar, F., & Antretter, T. (2016). 3D numerical study on microwave induced stresses in inhomogeneous hard rocks. Minerals Engineering, 90, 29–42.

Wang, G., Radziszewski, P., & Ouellet, J. (2008). Particle modeling simulation of thermal effects on ore breakage. Computational Materials Science, 43(4), 892–901.

Wang, Y., & Djordjevic, N. (2014). Thermal stress FEM analysis of rock with microwave energy. International Journal of Mineral Processing, 130, 74–81.

Wei, W., Shao, Z., Zhang, Y., Qiao, R., & Gao, J. (2019). Fundamentals and applications of microwave energy in rock and concrete processing–A review. Applied Thermal Engineering, 157, 113751.

Whittles, D. N., Kingman, S. W., & Reddish, D. J. (2003). Application of numerical modelling for prediction of the influence of power density on microwave-assisted breakage. International Journal of Mineral Processing, 68(1–4), 71–91.

Xu, T., He, L., Zheng, Y., Zou, X., Badrkhani, V., & Schillinger, D. (2020). Experimental and numerical investigations of microwave-induced damage and fracture formation in rock. Journal of Thermal Stresses, 44(4), 513–528.

Yao, J., Tao, M., Zhao, R., Hashemi, S. S., & Wang, Y. (2021). Effect of microwave treatment on thermal properties and structural degradation of red sandstone in rock excavation. Minerals Engineering, 162, 106730.

Zhao, Q. H., Zhao, X. B., Zheng, Y. L., Li, J. C., He, L., & Zou, C. J. (2020). Microwave fracturing of water-bearing sandstones: Heating characteristics and bursting. International Journal of Rock Mechanics and Mining Sciences, 136, 104495.

Zheng, Y., Ma, Z., Zhao, X., & He, L. (2020). Experimental investigation on the thermal, mechanical and cracking behaviours of three igneous rocks under microwave treatment. Rock Mechanics and Rock Engineering, 53(8), 3657–3671.

Zheng, Y L, Ma, Z. J., Yang, S. Q., Zhao, X. B., He, L., & Li, J. C. (2021). A microwave fracturability index (MFI) of hard igneous rocks. International Journal of Rock Mechanics and Mining Sciences, 138, 104566.

Zheng, Y L卌, Zhang, Q. B., & Zhao, J. (2017). Effect of microwave treatment on thermal and ultrasonic properties of gabbro. Applied Thermal Engineering, 127, 359–369.

"You know the expression it's been a pleasure, well it hasn't!"

Mike Ehrmantraut- Breaking Bad

Chapter 6: Discussion

The current thesis evaluates the potential application of microwave treatment as a rock preconditioning method to enhance mechanical excavation. Building upon a comprehensive review of the literature, knowledge gaps in both experimental and numerical research studies are identified. Previous experimental investigations have primarily concentrated on assessing the characteristics of rocks before and after microwave treatment, often neglecting the energy efficiency aspect of the method. Consequently, all experiments conducted in this research are analysed using an energy efficiency-based approach. This framework provides valuable insights into the method's efficiency, which is essential for its potential implementation in practical field applications.

Numerical simulation studies on microwave treatment remain relatively underdeveloped compared to experimental research, mainly due to the complex nature of the process. Microwave treatment consists of various physical phenomena, such as electromagnetic microwave irradiation, heat transfer, and mechanical analysis, among others. Previous literature has frequently relied on simplified assumptions, resulting in outcomes that diverge from experimental data and lack adequate validation of their numerical models. To address these challenges, this research has developed a fully coupled numerical model. This model undergoes quantitative and qualitative validation against benchmark experimental studies conducted as part of this research, ensuring its accuracy and reliability.

This chapter delves deeper into the results of the research and synthesizes the findings presented in the previous chapters. Drawing upon the extensive research conducted throughout this PhD study, this chapter aims to offer insights into the efficacy, challenges, opportunities, and limitations associated with utilizing microwave treatment for various mining operations. Through a systematic analysis of experimental and numerical results, this chapter aims to contribute to the advancement of microwave-based techniques in the mining sector.

6.1. Development of a numerical model

The primary objective of this research was to develop a numerical model capable of accurately capturing the heat transfer phenomena and energy absorption occurring in rock samples during microwave treatment. This attempt involved incorporating various physical phenomena, such as heat conduction, heat convection (both natural and forced), thermal radiation, and electromagnetic irradiation. The resulting numerical model represents one of the first in the field and has been rigorously validated against experimental data on microwave treatment of rocks, both quantitatively and qualitatively, particularly for temperature distribution and energy absorption. This achievement marks a significant milestone in advancing our understanding of microwave treatment in rock processing applications.

The results of the model highlight the increasing influence of natural and forced convection during microwave treatment of rocks with longer exposure times. As exposure time increases, air has more opportunity to cool down the sample surfaces, facilitating the dissipation of heat from concentrated areas within the sample to the surrounding surfaces in contact with air. This enhances the effect of convection, contributing to more pronounced cooling effects. The significance of thermal radiation depends largely on the temperature of the sample surfaces. Higher temperatures amplify the effect of thermal radiation. At the same microwave energy dosage, thermal radiation has a more pronounced effect at higher power levels. This is because higher power levels are required at shorter exposure times, reducing the time available for thermal conductivity to equalize temperature distribution within the rock. Consequently, higher power levels lead to higher maximum temperatures within samples and increased thermal radiation. Moreover, higher power levels also result in greater maximum temperatures and more intense thermal expansion and stress within the sample. This underscores the importance of utilizing higher powers for improved microwave treatment efficiency.

The insights from the numerical models provide deeper insights into phenomena observed in experimental practices, such as the enhanced microwave treatment efficiency achieved with higher power usage at the same energy dosage. Moreover, these models serve to address misunderstandings. Traditionally, for instance, researchers have predominantly focused on the imaginary part of dielectric properties as the primary parameter influencing sample energy absorption during microwave treatment. Consequently, it was expected that a rock sample with a higher imaginary part would exhibit better efficiency, even if their real dielectric properties differed. However, the numerical models reveal a more nuanced understanding. Specifically, when comparing two rock samples with the same value for the imaginary part, changing the real dielectric properties significantly affects the electromagnetic distribution within the cavity. This alteration subsequently impacts the intensity of electric and magnetic fields, thereby exponentially influencing energy absorption and temperature distribution in the samples. Essentially, changing the real dielectric properties can have even a more profound effect on microwave treatment efficiency compared to the imaginary part alone.

Another significant advantage of numerical models is their ability to evaluate situations where experimental investigation is challenging, such as field tests. Conducting field investigations to assess the potential of microwave treatment in improving excavation processes has numerous challenges, including safety hazards, high development costs, and operational learning curves. Prior to making significant investments, numerical models can potentially provide valuable feedback on the feasibility and effectiveness of the methodology, offering insights that can inform decision-making and optimize resource allocation.

6.2. Perspective on experimental data analysis

In this PhD thesis, a novel approach is employed to evaluate the effectiveness of microwave treatment in experimental investigations. This energy efficiency-based methodology assesses many changes in rock characteristics while emphasizing input microwave energy as a primary design factor. By adopting this approach, fresh insights into the application of microwave treatment in practical settings are achieved. For instance, it is observed that, at similar power levels, increasing exposure time typically results in decreased strength factors such as UCS and fracture toughness. However, an analysis from an energy efficiency perspective reveals that while this trend holds true, it is not always energy efficient to increase the energy dosage of the microwave treatment. Furthermore, this approach enables more meaningful comparisons between different treatment scenarios by considering both input and absorbed microwave energy. Insights derived from these energy metrics provide both quantitative and qualitative data, which can also serve as a benchmark for validating the numerical model used in the study.

In the context of field application, the new methodology aids researchers in two significant ways:

1) Current State: The energy efficiency-based methodology integrates both input and absorbed microwave energy as primary considerations in design assessments. This approach establishes a dependable quantitative criterion for evaluating microwave treatment efficiency, which is comprehensible to engineers in the field.
2) Future Potentials: Even if the current state indicates relatively low potential treatment efficiency values, the methodology proves invaluable in assessing microwave treatment's future potential as a rock pre-conditioning method. This predictive capability extends to two key fronts: heat absorption and treatment efficiency.

Regarding heat absorption, the methodology illuminates the extent of microwave energy wastage and identifies the potential benefits of utilizing this wasted energy. In terms of treatment efficiency, projections can be made by considering potential advancements such as higher power or reduced ramp-up time applications in microwave systems built in the future.

It should be mentioned that the same energy efficiency-based approach can be used in other similar mining operations focusing on using a new technology improving operational efficiencies.

6.3. Improving the efficiency of microwave treatment

Access to a fully validated numerical model offers engineers significant opportunities to enhance the energy efficiency of microwave treatment. Firstly, numerical models provide rapid and cost-effective insights into the energy absorption characteristics of the sample compared to experimental data. This efficiency in data acquisition can accelerate the optimization process. Secondly, numerical models have the capability to capture aspects that are often challenging to observe during experiments, such as the temperature distribution inside the sample. This detailed information is essential for fine-tuning the microwave treatment process to maximize its efficiency.

In this PhD research, the developed numerical model plays a significant role in deepening the understanding of the effects of microwave treatment on rocks and enhancing the method's efficiency. For instance, by focusing on the mineralogy of rocks, experimental data reveal that the presence of microwave-absorbing minerals intensifies the effectiveness of the microwave treatment. This phenomenon can be further evaluated using the numerical model, which offers insights from different perspectives, including mineral size, distribution, shape, and absorption capability within the matrix. Additionally, when evaluating the impact of microwave treatment on the fracture toughness of rocks, experimental results indicate that rock samples that are cut before microwave treatment undergo more intense microwave damage. Examination of this phenomenon using the numerical model reveals that sharp edges resulting from pre-cutting concentrate heat at the fracture edges, potentially explaining the observed reductions in experimental data. In summary, the numerical model significantly aids in the better and more accurate interpretation of experimental data, thereby advancing our understanding of microwave treatment effects.

In addition to aiding in better understanding the influence of microwave treatment on rocks, numerical models help in optimizing experiments for efficiency improvement. In this PhD research, the developed numerical model is effectively employed to enhance the energy efficiency of microwave treatment in the experimental phase. Firstly, the model is utilized to maximize the energy absorption of the samples, thereby improving microwave treatment efficiency. Additionally, the numerical model allows for the observation of temperature distribution within the sample. Understanding the temperature distribution aids in identifying high-intensity locations, which can be significant factors contributing to failure during microwave treatment.

6.4. Limitations and future work

The finding of this research work can be further verified and improved. The following points explain certain limitations within this research and potential ways to improve upon it:

- While the developed numerical model in this research successfully incorporates electromagnetic microwave irradiation, thermal conduction, convection, and radiation into a fully coupled format, one notable absence is mechanical analysis. Integrating mechanical analysis with these physics can enhance the depth of information provided by the numerical model. This addition would enable stress and strain analysis during microwave treatment, providing valuable insights into failure mechanisms during the process.

- The numerical model developed in this study primarily focuses on homogeneous rock samples. While the effect of heterogeneity is addressed by considering microwave-absorbing minerals within the samples and their impact on treatment efficiency, there remains room for improvement in this area. Initially, this can be addressed by incorporating a wider variety of minerals present within the sample, each with distinct material properties compared to the general rock matrix. Subsequently, the model can be refined to account for the variability of minerals within the sample, encompassing different properties. This approach holds significant potential for understanding the behaviour of heterogeneous rocks, such as kimberlite commonly encountered in Canadian mines, when subjected to microwave irradiation.
- The developed numerical model in this research focuses on the application of microwave treatment to improve excavation processes in mining, thus primarily concentrating on intact rock samples. However, there is potential to extend the application of the model to other mining operations, such as crushing and grinding, which involve particle-sized materials. By adapting the model to accommodate these different scenarios, a more comprehensive understanding of microwave treatment's efficacy across various mining processes can be achieved.
- The research outcomes were obtained by utilizing an industrial microwave system housed in the Geomechanics Laboratory of McGill University, capable of delivering up to 15 kW of microwave power to targeted samples. The findings underscore the significance of high power density in achieving improved microwave treatment outcomes. Conducting experiments at even higher power

densities holds promise for further enhancing the efficiency of microwave treatment methodologies.

- The application of high-power microwave energy to small samples faces a challenge posed by the ramp-up time inherent in microwave systems. This delay necessitates several seconds to reach the desired high power level. Consequently, although high power is theoretically applied to the small samples (UCS sized), the practical application is hindered by the time taken to reach peak power. As a result, the average received power experienced by the sample is technically slightly lower than what is theoretically anticipated.
- Ongoing advancements in microwave system development continually enhance the efficiency of microwave treatment. These improvements operate on two key fronts: 1) enhancing the energy absorption of the sample, and 2) modifying the temperature distribution within the sample to influence temperature concentration. The utilization of emerging microwave systems, such as solid-state microwaves, holds promise for further improving the efficiency of rock microwave treatment.
- While previous experiments in the literature, including those in this research, predominantly rely on well-established tests such as UCS, BTS, and fracture toughness, their ability to predict the impact of microwave treatment in practical field settings is limited. To enhance predictive accuracy, it is recommended to supplement these experiments with alternative approaches such as rock cutting experiments. By diversifying experimental methodologies, a more comprehensive understanding of the potential applications of microwave treatment in real-world scenarios can be achieved.
- Many research studies exploring the application of microwave treatment in the mining industry tend to focus on singular operations such as excavation, crushing,

grinding, and liberation, mirroring the scope of this study. However, a critical aspect often overlooked by researchers and engineers is the broader impact of microwave treatment on subsequent processes within the mining operation. For instance, while microwave treatment in excavation may enhance efficiency by prolonging cutter lifespan and increasing excavation rates, it also yields a different final product that can significantly influence the efficiency of downstream mine-to-mill processes. To gain a comprehensive understanding of the implications of microwave treatment in the mining industry, a thorough analysis of its effects across all mine-to-mill operations is imperative.

- Considering the application of microwave treatment in mining, it is imperative to account for the heterogeneous nature of rocks. Even rocks that are generally considered homogeneous by engineers, such as basalt, exhibit parameter variations from one sample to another. This variability is present in both treated and untreated samples. Figure 6.1 illustrates this point by showing all the data points used to calculate the average and standard deviation in Figure 5.8. Comparing the charts for all data points with those showing only average and standard deviation highlights several key points. First, even for untreated samples, analysing the UCS values—a commonly used metric for rock strength—reveals a variation between 183 MPa and 214 MPa. After applying microwave treatment, the variation among different samples becomes even more pronounced. This increased variability is due not only to differences between the rock samples themselves but also to the way microwave treatment induces crack formation, adding to the overall data point variation for each treatment scenario which makes it an important factor for field application considerations. Furthermore, the calculated R^2 values based on all the data points are lower than those derived from the average values. However, the overall trendline and its related equation remain consistent (Figure 6.1).

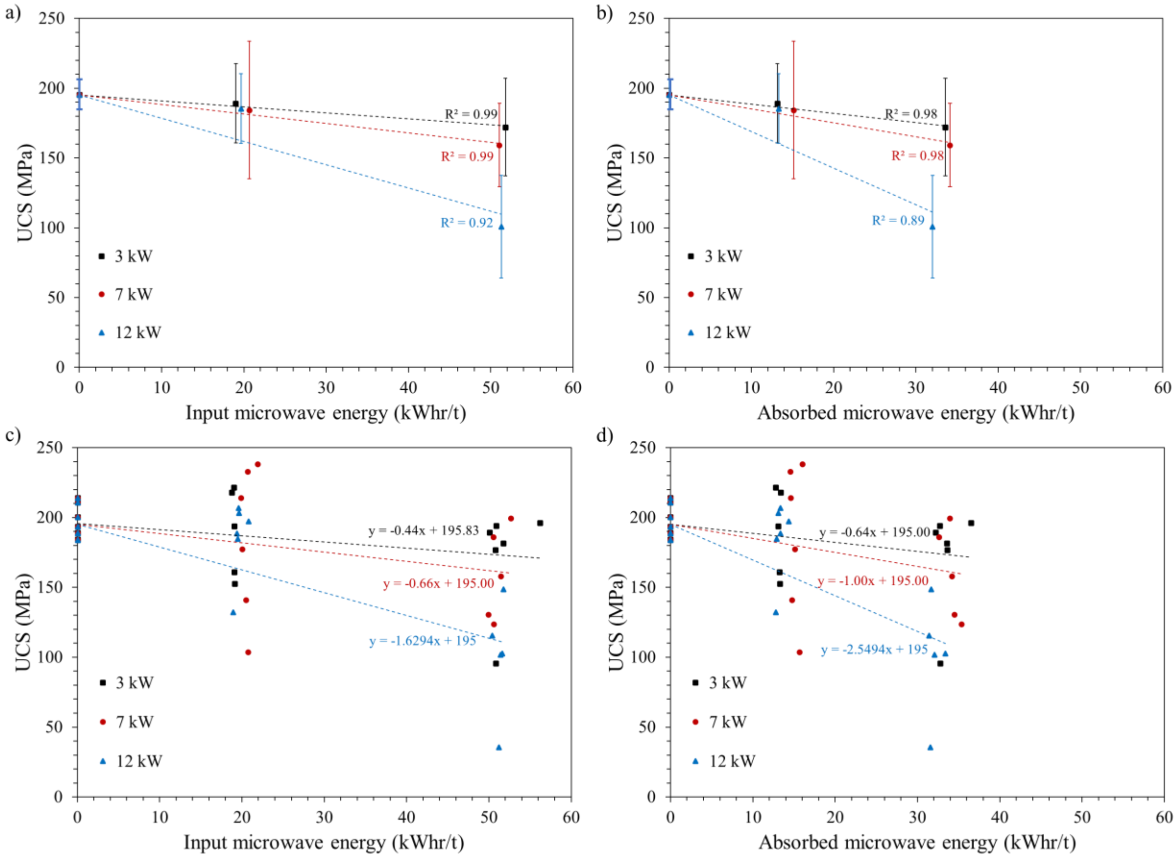

Figure 6.1 Comparison between the data analysis using all data points and average and standard deviation, a) UCS versus input microwave energy using average and standard deviation, b) UCS versus absorbed microwave energy using average and standard deviation, c) UCS versus input microwave energy using all data points, and d) UCS versus absorbed microwave energy using all data points.

"Better to be king for a night than a schmuck for a lifetime."

Rupert Pupkin- The King of Comedy

Chapter 7: Conclusion

This thesis investigates microwave treatment as a rock pre-conditioning method for potential improvement in mining excavation. The study employs two distinct approaches: experimental testing and numerical modelling. The combination of these viewpoints underscores the intricate interplay between electromagnetic energy and geological materials, revealing critical insights into energy absorption mechanisms, failure modes, and optimization strategies for enhanced treatment efficacy.

Chapter 2 focuses on the development and application of Finite Element Method (FEM)-based numerical models for simulating microwave treatment of rocks. By integrating mathematical formulations of heat transfer, fluid flow, thermal radiation, and Maxwell's equations, the developed model provides a robust framework for analysing the complex interactions between electromagnetic fields and geological substrates. The model's fidelity is demonstrated through validation against experimental benchmarks conducted in this thesis, showcasing its capability to accurately capture essential features of electromagnetic heating processes. Additionally, sensitivity analysis highlights the influence of different heat transfer phenomena, such as conduction, convection, and radiation, on microwave absorption characteristics. Notably, the developed numerical model is the first of its kind to undergo both quantitative and qualitative validation against experiments, including overall energy absorption and temperature distribution. This accomplishment establishes a solid foundation for future research in this field.

Investigations into failure mechanisms resulting from microwave treatment unveil a spectrum of behaviours influenced by sample heterogeneity, mineral composition, and heating patterns. Chapter 3 delves into the effect of microwave treatment on rhyolite rocks, revealing two distinct reactions observed in rocks: distributed and concentrated heating. Utilizing both numerical modelling and experimental findings, the study identifies the significance of microwave absorbent minerals and their role in inducing concentrated heating. This underscores the importance of understanding microscale material properties in optimizing treatment strategies. Such insights can empower engineers to manipulate the environment effectively, leading to more efficient mining practices.

In Chapter 4, the effect of microwave treatment on fracture mechanics is investigated through Mode I fracture toughness experimental techniques conducted alongside thermal imaging and calorimetric measurements. The developed numerical model is successfully utilized to optimize the energy absorption of the samples during microwave treatment. This chapter also explores the complications associated with experimental testing methods, such as fracture toughness. Specifically, the study investigates the effect of cutting the sample and creating notches on semi-circular samples before and after microwave treatment, revealing a significant difference between the two approaches. The results of the numerical model help justify this difference by showcasing temperature concentration on the samples' edges when cutting is performed before treatment, leading to a more significant reduction in the Mode I fracture toughness value.

Understanding the limitations of studying the effect of microwave treatment on the fracture mechanics characteristics of rocks leads to Chapter 5, wherein Uniaxial Compressive Strength (UCS) samples are considered as the criteria to evaluate the effectiveness of microwave treatment. This investigation is conducted through an energy efficiency-based perspective, offering novel interpretations of the results. One crucial aspect of UCS samples, compared to fracture toughness, is that the former involves all the created micro-macro cracks in the mechanical testing, providing a more realistic viewpoint on the influence of microwave treatment on rocks' properties. Additionally, quantitative data analysis reveals the potential application of microwave treatment in the field. While such applications may not be feasible currently, the ongoing improvement of microwave technology, coupled with its interaction with rocks, suggests high potential for future advancements.

The implications of microwave treatment extend beyond laboratory experiments to practical applications in mining excavation. Leveraging insights gained from numerical modeling and experimental analysis, engineers can plan treatment strategies to enhance excavation efficiency, reduce energy consumption, and mitigate operational challenges. Optimization of microwave power levels, exposure times, and sample geometries offers tangible improvements in excavation outcomes, paving the way for sustainable and resource-efficient mining practices.

References

Abali, B. E., & Reich, F. A. (2017). Thermodynamically consistent derivation and computation of electro-thermo-mechanical systems for solid bodies. *Computer Methods in Applied Mechanics and Engineering*, *319*, 567–595.

Ahmadihosseini, A., Aslam, A., & Ferri Hassani, A. S. (n.d.). *Investigating the Efficiency of Microwave Treatment in Mine-to-Mill Operations: An Energy-Based Analysis*.

Ahmadihosseini, A., Shadi, A., Rabiei, M., Samea, P., Hassani, F., & Sasmito, A. P. (2022). Computational study of microwave heating for rock fragmentation; model development and validation. *International Journal of Thermal Sciences*, *181*, 107746.

Ahmed, H. M., Ahmadihosseini, A., Hassani, F., Hefni, M. A., Ahmed, H. M., Saleem, H. A., Moustafa, E. B., & Sasmito, A. P. (2023). Numerical and experimental analyses of rock failure mechanisms due to microwave treatment. *Journal of Rock Mechanics and Geotechnical Engineering*, *15*(10), 2483–2495.

Ahmed, H. M., Hefni, M. A., Ahmed, H. A. M., Adewuyi, S. O., Hassani, F., Sasmitob, A. P., Saleem, H. A., Moustafa, E. B., & Hassan, G. S. A. (2022). Effect of Elevated Temperature on Rhyolitic Rocks' Properties. *Materials*, *15*(9), 3204.

Ali, A. Y., & Bradshaw, S. M. (2009). Quantifying damage around grain boundaries in microwave treated ores. *Chemical Engineering and Processing: Process Intensification*, *48*(11–12), 1566–1573.

Ali, A. Y., & Bradshaw, S. M. (2010). Bonded-particle modelling of microwave-induced damage in ore particles. *Minerals Engineering*, *23*(10), 780–790.

Aramendia, E., Brockway, P. E., Taylor, P. G., & Norman, J. (2023). Global energy consumption of the mineral mining industry: Exploring the historical perspective and future pathways to 2060. *Global Environmental Change*, *83*, 102745.

ASTM, E. (2006). *Standard test method for linear thermal expansion of solid materials by* *thermomechanical analysis*. ASTM E228-17, West Conshohocken, PA.

Bai, G., Sun, Q., Jia, H., Ge, Z., & Li, P. (2021). Variations in fracture toughness of SCB granite influenced by microwave heating. *Engineering Fracture Mechanics*, *258*, 108048.

Batchelor, A. R., Jones, D. A., Plint, S., & Kingman, S. W. (2015). Deriving the ideal ore texture for microwave treatment of metalliferous ores. *Minerals Engineering*, *84*, 116–129.

Bisai, R., Palaniappan, S. K., & Pal, S. K. (2020). Influence of individual and combined pre-treatment on the strength properties of granite and sandstone. *Arabian Journal of Geosciences*, *13*(1), 1–10.

Bobicki, E. R., Pickles, C. A., Forster, J., Marzoughi, O., & Hutcheon, R. (2020). High temperature permittivity measurements of selected industrially relevant ores: Review and analysis. *Minerals Engineering*, *145*, 106055.

Callister Jr, W. D., & Rethwisch, D. G. (2020). *Fundamentals of materials science and engineering: an integrated approach*. John Wiley & Sons.

Cecot, W. (2005). Modeling of electromagnetic fields in rectangular waveguides by coupled finite–infinite elements. *Computer Methods in Applied Mechanics and Engineering*, *194*(2–5), 549–558.

Chang, S.-H., Lee, C.-I., & Jeon, S. (2002). Measurement of rock fracture toughness under modes I and II and mixed-mode conditions by using disc-type specimens. *Engineering Geology*, *66*(1–2), 79–97.

Chen, H., Li, T., Wang, Z., Ye, R., & Li, Q. (2020). Effect of dielectric properties on heat transfer characteristics of rubber materials via microwave heating. *International Journal of Thermal Sciences*, *148*, 106162.

Chen, T. T., Dutrizac, J. E., Haque, K. E., Wyslouzil, W., & Kashyap, S. (1984). The relative transparency of minerals to microwave radiation. *Canadian Metallurgical Quarterly*, *23*(3), 349–351.

Chun, Y., Hassani, F., Zhou, K.-P., Feng, G. A. O., & Ameen, T. (2022). SPH-FEM simulations of microwave-treated basalt strength. *Transactions of Nonferrous Metals Society of China*, *32*(6), 2003–2018.

Cui, G., Chen, T., Feng, X., Chen, Z., Elsworth, D., Yu, H., Zheng, X., & Pan, Z. (2020). Coupled multiscale-modeling of microwave-heating-induced fracturing in shales. *International Journal of Rock Mechanics and Mining Sciences*, *136*, 104520.

D4543. (2019). *Standard practices for preparing rock core as cylindrical test specimens and verifying conformance to dimensional and shape tolerances*. ASTM International.

Deyab, S. M., Ahmadihosseini, A., Rafezi, H., Hassani, F., & Sasmito, A. P. (2023). Investigating Microwave Treatment of Rocks Based on Fracture Mechanics Analysis in Mode I Fracture Toughness Test. *Rock Mechanics and Rock Engineering, 56*, 5275–5291.

Deyab, S. M., Rafezi, H., Hassani, F., Kermani, M., & Sasmito, A. P. (2021). Experimental investigation on the effects of microwave irradiation on kimberlite and granite rocks. *Journal of Rock Mechanics and Geotechnical Engineering*, *13*(2), 267–274.

Deyab, S. M., Rafezi, H., Hassani, F., Sasmito, A. P., & Kermani, M. (2020). The effect of microwave irradiation on the mechanical properties of kimberlite and limestone. *Selçuk-Teknik Dergisi*, *19*(4), 97–109.

E1269-11, A. (2011). Standard test method for determining specific heat capacity by differential scanning calorimetry. *Am. Soc. Test. Mater*, *1*, 1–6.

Feng, G., Kang, Y., Meng, T., Hu, Y., & Li, X. (2017). The influence of temperature on mode I fracture toughness and fracture characteristics of sandstone. *Rock Mechanics and Rock Engineering*, *50*(8), 2007–2019.

Fowell, R. J., Hudson, J. A., Xu, C., & Zhao, X. (1995). Suggested method for determining mode I fracture toughness using cracked chevron notched Brazilian disc (CCNBD) specimens. *International Journal of Rock Mechanics and Mining Sciences and Geomechanics Abstracts*, *7*(32), 322A.

Gao, F., Shao, Y., & Zhou, K. (2020). Analysis of microwave thermal stress fracture characteristics and size effect of sandstone under microwave heating. *Energies*, *13*(14), 3614.

Ge, Z., Sun, Q., Xue, L., & Yang, T. (2021). The influence of microwave treatment on the mode I fracture toughness of granite. *Engineering Fracture Mechanics*, *249*, 107768.

Hartlieb, P., Kuchar, F., Moser, P., Kargl, H., & Restner, U. (2018). Reaction of different rock types to low-power (3.2 kW) microwave irradiation in a multimode cavity. *Minerals Engineering*, *118*, 37–51.

Hartlieb, P., Leindl, M., Kuchar, F., Antretter, T., & Moser, P. (2012). Damage of basalt induced by microwave irradiation. *Minerals Engineering*, *31*, 82–89.

Hartlieb, P., & Rostami, J. (2018). Rock mechanics implications of microwave treatment of rock as part of a hybrid system for mechanical excavation of rock for civil and mining applications. *ISRM EUROCK*, ISRM-EUROCK.

Hartlieb, P., Toifl, M., Kuchar, F., Meisels, R., & Antretter, T. (2016). Thermo-physical properties of selected hard rocks and their relation to microwave-assisted comminution. *Minerals Engineering*, *91*, 34–41.

Hassani, F. (2010). Review of explosive-free rock breakage (EFRB) technologies. *McGill University. Montreal, Canada*, 450.

Hassani, F, Nekoovaght, P. M., Radziszewski, P., & Waters, K. E. (2011). Microwave assisted mechanical rock breaking. *12th ISRM Congress*.

Hassani, Ferri, Nekoovaght, P. M., & Gharib, N. (2016). The influence of microwave irradiation on rocks for microwave-assisted underground excavation. *Journal of Rock Mechanics and Geotechnical Engineering*, *8*(1), 1–15.

Hassani, Ferri, Shadi, A., Rafezi, H., Sasmito, A. P., & Ghoreishi-Madiseh, S. A. (2020). Energy analysis of the effectiveness of microwave-assisted fragmentation. *Minerals Engineering*, *159*, 106642.

Hayt, W., & Buck, J. (2012). *Engineering electromagnetics*.

Holmberg, K., Kivikytö-Reponen, P., Härkisaari, P., Valtonen, K., & Erdemir, A. (2017). Global energy consumption due to friction and wear in the mining industry. *Tribology International*, *115*, 116–139.

Hutcheon, R., Jong, M. de, & Adams, F. (1992). A system for rapid measurements of RF and microwave properties Up to 1400° C. Part1: theoritical development of the cavity frequency-shift data analysis equations. *Journal of Microwave Power and Electromagnetic Energy*, *27*(2), 87–92.

Hutcheon, R., Jong, M. de, Adams, F., Wood, G., McGregor, J., & Smith, B. (1992). A System for Rapid Measurements of RF and Microwave Properties Up to 1400° C. Part 2: Description of Apparatus, Data Collection Techniques and Measurements on Selected Materials. *Journal of Microwave Power and Electromagnetic Energy*, *27*(2), 93–102.

Infrarde, E., & Termografije, E. (2018). Emissivity of aluminium alloy using infrared thermography technique. *Mater. Tehnol*, *52*, 323–327.

Iqbal, M. J., & Mohanty, B. (2007). Experimental calibration of ISRM suggested fracture toughness measurement techniques in selected brittle rocks. *Rock Mechanics and Rock Engineering*, *40*(5), 453–475.

Jin, J.-M., & Riley, D. J. (2008). *Finite element analysis of antennas and arrays*. John Wiley & Sons.

Jin, J.-M., Zunoubi, M., Donepudi, K. C., & Chew, W. C. (1999). Frequency-domain and time-domain finite-element solution of Maxwell's equations using spectral Lanczos decomposition method. *Computer Methods in Applied Mechanics and Engineering*, *169*(3–4), 279–296.

Jones, D A, Kingman, S. W., Whittles, D. N., & Lowndes, I. S. (2007). The influence of microwave energy delivery method on strength reduction in ore samples. *Chemical Engineering and Processing: Process Intensification*, *46*(4), 291–299.

Jones, Dafydd Aled, Kingman, S. W., Whittles, D. N., & Lowndes, I. S. (2005). Understanding microwave assisted breakage. *Minerals Engineering*, *18*(7), 659–669.

Kahraman, S., Canpolat, A. N., & Fener, M. (2020). The influence of microwave treatment on the compressive and tensile strength of igneous rocks. *International Journal of Rock Mechanics and Mining Sciences*, *129*, 104303.

Kahraman, S., Canpolat, A. N., Fener, M., & Kilic, C. O. (2020). The assessment of the factors affecting the microwave heating of magmatic rocks. *Geomechanics and Geophysics for Geo-Energy and Geo-Resources*, *6*(4), 1–16.

Keysight. (2017a). *Basics of measuring the dielectric properties of materials— application note*. http://literature.cdn.keysight.com/litweb/%0Apdf/5989-2589EN.pdf

Keysight. (2017b). *Keysight 85070E dielectric probe kit 200 MHz to 50 GHz—technical overview*. https://literature.cdn.keysight.com/%0Alitweb/pdf/5989-0222EN.pdf?id=364444

Kingman, S W, Jackson, K., Cumbane, A., Bradshaw, S. M., Rowson, N. A., & Greenwood, R. (2004). Recent developments in microwave-assisted comminution. *International Journal of Mineral Processing*, *74*(1–4), 71–83.

Kingman, S W, Jackson, K., Bradshaw, S. M., Rowson, N. A., & Greenwood, R. (2004). An investigation into the influence of microwave treatment on mineral ore comminution. *Powder Technology*, *146*(3), 176–184.

Kuruppu, M. D., Obara, Y., Ayatollahi, M. R., Chong, K. P., & Funatsu, T. (2014). ISRM-suggested method for determining the mode I static fracture toughness using semi-circular bend specimen. *Rock Mechanics and Rock Engineering*, *47*(1), 267–274.

Lan, W., Wang, H., Zhang, X., Fan, H., Feng, K., Liu, Y., & Sun, B. (2020). Investigation on the mechanism of micro-cracks generated by microwave heating in coal and rock. *Energy*, *206*, 118211.

Lee, G. L., Law, M. C., & Lee, V.-C. (2021). Numerical modelling and investigation of microwave heating and boiling phenomena in binary liquid mixtures using OpenFOAM. *International Journal of Thermal Sciences*, *159*, 106538.

Lehmann, G., Mayr, M., Käsling, H., & Thuro, K. (2023). Microwave pre-conditioning of granite and concrete and the implications on their geotechnical parameters. *International Journal of Rock Mechanics and Mining Sciences*, *164*, 105294.

Li, J., Kaunda, R. B., Arora, S., Hartlieb, P., & Nelson, P. P. (2019). Fully-coupled simulations of thermally-induced cracking in pegmatite due to microwave irradiation. *Journal of Rock Mechanics and Geotechnical Engineering*, *11*(2), 242–250.

Li, Q., Cheng, B., Li, X., Yin, T., & Huang, L. (2022). Fracture behaviour of microwave-heated granite under indentation: Experimental and numerical investigation. *Engineering Fracture Mechanics*, *269*, 108535.

Li, Q., Li, X., & Yin, T. (2021). Effect of microwave heating on fracture behavior of granite: An experimental investigation. *Engineering Fracture Mechanics*, *250*, 107758.

Li, R., Zhang, C., & Huang, Z. (2020). Quenching and rewetting of rock in liquid nitrogen: Characterizing heat transfer and surface effects. *International Journal of Thermal Sciences*, *148*, 106161.

Li, X., Wang, S., Xu, Y., Yao, W., Xia, K., & Lu, G. (2020). Effect of microwave irradiation on dynamic mode-I fracture parameters of Barre granite. *Engineering Fracture Mechanics*, *224*, 106748.

Liang, C.-G., Guo, Z.-S., Yue, X., Li, H., & Ma, P.-C. (2023). Microwave-assisted breakage of basalt: A viewpoint on analyzing the thermal and mechanical behavior of rock. *Energy*, *273*, 127225.

Lin, Bai-quan, Zhu, C., Wang, Z., Liu, J., Saffari, P., & Nie, W. (2020). Image and ultrasonic analysis-based investigation of coal core fracturing by microwave energy. *International Journal of Rock Mechanics and Mining Sciences*, *127*, 104232.

Lin, Baiquan, Li, H., Chen, Z., Zheng, C., Hong, Y., & Wang, Z. (2017). Sensitivity analysis on the microwave heating of coal: A coupled electromagnetic and heat transfer model. *Applied Thermal Engineering*, *126*, 949–962.

Lin, F., Feng, X.-T., Yang, C.-X., Li, S.-P., Zhang, J.-Y., Su, X.-X., & Tong, T.-Y. (2022). Experimental study on improving mechanical mining efficiency of deep banded iron ore by microwave presplitting. *International Journal of Rock Mechanics and Mining Sciences*, *159*, 105233.

Liu, H., Sun, H., Liu, X., Ye, Z., & Wang, H. (2023). Damage properties of basaltic rocks under multilevel stress loading and microwave irradiation. *Engineering Fracture Mechanics*, *289*, 109391.

Lu, G.-M., Feng, X.-T., Li, Y.-H., Hassani, F., & Zhang, X. (2019). Experimental investigation on the effects of microwave treatment on basalt heating, mechanical strength, and fragmentation. *Rock Mechanics and Rock Engineering*, *52*(8), 2535–2549.

Lu, G.-M., Feng, X.-T., Li, Y.-H., & Zhang, X. (2019). The microwave-induced fracturing of hard rock. *Rock Mechanics and Rock Engineering*, *52*(9), 3017–3032.

Lu, G. M., Li, Y. H., Hassani, F., & Zhang, X. W. (2016). Review of theoretical and experimental studies on mechanical rock fragmentation using microwave-assisted approach. *Chin J Geotech Eng*, *38*(8), 1497–1506.

Lu, Gao-ming, Li, Y., Hassani, F., & Zhang, X. (2017). The influence of microwave irradiation on thermal properties of main rock-forming minerals. *Applied Thermal Engineering*, *112*, 1523–1532.

Lu, Gaoming, Feng, X., Li, Y., & Zhang, X. (2020). Influence of microwave treatment on mechanical behaviour of compact basalts under different confining pressures. *Journal of Rock Mechanics and Geotechnical Engineering*, *12*(2), 213–222.

Lu, Gaoming, Zhou, J., Li, Y., Zhang, X., & Gao, W. (2020). The influence of minerals on the mechanism of microwave-induced fracturing of rocks. *Journal of Applied Geophysics*, *180*, 104123.

Ma, D., Duan, H., Li, X., Li, Z., Zhou, Z., & Li, T. (2019). Effects of seepage-induced erosion on nonlinear hydraulic properties of broken red sandstones. *Tunnelling and Underground Space Technology*, *91*, 102993.

Ma, D., Duan, H., Liu, J., Li, X., & Zhou, Z. (2019). The role of gangue on the mitigation of mining-induced hazards and environmental pollution: an experimental investigation. *Science of the Total Environment*, *664*, 436–448.

Measurements, A. C. E. on T. (2007). *Standard Test Method for Determining Thermal Diffusivity by the Flash Method*. ASTM International.

Meisels, R., Toifl, M., Hartlieb, P., Kuchar, F., & Antretter, T. (2015). Microwave propagation and absorption and its thermo-mechanical consequences in heterogeneous rocks. *International Journal of Mineral Processing*, *135*, 40–51.

Meng, Y., Yan, Y., Jiang, P., Zhang, M., Oladejo, J., Wu, T., & Pang, C. H. (2020). Investigation on breakage behaviour of oil shale with high grinding resistance: A comparison between microwave and conventional thermal processing. *Chemical Engineering and Processing-Process Intensification*, *151*, 107909.

Mineo, S., & Pappalardo, G. (2021). Rock emissivity measurement for infrared thermography engineering geological applications. *Applied Sciences*, *11*(9), 3773.

Motlagh, P. N. (2015). *Physical and mechanical properties of rocks exposed to microwave* *irradiation: potential application to tunnel boring*. McGill University (Canada).

Multiphysics, C. (1998). Introduction to comsol multiphysics®. *COMSOL Multiphysics, Burlington, MA, Accessed Feb, 9*(2018), 32.

Nasseri, M. H. B., Schubnel, A., & Young, R. P. (2007). Coupled evolutions of fracture toughness and elastic wave velocities at high crack density in thermally treated Westerly granite. *International Journal of Rock Mechanics and Mining Sciences*, *44*(4), 601–616.

Nejati, H., Hassani, F., & Radziszewski, P. (2012). Experimental investigation of fracture toughness reduction and fracture development in basalt specimens under microwave illumination. In *Earth and Space 2012: Engineering, Science, Construction, and Operations in Challenging Environments* (pp. 325–334).

Nekoovaght Motlagh, P. (2009). *An investigation on the influence of microwave energy on basic mechanical properties of hard rocks*. Concordia University.

Nicco, M., Holley, E. A., Hartlieb, P., & Pfaff, K. (2020). Textural and mineralogical controls on microwave-induced cracking in granites. *Rock Mechanics and Rock Engineering*, *53*, 4745–4765.

Ouchterlony, F. (1988). Suggested methods for determining the fracture toughness of rock. *International Journal of Rock Mechanics and Mining Sciences*, *25*(2), 71–96.

Ouchterlony, F. (1989). On the background to the formulae and accuracy of rock fracture toughness measurements using ISRM standard core specimens. *International Journal of Rock Mechanics and Mining Sciences & Geomechanics Abstracts*, *26*(1), 13–23.

Peinsitt, T., Kuchar, F., Hartlieb, P., Moser, P., Kargl, H., Restner, U., & Sifferlinger, N. (2010). Microwave heating of dry and water saturated basalt, granite and sandstone. *International Journal of Mining and Mineral Engineering*, *2*(1), 18–29.

Peinsitt, T., Kuchar, F., Kargl, H., Restner, U., Sifferlinger, N., & Moser, P. (2008). Microwave heating of rocks with different water content. In *Proceedings of Microwave*

Technology'08 (pp. 1–9).

Peng, K., Lv, H., Zou, Q., Wen, Z., & Zhang, Y. (2020). Evolutionary characteristics of mode-I fracture toughness and fracture energy in granite from different burial depths under high-temperature effect. *Engineering Fracture Mechanics*, *239*, 107306.

Pressacco, M., Kangas, J. J. J., & Saksala, T. (2022). Numerical Modelling of Microwave Heating Assisted Rock Fracture. *Rock Mechanics and Rock Engineering*, *55*(2), 481–503.

Rabiei, M., Samea, P., Shadi, A., & Ghoreishi-Madiseh, S. A. (2023). A discrete element analysis for general failure behavior of basalt. *International Journal of Rock Mechanics and Mining Sciences*, *167*, 105394.

Rafezi, H., Deyab, S. M., Hassani, F., Ghoreishi-Madiseh, S. A., & Micallef, D. (2020). A comparative study of the cooling-rate effect on rock strength reduction after microwave irradiation. *Experimental Results*, *1*.

Rasyid, M. A., Aslam, A., Rafiei, A., Hassani, F., & Sasmito, A. P. (2023). Application of instantaneous power draw analysis to investigate the impact of microwave heating on kimberlite ore crushing. *Applied Energy*, *352*, 121900.

Rizmanoski, V. (2011). The effect of microwave pretreatment on impact breakage of copper ore. *Minerals Engineering*, *24*(14), 1609–1618.

Rostami, J., & Ozdemir, L. (1993). A new model for performance prediction of hard rock TBMs. *Proceedings of the Rapid Excavation and Tunneling Conference*, 793.

Salsman, J. B., Williamson, R. L., Tolley, W. K., & Rice, D. A. (1996). Short-pulse microwave treatment of disseminated sulfide ores. *Minerals Engineering*, *9*(1), 43–54.

Samouhos, M., Taxiarchou, M., Hutcheon, R., & Devlin, E. (2012). Microwave reduction of a nickeliferous laterite ore. *Minerals Engineering*, *34*, 19–29.

Satish, H, Ouellet, J., Raghavan, V., & Radziszewski, P. (2006). Investigating microwave assisted rock breakage for possible space mining applications. *Mining Technology*, *115*(1), 34–40.

Satish, Hemanth. (2005). *Exploring microwave assisted rock breakage for possible space mining applications*.

Scott, G. (2006). *Microwave pretreatment of a low grade copper ore to enhance milling performance and liberation*. Stellenbosch: University of Stellenbosch.

Shadi, A., Ahmadihosseini, A., Rabiei, M., Samea, P., Hassani, F., Sasmito, A. P., & Ghoreishi-Madiseh, S. A. (2022). Numerical and experimental analysis of fully coupled electromagnetic and thermal phenomena in microwave heating of rocks. *Minerals Engineering*, *178*, 107406.

Shou, H. Z., Hu, Q., Zeng, J., He, L., Tang, H., Li, B., Chen, S., & Lu, X. (2019). Comparative study on the deterioration of granite under microwave irradiation and resistance-heating treatment. *Frattura Ed Integrità Strutturale*, *13*(50), 638–648.

Spierings, A. B., Schneider, M. u, & Eggenberger, R. (2011). Comparison of density measurement techniques for additive manufactured metallic parts. *Rapid Prototyping Journal*, *17*(5), 380–386.

Standard, A. (2010). D7012–10 (2010) Standard test method for compressive strength and elastic moduli of intact rock core specimens under varying states of stress and temperatures. *Annual Book of ASTM Standards, American Society for Testing and Materials, West Conshohocken, PA*, 495–498.

Toifl, M., Hartlieb, P., Meisels, R., Antretter, T., & Kuchar, F. (2017). Numerical study of the influence of irradiation parameters on the microwave-induced stresses in granite. *Minerals Engineering*, *103*, 78–92.

Toifl, M., Meisels, R., Hartlieb, P., Kuchar, F., & Antretter, T. (2016). 3D numerical study on microwave induced stresses in inhomogeneous hard rocks. *Minerals Engineering*, *90*, 29–42.

Vajdi, M., Moghanlou, F. S., Sharifianjazi, F., Asl, M. S., & Shokouhimehr, M. (2020). A review on the Comsol Multiphysics studies of heat transfer in advanced ceramics. *Journal of Composites and Compounds*, *2*(2), 35–43.

Walkiewicz, J. W., Clark, A. E., & McGill, S. L. (1991). Microwave-assisted grinding. *IEEE Transactions on Industry Applications*, *27*(2), 239–243.

Wang, G., Radziszewski, P., & Ouellet, J. (2008). Particle modeling simulation of thermal effects on ore breakage. *Computational Materials Science*, *43*(4), 892–901.

Wang, S., Li, X., Yao, J., Gong, F., Li, X., Du, K., Tao, M., Huang, L., & Du, S. (2019). Experimental investigation of rock breakage by a conical pick and its application to non-explosive mechanized mining in deep hard rock. *International Journal of Rock Mechanics and Mining Sciences*, *122*, 104063.

Wang, X., Guo, H., Wang, C., Chen, P., & Shi, Y. (1999). Relative dielectric constant from dry rocks. *Chinese Science Bulletin*, *44*, 2286–2293.

Wang, Y., & Djordjevic, N. (2014). Thermal stress FEM analysis of rock with microwave energy. *International Journal of Mineral Processing*, *130*, 74–81.

Wei, W., Shao, Z., Qiao, R., Chen, W., Zhou, H., & Yuan, Y. (2021). Recent development of microwave applications for concrete treatment. *Construction and Building Materials*, *269*, 121224.

Wei, W., Shao, Z., Zhang, Y., Qiao, R., & Gao, J. (2019). Fundamentals and applications of microwave energy in rock and concrete processing–A review. *Applied Thermal Engineering*, *157*, 113751.

Whittaker, B. N., Singh, R. N., & Sun, G. (1992). *Rock fracture mechanics. Principles, design and applications*.

Whittles, D. N., Kingman, S. W., & Reddish, D. J. (2003). Application of numerical modelling for prediction of the influence of power density on microwave-assisted breakage.

International Journal of Mineral Processing, *68*(1–4), 71–91.

Xu, T., He, L., Zheng, Y., Zou, X., Badrkhani, V., & Schillinger, D. (2020). Experimental and numerical investigations of microwave-induced damage and fracture formation in rock. *Journal of Thermal Stresses*, *44*(4), 513–528.

Xu, T., Yuan, Y., Heap, M. J., Zhou, G.-L., Perera, M. S. A., & Ranjith, P. G. (2021). Microwave-assisted damage and fracturing of hard rocks and its implications for effective mineral resources recovery. *Minerals Engineering*, *160*, 106663.

Xue, Y., Cao, Z., Dang, F., Ma, Z., & Gao, J. (2019). Numerical simulation of damage and permeability evolution mechanism of coal seam under microwave radiation. *Thermal Science*, *23*(3 Part A), 1355–1361.

Yang, X., Zhu, H., Zhou, X., & Nie, A. (2020). Experimental investigation on the evolution of structure and mechanical properties of basalt induced by microwave irradiation. *RSC Advances*, *10*(54), 32723–32729.

Yao, J., Tao, M., Zhao, R., Hashemi, S. S., & Wang, Y. (2021). Effect of microwave treatment on thermal properties and structural degradation of red sandstone in rock excavation. *Minerals Engineering*, *162*, 106730.

Yin, T., Wu, Y., Wang, C., Zhuang, D., & Wu, B. (2020). Mixed-mode I+ II tensile fracture analysis of thermally treated granite using straight-through notch Brazilian disc specimens. *Engineering Fracture Mechanics*, *234*, 107111.

Yuan, Y., Shao, Z., Qiao, R., Fei, X., & Cheng, J. (2020). Thermal response and crack propagation of mineral components in olivine basalt under microwave irradiation. *Arabian Journal of Geosciences*, *13*(14), 1–11.

Zeng, J., Hu, Q., Chen, Y., Shu, X., Chen, S., He, L., Tang, H., & Lu, X. (2019). Experimental investigation on structural evolution of granite at high temperature induced by microwave irradiation. *Mineralogy and Petrology*, *113*, 745–754.

Zhang, Y., Sun, Q., Ge, Z., Rui, F., & Li, J. (2022). Combined effects of microwave irradiation and water cooling on the deformation and failure behaviours of CSTBD granite. *Engineering Fracture Mechanics*, *275*, 108848.

Zhao, Q. H., Zhao, X. B., Zheng, Y. L., Li, J. C., He, L., He, J. L., & Zou, C. J. (2020). Heating characteristics of igneous rock-forming minerals under microwave irradiation. *International Journal of Rock Mechanics and Mining Sciences*, *135*, 104519.

Zhao, Q. H., Zhao, X. B., Zheng, Y. L., Li, J. C., He, L., & Zou, C. J. (2020). Microwave fracturing of water-bearing sandstones: Heating characteristics and bursting. *International Journal of Rock Mechanics and Mining Sciences*, *136*, 104495.

Zhao, Y., Gao, Y., Sun, Z., Gao, S., & Sun, C. (2022). Dielectric anisotropy effects on the microwave-induced thermodynamic response of coal: Numerical simulations and experiments. *Fuel*, *326*, 125038.

Zheng, Y., Ma, Z., Zhao, X., & He, L. (2020). Experimental investigation on the thermal, mechanical and cracking behaviours of three igneous rocks under microwave treatment. *Rock Mechanics and Rock Engineering*, *53*(8), 3657–3671.

Zheng, Y L, Ma, Z. J., Yang, S. Q., Zhao, X. B., He, L., & Li, J. C. (2021). A microwave fracturability index (MFI) of hard igneous rocks. *International Journal of Rock Mechanics and Mining Sciences*, *138*, 104566.

Zheng, Y L, Zhao, X. B., Zhao, Q. H., Li, J. C., & Zhang, Q. B. (2020). Dielectric properties of hard rock minerals and implications for microwave-assisted rock fracturing. *Geomechanics and Geophysics for Geo-Energy and Geo-Resources*, *6*(1), 1–17.

Zheng, Y L, Zhang, Q. B., & Zhao, J. (2017). Effect of microwave treatment on thermal and ultrasonic properties of gabbro. *Applied Thermal Engineering*, *127*, 359–369.

Zhu, J, Kuznetsov, A. V, & Sandeep, K. P. (2007). Mathematical modeling of continuous flow microwave heating of liquids (effects of dielectric properties and design parameters).

International Journal of Thermal Sciences, *46*(4), 328–341.

Zhu, Jingyi, Yi, L., Yang, Z., & Duan, M. (2021). Three-dimensional numerical simulation on the thermal response of oil shale subjected to microwave heating. *Chemical Engineering Journal*, *407*, 127197.

“Successes only last until someone screws them up. Failures are forever.”

Gregory House-House